TECHNISCHE UNIVERSITÄT MÜNCHEN

Fachgebiet für Peptidbiochemie

Identification of sequences of the interaction interface of β-amyloid peptide (Aβ) and islet amyloid polypeptide (IAPP) and synthesis and characterization of IAPP-derived inhibitors of Aβ aggregation

Erika Andreetto

Vollständiger Abdruck der von der Fakultät für Wissenschaftszentrum Weihenstephan für Ernährung, Landnutzung und Umwelt der Technischen Universität München zur Erlangung des akademischen Grades eines

Doktors der Naturwissenschaften

(Dr. rer. nat.)

genehmigten Dissertation.

Vorsitzende: Univ. -Prof. Dr. I. Antes

Prüfer der Dissertation: 1. Univ. -Prof. Dr. A. Kapurniotu

2. Univ. -Prof. Dr. Dr. h.c. H. Kessler

Die Dissertation wurde am 21.07.2011 bei der Technischen Universität München eingereicht und durch die Fakultät für Ernährung, Landnutzung und Umwelt des Wissenschaftszentrum Weihenstephan am 14.09.2011 angenommen.

Parts of this thesis have been published in:

Identification of hot regions of the Abeta-IAPP interaction interface as high-affinity binding sites in both cross- and self-association.
Andreetto E, Yan LM, Tatarek-Nossol M, Velkova A, Frank R, Kapurniotu A.
Angew Chem Int Ed Engl. 2010 Apr 12;49(17):3081-5.

Dissecting the Role of Single Regions of an IAPP Mimic and IAPP in Inhibition of Aβ40 Amyloid Formation and Cytotoxicity.
Andreetto E, Yan LM, Caporale A, Kapurniotu A.
Chembiochem. 2011 Jun 14;12(9):1313-22.

Other publications:

Handedness control of peptide helices by amino acid side-chain chirality: Ile/aIle peptides.
Andreetto E, Peggion C, Crisma M, Toniolo C.
Biopolymers. 2006;84(5):490-501.

IAPP mimic blocks Abeta cytotoxic self-assembly: cross-suppression of amyloid toxicity of Abeta and IAPP suggests a molecular link between Alzheimer's disease and type II diabetes.
Yan LM, Velkova A, Tatarek-Nossol M, **Andreetto E**, Kapurniotu A.
Angew Chem Int Ed Engl. 2007;46(8):1246-52.

Crystal-state 3D-structural characterization of novel, Aib-based, turn and helical peptides.
Crisma M, **Andreetto E**, De Zotti M, Moretto A, Peggion C, Formaggio F, Toniolo C.
J Pept Sci. 2007 Mar;13(3):190-205.

Exploiting cross-amyloid interactions to inhibit protein aggregation but not function: nanomolar affinity inhibition of insulin aggregation by an IAPP mimic.
Velkova A, Tatarek-Nossol M, **Andreetto E**, Kapurniotu A.
Angew Chem Int Ed Engl. 2008;47(37):7114-8.

MIF-chemokine receptor interactions in atherogenesis are dependent on an N-loop-based 2-site binding mechanism.
Kraemer S, Lue H, Zernecke A, Kapurniotu A, **Andreetto E**, Frank R, Lennartz B, Weber C, Bernhagen J.
FASEB J. 2011 Mar;25(3):894-906.

Interaction between Amyloid Beta Peptide and an Aggregation Blocker Peptide Mimicking Islet Amyloid Polypeptide.
Rezaei-Ghaleh N, **Andreetto E**, Yan LM, Kapurniotu A, Zweckstetter M.
PLoS One. 2011;6(5):e20289.

Abstract

Protein aggregation is linked to many cell degenerative diseases such as Alzheimer's disease (AD) and type 2 diabetes (T2D). AD is associated with the self-assembly of the 40-42 residue β-amyloid peptide (Aβ) whereas T2D is linked to the aggregation of the 37 residue long islet amyloid polypeptide (IAPP). Both polypeptides Aβ and IAPP share in addition to their amyloidogenicity a high degree of sequence similarity. It has been previously shown that non-fibrillar and non-toxic Aβ and IAPP species bind each other with low nanomolar affinity and that Aβ-IAPP hetero-association suppresses cytotoxic self-association and amyloidogenesis by both peptides. In addition clinical and pathophysiological studies suggest that the two diseases might be linked to each other. Therefore, the characterization of the Aβ-IAPP hetero-association interface is an important task of biomedical research. Toward this aim, the cross- and self-interaction interfaces of Aβ and IAPP were first characterized using synthetic membrane bound peptide arrays. Thereby, the N-methylated IAPP mimic IAPP-GI which is a soluble non-amyloidogenic IAPP mimic was used instead of IAPP. IAPP-GI was found to bind Aβ40 in the two regions Aβ(12-24) and Aβ(26-37). In addition, regions Aβ(11-21) and Aβ(23-37) were found to mediate Aβ40 self-association. These results showed that regions involved in the hetero-association of Aβ40 with IAPP are similar to the ones involved in Aβ40 self-association. On the other side, Aβ40 was found to bind IAPP strongly in the region IAPP(1-20) and weakly in the C-terminal part of IAPP. Similar results were obtained in the binding studies of IAPP-GI with IAPP suggesting that regions of IAPP involved in the hetero-association with Aβ40 are also mediating IAPP self-association. Next, the cross-interacting sequences of IAPP and Aβ40 were determined. IAPP(10-18) was found to bind strongly Aβ(26-37) and IAPP(20-29) interacted with the two Aβ regions Aβ(11-25) and Aβ(23-37). Aβ(15-24) and Aβ(25-35) showed strong binding to IAPP(1-20) and weak binding to the C-terminal IAPP part. These data suggested the presence of multiple cooperative interactions between specific Aβ and IAPP segments within the Aβ-IAPP interaction interface and together with other studies led to the identification of five short peptide segments of Aβ and IAPP as "hot spot regions" of Aβ-IAPP interface: Aβ(19-22), Aβ(27-32), Aβ(35-40), IAPP(8-18) and IAPP(22-28).

It has been previously shown that IAPP-GI binds Aβ with high affinity and blocks its cytotoxic self-assembly and fibrillogenesis. The next question which was addressed in my thesis was what is the role of the individual IAPP-GI and IAPP regions in inhibition of Aβ40 self-association and cytotoxicity. Thereby, the single segments IAPP(1-7), IAPP(8-18), IAPP(22-28)-GI, and IAPP(30-37) were found to not affect cytotoxic Aβ40 self-assembly. Surprisingly, the presence of the two hot regions alone of the Aβ-IAPP interaction interface IAPP(8-18) and IAPP(22-28)-GI in the partial IAPP sequence IAPP(8-28)-GI was found to be not

sufficient for inhibitory function on Aβ40 fibrillogenesis and cytotoxicity. By contrast, inclusion of the IAPP N-terminal part IAPP(1-7) as in IAPP(1-28)-GI resulted in a strong enhancement of the inhibitory effect. Inhibition of Aβ40 fibrillogenesis and cytotoxicity by IAPP(1-28)-GI was, however, not as efficient as in the case of IAPP-GI suggesting that the inhibitory effect of IAPP-GI on Aβ40 aggregation might function both via direct interaction of the hot regions and a structure stabilizing action of the N- and C-terminal IAPP parts. Studies on peptides (A1-3)IAPP(1-28)-GI and (A4-6)IAPP(1-28)-GI derived via a partial "Ala scan" of the IAPP(1-28)-GI sequence revealed similar inhibition potencies as in IAPP(1-28)-GI. By contrast, the peptides G7-IAPP(8-28)-GI and A7-IAPP(8-28)-GI exhibited weaker inhibitory effects. These results were consistent with an important role of the N-terminal region IAPP(1-7) and specific residues within this region in the inhibitory effect of IAPP-GI on Aβ aggregation and toxicity.

In the final part of my thesis, I focused on the design, synthesis and biochemical and biophysical studies of a novel class of IAPP-GI analogues as potential peptide inhibitors of Aβ40 aggregation and toxicity. These analogues consisted of the two IAPP hot regions of the Aβ-IAPP interaction interface IAPP(8-18) and IAPP(22-28)-GI which were covalently linked to each other by different linker structures. These structures consisted either of three identical amino acid residues or of non-natural amino acid residues with a backbone length corresponding to the length of three amino acids in extended conformation. Analogues with flexible hydrophobic or hydrophilic, non-natural linker structures, such as Aoc, Adc and PEG were found to be unable to affect Aβ40 self-assembly processes. The tripeptide SSN between the hot regions in IAPP(8-28)-GI was then replaced by three amino acid residue sequences with different hydrophobicity and steric hindrance in their side chains yielding analogues IAPP(8-18)G3(22-28)-GI, IAPP(8-18)A3(22-28)-GI, IAPP(8-18)V3(22-28)-GI, and IAPP(8-18)L3(22-28)-GI. In fact, the inhibitory capacity of these IAPP(8-28)-GI analogs was found to strongly improve by increasing the hydrophobicity and steric hindrance of the side chain of the tripeptide linker and IAPP(8-18)L3(22-28)-GI turned out to be the most potent inhibitor of this series of analogues. Next, rigid constrained linkers were exploited, yielding IAPP(8-18)L3(22-28)-GI-cyclo and IAPP(8-18)Amb-Ab(22-28)-GI. The cyclic constraint in IAPP(8-18)L3(22-28)-GI-cyclo was found to transform the potent inhibitor IAPP(8-18)L3(22-28)-GI in an ineffective one whereas IAPP(8-18)Amb-Ab(22-28)-GI carrying a rigid extended linker was found to be a strong inhibitor of Aβ40 self-assembly. The last category of the here synthesized and studied analogues contained β-hairpin stabilizing or destabilizing charged residues at the N- and C-termini of IAPP(8-18)A3(22-28)-GI or IAPP(8-28)-GI. K3-IAPP(8-18)A3(22-28)-GI-K3 containing the β-hairpin destabilizing K3 patches – likely via coulombic interaction of side chains - was found to be a strong inhibitor of Aβ40 aggregation and toxicity whereas E3-IAPP(8-18)A3(22-28)-GI-K3 with a likely β-hairpin stabilizing E3 and K3 patches had no effect. Studies on several truncated control peptides of the above two analogues

supported the idea that β-hairpin destabilization in the IAPP(8-28)-GI analogues may result in higher inhibitory potencies whereas β-hairpin stabilization is rather associated to weaker inhibitory effects.

Finally, the three most potent inhibitors of Aβ40 aggregation identified in this thesis IAPP(8-18)L3(22-28)-GI, IAPP(8-18)Amb-Ab(22-28)-GI, and K3-IAPP(8-18)A3(22-28)-GI-K3 were studied with regard to the IC_{50} of their inhibitory effects on formation of cytotoxic Aβ40 species and their ability to block cytotoxicity of pre-formed Aβ40 cytotoxic species. The IC_{50} of all three peptides were in the low nanomolar range and IAPP(8-18)L3(22-28)-GI proved to be the most effective analogue also with regard to blocking toxicity of already formed Aβ40 cytotoxic aggregates. IAPP(8-18)L3(22-28)-GI proved thus to have similar properties as the full length IAPP analogue IAPP-GI with regard to inhibition of Aβ40 cytotoxicity and fibrillogenesis. This analogue is, therefore, a promising peptide lead structure for the design and development of novel inhibitors of Aβ40 aggregation and toxicity.

Taken together the studies presented in this thesis contributed to the identification of hot regions of the Aβ-IAPP interaction interface and the characterization of the role of the individual region of IAPP in inhibition of Aβ40 aggregation and toxicity, and lead to the generation of a novel class of potent inhibitors of Aβ40 aggregation and toxicity consisting of covalently linked IAPP hot spot regions of the Aβ-IAPP interaction interface.

1 Introduction

1.1 Protein folding

Proteins are among the most important molecules in living organisms. There are approximately 20,500 protein-encoding genes in the human genome [1].

Protein folding is a natural process in which a polypeptide chain adopts its characteristic three-dimensional structure. This transition is crucial as the right fold is a prerequisite for a protein's long term stability and the ability to selectively interact with its partners [2].

In the early 1960 the pioneering work of Anfinsen on protein folding concluded that the native conformation of a polypeptide is encoded within its primary amino acid sequence [3, 4]. In addition proteins can fold reversibly and the functional fold should represent a global minimum on the energy landscape. Some years later, Levinthal stated that random search of a protein for the right conformation cannot be performed within microsecond to millisecond biological timescale of protein folding (Levinthal paradox) (Fig. 1A). Thus, he concluded that protein folding occurs through specific folding pathways [5].
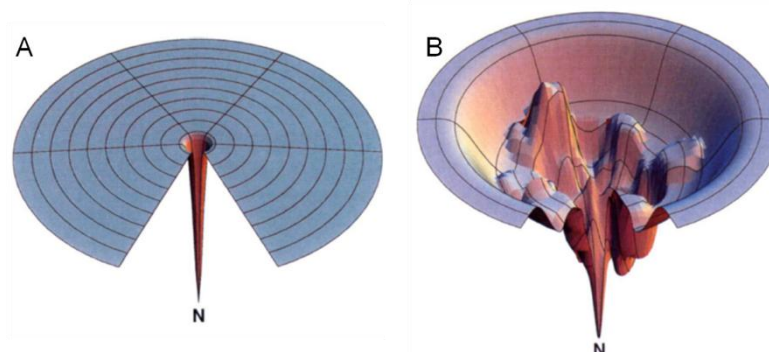
Fig. 1. (A) Energy landscape for random search (B) Energy landscape for multi-state folding in which N is the native conformation. (The figure was taken from Ref. [6])

The model of Dill et al., 1993 proposed that protein folding starts by a "hydrophobic collapse", with the burial of hydrophobic residues in a folding core [7]. Secondary and tertiary structures form then within this core with interactions such as disulfide bonds and salt bridges continuing to direct the folding, and thus the selection of conformation. This model however, may not be applicable to trans-membrane proteins since they will need to expose hydrophobic parts in order to be stable in the membrane environment. Another proposed mechanism is the nucleation-condensation model [8]. According to this model, secondary and tertiary structures form cooperatively as the whole protein condenses around a nucleus. This nucleus is formed by a few adjacent residues that have a high preference for early formation of secondary structure when stabilized by tertiary structure interactions. Together

these types of constraints limit the number of available conformations and allow the protein to fold in a biologically acceptable time span. All these models were necessary to understand how the folding process of a protein reaches a single stable state within the huge conformational space. In other words proteins are "funneled" down the energy landscape by energy barriers, kinetic traps and narrow pathways (Fig. 1B) [6, 9].

In the last decade, a number of studies suggested that a protein does not have to be folded in order to exhibit biological function [10-12]. In fact, a number of intrinsically disordered proteins have been found to be capable of biological function. It was found that 40% of all human proteins contain at least one intrinsically disordered segment and that 25% of the eukaryotic proteins are mainly disordered [11].

The knowledge about protein folding was obtained by computer prediction models and by in vitro experiments in which proteins were denatured and folded back into their original fold. However, the conditions in a living system are much more crowded and complex. Therefore, especially the folding of a large protein cannot take place without the help of the so-called quality control system.

1.1.1 Intracellular quality control

In the cell, ribosomes are responsible for the synthesis of proteins. Briefly, DNA sequence is copied into a messenger RNA (mRNA) that, in turn, is decoded by ribosomes for proteins synthesis. The decoding of genetic information to protein is called translation. In many cases, the ribosome binds to the outer membrane of the rough endoplasmic reticulum (ER) and releases the nascent protein inside the ER for later secretion to the extracellular milieu (Fig. 2). The process of folding in vivo often begins co-translationally, therefore the N-terminus of the protein begins to fold while the C-terminal portion of the protein is still being synthesized [13]. In other cases, other proteins fold in cytoplasm or in specific compartments as mitochondria and endoplasmatic reticulum. While the native conformation of a polypeptide is encoded within its primary amino acid sequence and is sufficient for protein folding in vitro, the condition in vivo is more complex. For that reason, specialized proteins called chaperones assist in the folding of other proteins [14]. Chaperones prevent protein aggregation or facilitate the forward folding and assembly of proteins into higher order structures [15]. There are two large families of molecular chaperones: ATP-dependent, such as folding machines, or ATP-independent, such as "holding" components or folding catalysts. One of the most known classes of ATP-dependent chaperones is the class of such heat-shock proteins, as Hsp70 and Hsp40 [15-18]. Another example of ATP-dependent folding machines includes the chaperonines which have a cylindrical shape that allows proteins to fold inside the cylinder.
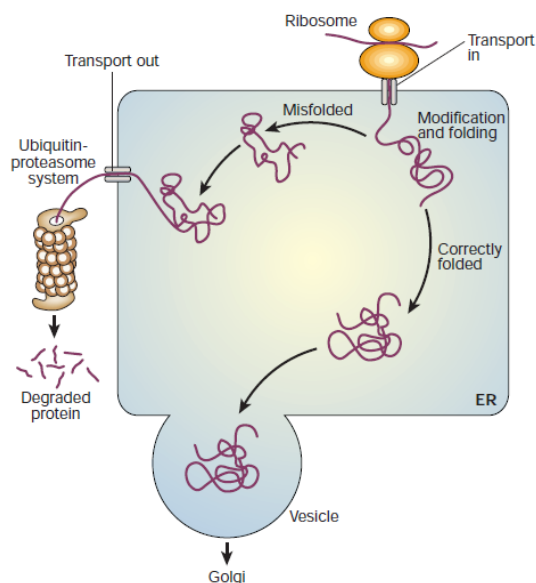
Fig. 2. Protein folding in the endoplasmatic reticulum. (The figure was taken from Ref. [2])

Incorrectly folded proteins are detected by the quality control system present in the cell [17]. These proteins follow a different pathway where they become first ubiquitinated and consequently degraded by proteasomes (Fig. 2) [19, 20].

1.1.2 Extracellular quality control

After the synthesis, proteins are translocated to the rough endoplasmic reticulum and thereafter to the compartments of the Golgi apparatus. Following the formation of vesicles that fuse with the plasma membrane, the proteins are secreted to the extracellular milieu. However, once in the extracellular space, the proteins are no longer under the surveillance of the intracellular protein folding quality control (QC) system. Recently, it has been proposed that an extracellular protein folding QC system exists which corresponds to the intracellular one [21, 22]. According to this model, a quality-control mechanism exists which is based on extracellular chaperones that are able to detect regions of increased hydrophobicity of non-correctly folded proteins as shown in Fig. 3. The extracellular chaperone would form a non-covalent complex with the non-correctly folded protein. Consequently, the complex would be recognized by cell-surface receptors and would enter the cell and be directed to intracellular degradation.

Recently identified extracellular chaperones include clusterin [23], haptoglobin [21], α2-macroglobulin [24] and serum amyloid P component [25]. It has been shown in vitro that extracellular chaperones can inhibit the aggregation of purified proteins subjected to chemical and physical stress by forming stable, non-covalent complexes with them [21, 23].
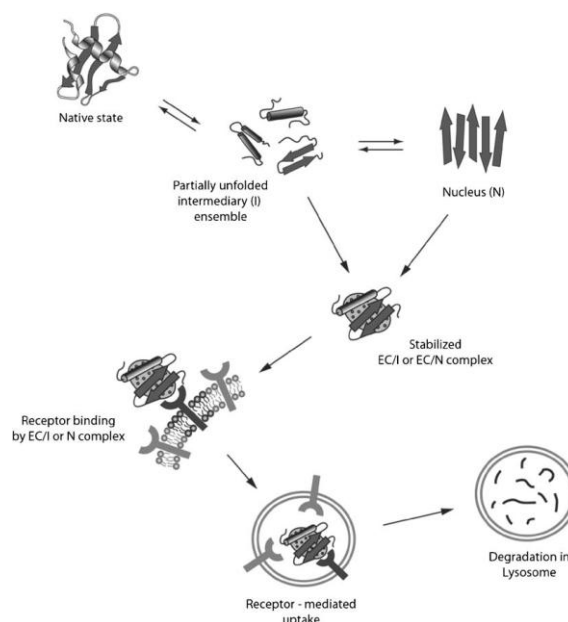
Fig. 3. Proposed extracellular quality control mechanism for protein folding. Extracellular chaperones bind to partially unfolded protein (I) or to preformed nucleus (N) generating a complex that is recognized by a receptor. Following endocytosis, the complex is degraded by lysosome. (The figure was taken from Ref. [26])

1.2 Protein misfolding diseases

Despite the many mechanisms that nature has generated to prevent protein misfolding and aggregation, there is a large number of diseases which are caused by the abnormal folding of proteins, the so-called protein misfolding diseases. This process can occur as a result of several post-translational modifications, such as premature degradation via the quality control system of the endoplasmic reticulum, as occurs in cystic fibrosis [27], or the inappropriate transport of a protein, as seen in early-onset emphysema [28]. However, the largest group of misfolding disorders involves a specific class of polypeptides or proteins that, by escaping all protective mechanisms, undergo a conversion from their functional soluble states into highly organized fibrillar aggregates. These structures are generally described as amyloid fibrils and are accumulating extracellularly such as β-amyloid peptide and amylin or intracellularly such as α-sinuclein and tau. In 1857, Rudolf Virchow used for the first time the term "amyloid" (starch-like) to describe extracellular deposits in the nervous system. The term amyloid was retained but with a meaning of proteinaceous deposit.

A large number of human diseases is related to the failure of proteins or peptides to fold correctly [29]. A list of known diseases that are associated with the formation of amyloid fibrils is given in Table 1**.**

Table 1. Human disorders characterized by protein misfolding and amyloid deposits. (The table was adapted from Ref. [29])

DISEASE	AGGREGATING POLYPEPTIDE
Neurodegenerative disease	
Alzheimer's disease	β-amyloid peptide
Spongiform encephalopathies	Prion protein or fragments
Parkinson's disease	α-Synuclein
Dementia with Lewy bodies	α-Synuclein
Frontotemporal dementia with Parkinsonism	Tau
Amyotrophic lateral sclerosis	Superoxide dismutase
Huntington's disease	Huntingtin with polyQ expansion
Spinocerebellar ataxias	Ataxins with polyQ expansion
Spinocerebellar ataxia 17	TATA box-binding protein with polyQ expansion
Spinal and bulbar muscular atrophy	Androgen receptor with polyQ expansion
Hereditary dentatorubral-pallidoluysian atrophy	Atrophin-1 with polyQ expansion
Familial British dementia	ABri
Familial Danish dementia	ADan
Non-neuropathic systemic amyloidoses	
AL amyloidosis	Immunoglobulin light chains or fragments
AA amyloidosis	Fragments of serum amyloid A protein
Familial Mediterranean fever	Fragments of serum amyloid A protein
Senile systemic amyloidosis	Wild-type transthyretin
Familial amyloidotic polyneuropathy	Mutants of transthyretin
Hemodialysis related amyloidosis	β2-microglobulin
ApoAI amyloidosis	N-terminal fragments of apolipoprotein AI
ApoAII amyloidosis	N-terminal fragment of apolipoprotein AII
ApoAIV amyloidosis	N-terminal fragment of apolipoprotein AIV
Finnish hereditary amyloidosis	Fragments of gelsolin mutants
Lysozyme amyloidosis	Mutants of lysozyme
Fibrinogen amyloidosis	Variants of fibrinogen α-chain
Icelandic hereditary cerebral amyloid angiopathy	Mutant of cystatin C
Non-neuropathic localized diseases	
Type II diabetes	Islet amyloid polypeptide (IAPP)
Medullary carcinoma of the thyroid	Calcitonin
Atrial amyloidosis	Atrial natriuretic factor
Hereditary cerebral hemorrhage with amyloidosis	Mutants of β-amyloid peptide
Pituitary prolactinoma	Prolactin
Injection-localized amyloidosis	Insulin
Aortic medial amyloidosis	Medin
Hereditary lattice corneal dystrophy	C-terminal fragments of kerato-epithelin
Corneal amyloidosis associated with trichiasis	Lactoferrin
Cataract	γ-Crystallins
Calcifying epithelial odontogenic tumors	Unknown
Pulmonary alveolar proteinosis	Lung surfactant protein C
Inclusion-body myositis	B-amyloid peptide
Cutaneous lichen amyloidosis	Keratins

The table is divided in: neurodegenerative diseases in which aggregation occurs in the brain, non-neuropathic systemic amyloidosis in which aggregation occurs in multiple tissues and

non-neuropathic localized amyloidosis in which aggregation occurs in a single tissue. Those diseases can be, in turn, grouped in sporadic (85%), hereditary (10%) and infectious (5%) [29]. For example Alzheimer's disease and Parkinson disease are predominantly sporadic diseases whereas many studies suggest also a possible hereditary component [29]. Spongiform encephalopathies can also be transmissible [29].

1.2.1 **Amyloid fibril structure**

As shown in Table 1, many different diseases are associated to protein misfolding [29]. The polypeptides involved in misfolding disorders do not share strong similarity between their primary, secondary or tertiary structures. However, they share many common physico-chemical and biological features in their aggregated states [29]. All amyloid fibrils are constituted of β-strands that run perpendicular to the long axis of the fibril (Fig. 4B-F) [30]. X-ray diffraction studies have revealed two distinct signals corresponding to the so-called "cross-β pattern" one at 4.7 Å and one perpendicular at 10 Å (Fig. 4A) [31]. The 4.7 Å signal corresponds to the distance between the β-strands and the 10 Å signal indicates spacing between the different interacting sheets.
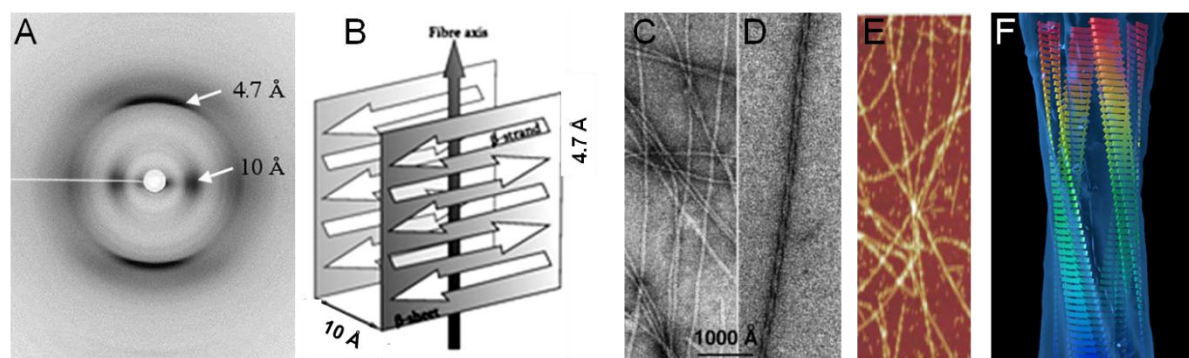
Fig. 4. (A) X-ray diffraction showing the characteristic cross-β diffraction signals on the meridian and equator at 4.7 Å and 10 Å, respectively. (The figure was taken from Ref. [32]) (B) Schematic representation of a cross-β structure. (The figure was taken from Ref [33]) (C) (D) Example of EM image of amyloid fibrils. (The figure was taken from Ref. [34]) (E) Example of AFM image of amyloid fibrils. (The figure was taken from Ref. [35]) (F) Overview of the fibril structure: twisting of the protofilaments around each other. Fibril model was based on cryo EM studies. (The figure was taken from Ref. [34])

In the last decade, much structural information on the fibril structure was obtained with biophysical methods including solid-state NMR [36] and cryo-electron microscopy [37]. Solid state NMR is able to provide detailed structural information of a non-crystalline compound such as fibril. Together with electron microscopy (EM) data, it contributed to the development of structural model of amyloid fibrils. Transmission electron microscopy (TEM) or atomic force microscopy (AFM) have suggested that fibrils can be composed of 2 to 6 protofilaments

[38] (Fig. 4C-D-E) (Fig. 5). These fibrillar subunits twist together to form unbranched fibers of 7-12 nm in diameter [30, 38]. In addition, amyloid deposits show specific optical behavior such as binding to thioflavin T (ThT) or Congo red (CR) [39]. While binding to ThT results in enhanced fluorescence intensity at 482 nm and a shift of the emission maximum of ThT from 430 nm to 482 nm, the binding to CR results in gold-green birefringence under polarized light. Although many similarities are observed in the structure and composition of fibrils, a certain degree of heterogeneity in the morphology and in particular in the position of the peptide chain within the fibrils, so-called polymorphism, has been also observed [34, 40, 41]. Clearly, the favored structure should be the one with the lowest free energy and fastest kinetic and it is regulated by the main polypeptide chain. However, different environmental conditions or side-chain interactions can affect the fibrils structure.

1.2.2 Amyloid fibril formation

Following the biosynthesis, a polypeptide chain can adopt many conformational states that are in equilibrium with each other. The interconversion from one state to another is normally regulated by the quality control system. However when such regulatory systems fail, conformational diseases can occur [29]. In that case, the concentration of the amyloidogenic species has to increase as much as the gain of enthalpy (due to favorable packing interactions) overcomes the loss of entropy. In other words, misfolding and aggregation of proteins are believed to be side effects of the conformational transitions of polypeptide and protein.
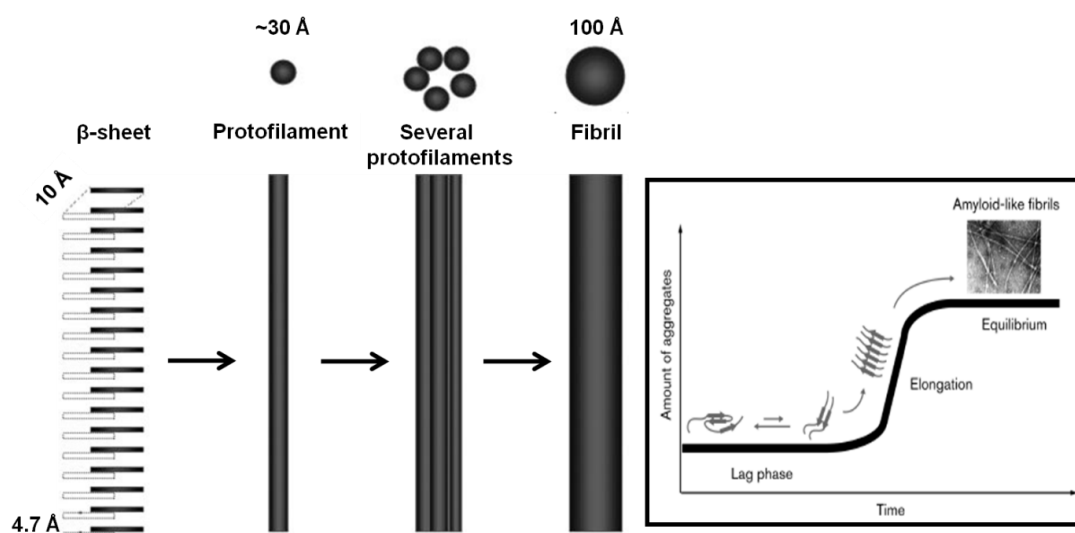
Fig. 5. Schematic diagram showing the probable hierarchical assembly of amyloid peptides from β-sheets to fibrils. (The figure was taken from Ref. [32]) In the inset a scheme of a typical kinetic trace of fibrillization is shown: amyloid fibril formation is characterized by a lag-phase followed by an elongation phase and a final steady-state phase.

Amyloid fibril formation has many characteristics of a "nucleated growth" mechanism. In particular, the conversion of a peptide or protein to its fibrillar form is characterized by a lag-phase that is followed by an elongation phase where a rapid exponential growth occurs, and eventually a steady state phase (Fig. 5) [29]. The lag-phase is the time required to reach the critical concentration to form the nucleus. It has been suggested that the nucleus is formed first by the self-association of a short sequence within the polypeptide chain. It has been also proposed that the nucleus can be formed by a "dry steric zipper" constituted of two tightly interdigitated β-sheets [42]. The formation of the nucleus is generally slow because it requires high-order oligomerization. In fact, amyloidogenic monomers are often in α-helical conformation or not structured while amyloid fibrils exhibit highly defined β-sheet structure. The lag-phase can be shortened or abolished by adding a preformed nucleus, so-called seed, by changing experimental conditions, or by mutations. During the lag-phase many different oligomers are formed by a series of thermodynamically unfavorable steps. Oligomeric species are important intermediates of the fibril formation pathway and in addition they have been suggested to be more cytotoxic than the fibrils themselves [43].

An increasing number of proteins have been found to form fibrils under certain conditions [44, 45]. These findings have suggested that the ability to form fibrillar structures is a generic property of polypeptide backbone. However, the nature of the amino acids sequence affects the stabilities of the different conformational states accessible to the peptide. Thus, the sequence will promote or prevent the conversion into fibrils. In fact, substitution of amino acids which are located within the amyloid core of an amyloidogenic peptide can reduce the aggregation propensity when the hydrophobicity of the inserted amino acid is less than the one of the original amino acid and vice versa [46, 47]. It has also to be taken into account that nature has avoided clusters of hydrophobic amino acids in soluble proteins [48]. Another key factor in protein aggregation is the total net charge. It has been observed that the capacity of a peptide to aggregate decreases when the total net charge becomes higher [49]. Several amyloidogenic proteins exhibit α-helical conformation in their native state hence, when misfolding occurs, the protein undergoes an α-helix → β-sheet transition. In this context, it has been demonstrated that proteins, which are found to be in α-helix conformation but with a β-sheet forming potential, are associated with amyloid fibril formation [50].

1.3 **Alzheimer´s disease**

Alzheimer's disease (AD) is a progressive neurodegenerative disorder described for the first time by the German psychiatrist and neuropathologist Alois Alzheimer in 1906. AD is the most common cause of dementia in elderly, accounting for 60-70% of all cases [51]. Since

age is the strongest risk factor for AD and as the life expectancy has become longer, the number of people affected by AD is expected to increase enormously which will result in high costs for the society. The two main neuropathological characteristics of AD are: intracellular neurofibrillar tangles consisting of hyperphosphorylated tau protein and extracellular deposits consisting of β-amyloid peptide. Tau proteins are mainly present in neurons and their function is to stabilize the microtubules. The hyperphosphorylation of tau can result in the self-assembly and consequently neurofibrillar tangle formation [52]. However, the senile plaques in AD have been found to be predominantly composed of β-amyloid-peptide (Aβ) fibrils [53]. Aβ is a 39-43 amino acid polypeptide derived from the cleavage of a large protein called amyloid precursor protein (APP). Aβ self-assembly is believed to be strongly associated – possibly causally - with AD pathogenesis [54]. The first symptoms of AD are often memory loss and difficulties in acquiring new information. When the disease is in an advanced stage, a general and progressive decline in cognitive functions is observed. AD patients are usually divided into two subgroups based on age of onset. Early onset AD, which accounts in about 5-10 % of all AD cases, is diagnosed before the age of 65 while the rest is diagnosed after the age of 65 years. Familial AD belongs to the group of the early-onset AD and is caused by mutations in at least three genes: β-amyloid precursor protein, Presenilin 1, or Presenilin 2.

1.3.1 β-amyloid precursor protein (APP) and the β-amyloid-peptide (Aβ)

β-amyloid precursor protein (APP) gene is located in the chromosome 21 [55]. APP is a type I transmembrane protein, with the N-terminus in the extracellular space, a single domain in the membrane and the C-terminus in the cytoplasm. The physiological role of APP is still not clear although cellular expression has been found in many cell types suggesting an important role [56]. APP was found to be critical in neuron growth, survival and post-injury repair [57].
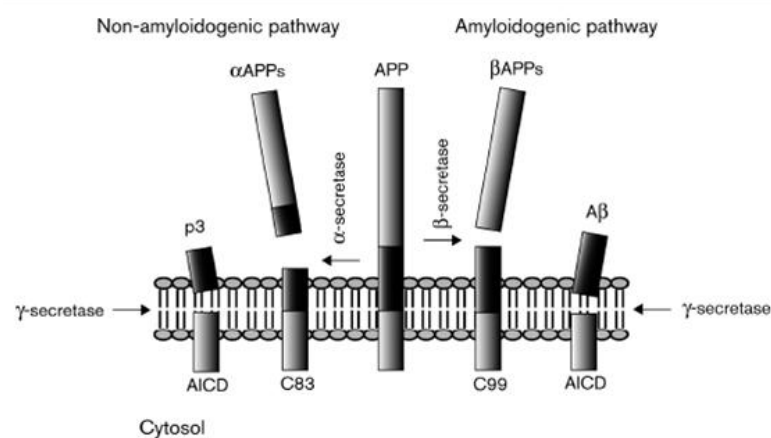
Fig. 6. Non-amyloidogenic and amyloidogenic pathways of APP.

During cellular metabolism APP can be cleaved at three different sites by proteases leading to different pathways: the amyloidogenic and the non-amyloidogenic pathway (Fig. 6) [58]. The amyloidogenic pathway occurs when the β-secretase cleaves APP between residues 596 and 597 in the extracellular region releasing a soluble fragment called βAPPs and a membrane-bound fragment C99. C99 is further cleaved by γ-secretase at position 639-640 that is located in the membrane. The second cleavage made by the γ-secretase generates β-amyloid-peptide (Aβ), a peptide of predominantly 40-42 amino acid residues which forms amyloid fibrils in AD. In the non-amyloidogenic pathway, which is predominant under normal physiological condition, APP is cleaved by α-secretase between residues 612 and 613 (within the Aβ sequence). This pathway generates a membrane bound peptide C83 and releases a soluble fragment αAPPs. Consequently C83 is cleaved by γ-secretase at position 639-640 yielding the extracellular peptide p3 and the intracellular AICD. The transmembrane γ-secretase is involved in both pathways and it is composed of presenilin 1 or 2, Pen-2, Aph-1 and nicastrin [59]. Mutations in the presenilins can cause increases in production of Aβ1-42 and are thus linked to familial AD [60]. The amyloidogenic pathway produces Aβ peptide that is composed of 36-43 residues. However the predominant form is Aβ40 while Aβ42 is characterized by a higher aggregation propensity than Aβ40.

$$D^1AEFRHDSGYEVHHQKLVFFAEDVGSNKGAIIGLMVGGVV^{40}IA^{42}$$

Fig. 7. Primary sequence of Aβ40 and Aβ42.

The Aβ peptide has a hydrophobic C-terminal (derived by the APP membrane domain) and a hydrophilic N-terminal (previous extracellular domain). Solid state NMR studies have proposed a model for Aβ40 fibrils in which the region Aβ(1-10) is disordered, the regions Aβ(12-24) and Aβ(30-40) form β-sheet structures and the region Aβ(25-29) contains a bend [61]. Hydrogen/deuterium-exchange NMR studies on Aβ42 have proposed as a model of fibrils structure, heterogeneity in the region Aβ(1-17), two β-strands involving regions Aβ(18-26) and Aβ(31-42), and a β-turn between the β-strands [62].

1.3.2 β-amyloid-peptide (Aβ) fibrils

The β-amyloid-peptide generated from the APP cleavage by the β- and γ-sectretases forms fibrils that are deposited in the brains of affected patients (so-called plaques). This wrong metabolism of APP has been proposed by Hardy and Higgins in 1992 to be the cause of AD pathogenesis and it has been called "the amyloid cascade hypothesis" [63]. This hypothesis consisted on the idea that Aβ should be the major neuropathological responsible in the

disease since it is found in the plaques surrounding degenerated neurons. Additionally, it has been shown that mutations on chromosome 21 (APP gene), 14 (PRE1 gene), and 1 (PRE2) are related to early onset of AD most likely by increasing the production of Aβ42. Furthermore, trisomy 21 patients (Down's syndrome) usually develop early onset of AD because chromosome 21 encodes for APP. Although increasing amounts of amyloid favors Aβ as the cause of AD, only a poor correlation has been found between amount of plaques and the severity of the disease. Therefore, the amyloid cascade hypothesis has been extended to include also soluble Aβ oligomers [54]. In fact, soluble Aβ species are now believed to be the main cause of neurodegeneration in AD because they are more neurotoxic than fibrils [43].

The structure of ex-vivo amyloid fibrils from cerebral cortex of AD patients has been studied by EM and X-ray fiber diffraction [64]. These two techniques have been widely used to characterize Aβ fibrils. For example in Fig. 8A-B-C is shown the negative stain TEM of Aβ40 synthetic fibrils in which is observed a mixture of straight and twisted fibrils [65]. Both types of fibrils were unbranched and with a average fiber size of around 70 Å. The helical pitch of the twisted fibers was around 460 Å. Interestingly, the extended form of Aβ40 would be around 140 Å long and according to the EM data the diameter of the fibril is around 70 Å. Based on this finding it has been suggested that Aβ40 exhibit a intersheet β-hairpin [66].
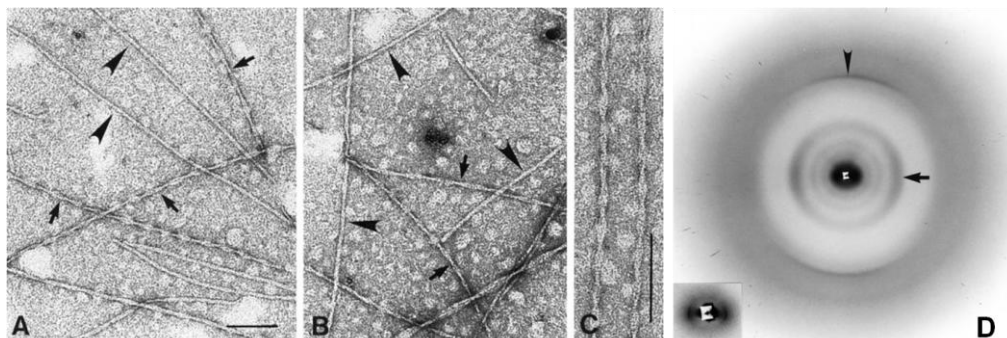
Fig. 8. (A)(B) EM of two types of Aβ40 fibrils: twisted (arrow) and straight (arrowhead). Scale bar, 1000 Å. (C) EM with higher magnification of twisted Aβ40 fibrils. Scale bar, 1000 Å. (D) X-ray diffraction of Aβ40: reflection on equator at 8.9 Å (arrow) and reflection on meridian at 4,7 Å (arrowhead). (The figure was taken from Ref. [65])

Another method used to characterize the fibrillar structure is X-ray diffraction that gives a distinctive pattern. The X-ray diffraction pattern of cross-β sheet structure contains two reflections: one meridian corresponding to the fibril axis at 4.7 Å and one equatorial corresponding to the distance between β-sheets at 10-12 Å (Fig. 8D) [32].

A detailed molecular structure of Aβ fibrils has been difficult to obtain because of their non-crystalline, insoluble structure. However, much progress has been made in the solid state NMR (SSNMR) field and based on these studies models of Aβ fibrils have been generated. Tycko's model has been obtained with Aβ40 fibrils generated using gentle agitation. In this

model, Aβ40 fibrils exhibited in-register parallel β-sheets [61, 67]. Residues 1-10 are structurally disordered, residues 10-22 and 30-40 form two β-strands. Thereby, G^{25}, S^{26}, and G^{29} are not part of β-strands (Fig. 9) [68]. A stabilizing intermolecular salt-bridge between D^{23} and K^{28} and contacts between I^{31}/G^{37} and M^{35}/G^{33} were also observed [61, 69]. The combination of NMR and TEM data is based on the hypothesis that the protofilament contains two layers of Aβ40 molecules that are mainly stabilized by hydrophobic interactions. In fact, it has been found that the side chains of L^{17}, F^{19}, A^{21}, A^{30}, I^{32}, L^{34} and V^{36} interact intramolecularly while side chains of I^{31}, M^{35} and V^{39} interact with the second layer at the interface. Polar or charged residues (except the one involved in the salt bridge) are placed in the outer part of the protofilament.
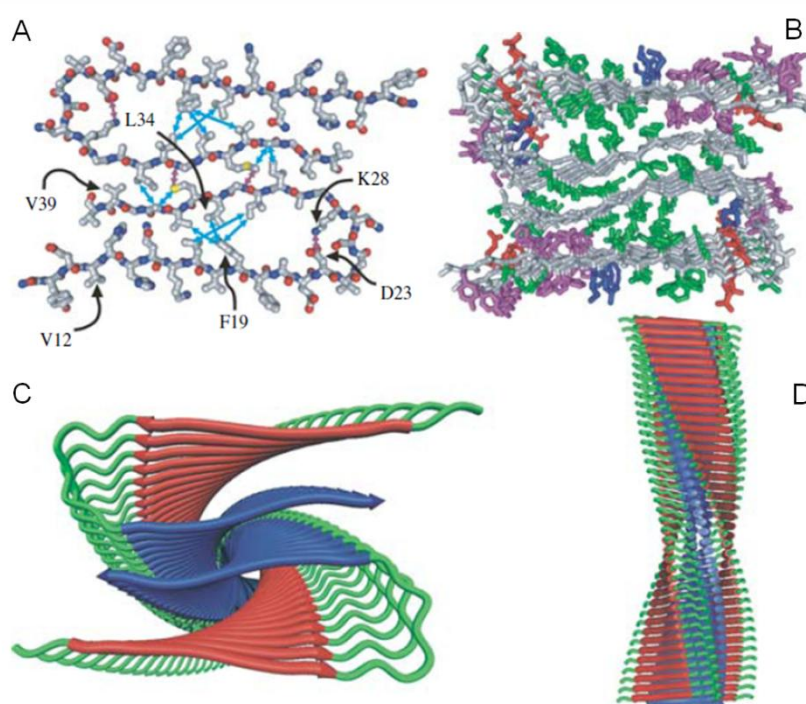
Fig. 9. Structural model of Aβ40 fibrils based on solid state NMR [69]. Residues of Aβ(1-8) are omitted because they are disordered. The axis of the fibril is perpendicular to the page in panels (A), (B), (C) and parallel and vertical to the page in panel (D). (A) Layer of the protofilament constituted of two Aβ40 molecules and four β-strands. Blue and violet double-headed arrows indicate respectively side-chain–side-chain and side-chain–backbone contacts. (B) Model of Aβ40 protofilament generated by SSNMR data. Amino acids side chains are visualized by using green (hydrophobic), purple (polar), red (negatively charged), blue (positively charged). The backbone is shown in grey colour. (C)(D) Cartoon representations of Aβ40 protofilament with residues 12–21 in red and residues 30–40 in blue with a left-handed twist of 0.833°/Å. (The figure was taken from Ref. [36])

Another model proposed by Riek has been obtained by hydrogen/deuterium-exchange NMR of Aβ42 fibrils oxidized at the M^{35} [62]. Oxidation of the methionine side chain has been found to be helpful in solution NMR studies [70]. In this model, residues 1–17 are disordered and two intermolecular, parallel, in-register β-sheets are formed by residues 18–26 (β1) and

31–42 (β2) (Fig. 10C). The two β-strands were connected by a loop. The main differences between the two models were: a) in Tycko´s model the side chain interactions are intramolecular between the strands belonging to the same molecule which is in contrast to the intermolecular nature of the side chain interactions in Riek´s model (Fig. 10A-B); b) the side chain interactions in Tycko´s model are between the odd residues of β1 and the odd residues of β2, which is in contrast to Riek´s model where the intermolecular contacts are between odd residues of β1 and even residues of β2; and c) Tycko´s model had two to four Aβ40 molecules per unit length while Riek´s model comprises only one Aβ42 molecule per protofilament unit length. The differences between the two models might found a justification in the polymorphism of Aβ due to different experimental conditions used to obtain the amyloid fibrils.
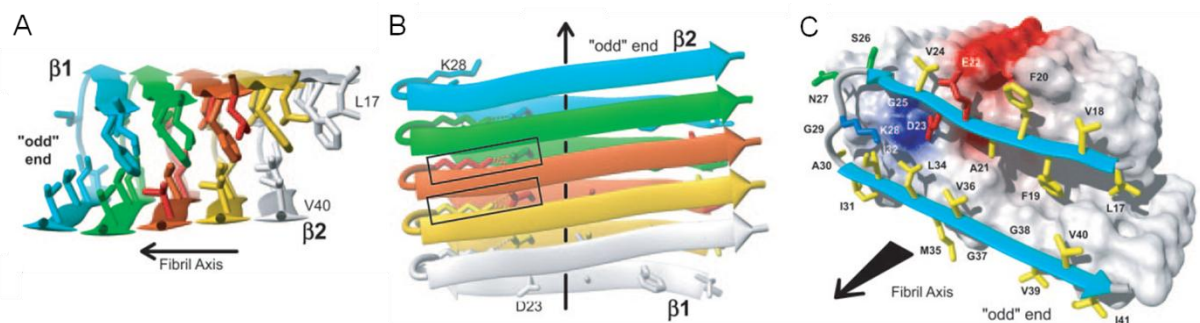
Fig. 10. 3D structure of a (35Mox)Aβ42 fibril as derived from NMR studies. (A)(B) Ribbon diagrams of the inter-β-strand interactions of residues 17–42. In (B) the intermolecular salt bridges between residues D23 and K28 are highlighted by rectangles. (C) Van der Waals contact surface polarity and ribbon diagram of the (35Mox)Aβ42 protofilament comprising residues 17–42. The hydrophobic, polar, negatively charged, and positively charged amino acid side chains are shown in yellow, green, red, and blue, respectively. Positively and negatively charged surface patches are shown in blue and red, respectively, and all others are shown in white. (The figure was taken from Ref. [62])

1.4 Biochemical approaches to target Aβ aggregation toxicity

In the past decades much effort has been invested in understanding the molecular mechanism of misfolding diseases and in finding compounds which can interact with amyloidogenic polypeptides and proteins. In the case of AD, no cure but only treatments that somewhat slow down disease progress have been available. However many compounds are currently under clinical trials [71]. Various different strategies to intervene with the Aβ aggregation pathway have been developed. In the following chapters some of these strategies are discussed.

1.4.1 **Blocking Aβ production**

A possible way to limit Aβ production is to suppress the cleavage of the amyloid precursor protein (APP) and several studies focus on discovering compounds that are able to inhibit the β- or γ-secretase.

Few reports on β-secretase inhibitors exist because the active site of the enzyme is quite large hence design of inhibitors is rather difficult [72]. β-Secretase is an aspartic-acid protease and, additionally, it is involved in the formation of myelin sheaths in peripheral nerve cells, making this target not suitable for inhibitors development [73].

γ-Secretase is a protease which cleaves transmembrane proteins. It has been found to process not only APP but also the Notch receptor which is important for cell differentiation [74]. Also in the case of γ-secretase, as for β-secretase is not possible to block completely the function of the enzyme but it is rather preferred to alter its activity. Substrate-targeting γ-secretase modulators (such as NSAIDs) have been shown to affect the production of Aβ by binding to APP in the Aβ region and thereby modulate γ-secretase cleavage and the levels of released Aβ42 [75, 76]. This kind of approach can bypass the obvious side effect of shutting down the enzyme activity but it could find therapeutic application only if APP or its cleavage products would not have any physiological function which is yet unknown.

1.4.2 **Immunotherapy**

Another attractive strategy is the use of antibodies for prevention and treatment of AD. The immunization concept has been developed by Schenk and coworkers who showed that antibodies generated against Aβ42 could lower amyloid formation and reduce pre-formed plaques in mice brain [77]. Thereby, fibrillar Aβ42 was injected to the mice in order to stimulate the immune response (Fig. 11a). This approach has been applied and confirmed by other groups [78, 79]. However, when 6% of the patients participating in the clinical trial of Aβ42 fibrils immunization developed meningoencephalities, the study was terminated [80, 81]. Nevertheless, to avoid such a strong immune response much effort is currently being invested in developing new active immunization approaches. For example, new studies have been using immunization with Aβ fragments, such as Aβ(1-15) which lack T-cell reactive sites of the full length Aβ42 but they are conjugated to a carrier protein that stimulates T-cell that in turn will allow B-cell to produce antibodies (Fig. 11b) [82-85]. In this way, T-cell response against Aβ is avoided. Another option would be the passive immunization which consists of the direct administration of monoclonal anti-Aβ antibody (Fig. 11c). This approach bypasses the problem of the stimulation of the immune response.
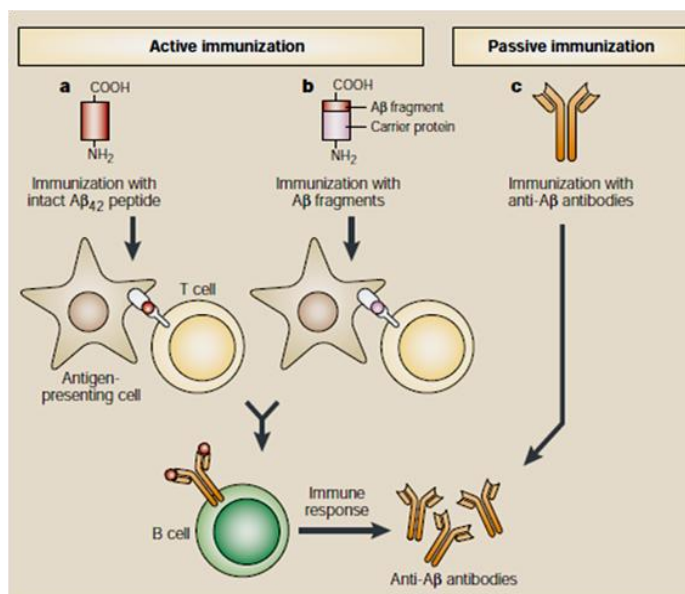
Fig. 11. Antibody approaches against Aβ: active and passive immunization. Active immunization might be achieved by (a) administration of Aβ42 or (b) Aβ fragment conjugated to a carrier protein that stimulates the T-cell response. (c) Passive immunization requires the direct injection of an anti-Aβ antibody. (The figure was taken from Ref. [86])

The mechanism of action of active or passive immunization has so far not been clarified. However, two possible ways have been proposed: either the antibody in the plasma shifts the equilibrium of the various Aβ species in the brain or by crossing the blood brain barrier helps in the phagocytosis of the plaques [77, 87].

1.4.3 Chaperones

As shortly described in chapters 1.1.1 and 1.1.2, molecular chaperones assist the correct folding of proteins [88]. Therefore, another kind of approach against Aβ self-assembly would be to stimulate the chaperone activity. In fact, it has been found that heat shock proteins Hsp70, Hsp40, and Hsp90 are able to inhibit the early stage of Aβ42 aggregation in vitro [89]. Heat shock proteins are normally present intracellularly but also in the extracellularly, where Aβ self-assembly occurs [90]. Clusterin, an extracellular chaperone, has been shown to interact and inhibit formation of pre-fibrillar amyloidogenic structures of Aβ42 in a substoichiometric manner [91]. Therefore, inducing the up-regulation of chaperones could be another way to intervene with the aggregation pathway. Indeed, Hsp90 inhibitor has been found to up-regulate Hsp70 and to suppress Aβ induced neurodegeneration in vitro [114].

1.4.4 Small molecule inhibitors

In the past years many small organic molecules have been found to interfere with Aβ aggregation and therefore they have been tested as inhibitors. An advantage of using small molecules as inhibitors is that they might be able to cross the blood brain barrier. These inhibitors include: surfactants, Cu/Zn chelators, bioactive molecules such as curcumin, melatonin, nicotine, rifampicin, and dyes such as Congo red and thioflavin T [92-99]. Although Congo red and thioflavin are the characteristic dyes used to detect amyloid plaques, they have been also shown to be able to inhibit fibril formation at high concentrations. Many of the above mentioned compounds are aromatic and they probably act at different stages of the Aβ aggregation pathway. For example, nicotine has been found to retard aggregation by stabilizing the α-helical structure of Aβ [96]. In another case, hydroxyaniline derivatives, RS-0466 and RS-0406, have been shown to inhibit Aβ oligomerization in cells and suppress cytotoxicity in HeLa cells [100, 101]. However, Glabe and coworkers systematically tested previously found inhibitors to determine whether oligomers are an intermediate stage in fibrillization pathway [102]. Based on their findings, they divided the small molecules inhibitors into three classes: compounds that inhibit oligomerization but not fibrillization, compounds that inhibit fibrillization but not oligomerization and compounds that inhibit both (Table 2). This study shed some light not only on the importance of small molecules as amyloid inhibitors but also on the aggregation mechanisms in particular with regard to the issue of the role of oligomers in fibrillizations. However, a limit of this study is that the oligomers have been detected by the anti-oligomer antibody (A11) which could recognize only some of the possible oligomers conformations.

Table 2. Classes of compounds that intervene with Aβ42 self-assembly. (The table was taken from Ref. [102])

Class I (compounds that inhibit oligomerization but do not inhibit fibrillization)	Class II (compounds that inhibit both oligomerization and fibrillization)	Class III (compounds that inhibit fibrillization but do not inhibit oligomerization)
Azure C	Meclocycline sulfosalicylate	Apigenin
Basic blue 41	Hemin	Chicago sky blue
R(-) Norapomorphine hydrobromide	o-Vanillin	Diallyltartar
Congo red	C16	Direct red
Rolitetracycline	Hematin	Orange G
Daunomycin hydrochloride	C17	
C16	Neocuproine	
1,2-Naphthoquinone	Lacmoid	
Nordihydroguaiaretic acid	Rifamycin SV	
C17	2,2′-Dihydroxybenzophenone	
Juglone	Rhodamine B	
Myrecitin	Phenol red	
ThT	Eosin y	
Curcumin		
Indomethacin		
Quinacrine mustard dihydrochloride		
Pherphenazine		

A disadvantage of small molecule drugs is that because of their size they might be not enough specific. Additionally, small molecules can bind the target compound only within a limited region.

1.4.5 **Peptide-based inhibitors**

To achieve higher specificity to the target, several strategies based on peptides have been developed. Several of the designed inhibitors have a sequence that resembles the amyloidogenic core of the protein whose aggregation should be inhibited but contains modifications such as N- and C-terminal ones, conformational restrictions, or D-amino acids. Tjernberg et al. has shown for the first time that the Aβ amyloid core region, KLVFF, was able to inhibit Aβ fibril formation (Fig. 12) [103]. Introducing lysines at N- or C-terminus of the KLVFF motif remarkably increased the binding affinity to Aβ possibly due to favorable coulombic interactions with full length Aβ [104]. The high affinity of these compounds to Aβ was accompanied by an increase in Aβ40 fibrillization rate and an inhibition of Aβ toxicity [105]. Soto et al. have developed inhibitors based on the concept of substituting amino acid in the amyloidogenic core with β-sheet breaking residues [106, 107]. In their case, proline was used as a β-sheet breaker which is well known to reduce β-sheet propensity and to interrupt the hydrogen bonding network. The shortest of these inhibitors, LPFFD, has been shown to inhibit fibril formation, to disassemble pre-formed fibrils and to reduce Aβ cytotoxicity (Fig. 12) [107].

A) KLVFF

B) LPFFD

C) K(N-Me)LV(N-Me)FF(N-Me)AE
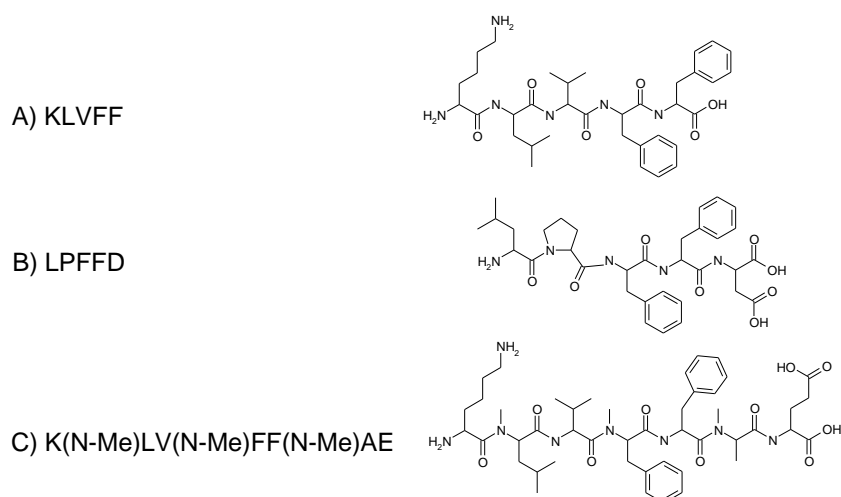
Fig. 12. Examples of peptide based inhibitors against Aβ: A) an inhibitor consisting of the Aβ amyloid core sequence KLVFF, B) LPFFD and C) K(N-Me)LV(N-Me)FF(N-Me)AE.

Later on, many groups followed the concept of designing inhibitors containing conformationally constrained amino acids such as N-methyl amino acids or α,α-disubstituted amino acids. The use of N-methyl amino acids contributes to: a) a good solubility of the

inhibitor, b) a higher resistance to proteolytic cleavage and c) a higher probability for the inhibitor to cross the blood brain barrier. Meredith et al. have designed K(N-Me)LV(N-Me)FF(N-Me)AE, a peptide based on the Aβ core region with three alternated N-methyl amino acids (Fig. 12). This peptide has been shown to inhibit Aβ fibril formation and to disassemble fibrils [108]. This inhibitor has been suggested to act as a "cap" of the amyloid fibrils and its sequence similarity to the Aβ amyloid core KLVFFA contribute to the binding to full length Aβ while the alternated N-methyl amino acids act to block the further aggregation on that side of the β-strand. Doig et al. reported also a study on a single N-methyl moiety introduced into Aβ(25-35) [109]. Out of the six N-methylated analogues only the one with (N-Me)Gly^{33} was able to inhibit both amyloid formation and cytotoxicity of the partial Aβ sequence Aβ(25-35). This result would suggest that the position of the N-methylation is crucial in the binding to the target molecule and in the structural design of the inhibitor.

1.5 Type II diabetes and IAPP

Diabetes is a chronic disease characterized by hyperglycemia. There are two major forms of diabetes: type I and type II. In the year 2000, the worldwide prevalence of diabetes has been estimated to 171 million, with 18 million suffering from type I diabetes [110, 111]. Type I diabetes is considered to develop as a consequence of an autoimmune destruction of the insulin producing pancreatic β-cells, preferentially in young people [112]. The most common form of diabetes is type 2 diabetes and is characterized by peripheral insulin resistance combined with impaired insulin production. In most of these patients deposits of amyloid are seen in the pancreatic islets. The amyloid deposits are associated with reduced β-cell mass and function [113]. Although the presence of amyloid deposits in pancreas has been first described 100 years ago, the protein composition of these deposits has been identified in 1986 [114, 115]. Their key component Islet Amyloid Polypeptide (IAPP) or amylin has been first isolated from amyloid deposits in a human insulinoma [114, 115]. IAPP is mainly expressed in pancreatic β-cells where it is stored together with insulin in secretory granules. The fact that amyloid has been originally described in the pancreas of a type II diabetic patient has led to the hypotheses that it may play a role in diabetes pathogenesis [114]. Humans with type 2 diabetes, as well as some animal models of type II diabetes, showed amyloid in more islets than age-matched controls [116-118]. Moreover, islet amyloid has been identified in humans with type 2 diabetes with a prevalence exceeding 80%, which could be compared to the 12% seen in non-diabetic subjects over the age of 40 years [117-120]. The exact initiation place of formation of islet amyloid is still not clarified. Some data suggest that IAPP aggregation is initiated intracellularly and becomes extracellular after the β-cell death, whereas other studies support the view of extracellular fibril formation at the site

of IAPP secretion from the cells [121, 122]. Amyloid deposits in the vicinity of the islet may contribute to a disturbed microenvironment of the islet cells and may lead to an impaired β-cell function [123]. Moreover, IAPP has been shown to disrupt phospholipid bilayer membranes and might therefore act as an inducer of cellular death by apoptosis in pancreatic islets [124]. In line with this, IAPP amyloid deposits have been reported to have a direct toxic effect on β-cells [125].

1.5.1 IAPP structure

ProIAPP is the precursor protein of IAPP and is produced in the pancreatic β-cells as a 67 amino acid residue containing protein. ProIAPP undergoes proteolysis to yield IAPP, the 37 amino acid polypeptide. The active form of IAPP contains an intramolecular disulfide bridge between the cysteine residues at positions 2 and 7 and a C-terminal amide group (Scheme 1) [126]. In 1988 it has been demonstrated that a short region of the human IAPP sequence, IAPP(20-29), is capable of self-associating into fibrils (Scheme 1) [127]. This region has been also found to have a different amino acid composition between different animal species and the various sequences differed in their fibrillogenic potentials [128-130]. In fact, species such as humans, primates, cats, dogs, monkeys, and raccoons develop islet amyloid while rodents do not develop IAPP-derived islet amyloid.

Human	KCNTATCATQRLANFLVHS**SNNFGAILSS**TNVGSNTY-NH2
Monkey	KCNTATCATQRLANFLVRS**SNNFGTILSS**TNVGSDTY-NH2
Cat	KCNTATCATQRLANFLIRS**SNNLGAILSP**TNVGSNTY-NH2
Rat	KCNTATCATQRLANFLVRS**SNNLGPVLPP**TNVGSNTY-NH2
Hamster	KCNTATCATQRLANFLVHS**NNNLGPVLSP**TNVGSNTY-NH2
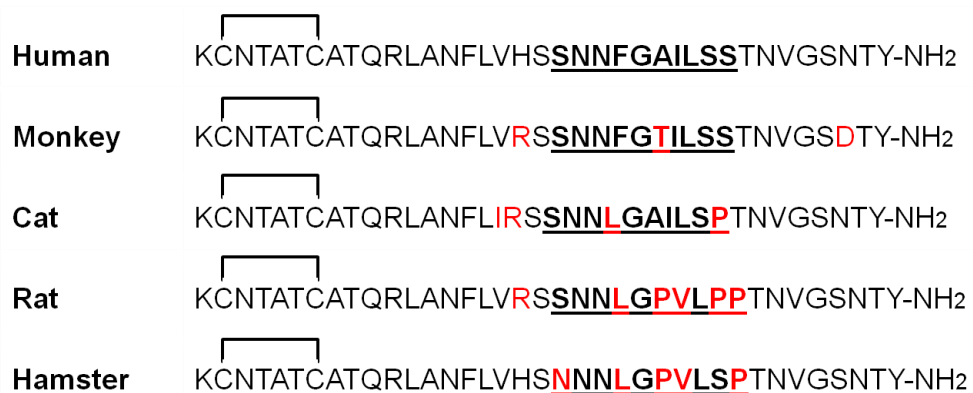
Scheme 1. Primary structure of human, monkey, cat, rat and hamster IAPP. The amyloidogenic sequence IAPP(20-29) is bold and underlined. Amino acid residues within the non-human sequence that differ from the respective residues of the human sequence are red. (The scheme was taken from Ref. [131])

The sequence of rat IAPP (rIAPP) differs from the human IAPP in 6 out of 37 amino acids and 5 of these 6 amino acids are located in the region between residues 20 and 29 (Scheme 1). Most importantly, the rat IAPP(20-29) (rIAPP(20-29)) region contains three prolines [132, 133]. Synthetic rIAPP and the corresponding rIAPP(20-29) sequences do not form amyloid fibrils consistent with the β-sheet breaking potential of proline [127, 129]. Substitution of residues Ala^{25}, Ser^{28} and Ser^{29} of hIAPP with three proline results in a peptide without

amyloidogenic potential at pH<5 which is now used as an insulin adjunctive in T2D treatment [134]. Additional studies have found that IAPP(30-37) and IAPP(8-20) are also able to form fibrils [135, 136]. These studies have shown that a big part of the IAPP sequence is highly amyloidogenic with the exception of the N-terminal part IAPP(1-7). Furthermore, rIAPP(8-20) was found to form also fibril as well as IAPP(30-37). By contrast full length rIAPP does not make fibrils which suggest that rIAPP(20-29) (containing three prolines) avoid rIAPP fibrillization and that IAPP(20-29) is the driving force of IAPP fibrillization [127, 129].

Two-dimensional IR with site-specific isotope labeling made during aggregation process suggest first the formation of the loop followed by a formation of the two parallel β-sheets [137]. Circular dichroism (CD) studies demonstrated that the IAPP monomer adopts random coil conformation that is converted to β-sheets with the time [138]. Results derived by denaturation studies of IAPP proposed that IAPP is able to adopt a non-amyloidogenic and an amyloidogenic conformation in equilibrium with each other [138]. This suggestion was supported by a results combinations of mobility mass spectrometry and molecular dynamics which have shown that two different types of conformers of IAPP monomers are present: an extended β-hairpin containing one and a helix-coil one [139]. The extended β-hairpin conformer is absent in the experiments performed on rIAPP suggesting that this conformer may play a crucial role in the aggregation pathway of human IAPP.

1.5.2 **IAPP fibrils**

IAPP as other amyloidogenic peptides form amyloid fibrils via a "nucleated growth" mechanism. Thereby, formation of a nucleus is a slow process and is followed by a fast further aggregation into protofilaments and fibrils. Two to five protofilaments associate to produce a fibril which is usually unbranched and exhibits a diameter of 10-30 nm [140]. Structural studies on IAPP have been particularly difficult because it has a poor kinetic solubility in aqueous solutions and forms fibrils rapidly. However, EPR measurements suggested that IAPP exhibits a very dynamic structure in solution and a highly ordered parallel structure in the fibrillar state [141]. In the fibrillar state, the same residues from different strands were found to be in close proximity to each other and the N-terminus showed an unordered structure [141]. Solid state NMR measurements of IAPP fibrils structure have been reported by Tycko [142]. This model has been obtained by a combination of solid state NMR, TEM, and Langevin dynamics simulations. In this model, IAPP fibrils form a parallel in-register assembly with a β-strand-loop-β-strand motif (Fig. 13). The two β-strands are IAPP(8-17) and IAPP(28-37). Fig. 13B-C reports two different sets of side chain contacts between the two β-sheets obtained from two independent runs.
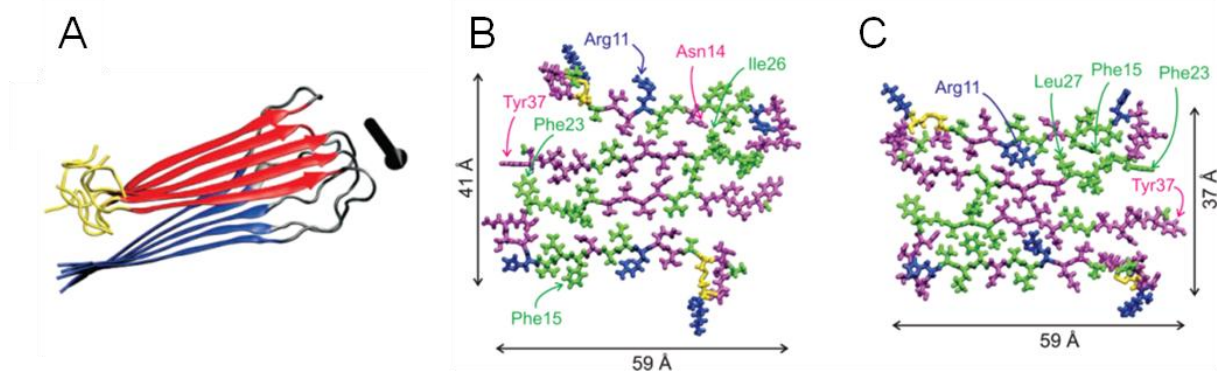
Fig. 13. IAPP fibril molecular structural model generated using restrained Langevin dynamics simulations. (A) Ribbon representation of one cross-β-molecular layer, with N- and C-terminal β-strand segments in red and blue, respectively. The black arrow indicates the fibril axis. (B) and (C) All-atom representations of two possible models, with hydrophobic residues in green, polar residues in magenta, positively charged residues in blue, and disulfide-linked cysteine residues in yellow. (The figure was taken from Ref. [142])

Attempts to crystallize full-length IAPP have been so far unsuccessful. Recently an IAPP fibril model based on x-ray diffraction data of cross-β spine structures of the two segments of human IAPP, IAPP(21-27) and IAPP(28-33), has been proposed [143]. This model differs from the one obtained with NMR with regards to the side chain packing but in principal it has similar topological features.

1.5.3 Inhibitors to target IAPP aggregation and toxicity

While many different compounds and chemical strategies to inhibit amyloid formation and cytotoxicity of Aβ have been developed, there are not so many reports available about IAPP aggregation inhibitors. A possible explanation could be that IAPP is one of the most insoluble and amyloidogenic polypeptides known with a critical concentration of aggregation which is lower than 100 nM [138]. Nevertheless, many small molecules found to inhibit aggregation of some of the amyloidogenic peptides have been also found to inhibit IAPP aggregation. Such inhibitors include aromatic organic compounds such as tetracycline, rifampicin and analogues, the amyloid specific dye congo red (CR), chalcones, and others [144-147]. Another approach is the design of peptidic inhibitors which are derived from the IAPP sequence. For example, studies on six overlapping hexapeptides spanning the IAPP amyloid core IAPP(20-29) demonstrated that IAPP(20-25) and IAPP(24-29) were strongly delaying the transition of IAPP to β-sheets and thus to inhibit IAPP amyloidogenesis [148].
The use of conformationally constrained amino acids to interrupt and/or prevent β-sheet formation was also applied to develop IAPP aggregation inhibitors. A study reported the design of short IAPP sequences containing α-aminoisobutyric acid (Aib) known to be a β-sheet breaker with high α-helical propensity [149]. The modified IAPP(14-20) analogues were

found to inhibit IAPP fibril formation. In another study the highly amyloidogenic sequence IAPP(20-29) was transformed into its peptoid and retro-peptoid and the peptoid was found to be not capable of self-assembly into fibril and to inhibit IAPP(20-29) fibril formation [150].

Another category of IAPP aggregation inhibitors introduces N-methyl amino acids in short peptides corresponding to the amyloid core of the IAPP sequence [151]. The generated peptides do not form β-sheet structure and are very good soluble [151]. Based on the information that IAPP(23-27) and IAPP(22-27) are the shortest IAPP sequences still able to make fibrils, two N-methyl moieties were introduced to those sequences on the same side of the β-strand (Scheme 2) [151, 152]. The double N-methylated hexapeptide [(N-Me)G24, (N-Me)I26]-IAPP(22-27) has been found to inhibit both amyloidogenicity and cytotoxicity of IAPP [151, 153].
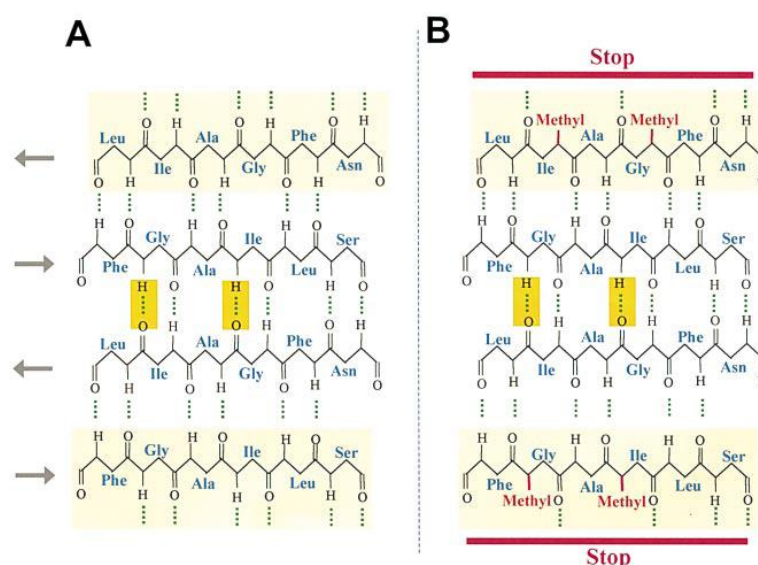
Scheme 2. A) Schematic model for IAPP(22-28) antiparallel β-sheet self-assembly based on rotational resonance (R2) solid state NMR of IAPP(20-29) [154]. B) Hypothetical mechanism of inhibition of IAPP fibril formation by introducing two N-methyl residues at G24 and I26. (The figure was taken from Ref. [151])

Based on these findings, the double N-methylated full length IAPP analog [(N-Me)G24, (N-Me)I26]-IAPP (IAPP-GI) has been designed and synthesized few years ago [155]. It has been shown that IAPP-GI is a highly soluble, non-amyloidogenic, and non-cytotoxic IAPP mimic and an IAPP receptor agonist [155]. Moreover, IAPP-GI has been shown to bind IAPP with low nanomolar affinity and to block IAPP cytotoxic self-assembly and fibrillogenesis with activity in the low nanomolar concentration range [155]. Importantly, IAPP-GI dissociates cytotoxic IAPP oligomers and fibrils and is able to reverse their cytotoxicity [155].

1.6 Links between AD and T2D

AD and T2D are chronic, age-related diseases. In AD, the neurodegeneration is related to the structural change, self-association, and amyloid fibril deposition of Aβ40 and Aβ42 [156]. T2D is characterized by insulin resistance and the deposition of amyloid fibrils consisting of islet amyloid polypeptide (IAPP) in pancreas (extracellular deposits) [157].

Many studies have demonstrated that there are several similarities between AD and T2D. In general, both diseases are characterized by extracellular amyloid deposition and associated cell degeneration. Numerous epidemiological studies have shown a two to five fold increased risk factor for T2D patients to develop AD and vice versa [158]. In fact, alterations in insulin signaling, a symptom of T2D, is likely associated to AD cognitive decline [159]. These findings are directly connected to the fact that the insulin receptor is not only expressed in the peripheral system but also in neurons and that it does not only regulate sugar blood level but it also acts as a growth factor in neurons [160]. Another study has shown that both diseases are characterized by insulin signaling abnormalities [161]. In addition it has been found that Aβ and IAPP share a similar degradation and clearance system carried out by insulin-degrading enzyme (IDE) [162]. A proteomic analysis on healthy pancreatic β-cells identified several proteins that are involved in AD pathogenesis [163]. Another proteomic study on transgenic mice brain discovered pancreatic islet proteins that are deregulated upon Aβ injection [164]. These findings suggest that AD and T2D contribute to the activation of pathways and proteins. Moreover Aβ and IAPP are present in similar concentration in serum and cerebrospinal fluid therefore the interaction between the two peptides is possible in vivo.
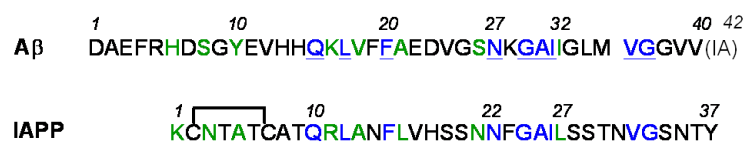
Fig. 14. Primary structures of Aβ and IAPP. Identical residues between sequences are indicated in blue and similar residues in green.

As least but not last, the two amyloidogenic peptides, Aβ and IAPP, share the 25% of sequence identity and circa the 50% of sequence similarity (Fig. 14).

1.7 Aβ-IAPP and Aβ-IAPP-GI interaction

In the above chapter, the similarities between AD and T2D on the pathophysiological and clinical level were discussed. Recently, a link between AD and T2D was found also on the molecular level. In fact, the key amyloid polypeptides of AD and T2D, Aβ and IAPP are two short, linear, and conformationally flexible polypeptides which exhibit high self-association

affinities and their aggregates are highly cytotoxic [45, 165]. Moreover, 25% of the residues of the two peptides are identical and they are normally located in the regions which are known to be important for the self-association such as Aβ(15-21) and IAPP(10-16) or Aβ(26–32) and IAPP(21–27) [61, 152, 166]. A recent study by our group has shown that Aβ40 binds IAPP with low nanomolar affinity ($K_{d,app}$= 48,5 ± 4,2 nM) and that pre-fibrillar Aβ40 attenuates IAPP aggregation into IAPP aggregates and fibrils and vice versa (Fig. 15) [167]. As both Aβ and IAPP are present at similar concentration in blood and cerebrospinal fluid an interaction in vivo would be possible.
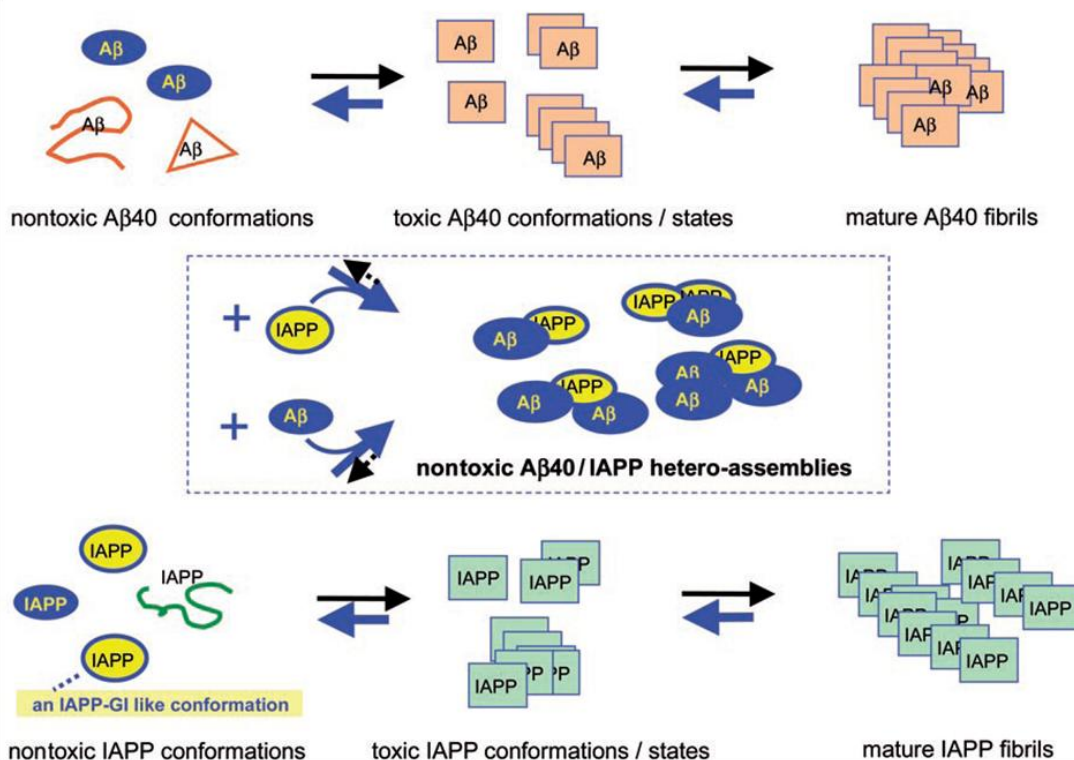
Fig. 15. Molecular model of the interaction between pre-fibrillar Aβ40 and IAPP resulting in attenuation of cytotoxic self-assembly and fibrillogenesis of both Aβ40 and IAPP (blue arrows). (The figure was taken from Ref. [167])

The discovery of the Aβ-IAPP interaction was the result of the finding that the IAPP mimic, IAPP-GI, has been found to bind with low nanomolar affinity pre-fibrillar Aβ40 ($K_{d,app}$= 41,2 ± 3,9 nM) and to strongly inhibit Aβ40 cytotoxic self-association and fibrillogenesis [167]. Additionally, IAPP-GI has been shown to redissociate already formed cytotoxic Aβ40 assemblies and fibrils [167]. The hetero-complex between Aβ40 and IAPP-GI is stabilized in a non-fibrillar and non-toxic soluble oligomeric form due to the high affinity of the Aβ-IAPP-GI interaction and the N-methylations in the amyloid core of IAPP-GI which is consistent with the high potency of the inhibitory effect of IAPP-GI (Fig. 16). In conclusion, IAPP-GI can be

considered as a high affinity ligand of both pre-fibrillar IAPP and Aβ and a cross-amyloid disease inhibitor [167].
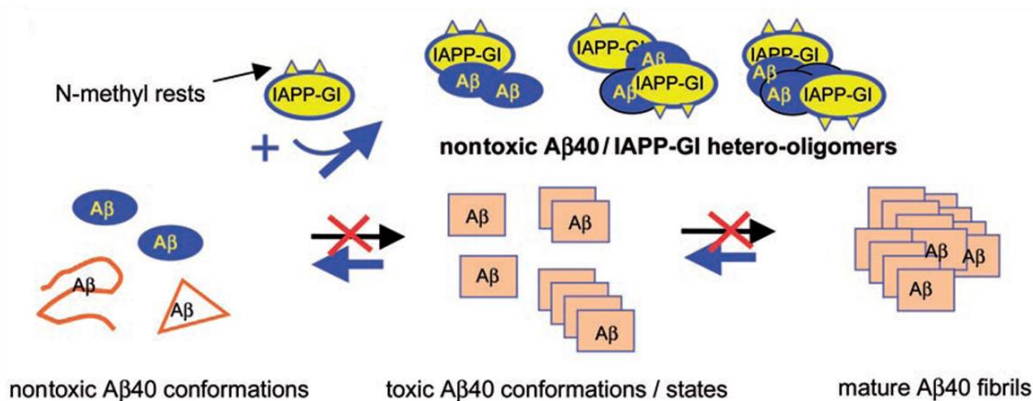
Fig. 16. Molecular model of the interaction between IAPP-GI and pre-fibrillar Aβ40 resulting in inhibition and reversal of cytotoxic self-assembly and fibrillogenesis of Aβ40 (blue arrows). (The figure was taken from Ref. [167])

1.8 Aims of the study

Based on the previous findings about the Aβ-IAPP and Aβ-IAPP-GI interaction the first part of this thesis had the following aims:

1. Identification of Aβ40 and IAPP regions involved in Aβ40-IAPP hetero- and in Aβ40 or IAPP self-association by using synthetic membrane-bound peptide arrays.
2. Characterization of the role of the single IAPP-GI and IAPP segments in the inhibitory effect on Aβ40 fibrillogenesis and cytotoxicity.
3. Studying the role of the N-terminal region of IAPP in inhibition of Aβ40 fibrillogenesis and cytotoxicity.

The second part of this thesis mainly focused on design, synthesis and biophysical and biochemical studies of novel Aβ40 aggregation inhibitors which were devised by using the "hot regions" of the Aβ40-IAPP (IAPP-GI) interaction interface as a template. Accordingly, inhibitors should consist of the IAPP segments, IAPP(8-18) and the N-methylated analog of IAPP(22-28) IAPP(22-28)-GI which were covalently connected to each other with different linkers. The applied linker structures between IAPP(8-18) and IAPP(22-28)-GI were:

a) A non-natural conformationally flexible hydrophobic or hydrophilic amino acids residue such as Aoc, Adc, PEG.
b) Segments of 3 natural amino acids which differed in the hydrophobicity and steric hindrance effect of their side chains.
c) A conformationally constrained linker or a cyclic constraint.
d) In addition, a subclass of analogs containing charged residues at the N- and C-termini which were introduced to modulate β-hairpin stability.

2 Materials and Methods

2.1 Materials

2.1.1 Chemicals

Chemical	Company (city or country)
Amino acids (Fmoc and side chain protected)	IRIS Biotech (Germany)
Acetaldehyde	Roth (Karlsruhe)
Acetic acid (100% ACS)	Merck (Darmstadt)
Acetic anhydride	Biosolve (Netherland)
Acetonitrile (HPLC-R)	Biosolve (Netherland)
Ammonium acetate	Fluka (Steinheim)
2-(7-Aza-1H-benzotriazole-1-yl)-1,1,3,3-tetramethyluronium hexafluorophosphate (HATU)	Merck (Darmstadt)
4-Benzyloxybenzyl Alcohol Resin (Wang resin)	IRIS Biotech (Germany)
Biotin	Sigma-Aldrich (Steinheim)
5(6)-Carboxyfluorescein (Fluo)	Sigma-Aldrich (Steinheim)
Chloranil	Fluka (Steinheim)
Dichloromethane (DCM)	Roth (Karlsruhe)
7-Diethylaminocoumarine-3-carboxylic acid (Dac)	Invitrogen (Eggenstein)
4-(2´,4´-Dimethoxyphenyl-Fmoc-aminomethyl)-phenoxyacetamido-norleucyl resin (Rink amide MBHA)	Merck (Darmstadt)
Dimethylsulfoxid (DMSO)	Roth (Karlsruhe)
N,N'-Diisopropylcarbodiimide	Sigma-Aldrich (Steinheim)
N,N-Diisopropylethylamine (DIEA)	Biosolve (Netherland)
3-[4,5-dimethylthiazol-2-yl]-2,5-diphenyltetrazolium bromide (MTT)	Aldrich (Steinheim)
Dimethysulfide (DMS)	Fluka (Steinheim)
Dimethylformamid (DMF)	Biosolve (Netherland)
Diethylether	Roth (Karlsruhe)
Dithiothreitol (DTT)	Sigma-Aldrich (Steinheim)
1,2-ethandithiol (>98% GC) (EDT)	Fluka (Steinheim)
Ethanol (>96%)	Roth (Karlsruhe)
Formic acid	Sigma-Aldrich (Steinheim)
Glycin	Fluka (Steinheim)
Guanidinium-HCl	Roth (Karlsruhe)
HCl	Sigma-Aldrich (Steinheim)
Hellmanex	Hellma
1,1,1,3,3,3-hexafluoro-2-propanol (grade 99+%) (HFIP)	Sigma-Aldrich (Steinheim)
H_2SO_4	Merck (Darmstadt)
1-Hydroxybenzotriazole (HOBt)	Fluka (Steinheim)

Isopropanol	Roth (Karlsruhe)
KCl	Merck (Darmstadt)
Methanol (p.a.)	Roth (Karlsruhe)
Milk powder (non-fat dried)	AppliChem (Darmstadt)
NaCl	KMF (Lohmar)
NaOH	Merck (Darmstadt)
NaH_2PO_4	Merck (Darmstadt)
$Na_2B_4O_7$	Merck (Darmstadt)
Na_2HPO_4	Merck (Darmstadt)
NH_4HCO_3	Fluka (Steinheim)
Ninhydrin	Fluka (Steinheim)
Phenol (99% A.C.S reagent)	Sigma-Aldrich (Steinheim)
Piperidin	Biosolve (Netherland)
Pyridin	Sigma-Aldrich (Steinheim)
Polylysine	Sigma-Aldrich (Steinheim)
2-propanol (p.a grade)	Merck (Darmstadt)
Proteinmarker-Muti Mark TM	Invitrogen (Karlsruhe)
Sodium acetate	Merck (Darmstadt)
Sodium dodecyl sulfate (SDS)	Merck (Darmstadt)
Super signal duration ECL staining solution	Pierce (USA)
N,N,N′,N′-Tetramethyl-O-(benzotriazol-1-yl)uronium tetrafluoroborate (TBTU)	IRIS Biotech (Germany)
Tentagel R PHB	Rapp Polymere GmbH Tübingen
Thioanisole (>99% GC) (THA)	Fluka (Steinheim)
Thioflavin T (ThT)	Sigma (Steinheim)
Trifluoroacetic acid (>99.5%) (TFA for synthesis)	Biosolve (Netherland)
Trifluoroacetic acid (>99.9%) (TFA for HPLC)	Biosolve (Netherland)
Triisopropylsilan (TIS)	Sigma-Aldrich (Steinheim)
2-Amino-2-(hydroxymethyl)-1,3-propanediol, hydrochloride (Tris-HCl)	Roth (Darmstadt)
Triton X-100	Sigma (München)
Trypsin/EDTA	Invitrogen (Karlsruhe)
Tween 20	Fluka (Steinheim)

2.1.2 Assay kits

Assay kit	Company (city or country)
Micro bicinchoninic acid (BCA) protein assay kit	Pierce (USA)
SuperSignal West Dura Extended Duration Substrate	Pierce (USA)

2.1.3 Materials

Material	Company (city or country)
Black microwell-plate (96-well)	NUNC (Denmark)
96 well cell culture plate	Greiner Bio-One (Frickenhausen)

Quartz CD cells	Hellma (Mullheim)
Eppendorf tube (1.5 ml)	Sarstedt (Nümbrecht)
Syringe needle 20G 1½ ″ - Nr.1 (0.9X40 mm, sterile)	DB Microlance TM (Ireland)
Syringe needle 27G ¾ ″- Nr.20 (0.4X19 mm,sterile)	DB Microlance TM (Ireland)
Single-use syringe 1 ml (sterile)	B. BRAUN (Melsungen)
Syringe 20 ml (sterile)	DB Discardit TM (Spain)
Filter Millex-FG (0.2 µm pore size, 4 mm)	Millipore (Japan)
Filter Millex-FG (0.2 µm pore size, 25 mm)	Millipore (Japan)
Filter (0.2 µm pore size, unsterile)	Schleicher & Schuell MicroScience (Dassel)
Filter (0.2 µm pore size, sterile)	Schleicher & Schuell MicroScience (Dassel)
Tissue culture flasks (75 cm^2, 250 ml, PS, filter cap, sterile)	Greiner Bio-One (Frickenhausen)

2.1.4 Cell culture media

Cell culture media	Company (city or country)
Fetal calf serum (FCS)	GIBCO^{TM} (UK)
Glutamine	GIBCO^{TM} (UK)
Horse serum	GIBCO^{TM} (UK)
Penicillin/Streptomycin	GIBCO^{TM} (UK)
RPMI-1640	GIBCO^{TM} (UK)
Trypsin	GIBCO^{TM} (UK)

2.1.5 Antibodies

Antibodies	Company (city or country)
Rabbit anti-amylin (human) IgG	Bachem (Switzerland)
Anti-β-amyloid-protein (1-40) (Rabbit)	Bachem (Switzerland)
Donkey anti-rabbit IgG-POD	Amersham (UK)
Anti-biotin streptavidin-POD conjugate	Roche (Switzerland)

2.2 Methods

2.2.1 Solid phase peptide synthesis (SPPS) using the Fmoc-strategy

According to the Fmoc-strategy an orthogonal protection scheme was applied with the Fmoc-group as a temporary protection of the N$^\alpha$ group and tBu- and Trt-based side chain protecting groups. Fmoc-cleavage was achieved by 25% piperidine in DMF according to the protocol shown in Table 3. Couplings were performed using the amino acid (Fmoc and side chain protected) (Fmoc-AA) and TBTU (3-fold molar excess) in the presence of DIEA (4,5-fold molar excess) (Table 3). The following Fmoc-protected amino acid derivatives were applied: Asp(OtBu), Glu(OtBu), Gln(Trt), Cys(Trt), His(Trt), Lys(Boc), Thr(tBu), Ser(tBu), Arg(Pbf),

and Tyr(tBu). The side chain protecting groups of the residues that were covalently linked via side chain-to-side chain were: 2-phenyl-isopropyl ester (OPip) for Asp, 4-methyl-trityl (Mtt) for Dap [168]. Coupling efficiencies were checked by the Kaiser test, chloranil test for the N-methylated amino acid [169, 170]. In difficult part of the synthesis, either the determination of the substitution level was measured by cleaving the Fmoc-group of a small amount of resin with 25% piperidine followed by the measurement of the UV absorbance or a small sample of peptide resin was subjected to TFA treatment to cleave the peptide from the resin and the resulting solution containing the crude product was examined by reversed-phase high performance liquid chromatography (RP-HPLC) and/or mass spectroscopic analysis (MS).

Table 3. Protocol for SPPS using Fmoc-chemistry.

Synthesis step	Reagent	Time
Fmoc cleavage	25% piperidine / DMF	1 x 5 min
Fmoc cleavage	25% piperidine / DMF	1 x 10 min
Wash	DMF	4 x 1 min
Coupling	Fmoc-AA / TBTU / DIEA (Eq: 3 / 3 / 4,5)	2 x 40 min
Wash	DMF	3 x 1 min
Acetylation	Ac_2O / DIEA (Eq: 10 / 10)	45 min
Wash	DMF	3 x 1 min

2.2.1.1 Attachment of the C-terminal amino acid to the resin

For the synthesis of peptide in a C-terminal amide form (as in the case of IAPP, the several analogues or fragment) the 4-(2´,4´-dimethoxyphenyl-Fmoc-aminomethyl)-phenoxyacetamido-norleucyl resin (Rink amide MBHA) was used. Thereafter, attachment of the C-terminal residue was achieved using the same protocol as described in Table 3. Coupling time was settled depending on the desired substitution level. For example, peptides with high aggregation propensities were kept with a low substitution level by performing a single coupling for 1 h (3-fold excess). Following the substitution level determination, unreacted amino groups were capped (Ac_2O / DIEA in DMF, 10-fold molar excess each with regard to the free NH_2-groups of the resin) for 1 hr.

For the synthesis of peptide in a C-terminal acid form, resins with linkers containing a free alcoholic group were used, i.e. 4-benzyloxybenzyl alcohol Resin (Wang resin) (Aβ40-fragments) or Tentagel R PHB (Aβ40). Attachment of the C-terminal residue was achieved using 3-fold molar excess Fmoc-AA, TBTU, HOBt (3-fold molar excess) in the presence of DIEA (6-fold molar excess) for 1-2 hr depending on the desired substitution level. As mentioned above for the synthesis of peptide in a C-terminal amide form, following the substitution level determination, unreacted amino groups were capped for 1 hr.

2.2.1.2 Determination of the substitution level of resin in Fmoc-strategy

Estimation of the substitution level of Fmoc-protected peptide resin was performed by measuring the absorbance of the piperidine-dibenzofulvene adduct that is generated after Fmoc-cleavage. Three aliquots of the dry peptide resin (3-4 mg) were weighted in a volumetric flask (10 ml), which was then filled with 25% piperidine in DMF and left to stand for 10 min. Thereafter, the absorbance at 290 nm was measured and the substitution level of the peptide resin was estimated by the formula:

$$\text{Substitution Level} = \frac{A \times V}{\varepsilon \times m}$$

A: absorbance of sample at 290 nm

V: volume of the sample (ml)

ε: molecular coefficient of piperidine-dibenzofulvene at 290 nm = 5800

m: weight of peptide resin (g)

The resin was acetylated (Ac$_2$O / DIEA 10-fold molar excess in DMF) for 1 hr prior proceeding with the synthesis.

2.2.1.3 Coupling of Cys residues in Fmoc-SPPS

Coupling of Fmoc-Cys(Trt)-OH was performed with different methods. The reason is that the activation of Fmoc-Cys(Trt)-OH when performed with TBTU in the presence of base as normally performed in Fmoc-strategy can cause significant racemization of Cys [171]. Therefore, Cys couplings were performed using an in situ activation protocol via 1-hydroxybenzotriazole (HOBt) and diisopropylcarbodiimide (DIC). For this activation no addition of base was necessary. Specifically, equimolar amounts of Fmoc-Cys(Trt)-OH , HOBt, and DIC (4-fold molar excess each with regard to the amino groups) were dissolved in DMF (concentration 0.15 M each). Following stirring of the reaction mixture at 4 °C for 45 min, the solution containing the OBt-ester of Fmoc-Cys(Trt) was added to the N^α-deprotected peptide resin. Coupling was performed for 60-90 min. A second activation / coupling cycle was also performed using the same methodology. Coupling efficiency was estimated by the Kaiser test and prior to proceeding with the synthesis a capping step (Ac$_2$O / DIEA in DMF, 10-fold molar excess each) was usually performed.

Alternatively, Cys couplings were performed using the 3-fold molar excess of Fmoc-Cys(trt)-OH and TBTU; DIEA was added until a neutral pH was reached. Coupling was performed twice for 60 min.

2.2.1.4 Coupling of N-methyl residues and on N-methyl residues

For the coupling of N-methyl (N-Me) residues the standard TBTU coupling as described in 2.2.1 was applied. Coupling times were often longer than the ones used for non-N-methylated amino acids. Coupling of amino acids on N-methyl residues was more difficult than the coupling of N-methyl amino acids because of the steric hindrance caused by the N-Me residue on the amino group. The coupling efficiency could only be evaluated by the acetaldehyde/chloranil test [170]. In the case of positive chloranil test (free amino groups) after two couplings a third coupling was carry out by using 2-(7-Aza-1H-benzotriazole-1-yl)-1,1,3,3-tetramethyluronium hexafluorophosphate (HATU) as coupling reagent. Thereafter, a capping step (Ac$_2$O / DIEA in DMF, 10-fold molar excess) was performed.

2.2.1.5 Side chain-to-side chain cyclization of resin bound peptides

In IAPP(8-18)L3(22-28)-GI-cyclo the side chains of residues Dap[18] and Asp[22] were covalently linked to each other by using the following method. After incorporation of residue Dap whose side-chain was protected by 4-methyltrityl (MTT), the peptide resin was washed with distilled DCM. For the side-chain protection of Asp 2-phenyl-isopropyl ester (OPip) was applied. A mixture of triisopropylsilane (TIS) (5%) (v/v) and TFA (1%) (v/v) in 99,9% DCM was then added to cleave the side chain groups OPip and Mtt following the protocol presented in Table 4. The completeness of the cleavage reaction was followed by Kaiser Test. After that, the peptide resin was finally washed with DCM and DMF and neutralized with 1% DIEA in DMF followed by washes with DMF. The cyclization reaction was performed by the addition of HATU (4-fold molar excess) and DIEA (4-fold molar excess) in DMF. The completeness of the reaction after 16 h was checked by the Kaiser test. A second cyclization reaction for 5 hrs was performed. Thereafter, capping of the peptide resin was carried out with acetic anhydride and DIEA in DMF (10-fold molar excess each) for 45 min.

Table 4. Protocol of cleavage of MTT-/OPip- and side chain-to-side chain cyclization in Fmoc-SPPS.

Synthesis cycle:	Reagent:	Time:
Wash	DCM	3 x 1 min
MTT-/OPip- deprotection	TIS / TFA (5% / 1%) in DCM	2 x 2 min
MTT-/OPip- deprotection	TIS / TFA (5% / 1%) in DCM	6 x 10 min
Wash	DCM	3 x 1 min
Wash	DMF	3 x 1 min
Neutralize	1% DIEA / DMF	2 x 2 min
Wash	DMF	3 x 1 min
Cyclization	HATU / DIEA (Eq: 4 / 4) in DMF	1 x 16 hrs 1 x 4 hrs
Wash	DMF	3 x 1 min

Acetylation	Ac$_2$O / DIEA (Eq: 10 / 10) in DMF	45 min
Wash	DMF	3 x 1 min

2.2.1.6 Kaiser test

The Kaiser test is a qualitative colorimetric test for determining the presence or absence of free primary amino groups on a peptide resin (following deprotection and coupling steps) [169]. The following three solutions are prepared:

- Ninhydrin in ethanol (5 gr in 100 ml ethanol)
- Phenol in ethanol (40 gr in 10 ml ethanol)
- An aqueous solution of potassium cyanide in pyridine (2 ml of aqueous 0.001 M KCN in 100 ml pyridine)

A small sample of resin is placed into a glass test tube and washed with ethanol. Two drops of each of the above solutions are then added to the resin and the mixture is mixed thoroughly and heated at 110 °C for 5 min. Blue beads and blue solution indicate the presence of more than 95% free amino groups while a yellow solution and yellow beads indicate that the coupling is more than 99% complete. However some amino groups (such as in Ser, Asn, Asp, Cys and Thr) do not show the expected dark blue colour that is typical for more than 95% free primary amino groups. Additionally, the test cannot be applied in the case of the imino-acid Pro or N-methylated amino acids because it can detect only primary amino groups.

2.2.1.7 The Acetaldehyde/Chloranil Test

This sensitive test has been used for the detection of secondary amino groups such as the ones present in N-methylated amino acids. It can also detect primary amines [170]. Only the beads will be colored in case of a positive test. For the Acetaldehyde/Chloranil Test the following two solutions are prepared:

- 2% acetaldehyde in DMF
- 2% chloranil in DMF

A few beads of resin are placed in a small test tube and 2-5 drops of each solution are added. After a short mixing the mixture is left at room temperature for 5 min and the beads are inspected. Dark blue to green beads indicate the presence of free amino group while colorless to yellowish beads indicate that the coupling has been accomplished.

2.2.1.8 Final deprotection of side chains and peptide cleavage from the resin

A 95% aqueous trifluoracetic acid (TFA) solution is the typical reagent to perform the final cleavage of the peptide from the resin together with the removal of the side chain protecting groups in Fmoc-based SPPS. During the reaction highly reactive carbocations are generated and it is necessary to trap them to avoid undesired reactions with sensitive amino acids such as Cys, Met, Ser, Thr, Trp, Tyr. This effect can be suppressed by the addition of scavengers to the cleavage solution. Water is a moderately efficient scavenger and can be used as single scavenger for the cleavage of peptides devoid of Cys, Met and Trp. In the presence of the previous mentioned residues the cleavage of side chain protecting groups and the peptide from the resin was carried out by treatment of the resin with a slight modification of reagent K [TFA / water / thioanisole (THA) / ethandithiol (EDT) / phenol: 83 / 4,5 / 4,5 / 2 / 6 (v/v/v/v/w)] [172]. Cleavage of the peptide resins with sequence containing Cys, Met or Trp were carried out using of 20-50 mg resin per 0,5 ml reagent K for 3 hrs at room temperature. After filtering the reaction mixture through a syringe equipped with a frit to a centrifuge glass containing water, the resin was washed three times with TFA. The aqueous solution was then extracted with cold diethyl ether (three times at 4 °C). Extraction was performed as follows: diethyl ether was added to the solution and mixed, the solution was then centrifuged (2500g, 3 min) and the ether layer was discarded. Thereafter, the aqueous layer was lyophilized.

2.2.2 Disulfide bridge formation in the IAPP analogues

After the synthesis, IAPP analogues were subjected to air oxidation for the formation of the disulfide bridge between Cys^2 and Cys^7. Oxidations were performed in aqueous 0.1 M NH_4HCO_3, containing 3 to 6 M Gdn HCl (pH 8) at 1 mg crude product/ml solution to improve oxidation yields and solubility of the peptides. The completion of the oxidation was monitored by RP-HPLC and for the here synthesized IAPP analogues 2-4 hrs were usually required for the oxidation to be accomplished.

2.2.3 N-terminal labeling of peptides with fluorescein (Fluo-), 7-diethylamino coumarin-3-carboxylic acid (Dac-) and Biotin

N^α-fluorescein label was introduced as follows: after SPPS of the fully protected peptide chain and N^α-Fmoc-cleavage, fluorescein was coupled twice using: 5(6)-carboxyfluorescein (3-fold excess) in the presence of TBTU (3-fold excess) and DIEA (4,5-fold excess) in DMF for 2 h.

The "Dac" label was introduced at the free N^{α}-terminus of the Aβ40 peptide resin via 7-diethylaminocoumarin-3-carboxylic acid (Dac) (3-fold excess) in the presence of TBTU (3-fold excess) and DIEA (4,5-fold excess) in DMF two times for 2 h.

Biotinylated peptides were obtained, first, by introducing N-ε-Fmoc-aminohexanoic acid (Fmoc-Ahx-OH) as spacer between biotin and the peptide. The coupling was performed using Fmoc-Ahx-OH (3-fold excess), TBTU (3-fold excess) and DIEA (4,5-fold excess) two times 1 h. After deprotection of N^{α}-terminus, Biotin (3-fold excess) in the presence of TBTU (3-fold excess) and DIEA (4,5-fold excess) was coupled twice for 2 h.

The three differently labelled peptides were cleaved by TFA cleavage protocol as described under 2.2.1.8.

2.2.4 Purification and characterization of the peptides

2.2.4.1 RP-HPLC

Purification of the products (Aβ40, IAPP analogues and fragments) was carried out by RP-HPLC on a C18 Nucleosil column with a length of 25 cm, internal diameter of 8 mm and 7 µm particle size. The device consisted of a PU-2098 Pump (Jasco), a UV-2075 Detector (Jasco) and a C-R6A integrator (Shimadzu). The second device consisted of PU-2080 Plus Intelligent HPLC-Pump (Jasco), a DG-2080-53 3-Line Degasser (Jasco), a LG-2080-02 Ternary Gradient Unit (Jasco), a UV-2077 Plus 4-λ Intelligent UV/Vis detector (Jasco). The flow rate was 2 ml/min and eluting buffers were:

- Buffer A: 0.058% (v/v) TFA in water
- Buffer B: 0.05% (v/v) TFA in 90% ACN / water

Peptides were detected at 214 nm and the gradient programs that were applied are shown in Table 5. Eluates containing peptide peaks were immediately frozen in dry ice, and lyophilized.

Table 5. The usually applied HPLC gradient programs to purify the synthetic peptides.

Slow Program	Time	Buffer A	Buffer B
	0	70%	30%
	7	70%	30%
	37	40%	60%

Fast Program	Time	Buffer A	Buffer B
	0	90%	10%
	1	10%	90%
	31	10%	90%

2.2.4.2 Laser Desorption Ionization Mass Spectroscopy (MALDI-MS)

Characterization of the HPLC purified peptides was performed by MALDI-MS with a MALDI-TOF/TOF (Bruker Daltonik, Bremen, Germany). Peptides were dissolved in an aqueous mixture of 30% ACN 0,1% TFA and then mixed (1:1) with a saturated solution of cyano-4-hydroxycinnamic acid (HCCA) in 30% ACN 0,1% TFA (matrix). 0,5 µl of the mixture was placed on the target, dried and then the spot was washed with 10 mM $NH_4H_2PO_4$ with 0,1% TFA to quench the signal of adduct ions (such as Na^+ K^+ etc.). The mass was recorded on the positive ion mode and monoisotopic mass was determined as $[M+H]^+$. The average expected mass of the peptides was calculated using the Peptide Companion software (WindowChem Software, North Fairfield, USA).

2.2.5 Preparation of stock solutions of the HPLC-purified peptides

2.2.5.1 Aβ40 stock solution

Aβ40 was dissolved at 1 mg/ml in a mixture of 72% CH_3CN in water containing 0.04% TFA, aliquoted, lyophilized and stored at –20 °C. Aβ40 stocks were freshly made by reconstituting freshly lyophilized Aβ40 aliquots with HFIP (1 mg/ml) on ice. Concentrations of the Aβ40 stocks were determined using the bicinchoninic acid assay (BCA). The stock solution of Aβ40 was kept on ice and used within one day.

2.2.5.2 Concentration determination of IAPP and IAPP-GI solutions with UV spectroscopy

HPLC purified peptides were stored in lyophilized form at –20 °C. Peptide stock solution was made by dissolving the peptide in HFIP to a final concentration of about 500 µM. the solution was then filtered (0,2 µm PTFE filter). The exact concentration was determined by UV-spectroscopy with a Jasco V630 spectrophotometer. UV absorbance of the peptide solution was measured between 200 and 400 nm and the absorbance at 274.5 nm was used to determine the exact peptide concentration. At this wavelength, the extinction coefficient of the Tyr residue (ε=1370 M^{-1} cm^{-1}) and the disulfide bridge of Cys^1 and Cys^7 (ε=70 M^{-1} cm^{-1}) was 1440 M^{-1} cm^{-1}. Peptide concentrations (C) were calculated according to the Beer-Lambert law:

$$C = \frac{A}{\varepsilon \times l}$$

A= absorbance of sample at 274,5 nm

ε= molecular extinction coefficient of peptides at 274.5nm

l= length of the cell (1 cm)

2.2.5.3 Concentration determination of fluorescein-labeled (Fluo-labeled) peptides and Dac-Aβ40 using UV spectroscopy

HPLC purified peptides were first dissolved in HFIP and then filtered (0,2 µm PTFE filter). UV absorbance of the peptide solution was measured between 200 and 600 nm and the absorbance at 432 nm (for Fluo-labeled peptides) or 445 nm (for Dac-Aβ40) was used to determine the exact peptide concentration. At this wavelength, the extinction coefficient was determined to be [173, 174]:

ϵ_{432}= 22770 M^{-1} cm^{-1} (Fluo-labeled peptide)

ϵ_{445}= 75940 M^{-1} cm^{-1} (Dac-labeled peptide)

Peptide concentrations were calculated according to the Beer-Lambert law.

2.2.6 Bicinchoninic acid (BCA) protein assay

The BCA Protein Assay combines the reduction of Cu^{2+} to Cu^{1+} by a protein in an alkaline medium with the highly sensitive and selective colorimetric detection of the cuprous cation (Cu^{1+}) by BCA. The BCA/copper complex exhibits a strong linear absorbance at 562 nm with increasing protein concentrations. This kit was used to determine the exact amount of Aβ40 which was obtained after HPLC purification. Aliquots of Aβ40 (1, 2,5 and 5 µg) from HFIP stock solution were added to a 96-well plates. After evaporation of HFIP, 50 µl of aqueous 10 mM sodium phosphate buffer pH 7,4 were added, followed by 150 µl of a freshly made solution of BCA kit. The plate was sealed and then incubated for 2h at 37°C. The absorbance of the plate was then measured at 570 nm using a 2030 Multilabel Reader VictorX3 (PerkinElmer). The exact amount of Aβ40 was derived from the calibration curve of known amounts of Aβ40.

2.2.7 Binding assays with membrane-bound peptide arrays

Decamers corresponding to consecutive overlapping sequences of Aβ40, IAPP and IAPP-GI were synthesized on APEG-amino-cellulose membrane (AIMS Scientific Products) in the laboratory of Dr. R. Frank (Department of Chemical Biology, Braunschweig - Germany) [175]. Membranes were blocked with 2% skim milk powder in aqueous TBSn solution (20 mM Tris HCl and 150 mM NaCl containing 0,01% Tween 20) for 1 h at room temperature or overnight at 4°C. Membranes were incubated with N^{α}-amino-terminal biotinylated (biotin-ε-aminocaproic acid-labeled) peptides in 10 mM sodium phosphate buffer, pH 7.4 at room temperature. Membrane bound biotinylated peptides were detected following incubation with streptavidin-POD conjugate for 90 min at room temperature and the SuperSignal West Dura

Chemiluminescence Reagent. Membranes were also incubated with Aβ40 in the same way described above but they were incubated overnight (at 4°C) with an anti-β-amyloid-protein (1-40) (Rabbit) (Bachem) followed by anti-rabbit IgG-POD (donkey) (Amersham) secondary antibody in combination with the above mentioned chemiluminescence (ECL) detection reagent.

Thereafter, the membranes were stripped with a solution consisting of 2% SDS, 100 mM β-mercaptoethanol in 50 mM aqueous Tris HCl (pH 6,8) to remove the streptavidin-POD conjugate or antibodies. To remove the biotinylated-peptide or Aβ40, harsh conditions have been used as follows:

- Aqueous 50% EtOH - 10% AcOH
- Aqueous 8 M urea - 1% SDS - 0,1% mercaptoethanol
- 100% HFIP
- Aqueous 6M guanidinium HCl in 0,1M NH_4HCO_3
- 95% TFA 5% H_2O

2.2.8 Assessment of cytotoxicity via the MTT reduction assay

PC-12 cells were cultured in RPMI 1640 medium containing 10% heat-inactivated horse serum, 5% fetal calf serum, 25 units/ml penicillin, and 25 µg/ml streptomycin [176]. 24 h prior to the cell viability assay, PC-12 cells were trypsinised and plated at a density of $1x10^5$ cells/ml in polylysine-coated 96-well plates. At the indicated time points, aliquots of the peptide incubations were diluted with cell culture medium and added to the cells at the indicated final concentrations. PC-12 cells were first incubated with 3-[4,5-dimethylthiazol-2-yl]-2,5-diphenyltetrazolium bromide (MTT) (1 mg/ml) for 90 minutes at 37°C. Thereafter, cell lysis buffer (10% SDS in 20 mM HCl, pH 4.5) was added and cellular MTT reduction was measured at 570 nm after overnight incubation at room temperature using a 2030 Multilabel Reader VictorX3 (PerkinElmer). All Aβ40 cell toxicity studies were performed in combination with the ThT binding assay. Peptide incubations were performed in ThT assay buffer (50 mM sodium phosphate buffer, pH 7.4, containing 100 mM NaCl and 1% HFIP) at an Aβ40 concentration of 16.5 µM.

Complete inhibition of cell function (0% viability) was defined as the absorbance value obtained in wells containing 0.1% Triton X-100. 100% MTT reduction was defined as the absorbance value obtained in wells containing vehicle alone. For the calculation of cell viability (% of control) the following formula was used:

$$\% \text{ MTT reduction} = \frac{A(\text{sample}) - A(0.1 \% \text{ Triton})}{A(\text{medium}) - A(0.1 \% \text{ Triton})} \times 100$$

For the studies of the effects of IAPP analogues on Aβ40 cytotoxicity and fibrillogenesis incubations of Aβ40 (16,5 µM) with inhibitors 1/1 in 50 mM sodium phosphate buffer, pH 7.4, containing 100 mM NaCl and 1% HFIP (ThT buffer) were performed as described in Ref. [167]. Peptide solutions were incubated at room temperature and added to PC-12 cells (at final concentrations between 1 µM and 1 nM) at various time points.

For determination of the IC_{50} of the inhibitory effect of the best inhibitors on toxicity of Aβ40, incubation of Aβ40 (16,5 µM) was mixed with the IAPP analogues with peptide ratios between 1:0.1 and 1:20. The solutions, including a control Aβ40 alone, were incubated at room temperature for 3 days and thereafter they were added to PC-12 cells at a final concentration of Aβ40 on cells between 1 µM and 1 nM.

To assess the effect of the best inhibitors on cytotoxicity of fibrillar Aβ40, Aβ40 was aged for 7 days (16.5 M in ThT buffer). Aβ40 was diluted 10 times (1.65 M in ThT buffer) and added to the dry peptide at molar ratios of 1/100 Aβ40/peptide. Following 24 h incubation, the solutions including a control fibrillar Aβ40 alone were added to PC-12 (at final concentrations between 1 µM and 1 nM).

2.2.9 Thioflavin T (ThT)-Binding Assays

ThT binding was measured on aliquots of incubations of Aβ40, or mixtures of Aβ40 and peptides at 1:1 (16,5 µM) made in ThT assay buffer (50 mM sodium phosphate buffer, pH 7.4, containing 100 mM NaCl and 1% HFIP). Incubations were performed at room temperature (see 2.2.8), and kinetics of fibrillogenesis were followed up to 7 days. At the indicated time points, aliquots of the solutions were mixed with a Thioflavin T solution (20 µM ThT in 0.05 M glycine/NaOH, pH 8.5), and ThT binding was determined immediately by measuring fluorescence emission at 485 nm after excitation at 450 nm using a 2030 Multilabel Reader VictorX3 (PerkinElmer).

2.2.10 Far-UV CD spectroscopy

Peptide incubations were performed in 10 mM sodium phosphate buffer, pH 7.4, with 1% HFIP in quartz cells (Hellma) at room temperature. CD spectra were collected at various peptide concentrations using a Jasco 715 spectropolarimeter. Spectra were collected between 195/200 and 250 nm at 0,1 nm intervals, a response time of 8 seconds and at room temperature. CD spectra are presented after subtracting the spectra of buffer alone. To allow comparison between different lengths of peptides or different cell lengths, row data in millidegrees were converted in mean residue ellipticities (MRE) (deg x cm^2 x $dmol^{-1}$).

$$MRE = \frac{millidegrees}{\# \, AA \, \times \, peptide \, concentration \, (M) \times cell \, lenght \, (cm) \times 10}$$

AA= number of amino acids of the peptide

All stock solutions were made freshly and dissolved in HFIP at 100-fold higher concentrations than the final ones in the cuvett. Peptides stock solutions in HFIP were pipetted directly into the buffer (10 mM sodium phosphate pH 7.4) in order to have 1% HFIP in the final solution. Mixing was performed by gentle pipetting and the CD spectrum was then measured. For the concentration dependence assays, measurements were made in 10 mM sodium phosphate buffer, pH 7.4, containing 1% HFIP at different peptide concentrations. For the trifluoroethanol (TFE) titration assays, the peptide stock solutions (1 mM) in HFIP were diluted in a mixture of 10 mM sodium phosphate buffer, pH 7.4, with the indicated amounts of TFE.

2.2.11 Peptide-peptide interaction studies using Fluorescence Spectroscopy

Fluorescence measurements were performed with a Spex Fluorolog 2 spectrophotometer or a Jasco FP-6500 spectrofluorometer. All titrations were carried out using synthetic N^{α}-amino-terminal fluorescein- (Fluo-) or 7-Diethylaminocoumarine-3-carboxylic acid-labeled (Dac-) peptides (see 2.2.3) and increasing amount of not labeled peptides as described below [167, 177]. For the binding studies between Dac-Aβ40 and the IAPP analogues, excitation was at 430 nm and emission spectra were collected between 440 and 550 nm. For the Fluo-IAPP, Fluo-IAPP-GI and self-association binding studies an excitation wavelength of 492 nm was applied and fluorescence emission spectra were recorded between 500 and 600 nm. Fluorescence measurements were performed in freshly made solutions containing Dac-Aβ40 (10 nM) or Fluo-peptide (5 nM) and different amounts of non-labeled peptides in 10 mM sodium phosphate buffer, pH 7.4, containing 1% HFIP at room temperature. The spectrum was recorded within 2-5 min after solution preparation. The changes at 522 nm (Fluo-labeled peptide) or at 465 nm (Dac-labeled peptide) were used to generate the binding curve.

Apparent affinities (app. K_ds) were estimated using 1/1 binding models which was in accordance with the observed stoichiometries of inhibitory effects. Sigmoidal curve fittings and estimation of affinities of interaction ($K_{d,app}$s) were performed with Origin software using:

$$F = F_0 + \frac{[(F_{max} - F_0)]}{1 + 10^{[(logKd-L)\times slope]}}$$

F: fluorescence intensity

F_0: fluorescence intensity of the Fluo-labeled peptide

F_{max}: maximal fluorescence intensity

logKd: logarithm of the dissociation constant

L: concentrationof the ligand

Slope: slope of the curve

3 Results

3.1 Identification of Aβ40 and IAPP regions which are important for the Aβ40-IAPP interaction

The sequences of Aβ40 and IAPP (Fig. 17) are 25% identical and 50% similar, while high degrees of identity and similarity are shared between the short sequences Aβ(15–21) and IAPP(10–16) or Aβ(26–32) and IAPP(21–27), which are believed to participate in Aβ40 or IAPP self-assembly [61, 62, 142, 152, 166, 178].
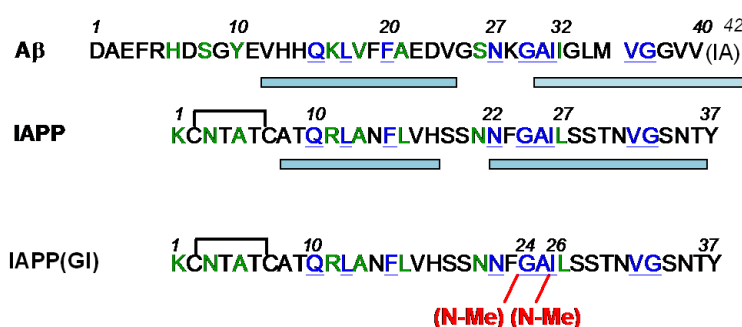
Fig. 17. Primary structures of Aβ, IAPP and IAPP-GI. Identical residues between sequences are indicated in blue and similar residues in green. Domains previously suggested to be involved in self-association are underlined (light blue) [61, 62, 142, 152, 166, 178].

In the following, a systematic study of the cross- and self-interaction interface of Aβ40 and IAPP will be presented. To address the question as to what regions of Aβ40 bind IAPP and vice versa, membrane-bound peptide arrays were used [175, 177]. The interaction interface of Aβ40 and IAPP was determined by the above assays and characterized thereafter more precisely via fluorescence titration binding assays [177]. The combination of the results of these two methods led to the identification of short peptides as "hot spot regions" of the cross-interaction interface of Aβ40 and IAPP.

3.1.1 Identification of Aβ40 and Aβ42 domains involved in Aβ40- and Aβ42-IAPP hetero- and Aβ40 and Aβ42 self-association by using membrane-bound peptide arrays

To obtain a first insight into the domains involved in Aβ40-IAPP hetero-association, membrane-bound peptide arrays were used. Decamer peptides corresponding to consecutive overlapping fragments of the Aβ40 sequence were incubated with 25 µM N-terminal biotinylated IAPP-GI (Biotin-IAPP-GI) in 10 mM phosphate buffer pH 7,4 overnight

(Fig. 18, membrane A). Decamers that bound Biotin-IAPP-GI were detected following incubation with streptavidin–conjugate peroxidase (POD) by using the enhanced chemiluminescence detection method (ECL).

Fig. 18. Identification of Aβ40 regions that bind IAPP-GI (membrane A), Aβ40 (membrane B) or Aβ42 (membrane C). The Aβ40 decamers shown in bold were incubated with 25 µM Biotin-IAPP-GI (A), 10 µM Biotin-Aβ40 (B) or 1 µM Biotin-Aβ42 (C) in 10 mM phosphate buffer pH 7,4 and detected following incubation with streptavidin–POD and development by ECL. Red boxes are binding sites of Aβ40 from the binding to IAPP-GI while blue boxes are binding sites of Aβ40 self-association. Membranes are from 2-3 assays.

Initially, the membrane containing the thirty-one decamers was incubated with 10 µM Biotin-IAPP in 10 mM phosphate buffer pH 7,4 (data not shown). However, as Biotin-IAPP aggregated, only non-specific binding was detected. Therefore, Biotin-IAPP-GI was used as a soluble, non-amyloidogenic mimic of Biotin-IAPP [155]. After ECL development, two IAPP binding regions were detected in Aβ40: the first was Aβ(12-24) and the second one Aβ(26-37) (Fig. 18, membrane A). These regions were reminiscent of sequences which have been earlier suggested to be involved in Aβ40 self-association [61, 62]. To confirm this observation, the regions mediating Aβ40 self-association were determined as follows: the above Aβ40 membrane, after having been stripped and washed, was incubated with 10 µM Biotin-Aβ40 in 10 mM phosphate buffer (pH 7,4) overnight and following incubation with streptavidin POD and ECL. Also in this case two regions were identified: the first one involved residues Aβ(11-21) and the second one Aβ(23-37) (Fig. 18, membrane B). Of note,

similar regions have been found in previous solid state NMR study where Aβ(12–24) and Aβ(30–40) have been shown to adopt β-strand conformations and form parallel β-sheets through intermolecular hydrogen bonding [61]. These results indicated that regions that are involved in the hetero-association of Aβ40 with IAPP are very similar to the ones involved in the self-association of Aβ40. Finally, the Aβ domains involved in Aβ42 self-association were determined. To this end, the Aβ40 10-mer containing membrane was incubated with Biotin-Aβ42 (Fig. 18, membrane C). Regions Aβ(8-22) and Aβ(23-37), which were very similar to the ones found to be important for Aβ40 self-association, were thus identified as important for Aβ42 self-association as well.

3.1.2 Identification of IAPP domains involved in IAPP-Aβ40 hetero- and IAPP self-association by using membrane-bound peptide arrays

To identify which domains of IAPP were involved in the interaction with Aβ40, twenty-eight 10-mer IAPP peptide sequences, spanning full length IAPP and positionally shifted by one residue were synthesized on a cellulose membrane. Additionally, a membrane consisting of non-amyloidogenic decamers spanning sequence IAPP(15-35)-GI, i.e. the IAPP sequence between residue 15-35 with 2 N-methylated amino acids at position G^{24} and I^{26} was synthesized, to exclude the possibility that aggregation of the cellulose-bound peptide chains might hinder interaction with Aβ. Membranes were incubated with 2 µM Aβ40 (10 mM phosphate buffer, pH 7,4 for 5 hours) (Fig. 19, membrane B) and bound peptide was detected with anti-Aβ40 antibody. Decamers within IAPP(1-20) were found to bind Aβ40 while only a very weak binding was observed in the C-terminal part of IAPP (Fig. 19, membrane B). However, examination of binding of the membrane IAPP(15-35)-GI showed that this region was in fact able to bind Aβ40 (Fig. 19, membrane D). These results were consistent with the suggestion that the membrane bound peptides within the C-terminal region of IAPP have a high self-association propensity which prohibited their interaction with Aβ40. Next, to identify the regions of IAPP which are mediating its self interaction, the IAPP and IAPP-GI membranes were incubated with 25 µM Biotin-IAPP-GI (10 mM phosphate buffer, pH 7,4; overnight) (Fig. 19 membrane C and F). The biotinylated peptide bound very strong the IAPP(1-20) region while weak binding was observed for the C-terminus of IAPP (Fig. 19 membrane C). Biotin-IAPP-GI did not bind IAPP-GI-decamer containing membrane (Fig. 19 membrane F). A possible reason for this observation might be the fact that all decamers and Biotin-IAPP-GI were N-methylated at G^{24} and I^{26}. The above results suggested that regions of IAPP that are important for the hetero-association with Aβ40 are also mediating self-association.
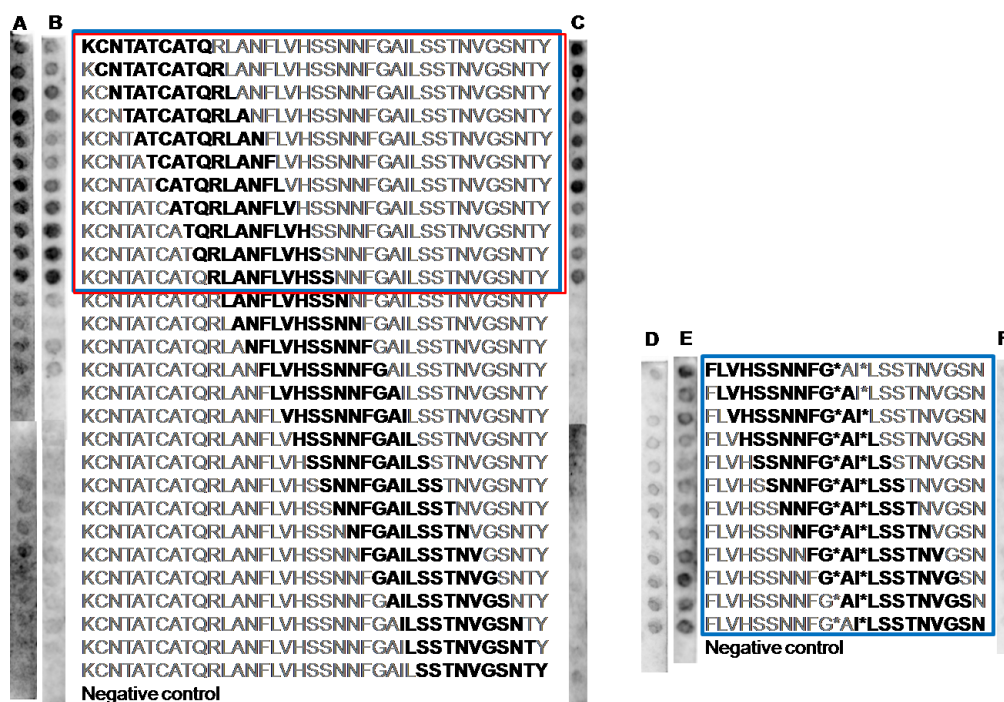
Fig. 19. Identification of Aβ42, Aβ40 or IAPP-GI regions that bind to IAPP or IAPP-GI. Decamers corresponding to overlapping IAPP sequences (bold) were incubated with 1 µM Biotin-Aβ42 (membrane A), 2 µM Aβ40 (membrane B) or 25 µM Biotin-IAPP-GI (membrane C) in 10 mM phosphate buffer pH 7,4. Membranes on the right side consist of the decamers spanning IAPP(15–35)-GI which were also probed for binding to Aβ42 (membrane D), Aβ40 (membrane E) or IAPP-GI (membrane F). Blue boxes indicate strong binding sites of IAPP to Aβ40 while red boxes indicate strong binding sites of IAPP to IAPP. Membranes are from 2-3 assays.

Subsequently, the IAPP domains involved in Aβ42 hetero-association were determined. IAPP and IAPP(15-35)-GI bound peptide decamers were incubated with 1 µM Biotin-Aβ42 (10 mM phosphate buffer; 6 hours) followed by incubation with streptavidin–conjugate peroxidase (POD) (Fig. 19 membrane A and D). The biotinylated peptide bound strongly the IAPP(1-20) region though weaker binding was observed for the C-terminus of IAPP (Fig. 19, membrane A). Interestingly, Biotin-Aβ42 clearly bound some of the N-methylated peptides of the IAPP(15-35)-GI sequence albeit weaker than Biotin-Aβ40 (Fig. 19, membrane D). Thus, Biotin-Aβ42 interacted with IAPP and IAPP-GI decamers in a similar manner as found for Biotin-Aβ40 (Fig. 19).

3.1.3 Identification of the cross-interacting pairs of the Aβ40 and IAPP interaction interface

To determine the cross-interacting couples, the membrane containing Aβ40 decamers (see 3.1.1) was next probed for binding with Biotin-IAPP(10-18) and Biotin-IAPP(20-29). These

two regions were found by fluorescence-based binding assays to be sufficient for binding full length Aβ40 with an affinity in the submicromolar to low micromolar range [177].

Aβ40 membrane was incubated with 140 µM Biotin-IAPP(10-18) (10 mM phosphate buffer, pH 7,4; overnight) and bound peptides were thereafter detected with streptavidin–conjugate peroxidase (POD) (Fig. 20, membrane A). A strong binding with Aβ(26-37) was found. When the Aβ40 membrane was incubated with 100 µM Biotin-Aβ(20-29) (10 mM phosphate buffer, pH 7,4; overnight) two binding regions were found: Aβ(11-25) and Aβ(23-37) (Fig. 20, membrane B).
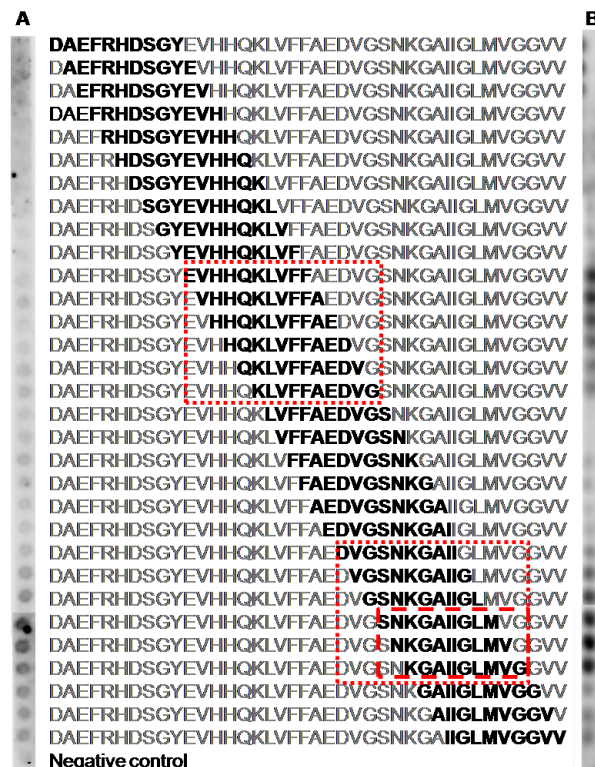
Fig. 20. Identification of Aβ40 regions that bind IAPP(10-18) (membrane A) or IAPP(20-29) (membrane B). The Aβ40 membrane bound decamers shown in bold were incubated with 140 µM Biotin-IAPP(10-18) (membrane A) or 100 µM Biotin- IAPP(20-29) (membrane B) in 10 mM phosphate buffer pH 7,4. Bound biotin-peptides were detected following incubation with streptavidin-POD and development by ECL. Red dashed boxes are binding sites of Aβ40 to IAPP(10-18) while red dotted boxes are binding sites of Aβ40 to IAPP(20-29). Membranes are from 1 assay.

Next, the membrane containing the IAPP and IAPP(15-35)-GI decamers (see 3.1.2) was probed for binding with Biotin-Aβ(15-24) and Biotin- Aβ(25-35). These two regions have been found by fluorescence-based binding assays to be sufficient for binding full length IAPP with an affinity in the submicromolar to low micromolar range [177]. IAPP and IAPP-GI decamer containing membranes were incubated with 90 µM Biotin-Aβ(15-24) (10 mM sodium phosphate buffer, pH 7,4; overnight) (Fig. 21 membrane A and C). Strong binding was detected within the region IAPP(1-20) (Fig. 21 membrane A). Binding was also observed in

the C-terminal part of the IAPP region, IAPP(16-29), and this result was further confirmed by the results obtained with the IAPP-GI peptide membrane (Fig. 21 membrane C). Next, IAPP/IAPP-GI decamer containing membranes were incubated with 50 µM Biotin-Aβ(25-35) (sodium acetate buffer pH 4,2; overnight) (Fig. 21 membrane B and D). The binding studies with Biotin-Aβ(25-35) had to be performed in acidic condition (5 mM sodium acetate buffer pH 4,2) because this peptide precipitated during incubation in the phosphate buffer (pH 7,4). Biotin-Aβ(25-35) was found to bind IAPP(1-20) whereas weaker binding was observed in the C-terminus of IAPP. IAPP-GI membrane also contained a binding region which was between residues 15 to 25. These results suggested that two IAPP binding sites of the Aβ40 sequence interact with the same binding site of IAPP which is within the sequence IAPP(1-20).
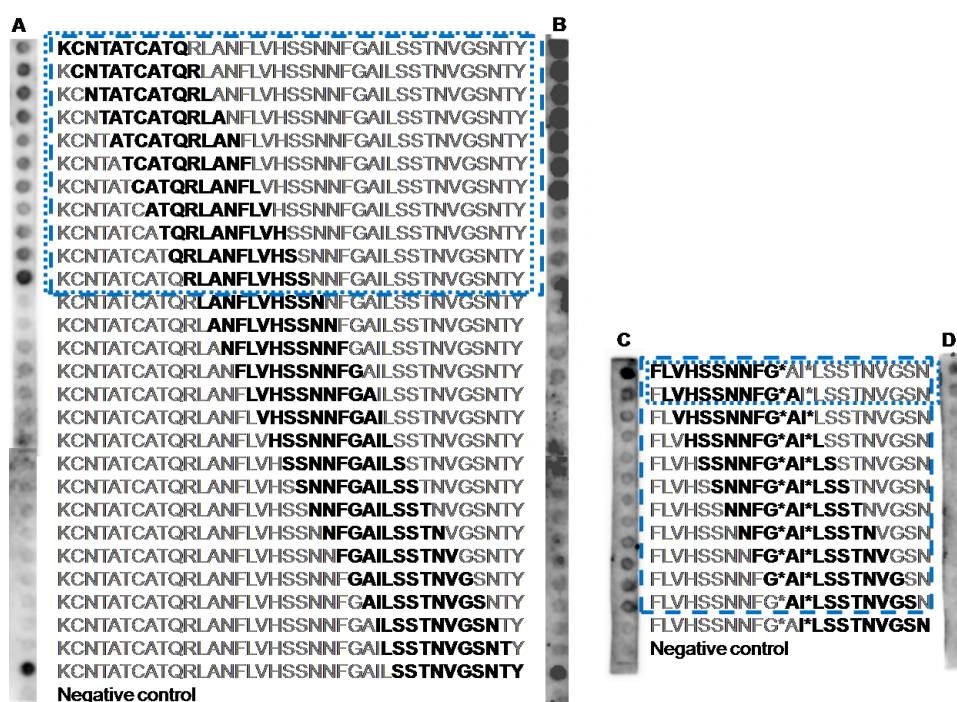
Fig. 21. Identification of IAPP or IAPP-GI sequences that bind Aβ(15-24) (membrane A) or Aβ(25-35) (membrane B) regions. Decamers corresponding to overlapping IAPP sequences (bold) were incubated with 90 µM Biotin-Aβ(15-24) (membrane A) in 10 mM phosphate buffer pH 7,4 or 50 µM Biotin- Aβ(25-35) (membrane B) in 5 mM acetate buffer pH 4,2. Bound biotin-peptides were detected following incubation with streptavidin-POD and ECL. The membranes on the right sides consist of the decamers spanning IAPP(15–35)(GI) which were also probed for binding to Aβ(15-24) (membrane C) or Aβ(25-35) (membrane D). Blue dashed boxes are binding sites of IAPP to Aβ(15-24) while blue dotted boxes are binding sites of IAPP to Aβ(25-35). Membranes are from 1 assay.

3.1.4 Identification of Aβ40 and IAPP domains involved in the interaction with rIAPP by using membrane-bound peptide arrays

In the following, the interaction between rIAPP and Aβ40, IAPP and IAPP-GI was examined. rIAPP is a natively non-amyloidogenic and non-cytotoxic IAPP analog that differs from (human) IAPP in six residues that are located in the region between residues 20 and 29 (see 1.5.1 Scheme 1).

Fig. 22. Identification of Aβ40, IAPP and IAPP-GI sequences that bind rIAPP. Biotin-rIAPP (25 µM) was incubated with decamers corresponding to overlapping sequences within Aβ40 (left, membrane A) in 10 mM phosphate buffer pH 7,4. Biotin-rIAPP (16 µM) was incubated with decamers corresponding to overlapping sequences within IAPP (right, membrane B) and IAPP(15-35)-GI (left, membrane C) in 10 mM phosphate buffer pH 7,4. Bound biotin-peptides were detected following incubation with streptavidin-POD and ECL. Green boxes are the identified 10-mer sequences of Aβ40, IAPP and IAPP(15-35)-GI that bound to rIAPP. Membranes are from 1 assay.

The membrane containing Aβ40 decamers was incubated with 25 µM Biotin-rIAPP (10 mM phosphate buffer, pH 7,4; overnight) and bound peptides were detected with streptavidin–conjugate peroxidase (POD) (Fig. 22, membrane A). Two regions were identified: the first one involved residues Aβ(1-19) and the second one Aβ(24-37). Next, to identify the regions of IAPP which are mediating the interaction with rIAPP, the IAPP and IAPP-GI membranes were incubated with 16 µM Biotin-rIAPP (10 mM phosphate buffer, pH 7,4; 6 h) (Fig. 22, membrane B and C). The biotinylated peptide bound strong the IAPP(1-16) (Fig. 22, membrane B). Biotin-rIAPP did not bind IAPP(15-35)-GI-decamer containing membrane (Fig.

22, membrane C). These results together with the results of Fig. 18 (membrane A) indicated that rIAPP bound different sequence parts of Aβ40 than IAPP-GI which are mainly located at the N-terminus. By contrast, rIAPP is found to bind to similar N-terminal regions of IAPP as IAPP-GI does (Fig. 19 membrane C-F). Therefore, regions that were involved in the hetero-association of Aβ40 with IAPP are specific and selective for that interaction.

3.2 Identification of the partial IAPP and IAPP-GI sequences which are able to inhibit Aβ40 fibrillogenesis and cytotoxicity

As previous studies of our group have shown that IAPP-GI is a very efficient inhibitor of Aβ40 fibrillization and cytotoxicity, the next question to be addressed was whether and which partial IAPP and IAPP-GI sequences might be also able to inhibit Aβ40 fibrillization and cytotoxicity [167]. To address this question, a number of peptide sequences derived via "deletion" of parts of the IAPP sequence were synthesized and tested (Fig. 23). First, the N-terminus and C-terminus were removed from the full sequence of IAPP-GI, yielding the peptides IAPP(8-37)-GI and IAPP(1-28)-GI. Of note, the C- and N-terminal sequences IAPP(30-37) and IAPP(1-7) have been previously shown by fluorescence studies to be unable to bind Aβ40 [177]. Thereafter, the sequence without C- and N-terminal parts, i. e. IAPP(8-28)-GI, was synthesized. This peptide contained both "hot regions" of the Aβ40-IAPP interface. In addition the following sequences were synthesized and tested: IAPP(1-7), IAPP(22-28)-GI, IAPP(30-37), IAPP(8-18), and IAPP(1-18).

Fig. 23. Primary structure of IAPP-GI. Domains of IAPP-GI which were studied with regard to their interaction with Aβ40 within this chapter: IAPP(8-37)-GI (red), IAPP(1-28)-GI (green), IAPP(8-28)-GI (blue), IAPP(1-7) (cyan), IAPP(30-37) (magenta), IAPP(22-28)-GI (dark cyan), IAPP(1-18) and IAPP(8-18) (grey).

Peptides were synthesized by solid phase peptide synthesis methodology (SPPS) utilizing the Fmoc-strategy. They were purified by RP-HPLC and MALDI mass spectrometry confirmed the expected mass as it is shown in Table 6.

Table 6. Characterization of the synthetic partial IAPP (IAPP-GI) peptide sequences of Fig. 23 (C-terminal amides except IAPP(1-18) and IAPP(8-18) that were C-terminal acids) via HPLC and MALDI-MS (monoisotopic mass).

	HPLC prg.	rt (min)	[M+H]+ expected	[M+H]+ found
IAPP(8-37)-GI	Slow	19,6´	3184	3184
IAPP(1-28)-GI	Slow	24,3´	3006	3006
IAPP(8-28)-GI	Fast	19´	2288	2287
IAPP(1-7)	Fast	21,1´	738	739
IAPP(22-28)-GI	Fast	17,5´	748	748
IAPP(1-18)	Fast	17,2´	1992	1992
IAPP(8-18)	Fast	18,5´	1270	1270

The effects of these peptides on Aβ40 fibrillogenesis and cytotoxicity were studied by the thioflavin T and MTT reduction assay. Amyloid fibrils of polypeptides and proteins, including Aβ40, bind the fluorescent dye ThT and the increase in fluorescence emission is broadly used as a specific and quantitative assay for fibril formation [179, 180]. Thereby, Aβ40 and the 1/1 mixture of Aβ40 with each of the peptides (16.5 μM each) were incubated in ThT buffer (50 mM sodium phosphate buffer, pH 7.4, containing 100 mM NaCl and 1% HFIP) for several days. At the time points shown in Fig. 24A aliquots of the incubations were mixed with a ThT solution and, following excitation at 450 nm, fluorescence emission of the solution at 485 nm was measured. For the cell viability assays, aliquots of the solutions used in the ThT assay were diluted with cell culture medium at incubation time points 72 and 168 h and added to PC-12 cells at the indicated final concentrations. Following incubation for 24 h with the cells, cell viabilities were assessed by measuring the cellular reduction of MTT [181]. As shown in Fig. 24A, peptides IAPP(1-28)-GI, IAPP(30-37), IAPP(1-18) and IAPP(8-18) delayed or suppressed fibril formation by Aβ40. Thereby, IAPP(1-28)-GI proved to be the most potent inhibitor although not as efficient as IAPP-GI. By contrast, IAPP(8-37)-GI, IAPP(8-28)-GI, IAPP(1-7) and IAPP(22-28)-GI did not affect Aβ40 fibrillogenesis. The difference between the effects of IAPP(1-28)-GI and IAPP(8-28)-GI or IAPP(1-37)-GI and IAPP(8-37)-GI suggested that the N-terminus IAPP(1-7) is important for the inhibitory effect of IAPP-GI on Aβ40 aggregation [167]. MTT assay of the 72 h aged Aβ40 solution showed the presence of cytotoxic Aβ40 aggregates at that time point of incubation (Fig. 24B-C). The 72 h aged mixtures (1:1) of Aβ40 with IAPP(1-7), IAPP(8-18), IAPP(22-28)-GI, IAPP(30-37) (Fig. 24B), IAPP(8-37)-GI and IAPP(8-28)-GI were similarly cytotoxic as Aβ40 alone (Fig. 24C). By contrast, the 72 h aged mixtures of Aβ40 with IAPP(1-18) (Fig. 24B) and IAPP(1-28)-GI (Fig. 24C) were not cytotoxic. IAPP(1-28)-GI proved thus to be the most potent inhibitor also with regard to Aβ40 cytotoxicity, demonstrating that the results of the ThT and

MTT assays were in good agreement. The effects of the two peptides IAPP(1-18) and IAPP(1-28)-GI which were found to be capable of inhibiting Aβ40 cytotoxicity at the incubation time point of 72 h, were also examined after 7 days of incubation. 168 h aged Aβ40 was more cytotoxic than the 72 h aged solution and the presence of the peptides did not affect its cytotoxicity. By contrast, in the presence of IAPP-GI (1/1) no cytotoxicity was found in the 168 h aged Aβ40 solution which was in agreement to previous findings (Fig. 24D) [167].

In conclusion, the two IAPP hot regions of the Aβ-IAPP interaction interface IAPP(8-18) and IAPP(22-28)-GI when linked together by the tripeptide SSN, as it occurs in IAPP(8-28)-GI, were not able to inhibit Aβ40 fibrillogenesis and cytotoxicity. This result was surprising as a) IAPP-GI which is a N- and C-terminal extended version of IAPP(8-28)-GI is a highly potent inhibitor of Aβ40 fibrillogenesis and cytotoxicity and b) the IAPP sequence parts IAPP(1-7) and IAPP(30-37) were found to not interact with Aβ40 [167, 177]. The addition of the N-terminal part IAPP(1-7) to IAPP(8-28)-GI resulted in IAPP(1-28)-GI which was a strong inhibitor of Aβ40 fibrillogenesis and cytotoxicity. However, IAPP(1-28)-GI was not as effective as IAPP-GI [167]. As it was shown that IAPP(30-37) or IAPP(8-37)-GI were not able to inhibit Aβ40 fibrillogenesis and cytotoxicity, it appeared that the N-terminus IAPP(1-7) may act by stabilizing a specific conformation of IAPP-GI which is important for its interaction with Aβ40 and the inhibition of Aβ40 fibril formation and cytotoxicity.
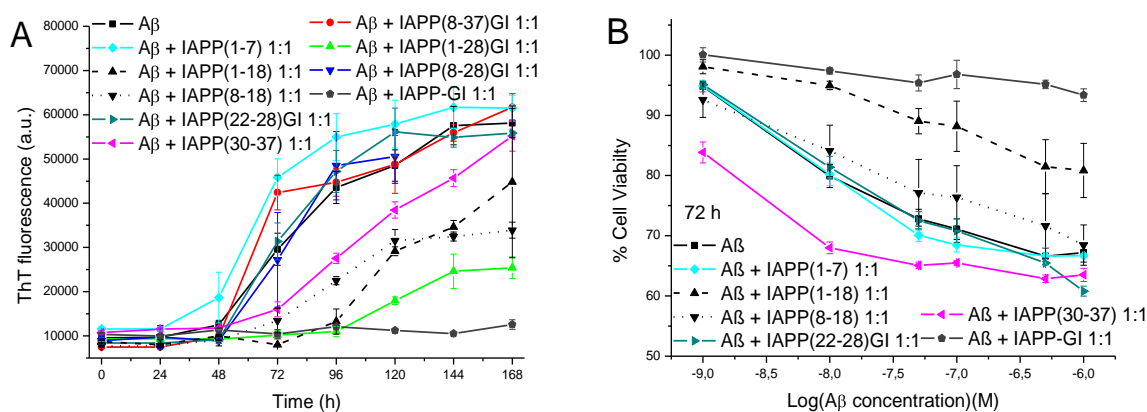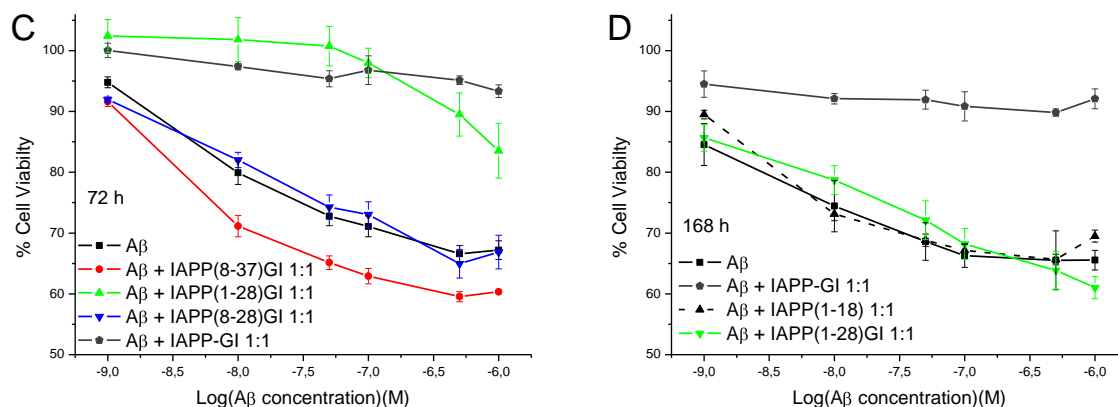
Fig. 24. Effect of IAPP(8-37)-GI, IAPP(1-28)-GI, IAPP(8-28)-GI, IAPP(1-7), IAPP(30-37), IAPP(22-28)-GI, IAPP(8-18), IAPP(1-18) and IAPP-GI, on Aβ40 fibrillogenesis and cytotoxicity. (A) Fibrillogenesis of Aβ40 (16.5 µM in 50 mM sodium phosphate buffer, pH 7.4, containing 100 mM NaCl and 1% HFIP) and of 1:1 mixtures of Aβ40 with peptides was followed by the ThT binding assay. (B) (C) Aβ40 and a mixture of Aβ40 with peptide (16.5 µM in 50 mM sodium phosphate buffer, pH 7.4, containing 100 mM NaCl and 1% HFIP) were incubated for 3 days. Aliquots were then diluted with cell culture medium and added to PC-12 cells at the indicated final concentrations. Following 24 h incubation at 37°C cell viabilities were assessed via the MTT reduction assay. (D) Aβ40-inhibitor mixtures which were found to inhibit following 3 days incubation were added to PC-12 cell at the time point 7 days. Cell viabilities were determined as under (B) and (C). Data are means (±SEM) of 3 assays (performed in triplicates).

Next, a fluorescence titration binding assay was used to determine whether different Aβ40 binding affinities cause the different inhibitory effects of these peptides segments on Aβ40 fibril formation and cytotoxicity. In addition, the binding affinities of the peptides to IAPP, IAPP-GI and to themselves were examined in order to test whether they are similar to the affinities of the interaction with Aβ40 as found for the hot regions [177] (Table 7). The principle of this assay is the following; N^{α}-amino terminal labeled peptide is titrated with an unlabeled peptide. Through the interaction of the peptide with the labeled one, the intensity of the fluorescence emission of the label may increase or decrease in a ligand concentration dependent manner. To ensure that the peptides were in a non-aggregated status at the beginning of the experiment, the stock solutions were made in hexafluoroisopropanol (HFIP). The concentration of the labeled peptides was kept as low as possible to guarantee a non-aggregated peptide and at the same time a reasonable fluorescence signal. 5(6)-carboxyfluorescein (Fluo) was normally used as the fluorophore and was coupled to the N^{α}-amino terminal IAPP, IAPP-GI, or for the self association studies to the peptide segments by themselves. The concentration of the fluorescein labeled peptide (Fluo-peptide) was 5 nM and, following mixing with increasing amount of peptide ligands, fluorescence emission spectra were recorded between 500-600 nm with excitation wavelength at 492 nm. For measuring the affinities of the peptides to Aβ40, Aβ40 was labeled at the N-terminus with 7-

diethylaminocoumarine-3-carboxylic acid (Dac). The concentration of Dac-Aβ40 was 10 nM and, following mixing with increasing amounts of peptide ligands, fluorescence emission spectra were recorded between 450-550 nm with excitation wavelength at 430 nm. Binding curves were obtained by plotting the maximum of fluorescent emission (522 nm for Fluo-peptide and 465 nm for Dac-Aβ40) versus the logarithm of the concentration of the non-labeled peptide. Apparent affinities (app. K_ds) were estimated using 1/1 binding-based models which was in accordance with the observed stoichiometry of the inhibitory effect of IAPP-GI on Aβ40 aggregation [167].

Table 7. Apparent affinities (app. K_d) of interaction of IAPP(8-37)-GI, IAPP(1-28)-GI, IAPP(8-28)-GI with Dac-Aβ40, Fluo-IAPP, Fluo-IAPP-GI and their N-terminal Fluo labeled form as determined by fluorescence titration binding assays. The measurements were carried out in 10 mM sodium phosphate buffer, pH 7.4, 1% HFIP and at room temperature. The concentration of the fluorescently labeled peptide was 10 nM for Dac-Aβ40 and 5 nM for Fluo-peptide. $K_{d,app}$ values were determined from one or three binding curves (± SEM where indicated).

	Dac-Aβ40	Fluo-IAPP	Fluo-IAPP-GI	Self-Ass.
IAPP(8-37)-GI	74 nM	500 nM	411 nM	168 nM
IAPP(1-28)-GI	192±10 nM	17 nM	52 nM	44±2 nM
IAPP(8-28)-GI	196±20 nM	195 nM	126 nM	71±10 nM

All tested IAPP-GI fragments were found to be able to interact and bind with high affinity Dac-Aβ40, Fluo-IAPP, and Fluo-IAPP-GI. IAPP(1-28)-GI which was the most potent inhibitor as compared to IAPP(8-28)-GI and IAPP(8-37)-GI appeared to have an app. K_d to Dac-Aβ40 which was in the same range as the affinities of IAPP(8-28)-GI or IAPP(8-37)-GI. These results indicated that there is no direct correlation between binding affinities of these sequences and their effects on Aβ40 fibrillogenesis and cytotoxicity.

3.3 Role of the IAPP N-terminal sequence IAPP(1-7) for its interaction with Aβ40

3.3.1 Function of the N-terminus related to IAPP(8-28)-GI analogs

The results of the studies of chapter 3.2 indicated that the N-terminus of IAPP (IAPP(1-7)) may play an important role in the Aβ40-IAPP interaction. To address this issue, the properties of the sequences IAPP(8-28)-GI vs. IAPP(1-28)-GI and two analogs were further studied. Starting from the point that the two hot regions of the IAPP-GI-Aβ40 interaction were IAPP(8-18) and IAPP(22-28)-GI, these two regions were connected by a sequence of three amino acids as in the case of the native IAPP (see 3.1 and Ref. [177]). Thereby, various analogues were designed and the two of them which will be discussed now were generated in two different forms: in the IAPP(8-28)-GI and in the IAPP(1-28)-GI form. In the first

analogue the three amino acids were glycines and in the second one the three amino acids were alanines. These two analogs were: a) IAPP(8-18)G3(22-28)-GI and IAPP(1-18)G3(22-28)-GI and b) IAPP(8-18)A3(22-28)-GI and IAPP(1-18)A3(22-28)-GI (Fig. 25).
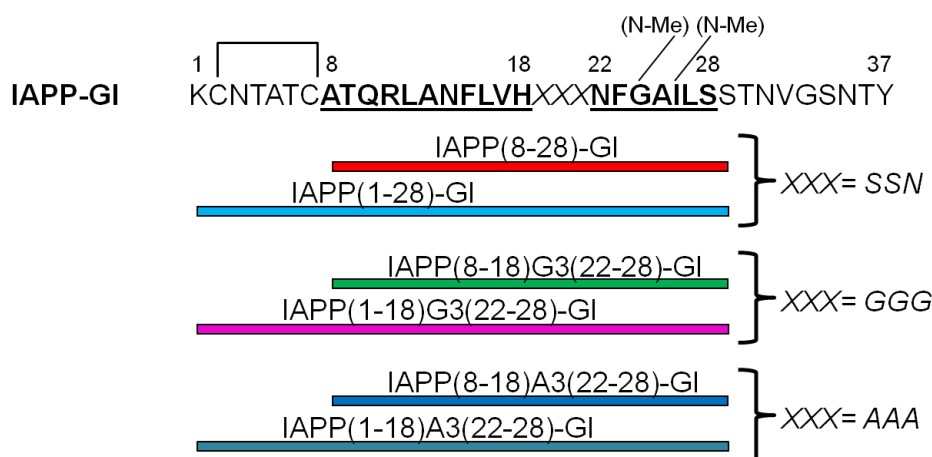

Fig. 25. Primary structure of IAPP-GI. Domains found to be hot regions for the Aβ40-IAPP interface are bold and underlined. Schematic presentation of designed IAPP-GI analogs: IAPP(8-28)-GI (red), IAPP(8-18)G3(22-28)-GI (green), IAPP(8-18)A3(22-28)-GI (blue), IAPP(1-28)-GI (cyan), IAPP(1-18)G3(22-28)-GI (magenta) and IAPP(1-18)G3(22-28)-GI (dark cyan).

Peptides were synthesized by solid phase peptide synthesis (SPPS) utilizing Fmoc-strategy. They were purified by HPLC and MALDI mass spectrometry was used to determine their mass as shown in Table 8.

Table 8. Characterization of peptides synthesized by Fmoc-chemistry (C-terminal amides) via their HPLC retention time (rt) and MS.

	HPLC prg.	rt (min)	[M+H]+ expected	[M+H]+found
IAPP(8-18)G3(22-28)-GI	Fast	18,7´	2171	2171
IAPP(1-18)G3(22-28)-GI	Slow	23,3´	2892	2892
IAPP(8-18)A3(22-28)-GI	Slow	24,1´	2213	2213
IAPP(1-18)A3(22-28)-GI	Fast	29´	2931	2931

Next, the question was addressed whether these IAPP-GI analogs could intervene with Aβ40 self-assembly into fibrils and affect formation of cytotoxic Aβ40 aggregates. Aβ40 alone (16.5 µM, pH 7.4) and the mixture of Aβ40 with peptides (16.5 µM each, pH 7.4) were incubated for 7 days and fibrillogenesis and cytotoxicity were followed by the ThT binding and the MTT reduction assay.

According to the ThT binding assay, Aβ40 fibrillogenesis exhibited a lag-time of ~48 h and reached completion between 96 and 120 h (Fig. 26A). In the presence of IAPP(8-18)A3(22-

28)-GI formation of Aβ40 fibrils was suppressed while IAPP(8-28)-GI and IAPP(8-18)G3(22-28)-GI had no or only little influence on Aβ40 fibrillogenesis. However, IAPP(8-18)A3(22-28)-GI was found to inhibit Aβ40 fibrillogenesis. Moreover the IAPP(1-28)-GI analogs, i. e. IAPP(1-28)-GI, IAPP(1-18)G3(22-28)-GI, and IAPP(1-18)A3(22-28)-GI blocked Aβ40 fibrillogenesis. These results suggested that both the linker connecting the "hot regions" and the N-terminal region of IAPP are important for inhibition of Aβ40 fibrillogenesis.

To examine whether these analogs may also inhibit formation of cytotoxic Aβ40 aggregates, aliquots of mixtures of Aβ40 with each of them (16.5 µM each, pH 7.4) and an incubation of Aβ40 alone (16.5 µM) (solutions used for the ThT binding) were added to PC-12 cells at various time points of the fibrillogenesis process (between 0 h and 7 days) and cell viability was assessed by the MTT reduction assay. Aβ40 alone was not toxic when added to the cells immediately after solution preparation (data not shown). After 72 h incubation, Aβ40 cytotoxicity increased whereas in the mixture of Aβ40 with IAPP(8-18)A3(22-28)-GI formation of Aβ40 cytotoxic species was found to be partially inhibited (Fig. 26B). By contrast, the mixtures of Aβ40 with IAPP(8-28)-GI or IAPP(8-18)G3(22-28)-GI were as toxic as Aβ40 alone (Fig. 26B). Thus, IAPP(8-18)A3(22-28)-GI was an inhibitor of Aβ40 cytotoxicity which was in good agreement with the results of ThT assay. Also in the mixtures of Aβ40 with IAPP(1-28)-GI, IAPP(1-18)G3(22-28)-GI, IAPP(1-18)A3(22-28)-GI no cytotoxic species after 72 h incubation were found (Fig. 26C). Therefore, the MTT assay on the effects of the analogs of IAPP(1-28)-GI on Aβ40 cytotoxicity was also performed at 7 days incubation (Fig. 26D) and IAPP(1-18)G3(22-28)-GI was found to be still able to inhibit cytotoxic Aβ40 self-assembly. The mixture of Aβ40 with IAPP(1-18)A3(22-28)-GI was slightly less toxic than Aβ40 alone while IAPP(1-28)-GI did not suppress Aβ40 cytotoxicity. These results indicated that the ability of partial IAPP-GI sequences to inhibit Aβ40 fibrillogenesis and cytotoxicity can be modulated by a) changing the linker between the "hot regions" of the IAPP-GI-Aβ40 interaction interface and b) by including the N-terminal IAPP(1-7) region.
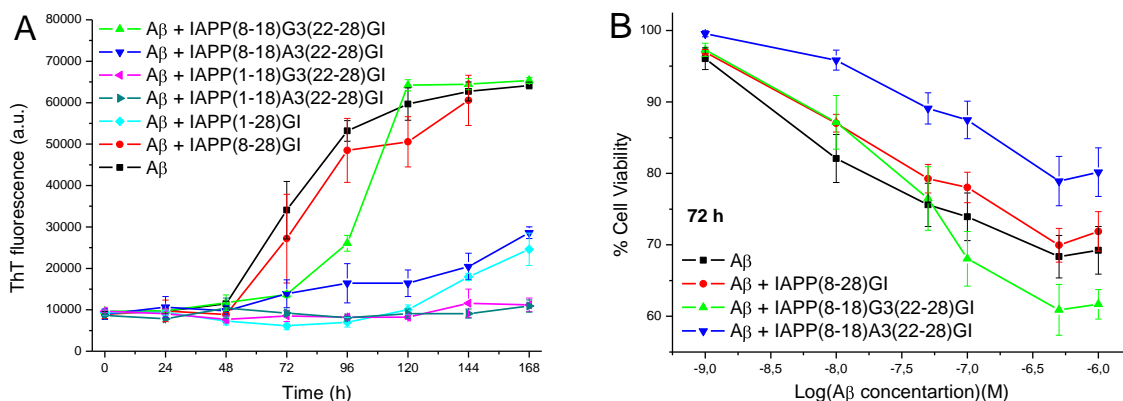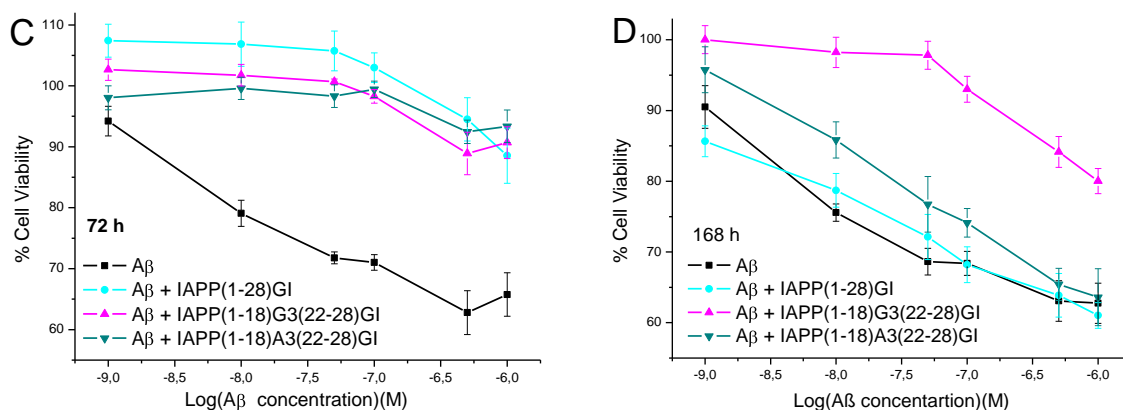
Fig. 26. Effect of IAPP(8-28)-GI, IAPP(8-18)G3(22-28)-GI, IAPP(8-18)A3(22-28)-GI, IAPP(1-28)-GI, IAPP(1-18)G3(22-28)-GI and IAPP(1-18)A3(22-28)-GI on Aβ40 fibrillogenesis and cytotoxicity. (A) Fibrillogenesis of Aβ40 (16.5 μM in 50 mM sodium phosphate buffer, pH 7.4, containing 100 mM NaCl and 1% HFIP) and of a mixture of Aβ40 with peptides (1:1) was followed by the ThT binding assay. (B)(C) Aβ40 and mixtures (1:1) of Aβ40 with peptides (16.5 μM in 50 mM sodium phosphate buffer, pH 7.4, containing 100 mM NaCl and 1% HFIP) were incubated for 3 days. Aliquots were then diluted with cell culture medium and added to PC-12 cells at the indicated final concentrations. Following 24h incubation at 37°C, cell viabilities were assessed via the MTT reduction assay. (D) Aβ40 and IAPP-GI analogues mixtures which were found to inhibit at the time point of 3 days were added to PC-12 cells at the time point of 7 days. Cell viabilities were determined as under (B) and (C). Data are means (±SEM) of 3 assays (performed in triplicates).

Next, the conformations of the above peptides were determined by far-UV CD spectroscopy. For these measurements, peptides were dissolved in 10 mM sodium phosphate buffer, pH 7.4, containing 1% HFIP and CD spectra were recorded. First, CD spectra of the peptides were measured at different peptide concentrations (5-200 μM) to determine their aggregation propensities. In general, the CD spectra of all tested peptides exhibited a pronounced minimum around 200 nm which indicated the presence of significant amounts of unordered structure and a second minimum around 225 nm which was indicative of more ordered most likely β-sheet- and/or β-turn-containing conformations (Fig. 27). Of note, IAPP(22-27) has been previously shown to have a pronounced minimum at about 200 nm, indicative of a predominantly random coil structure, while the spectrum of IAPP(22-27)-GI had a strong minimum at about 225 nm and a maximum at about 198 nm, suggesting an ordered and β-turn/β-sheet containing structure [151]. Therefore, the structure formed due to N-methylation of G^{24} and I^{26} is one major contributor of the secondary structure contents corresponding to the minimum at 225 nm. Accordingly, the magnitude of the signal at 225 nm differs in the CD spectra of the various peptides consistent with peptide specific contributions to the β-turn/β-sheets conformations of the analogues.

The critical concentrations for the oligomerization of IAPP(8-28)-GI, IAPP(8-18)G3(22-28)-GI and IAPP(8-18)A3(22-28)-GI were found to be between 50-100 μM while above a peptide

concentration of 50 µM a decrease of signal was observed consistent with formation of soluble oligomers (Fig. 27A-C-E).

The CD spectra of IAPP(1-28)-GI, IAPP(1-18)G3(22-28)-GI, and IAPP(1-18)A3(22-28)-GI exhibited the same two minima as the IAPP(8-28)-GI analogs at 200 and 225 nm (Fig. 27B-D-F). However, the ratios between the two minima were significantly different from the ratio of the minima in the IAPP(8-28)-GI. Thus, β-sheet- and/or β-turn content in the IAPP(1-28)-GI analogs appeared to be similar to the amount of IAPP(8-28)-GI analogs but the random coil content in the IAPP(1-28)-GI analogs was significantly lower than in the IAPP(8-28)-GI analogs. This suggests that the IAPP(1-28)-GI analogs have a more ordered structure than the IAPP(8-28)-GI sequences. In addition, the CD spectra of IAPP(1-28)-GI, IAPP(1-18)G3(22-28)-GI showed no concentration dependence up to 100 µM. The spectra of IAPP(1-18)A3(22-28)-GI indicated that aggregation started already at 5-10 µM. In fact, the CD spectrum of this peptide exhibited a pronounced β-sheet/β-turn signal and only a small random coil signal while by increasing the peptide concentration both β-sheet and the random coil minima became less.
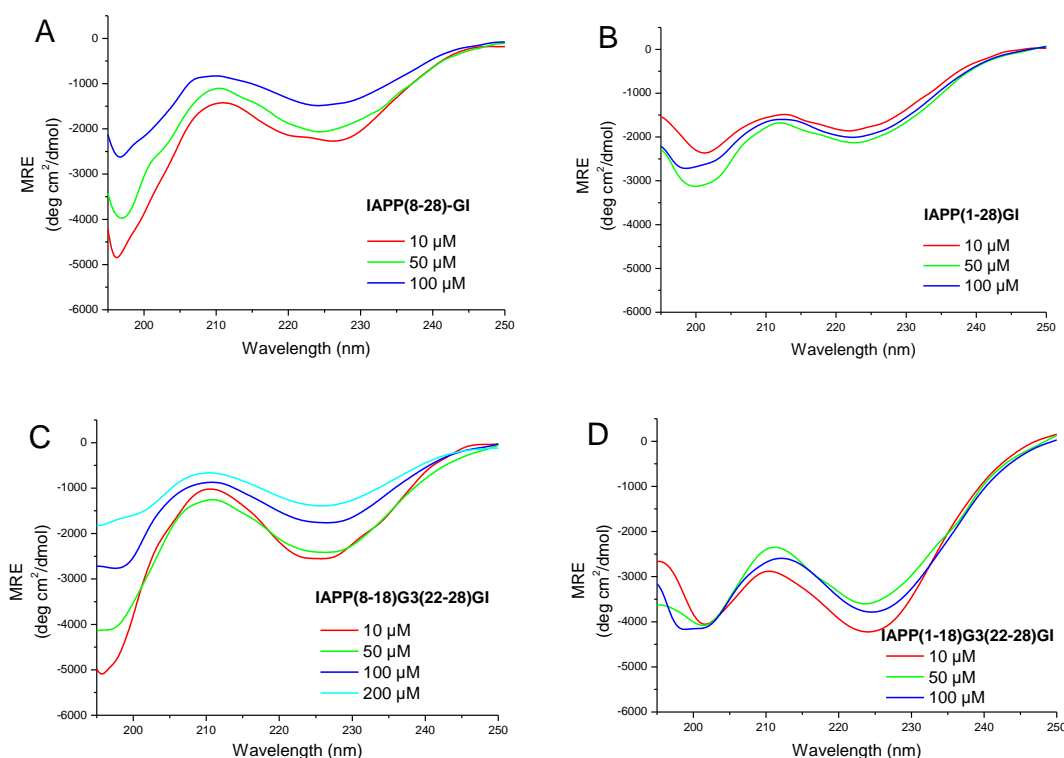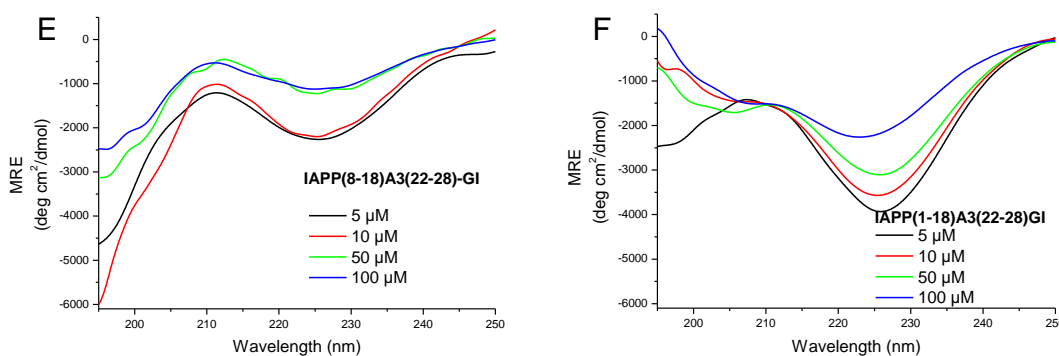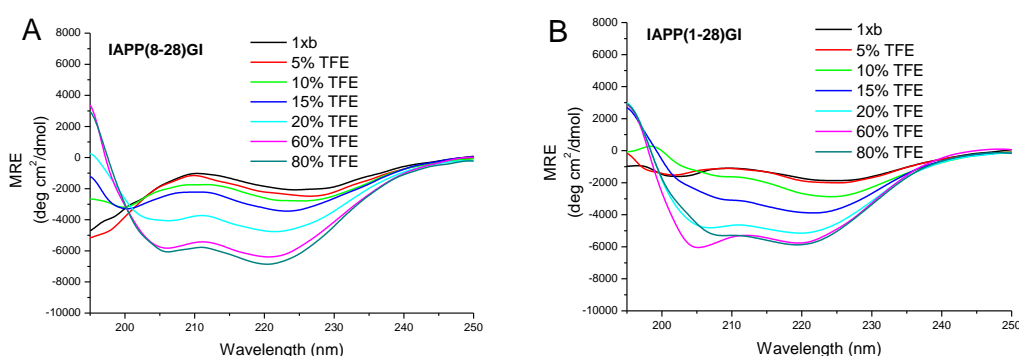
Fig. 27. Concentration dependence of the conformation of IAPP(8-28)-GI (A), IAPP(1-28)-GI (B), IAPP(8-18)G3(22-28)-GI (C), IAPP(1-18)G3(22-28)-GI (D), IAPP(8-18)A3(22-28)-GI (E) and IAPP(1-28)-GI (F) as assessed by far-UV CD spectroscopy. Experiments were performed in 10 mM sodium phosphate buffer, pH 7.4, containing 1% HFIP.

Next, the effects of trifluoroethanol (TFE) on the conformation of the above peptides were investigated. TFE promotes unfolding and intramolecular hydrogen bonds in proteins [182]. At low concentrations, TFE can destabilize thus specific tertiary interactions of proteins whereas at higher concentrations it is known to stabilize α-helical structures in polypeptides with α-helical propensity or non-natively folded states [182].

As mentioned above, the CD spectra of the peptides obtained in pure aqueous buffer (pH 7.4) showed a minimum at circa 200 nm which was typical of unordered conformation and a minimum at 225 nm which was typical of β-sheet- and/or β-turns. By increasing the amount of TFE, however, strong CD changes were observed and they were indicative of α-helix formation (two minima around 208 nm and 222nm) (Fig. 28). In addition, the CD spectra at different amount of TFE of IAPP(8-28)-GI, IAPP(8-18)A3(22-28)-GI and IAPP(1-18)G3(22-28)-GI were characterized by an isodichroic point at circa 200 nm indicating a two state transition (Fig. 28) [183].
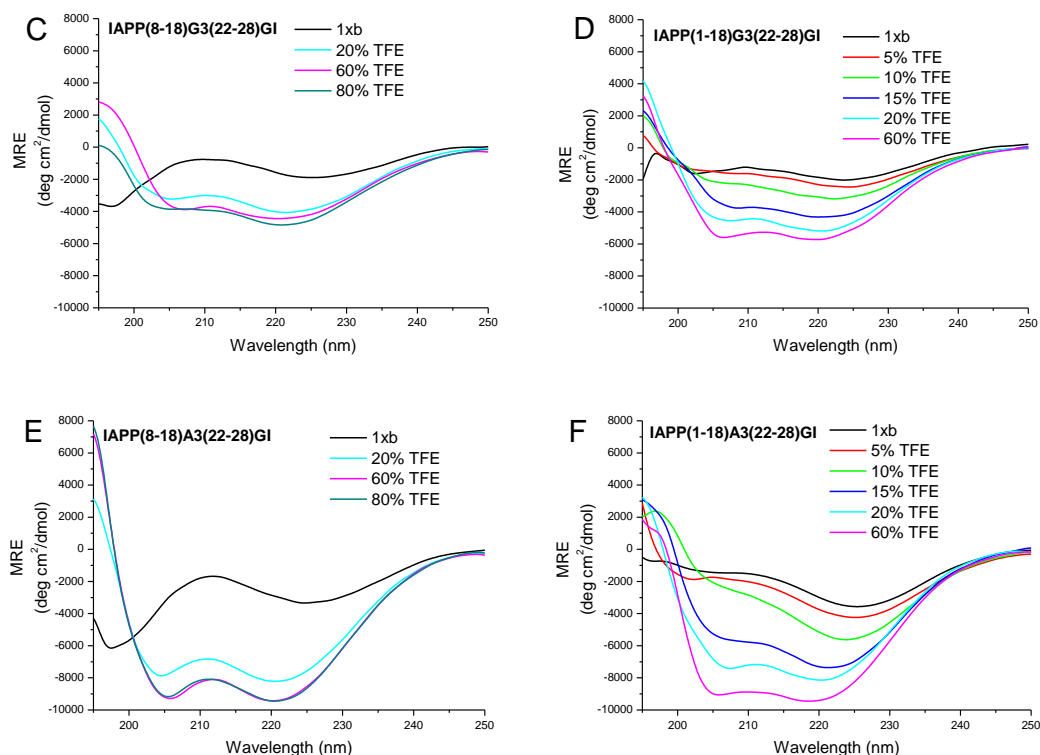
Fig. 28. Effects of TFE on conformation of aqueous solution of IAPP(8-28)-GI (A), IAPP(8-18)G3(22-28)-GI (B), IAPP(8-18)A3(22-28)-GI (C), IAPP(1-28)-GI (D), IAPP(1-18)G3(22-28)-GI (E) and IAPP(1-18)A3(22-28)-GI (F) assessed by far-UV CD spectroscopy. Experiments were performed at peptide concentrations of 10 μM in 10 mM sodium phosphate buffer, pH 7.4, containing 1% HFIP with the indicated amounts of TFE.

In general, all peptides had similar behavior in TFE, which indicated that they have a similar tendency to adopt an α-helical conformation in the presence of TFE. The transition curves constructed by plotting the intensity at 222 nm against the TFE concentration showed a sigmoidal trend (Fig. 29A) indicating that the induction of helical structure by TFE is a cooperative process [184, 185]. The midpoint of the transition of each peptide was between 12 and 16% of TFE (Fig. 29A). Interestingly, the peptides differed from each other with respect to the maximum amount of α-helical structure as induced by TFE. This is evident in Fig. 29B where the difference between the MRE at 222 nm of each peptide in aqueous buffer and the MRE in 60% TFE was plotted. Accordingly, IAPP(8-28)-GI, IAPP(1-28)-GI, IAPP(8-18)G3(22-28)-GI, and IAPP(1-18)G3(22-28)-GI exhibited similar α-helical contents whereas IAPP(8-18)A3(22-28)-GI and IAPP(1-18)A3(22-28)-GI exhibited higher maximum amounts of α-helix. It appears that the three alanines, placed between the two hot region, promoted helix formation [186].

Interestingly, no significant differences between the helical stabilization of IAPP(8-28)-GI and IAPP(1-28)-GI analogs were observed. These results suggested that the IAPP(1-7) region

does not contribute in stabilization of helical conformation. Thus, no correlation between Aβ40 aggregation inhibitory capacity and α-helix propensity could be deduced.
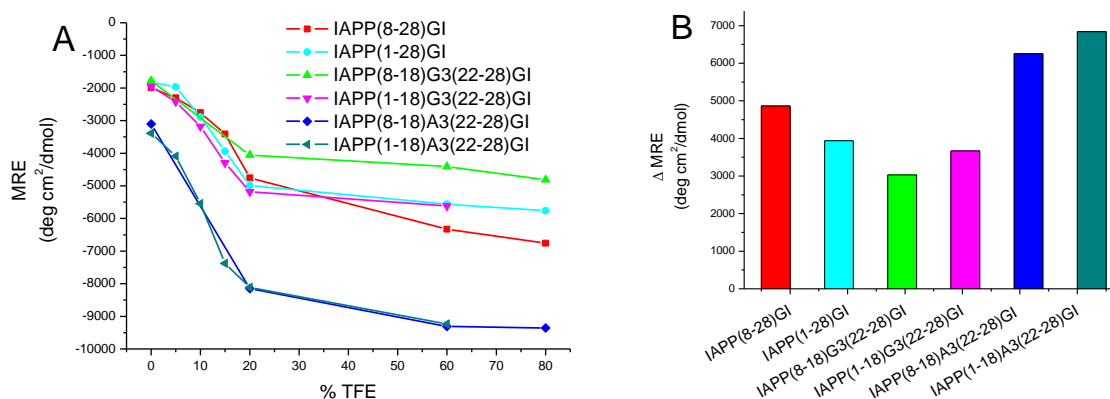

Fig. 29. (A) Plots of minima at 222 nm versus the % TFE contents of the CD spectra of the peptides shown in Fig. 28. (B) Plot of the difference between the MRE in pure acqueus buffer and the MRE in 60% TFE (maximum helical content) at 222 nm of the CD spectra of Fig. 28.

Next, to investigate the effect of the presence of the N-terminus IAPP(1-7) on the binding affinities to Aβ40, IAPP, and IAPP-GI, fluorescence titration binding assays were performed (Table 9). All tested peptides bound Dac-Aβ40 and their binding affinities were found to be in the micro- to low nanomolar range. In the group of the IAPP(1-28)-GI analogs, the strongest Aβ40 ligand was IAPP(1-18)G3(22-28)-GI ($K_{d,app}$= 8 nM) while the weakest one was IAPP(1-18)A3(22-28)-GI. In the group of the IAPP(8-28)-GI analogs, the best Aβ40 binder was IAPP(8-18)A3(22-28)-GI ($K_{d,app}$= 49 nM) while IAPP(8-28)-GI ($K_{d,app}$= 196±20 nM) and IAPP(8-18)G3(22-28)-GI ($K_{d,app}$= 1 μM) were weaker binders.

Table 9. Apparent affinities (app. K_d) of interaction of IAPP(8-28)-GI, IAPP(1-28)-GI, IAPP(8-18)G3(22-28)-GI, IAPP(1-18)G3(22-28)-GI, IAPP(8-18)A3(22-28)-GI and IAPP(1-18)A3(22-28)-GI with Dac-Aβ40, Fluo-IAPP, Fluo-IAPP-GI and their N-terminal Fluo labeled form as determined by fluorescence titration binding assays. The measurements were carried out in 10 mM sodium phosphate buffer, pH 7.4, 1% HFIP and at room temperature. The concentration of the fluorescently labeled peptide was 10 nM for Dac-Aβ40 and 5 nM for Fluo-peptide. $K_{d,app}$ values were determined from one or three binding curves (± SEM where indicated).

	Dac-Aβ40	Fluo-IAPP	Fluo-IAPP-GI	Self-Ass.
IAPP(8-28)-GI	196±20 nM	195 nM	126 nM	71±10 nM
IAPP(1-28)-GI	192±10 nM	17 nM	52 nM	44±2 nM
IAPP(8-18)G3(22-28)-GI	1 μM	913 nM	615 nM	91 nM
IAPP(1-18)G3(22-28)-GI	8 nM	48 nM	31 nM	58 nM
IAPP(8-18)A3(22-28)-GI	49 nM	24 nM	393 nM	2,7 μM
IAPP(1-18)A3(22-28)-GI	355 nM	44 nM	28 nM	47 nM

In general the affinities of the IAPP(1-28)-GI analogs to Fluo-IAPP or Fluo-IAPP-GI were found to be higher than the affinities to Dac-Aβ40. By contrast, similar binding affinities were found in the case of IAPP(8-28)-GI analogs toward either Fluo-IAPP (Fluo-IAPP-GI) or Dac-Aβ40. These findings suggested that the binding affinities to IAPP become stronger by increasing the sequence similarity of the analogs to IAPP which was done by their N-terminal elongation. Of note, in the case of IAPP(8-18)G3(22-28)-GI, the incorporation of N-terminal region IAPP(1-7) as IAPP(1-18)G3(22-28)-GI was found to result to a very strong increase of binding affinity to Dac- Aβ40 (> 100x).

3.3.2 Studies on the role of specific residues within the N-terminus IAPP(1-7) for the interaction with Aβ40

In chapter 3.3.1 it was shown that the presence of the N-terminal sequence, IAPP(1-7), significantly contributed to the inhibitory effect of IAPP(1-28)-GI (or analogs) on formation of cytotoxic Aβ40 species and fibrils. To investigate the role of specific residues within IAPP(1-7) on the above effect, five peptides were synthesized. Their effect on Aβ40 cytotoxicity and fibrillogenesis were determined and compared to the effect of IAPP(1-28)-GI (Fig. 30). First, the IAPP(1-28)-GI analogue G7-IAPP(8-28)-GI was designed, where all residues of the IAPP(1-7) region were exchanged by glycines. Glycines would ensure the same number of amino acids and hydrogen bonds as in IAPP(1-28)-GI whereas the effect of a $(Gly)_7$ sequence on overall conformation, i. e. helix formation, would be expected to be not as strong due to the maximal freedom of the phi-psi angle. By contrast, in order to get a helix inducer sequence, the second analog was designed to contain seven alanines instead IAPP(1-7) sequence, leading to A7-IAPP(8-28)-GI. To investigate which residues might be crucial for the interaction with Aβ40, a partial Ala-scan of the region IAPP(1-7) was performed: first, residues 1 and 3 were substituted with alanine ((A1-3)IAPP(1-28)-GI) and in the second case residues 4 and 6 ((A4-6)IAPP(1-28)-GI). Of note, in the native sequence of IAPP (IAPP-GI), Cys^2 and Cys^7 are linked by a disulfide bridge. In order to address the question whether the disulfide bridge is important, the reference peptide, IAPP(1-28)-GI, with the two cysteine in non disulfide-linked (reduced) form was also synthesized (IAPP(1-28)-GI-red).
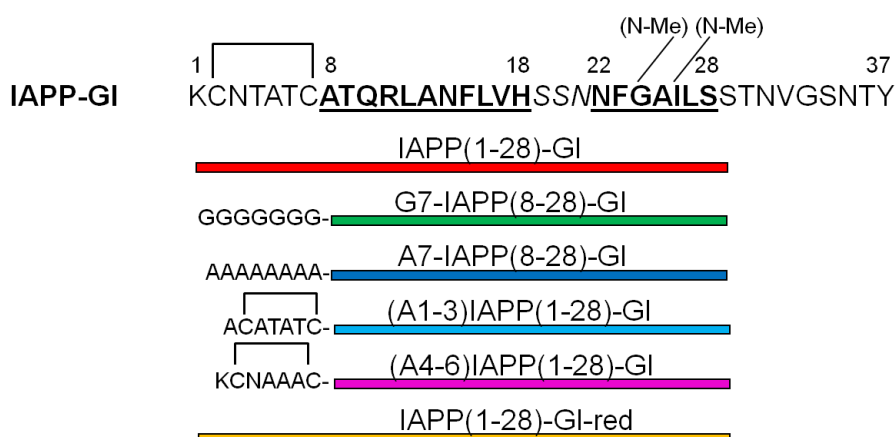
IAPP-GI

```
                                            (N-Me) (N-Me)
              1        8        18    22    /    /28        37
IAPP-GI       KCNTATC**ATQRLANFLVH**SS*N***NFGAILS**STNVGSNTY
```

IAPP(1-28)-GI

GGGGGGG- G7-IAPP(8-28)-GI

AAAAAAAA- A7-IAPP(8-28)-GI

ACATATC- (A1-3)IAPP(1-28)-GI

KCNAAAC- (A4-6)IAPP(1-28)-GI

IAPP(1-28)-GI-red

Fig. 30. Primary structure of IAPP-GI. Domains suggested to be hot regions of the Aβ40-IAPP interaction interface are bold and underlined. Schematic representation of the designed peptides studied in this chapter using colored bars: IAPP(1-28)-GI (red), G7-IAPP(8-28)-GI (green), A7-IAPP(8-28)-GI (blue), (A1-3)IAPP(1-28)-GI (cyan), (A4-6)IAPP(1-28)-GI (magenta) and IAPP(1-28)-GI-red (orange).

Peptides were synthesized by solid phase peptide synthesis (SPPS) utilizing Fmoc-strategy. They were purified by HPLC and MALDI mass spectrometry was used to determine their mass as shown in Table 10.

Table 10. Characterization of peptides synthesized by Fmoc-chemistry (C-terminal amides) via their HPLC retention time (rt) and MS

	HPLC prg.	rt (min)	[M+H]+ expected	[M+H]+ found
G7-IAPP(8-28)-GI	Slow	21´	2688	2688
A7-IAPP(8-28)-GI	Slow	24´	2786	2786
(A1-3)IAPP(1-28)-GI	Slow	26´	2908	2909
(A4-6)IAPP(1-28)-GI	Slow	25´	2948	2949
IAPP(1-28)-GI-red	Slow	23´	3008	3008

To answer the question whether these peptides were capable of inhibiting Aβ40 as effectively as IAPP(1-28)-GI, Aβ40 and the 1/1 mixture of Aβ40 and each of the peptides were incubated for 7 days in ThT buffer (50 mM sodium phosphate buffer, pH 7.4, containing 100 mM NaCl and 1% HFIP). The amount of fibrils was quantified via the ThT assay (Fig. 31A) and the Aβ40 cytotoxicity was measured after incubation for 3 and 7 days via the MTT reduction assay (Fig. 31B-C). According to the ThT assay Aβ40 fibrillogenesis exhibited a lag time of 48 h and reached completion at 96 h. In the presence of G7-IAPP(8-28)-GI or A7-IAPP(8-28)-GI, fibrillogenesis was somewhat delayed whereas the ThT fluorescence of the mixture at 7 days was comparable to the ThT of Aβ40 alone. By contrast, (A1-3)IAPP(1-28)-GI and (A4-6)IAPP(1-28)-GI were found to block nearly completely Aβ40 fibrill formation.

In fact, the two latter peptides exhibited a similar inhibitory effect as the reference peptide, IAPP(1-28)-GI, demonstrating that the substitution of two residues in IAPP(1-7) with alanine did not have any effect on the inhibitory capacity of IAPP(1-28)-GI on Aβ40 fibrillogenesis. To examine whether the IAPP(1-28)-GI analogues also affected formation of cytotoxic Aβ40 assemblies, aliquots of the incubations for the ThT binding assays were added to PC-12 cells at various time points of the fibrillogenesis process and cell viabilities were assessed by the MTT reduction assay (Fig. 31B-C). Non-aged Aβ40 and non-aged mixtures were non-toxic at time 0 (data not shown). At 72 h, Aβ40 alone and the mixture were at the beginning of the fibrillization phase (Fig. 31A) and the solution of Aβ40 alone was more cytotoxic than its mixtures with each of the peptides (Fig. 31B). Thereby, the 72 h aged mixtures with (A1-3)IAPP(1-28)-GI and (A4-6)IAPP(1-28)-GI, which were still in the fibrillization lag-phase, were not cytotoxic whereas the Aβ40 mixtures with G7-IAPP(8-28)-GI and A7-IAPP(8-28)-GI were partially cytotoxic albeit not as toxic as Aβ40 alone. Thus, (A1-3)IAPP(1-28)-GI and (A4-6)IAPP(1-28)-GI proved to be more effective inhibitor of Aβ40 aggregation than G7-IAPP(8-28)-GI and A7-IAPP(8-28)-GI. The partial Ala-scan peptides appear actually to intervene with Aβ40 aggregation in a similar manner as IAPP(1-28)-GI. At the time point of 7 days, the fully fibrillized mixtures of Aβ40 with G7-IAPP(8-28)-GI or A7-IAPP(8-28)-GI and also partially fibrillized mixtures of Aβ40 with IAPP(1-28)-GI, (A1-3)IAPP(1-28)-GI or (A4-6)IAPP(1-28)-GI, were found to be as cytotoxic as fully fibrillized Aβ40 (Fig. 31C).

Further, as shown in Fig. 31D, the reduced form of IAPP(1-28)-GI, IAPP(1-28)-GI-red, was also found to inhibit Aβ40 cytotoxicity (72 h) and fibrillogenesis as effective as the disulfide bridge containing peptide IAPP(1-28)-GI. Thus, the disulfide bridge occurring between Cys^2 and Cys^7 does not play an important role in the inhibitory potency of IAPP(1-28)-GI on Aβ40 cytotoxicity and fibrillogenesis.

In conclusion, the substitution of all 7 residues in the region IAPP(1-7) of IAPP(1-28)-GI, as in G7-IAPP(8-28)-GI and A7-IAPP(8-28)-GI resulted in a strong reduction of the inhibitory potency of IAPP(1-28)-GI on Aβ40 fibrillogenesis and cytotoxicity. However, the two latter peptides were clearly stronger inhibitors of Aβ40 aggregation and toxicity than IAPP(8-28)-GI (Fig. 26). In addition, the substitution of two residues within IAPP(1-7) as in (A1-3)IAPP(1-28)-GI and (A4-6)IAPP(1-28)-GI did not affect the inhibitory capacity of IAPP(1-28)-GI; in fact both peptides were found to inhibit in a similar manner as IAPP(1-28)-GI.
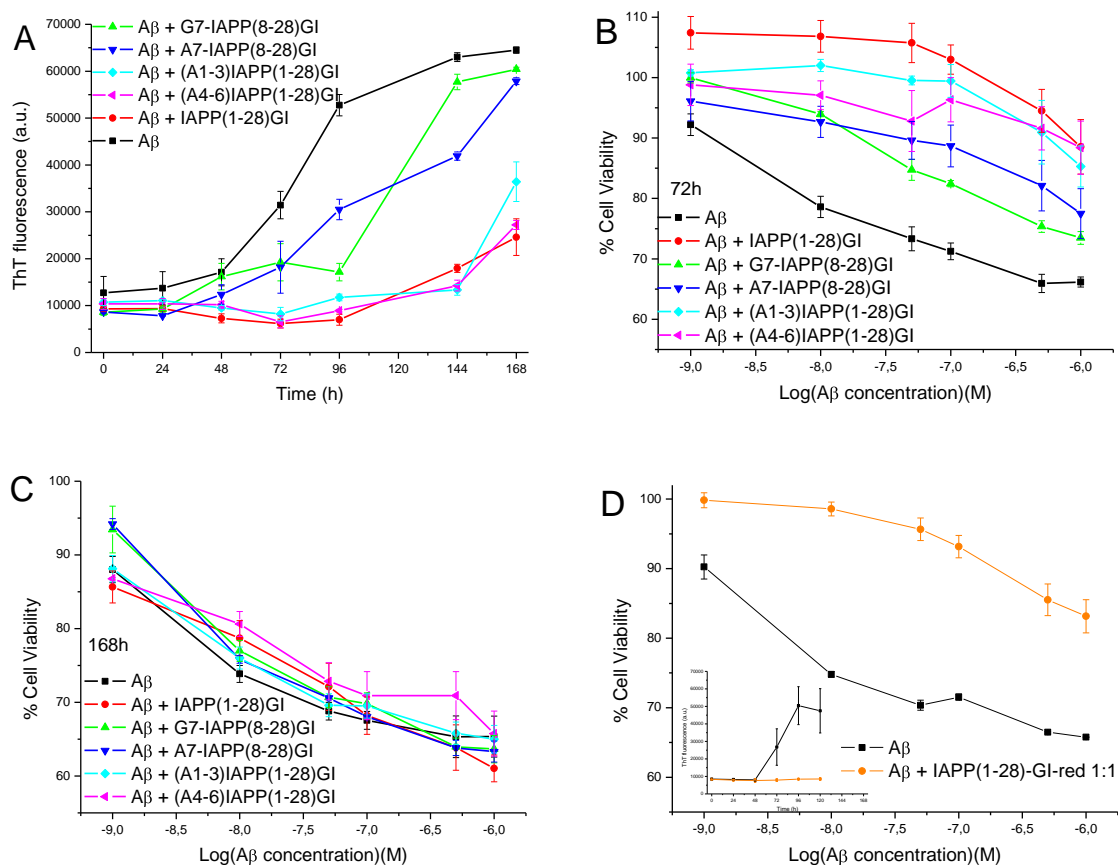
Fig. 31. Effect of IAPP(1-28)-GI, G7-IAPP(8-28)-GI, A7-IAPP(8-28)-GI, (A1-3)IAPP(1-28)-GI and (A4-7)IAPP(1-28)-GI on Aβ40 cytotoxicity and fibrillogenesis. (A) Fibrillogenesis of Aβ40 (16.5 µM in 50 mM sodium phosphate buffer, pH 7.4, containing 100 mM NaCl and 1% HFIP) and of a mixture of Aβ40 and peptides (1:1) was followed by ThT binding assay. (B)(C) Aβ40 and a mixture of Aβ40 with peptides (16.5 µM in 50 mM sodium phosphate buffer, pH 7.4, containing 100 mM NaCl and 1% HFIP) were incubated for 3 days (B) or 7 days (C). Aliquots were then diluted with cell culture medium and added to PC-12 cells at the indicated final concentrations. Following 24 h incubation at 37°C cell viabilities were assessed via the MTT reduction assay. (D) MTT reduction assay (after 3 days of incubation) and ThT assay (inset) of a mixture of Aβ40 with IAPP(1-28)-GI-red as compared to Aβ40 alone. Data are means (±SEM) of 3 assays (performed in triplicates).

The conformation of these peptides and their tendency to self-associate were next examined by CD spectroscopy. Solutions of IAPP-GI analogs at different peptide concentrations were prepared in 10 mM phosphate buffer, pH 7.4 and 1% HFIP and CD spectra were measured immediately thereafter (Fig. 32). The spectra of all peptides had a minimum around 200 nm indicating the presence of significant amounts of random coil structure and a second minimum around 225 nm which indicated more ordered, most likely β-sheet- and/or β-turn-containing, conformations. The ratios between the two minima were dependent on the type of peptide and on the concentration. As discussed in chapter 3.3.1, the spectra of IAPP(1-28)-GI did not show any change when the concentration was increased up to 100 µM and the

overall MRE signal was relatively small (Fig. 32A). G7-IAPP(8-28)-GI and A7-IAPP(8-28)-GI exhibited high amounts of random coil at 10 µM; however, both started to form more structured soluble oligomers around 50 and 100 µM. Thus, the intensities of the CD spectrum signal of G7-IAPP(8-28)-GI and A7-IAPP(8-28)-GI at 200 µM were about half as much as the ones at 10 µM (Fig. 32C-D). (A1-3)IAPP(1-28)-GI exhibited reduced random coil and β-sheet contents already at 10 µM and the intensity of the signal at 50 µM was less than the half of the 10 µM signal (Fig. 32E). By contrast, (A4-6)IAPP(1-28)-GI lost part of its CD signal only up 50 µM consistent with the suggestion that the N-terminal region plays an important role in the aggregation propensity of IAPP(1-28)-GI (Fig. 32F).

In Fig. 32B the absolute MRE value of each of the peptides is shown at 200 nm (random coil) and at 225 nm (β-sheet / β-turn) at a peptide concentration. It becomes clear that substitution of all residues within IAPP(1-7) by glycine or alanine resulted in significant increase of the random coil contents; peptides G7-IAPP(8-28)-GI and A7-IAPP(8-28)-GI exhibited the highest amounts of unordered conformation. The random coil signal of (A1-3)IAPP(1-28)-GI and (A4-6)IAPP(1-28)-GI exhibited a value between the one of IAPP(1-28)-GI and G7-IAPP(8-28)-GI or A7-IAPP(8-28)-GI. These results suggested that by increasing the number of substitutions within the N-terminus the peptide became more unordered. On the other hand, the amount of β-sheet/β-turn contents did not change significantly by these substitutions. These results indicated that a part of ordered peptide structure is not affected by the substitution in the N-terminal region of IAPP. The substitution within IAPP(1-7) resulted in an increase of conformational flexibility at the expense of structural components other than β-sheet/β-turn ones. However, since it appears that the here studied solutions contained oligomers, the CD-results do not allow for an exact quantification of secondary structural contents.
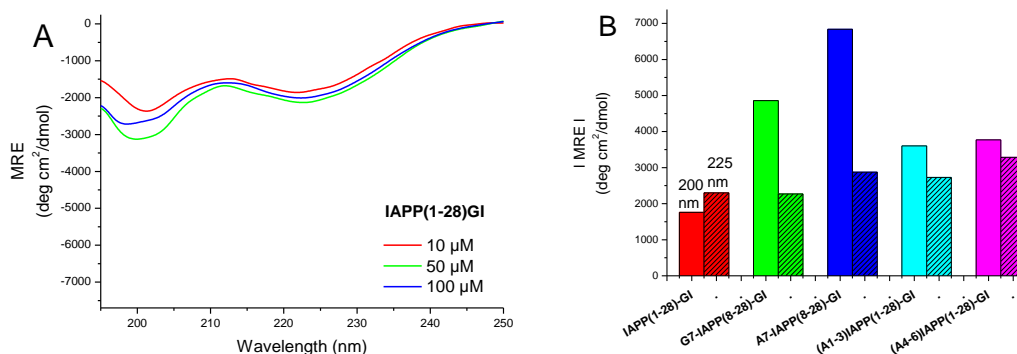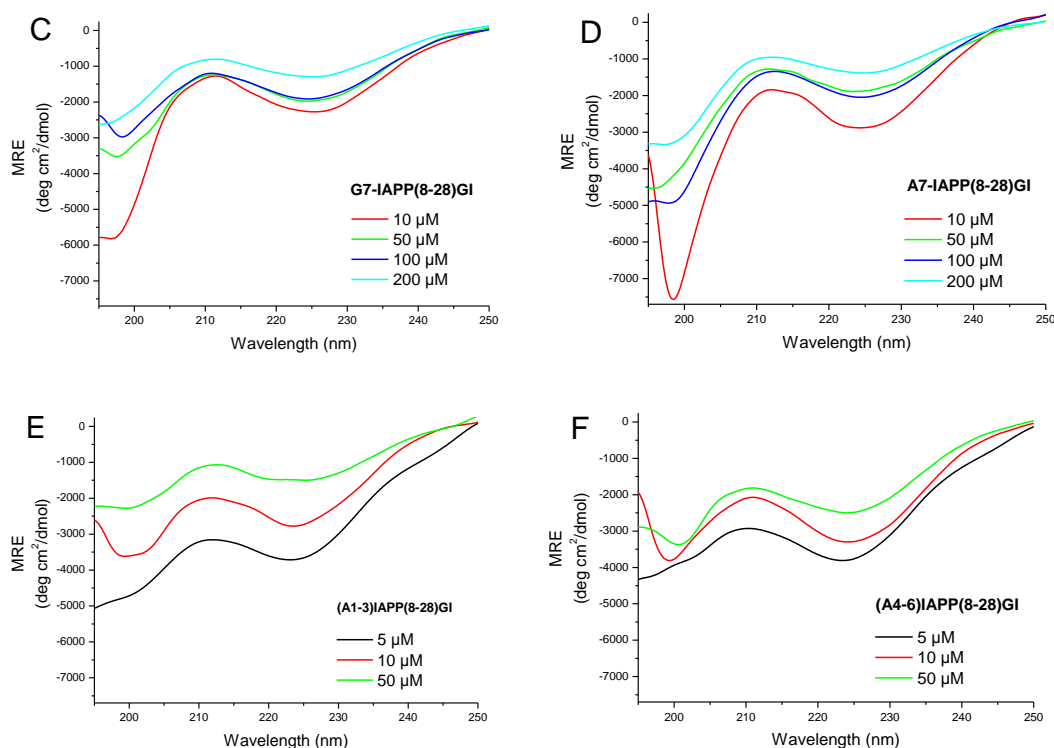
Fig. 32. Concentration dependence of the conformation of IAPP(1-28)-GI (A), G7-IAPP(8-28)-GI (C), A7-IAPP(8-28)-GI (D), (A1-3)IAPP(8-28)-GI (E) and (A4-6)IAPP(8-28)-GI (F) as assessed by far-UV spectroscopy. Measurements were performed in 10 mM sodium phosphate buffer, pH 7.4, containing 1% HFIP. (B) Absolute value of MRE at 200 nm (no pattern) and at 225 nm (striped pattern) for each of the peptides at 10 µM.

Next, the effects of TFE on the conformation of these peptides were investigated (Fig. 33). As shown above, the CD spectra of the peptides in 10 mM aqueous sodium phosphate buffer (pH 7,4)(1% HFIP) showed a minimum at 195-200 nm (random coil) and a minimum at circa 225 nm (β-sheet/β-turn). When TFE was added to the aqueous buffer, the peptide backbone (195-250 nm) was found to undergo significant spectral CD changes, indicative of α-helix formation (two minima around 208 and 222nm) (Fig. 33). Each one of the peptides was found to be able to adopt α-helix conformation in the presence of TFE and the maximum amount of helix was reached at 60% TFE. CD spectra collected for G7-IAPP(8-28)-GI and A7-IAPP(8-28)-GI following TFE titration revealed the presence of an isodichroic point around 200 nm indicating the presence of a two state system [183]. By plotting the minimum at 222 nm against the TFE content of the CD buffer (Fig. 33B), the midpoints of all titration curves were found to be between 10-15% TFE and sigmoidal curves were obtained indicative of cooperative transitions [184, 185]. The highest amount of α-helix content was observed in A7-IAPP(8-28)-GI as expected by the presence of the 7 alanines which are well known to be helix-inducing residues [186]. G7-IAPP(8-28)-GI appears to be the analogue with the lowest amount of α-helix consistent with the fact that glycine has a high

conformational freedom. In good agreement with the above findings, the peptides with two Ala substitutions, i. e. (A1-3)IAPP(1-28)-GI and (A4-6)IAPP(1-28)-GI, were found to have maximum α-helical contents between the content of the native sequence IAPP(1-28)-GI and A7-IAPP(8-28)-GI.

In conclusion, the α-helix propensities of all here studied IAPP(1-28)-GI analogs were higher than the propensity of the reference peptide, IAPP(1-28)-GI, consistent with the hypothesis that suitable substituents in the N-terminal region IAPP(1-7) can modulate the α-helical propensity of IAPP(1-28)-GI [187, 188].
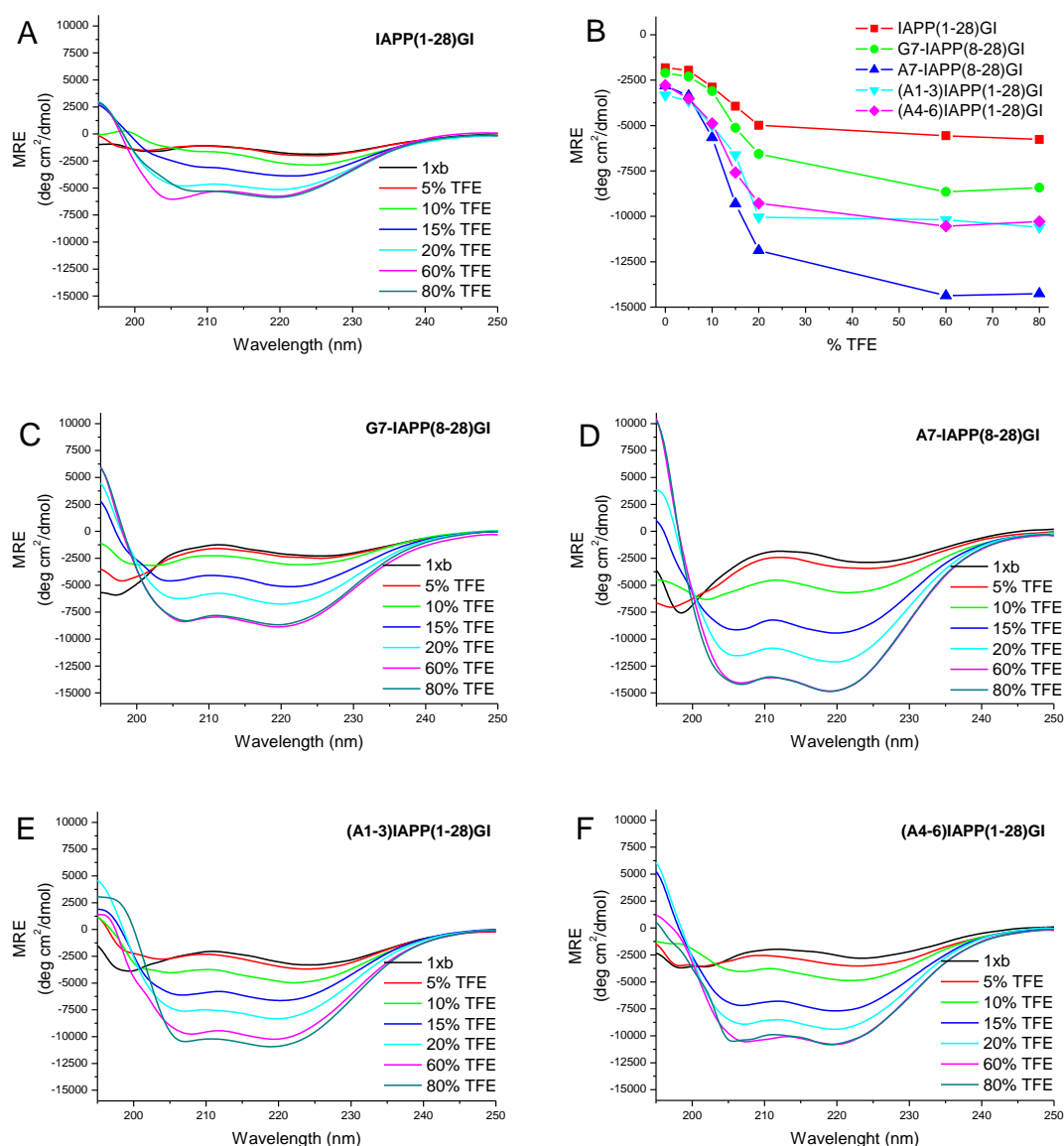

Fig. 33. Effects of TFE on conformation of aqueous solution of IAPP(1-28)-GI (A), G7-IAPP(8-28)-GI (C), A7-IAPP(8-28)-GI (D), (A1-3)IAPP(1-28)-GI (E), (A4-6)IAPP(1-28)-GI (F) assessed by far-UV CD spectroscopy. Experiments were performed at peptide concentrations of 10 µM in 10 mM sodium phosphate buffer, pH 7.4,

containing 1% HFIP and various amounts of TFE as indicated. (B) Plot of MRE at 222 nm of the CD spectra shown in (A, C, D, E, F) versus %TFE contents of the aqueous CD solutions.

Next, the affinity of the interaction of the peptides with Aβ40 was characterized by using fluorescence spectroscopy (Table 11). All tested IAPP(1-28)-GI analogs were found to bind with high affinity Dac-Aβ40. The dissociation constants (app. K_d) were similar to each other and were all in the nanomolar range (~100 nM). The affinities of the interaction of the peptides with Fluo-IAPP (and Fluo-IAPP-GI) were also determined. The determined $K_{d,app}$ values towards IAPP (or IAPP-GI) were in the nanomolar range and similar to the $K_{d,app}$ values of their interaction with Dac-Aβ40. Moreover, each peptide was found to self-associate into soluble low molecular weight oligomers with apparent dissociation constants in the nanomolar range.

Table 11. Apparent affinities (app. Kd) of interaction of IAPP(1-28)-GI, G7-IAPP(8-28)-GI, A7-IAPP(8-28)-GI, (A1-3)IAPP(1-28)-GI and (A4-6)IAPP(1-28)-GI with Dac-Aβ40, Fluo-IAPP, Fluo-IAPP-GI and their N-terminal Fluo labeled form as determined by fluorescence titration binding assays. The measurements were carried out in 10 mM sodium phosphate buffer, pH 7.4, 1% HFIP and at room temperature. The concentration of the fluorescently labeled peptide was 10 nM for Dac-Aβ40 and 5 nM for Fluo-peptide. $K_{d,app}$ values were determined from one or three binding curves (± SEM where indicated).

	Dac-Aβ40	Fluo-IAPP	Fluo-IAPP-GI	Self-Ass.
IAPP(1-28)-GI	192±10 nM	17 nM	52 nM	44±2 nM
G7-IAPP(8-28)-GI	158 nM	306 nM	56 nM	91 nM
A7-IAPP(8-28)-GI	58 nM	58 nM	45 nM	178 nM
(A1-3)IAPP(1-28)-GI	117 nM	151 nM	133 nM	76 nM
(A4-6)IAPP(1-28)-GI	65 nM	59 nM	93 nM	204 nM

In conclusion, the substitutions of all 7 amino acids in the N-terminus, as for G7-IAPP(8-28)-GI and A7-IAPP(8-28)-GI, resulted in a strong reduction of the inhibitory effect on Aβ40 cytotoxicity and fibrillogenesis providing evidence that IAPP(1-7) is important for the interaction and the inhibitory effect of IAPP(1-28)-GI with Aβ40. On the other hand, replacing of only two amino acids within IAPP(1-7) by alanine did not result in a significant change of the effect on Aβ40 aggregation and cytotoxicity as compared to the reference peptide IAPP(1-28)-GI. In addition, enhancing the α-helical propensity of IAPP(1-28)-GI by introducing α-helix inducing residues i.e. seven alanines within IAPP(1-7) did not prove to improve the inhibitory potential of IAPP(1-28)-GI on Aβ40 fibrillogenesis and cytotoxicity.

3.4   Exploiting the hot-spot regions of the Aβ40-IAPP interaction interface to devise inhibitors of Aβ40 aggregation and cytotoxicity

It has been previously shown that the designed 37-residue polypeptide IAPP-GI is a low nanomolar affinity Aβ40 ligand and a nanomolar activity inhibitor of Aβ40 cytotoxic oligomerization and fibrillogenesis. Additionally, IAPP-GI is the only known peptide-derived compound which binds with high affinity both IAPP and Aβ40 and blocks and reverses cytotoxic self-assembly of both polypeptides [167]. As shown in 3.1 and in Ref. [177], systematic studies on the Aβ-IAPP interaction interface identified IAPP(8-18) and IAPP(22-28) as the shortest sequences that are still able to bind Aβ40 with nanomolar affinities.

Here, a strategy was explored to devise inhibitors of Aβ40 aggregation based on the identified IAPP hot regions of the Aβ-IAPP interaction interface. The basic inhibitor structure consisted of the two hot regions IAPP(8-18) and IAPP(22-28). Thereby, IAPP(22-28) was applied in its N-methylated form ((N-Me)G^{24} and (N-Me)I^{26} as in IAPP-GI) to yield IAPP(22-28)-GI. The N-methylated sequence was used, instead of the natively occuring one, to ensure the solubility of the peptide since IAPP(22-27) was previously shown to aggregate into β-sheet-containing amyloid fibrils [152]. Of note, the segments IAPP(8-18) and IAPP(22-28)-GI by themselves are unable to block Aβ40 fibrillogenesis and cytotoxicity (see Fig. 24). As shown in chapter 3.2, when the two hot regions IAPP(8-18) and IAPP(22-28)-GI were linked together by the tripeptide sequence SSN, which is the sequence between residue 19 and 21 of native IAPP, the resulting peptide IAPP(8-28)-GI could not inhibit Aβ40 fibrillogenesis and cytotoxicity. Therefore, different kind of linkers between IAPP(8-18) and IAPP(22-28)-GI were applied here. The peptides were then studied with regard to their ability to interact with Aβ40 and to block fibrillogenesis and cytotoxicity.

3.4.1   Effects of peptides containing hydrophobic and hydrophilic linkers between IAPP(8-18) and IAPP(22-28)-GI on Aβ40 fibrillogenesis and cytotoxicity

Here, two hydrophobic and one hydrophilic linker were examined. The linker entity replaced the sequence SSN which links His^{18} and Asn^{22} in the native IAPP sequence (Fig. 34). The hydrophobic linkers were: 8-aminooctanoic acid (Aoc) and 10-aminodecanoic acid (Adc). In addition to their hydrophobicity, these linkers have the property that they are very flexible and do not engage in hydrogen bond formation. The Aoc-linker has a length comparable to the length of a tripeptide (in an extended conformation) while the Adc-linker has nearly a tetrapeptide length (Fig. 34inset). 8-Amino-3,6-dioxaoctanoic acid (PEG) was employed as a flexible and hydrophilic linker. This type of linker, which consists of polyethylene glycol, is known to be water-soluble and likely able to transfer its hydrophilicity to the connected sequence, thus decreasing the potential for aggregation and precipitation of the peptide

[189]. The length of the PEG spacer was similar to the length of an extended tripeptide (Fig. 34inset).
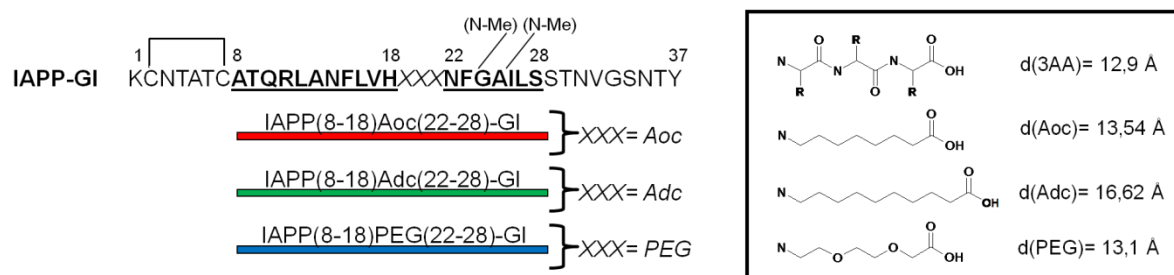

Fig. 34. Primary structure of IAPP-GI and schematic representation of the linked peptides sequences studied in this chapter: IAPP(8-18)Aoc(22-28)-GI (red), IAPP(8-18)Adc(22-28)-GI (green) and IAPP(8-18)PEG(22-28)-GI (blue). Domains suggested to be hot regions for the Aβ40-IAPP interaction interface are bold and underlined. (Inset) Structure and length of the linkers: a three amino acids long sequence in extended conformation, 8-aminooctanoic acid (Aoc), 10-aminodecanoic acid (Adc) and 8-amino-3,6-dioxaoctanoic acid (PEG).

The peptides were synthesized by solid phase peptide synthesis (SPPS) utilizing Fmoc-strategy. They were purified by RP-HPLC and MALDI mass spectrometry was used to determine their mass as shown in Table 12.

Table 12. Characterization of peptides synthesized by Fmoc-chemistry (C-terminal amides except IAPP(8-18)Aoc(22-28)-GI that was C-terminal acid) via their HPLC retention time (rt) and MS.

	HPLC prg.	rt (min)	[M+H]+ expected	[M+H]+ found
IAPP(8-18)Aoc(22-28)-GI	Fast	20,3´	2143	2143
IAPP(8-18)Adc(22-28)-GI	Fast	21,3´	2169	2169
IAPP(8-18)PEG(22-28)-GI	Fast	18,5´	2146	2146

To investigate if the interaction of the above peptides with Aβ40 could inhibit Aβ40 aggregation, incubations of Aβ40 in the absence or presence of the peptides (at 1/1) were performed and fibrillogenesis and cytotoxicity were assessed by ThT binding and MTT reduction assays. As shown in Fig. 35A, ThT fluorescence of Aβ40 alone started to increase after a lag-time of 48 h. This increase was followed by a plateau (at about 96-120 h) which indicated the end of the fibrillization process. In the presence of IAPP(8-18)Aoc(22-28)-GI and IAPP(8-18)PEG(22-28)-GI the ThT fluorescence also increased as Aβ40 alone. By contrast, in the presence of IAPP(8-18)Adc(22-28)-GI, Aβ40 fibrillogenesis was significantly delayed albeit not completely blocked. The other two analogues, IAPP(8-18)Aoc(22-28)-GI and IAPP(8-18)PEG(22-28)-GI, did not significantly affect Aβ40 fibrillogenesis. To examine if the interaction of these three peptides with Aβ40 could interfere with the formation of cytotoxic Aβ40 aggregates, aliquots of the 72 h aged incubations of the ThT binding assays

were added to PC-12 cells and cell viability was assessed by the MTT reduction assay (Fig. 35B). Aβ40 formed cytotoxic aggregates at 72 h and the mixtures with IAPP(8-18)Aoc(22-28)-GI and IAPP(8-18)PEG(22-28)-GI (at 1:1) were similarly cytotoxic. Thus, IAPP(8-18)Aoc(22-28)-GI and IAPP(8-18)PEG(22-28)-GI were unable to suppress formation of cytotoxic Aβ40 assemblies and fibrils. However, IAPP(8-18)Adc(22-28)-GI was found to partially inhibit formation of cytotoxic Aβ40 species at the 72 h incubation time point whereas no inhibitory affect was found at the incubation time point of 7 days (data not shown).

These results showed that peptides consisting of IAPP(8-18) and IAPP(22-28)-GI linked to each other by an hydrophobic linker such as Aoc or an hydrophilic linker such as PEG were not able to interfere with Aβ40 fibrillogenesis and cytotoxicity processes. On the other hand, IAPP(8-18)Adc(22-28)-GI partially inhibited formation of Aβ40 fibrils and cytotoxic aggregates, suggesting that the length of the linker may play an important role in the interaction with Aβ40.
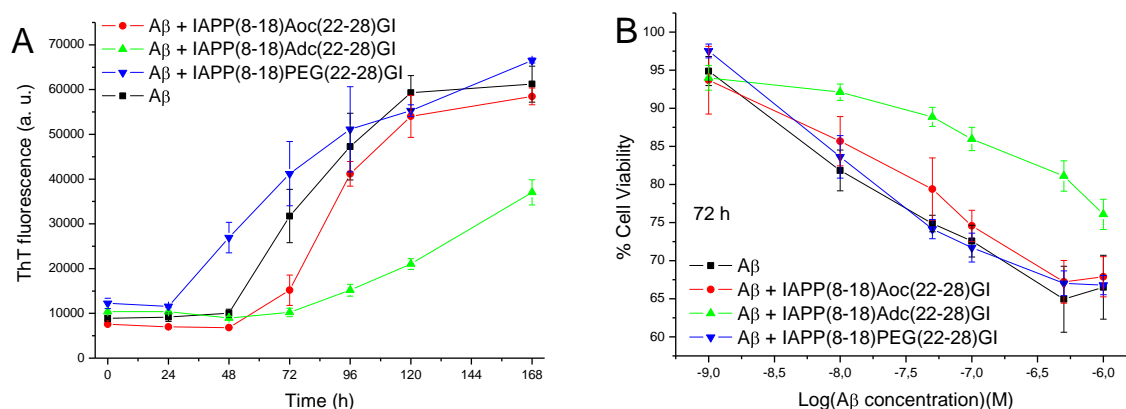

Fig. 35. Effect of the peptides IAPP(8-18)Aoc(22-28)-GI, IAPP(8-18)Adc(22-28)-GI and IAPP(8-18)PEG(22-28)-GI on Aβ40 fibrillogenesis and cytotoxicity. (A) Fibrillogenesis of Aβ40 alone (16.5 µM in 50 mM sodium phosphate buffer, pH 7.4, containing 100 mM NaCl and 1% HFIP) and of a mixtures of Aβ40 with the peptides (1:1) was followed by ThT binding assay. (B) Aβ40 and mixtures of Aβ40 with peptides (16.5 µM in 50 mM sodium phosphate buffer, pH 7.4, containing 100 mM NaCl and 1% HFIP) were incubated for 3 days. Aliquots were then diluted with cell culture medium and added to PC-12 cells at the indicated final concentrations. Following 24 h incubation at 37°C cell viabilities were assessed via the MTT reduction assay. Data are means (±SEM) of 3 assays (performed in triplicates).

Next, the conformations of the peptides were determined by far-UV CD spectroscopy. First, CD spectra of each peptide were measured at different peptide concentrations in aqueous solution (pH 7.4) to determine their aggregation propensity (Fig. 36A-C-E). Thereafter, the effect of increasing amounts of trifluoroethanol (TFE) on the peptide conformation was studied (Fig. 36B-D-F).

For the CD concentration dependence studies, peptides were dissolved in 10 mM sodium phosphate buffer, pH 7.4, containing 1% HFIP. At 5 µM IAPP(8-18)Aoc(22-28)-GI showed a minimum at around 200 nm which was indicative of random coil and a second minimum around 225 nm consistent of β-sheet/β-turn contents (Fig. 36A). At 10 µM, the CD spectrum exhibited a lower intensity at both 200 and 225 nm as compared to the spectrum at 5 µM whereas at 50 and 100 µM only the β-sheet minimum was still present though with lower intensity. This data suggested that IAPP(8-18)Aoc(22-28)-GI aggregates already at concentration above 5 µM into soluble β-sheets. The CD spectrum of IAPP(8-18)Adc(22-28)-GI, however, exhibited no random coil and was characterized by a clear β-sheet minimum at 217 nm (Fig. 36C). CD concentration dependence studies showed almost no signal at 50 µM peptide concentration. This data suggested that IAPP(8-18)Adc(22-28)-GI formed β-sheet aggregates already at 5 µM which then further aggregated into likely soluble oligomers already at 50 µM. Of note, the CD spectra of IAPP(8-18)Adc(22-28)-GI were indicative of a much higher β-sheet contents than the CD spectra of IAPP(8-18)Aoc(22-28)-GI. In fact, the value of the MRE at 225 nm of IAPP(8-18)Adc(22-28)-GI exhibited the double intensity than the one of IAPP(8-18)Aoc(22-28)-GI. By contrast, a completely different shape was observed in the spectra of IAPP(8-18)PEG(22-28)-GI as compared to the ones of the IAPP(8-18)Adc(22-28)-GI peptide and no concentration dependence was found up to 200 µM (Fig. 36F). The spectra of that peptide exhibited two minima at 197 and 227 nm which were indicative of random coil and β-sheet/β-turn contents. However, the concentration dependence studies in aqueous buffer of IAPP(8-18)PEG(22-28)-GI showed that there was no concentration dependence of the CD-spectra up to 200 µM. This data suggested that IAPP(8-18)PEG(22-28)-GI either did not aggregate or that it was a stable oligomer already at 10 µM. Taken together, the CD concentration dependence studies demonstrated that the difference between the linkers can strongly affect the conformation and the aggregation potential of the analogs. Next, TFE titration studies were performed and indicated that IAPP(8-18)Aoc(22-28)-GI and IAPP(8-18)Adc(22-28)-GI were able to populate α-helical states in part although the α-helix content was not higher than the one in aqueous buffer (Fig. 36B-D). These results suggested that the presence of the hydrophobic linker in IAPP(8-18)Aoc(22-28)-GI and IAPP(8-18)Adc(22-28)-GI does not favor an α-helical conformation which was in good agreement with the lack of hydrogen bond donor/acceptor moieties in these linkers. By contrast, the hydrophilic linker present in IAPP(8-18)PEG(22-28)-GI was found to significantly promote α-helix formation in TFE as compared to the CD spectrum in aqueous buffer (Fig. 36F).
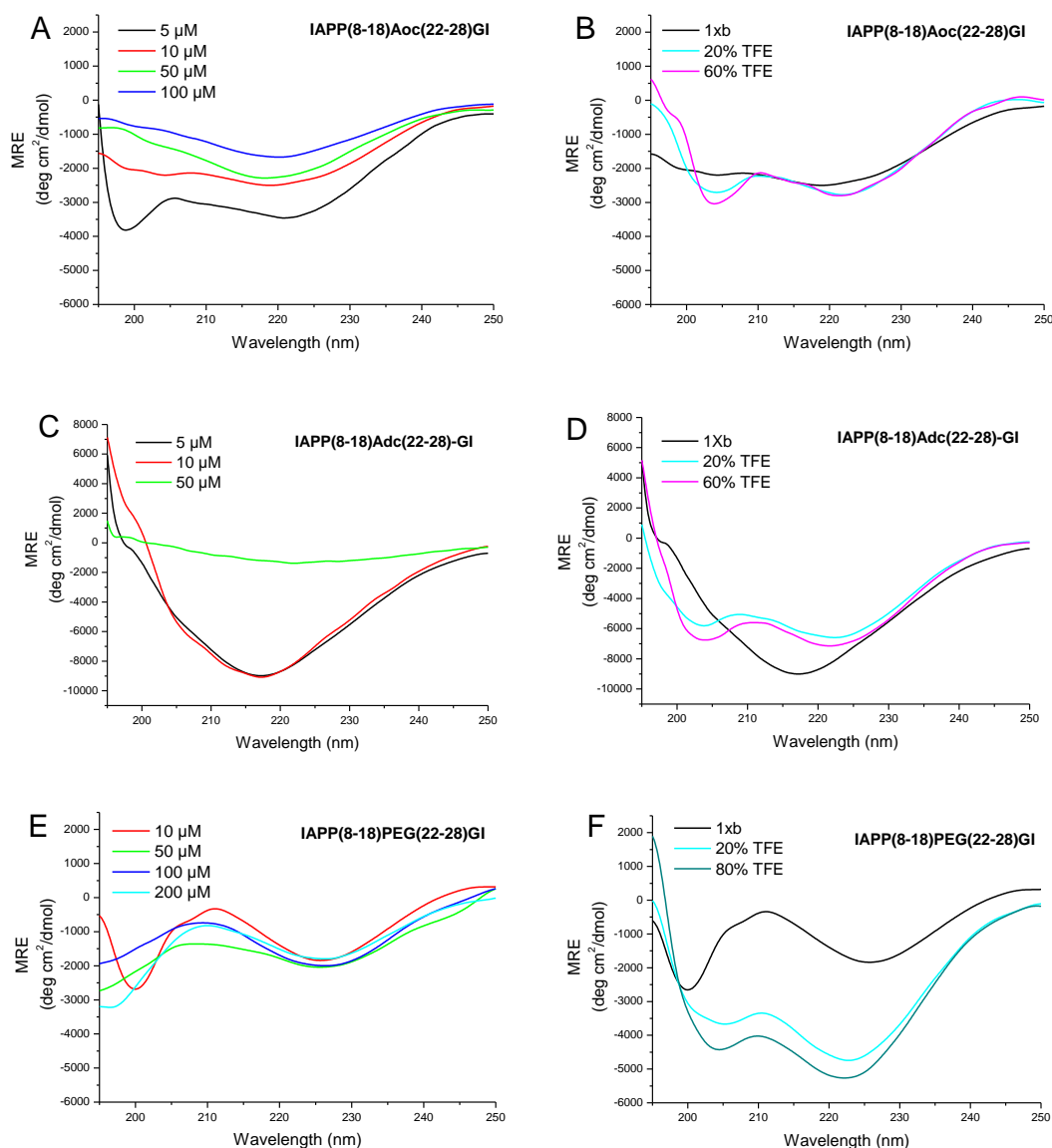
Fig. 36. Concentration dependence of the conformation of IAPP(8-18)Aoc(22-28)-GI (A), IAPP(8-18)Adc(22-28)-GI (C), IAPP(8-18)PEG(22-28)-GI (E) as assessed by far-UV spectroscopy. Experiments were performed at the indicated peptide concentration in 10 mM sodium phosphate buffer, pH 7.4, containing 1% HFIP. Effects of TFE on conformation of aqueous solution of IAPP(8-18)Aoc(22-28)-GI (B), IAPP(8-18)Adc(22-28)-GI (D), IAPP(8-18)PEG(22-28)-GI (F) assessed by far-UV spectroscopy. Experiments were performed at a peptide concentration of 10 μM in 10 mM sodium phosphate buffer, pH 7.4, containing 1% HFIP with the indicated amounts of TFE.

To characterize the affinity of the interaction of these peptides with Aβ40, IAPP and IAPP-GI, fluorescence titration binding assays were performed (Table 13). All three tested peptides bound Dac-Aβ40 and their apparent binding affinities were in the low micro- to the upper nanomolar range. Further, all three peptides were found to bind Fluo-IAPP and Fluo-IAPP-GI in the low micro- to upper nanomolar range. All tested peptides showed strong self-association constants in the low nanomolar range suggesting a high aggregation potential as also indicated by the results of CD studies. Concerning IAPP(8-18)PEG(22-28)-GI, the high

self-association propensity determined by fluorescence titration studies and the low aggregation potential found in the CD measurements would be consistent with the formation of only dimers or soluble low molecular weight oligomers in the nano- to low micromolar range.

Table 13. Apparent affinities (app. Kd) of interaction of IAPP(8-18)Aoc(22-28)-GI, IAPP(8-18)Adc(22-28)-GI and IAPP(8-18)PEG(22-28)-GI with Dac-Aβ40, Fluo-IAPP, Fluo-IAPP-GI and their N-terminal Fluo labeled form as determined by fluorescence titration binding assays. The measurements were carried out in 10 mM sodium phosphate buffer, pH 7.4, 1% HFIP and at room temperature. The concentration of the fluorescently labeled peptide was 10 nM for Dac-Aβ40 and 5 nM for the Fluo-peptide. $K_{d,app}$ values were determined from one or three binding curves (± SEM where indicated).

	Dac-Aβ40	Fluo-IAPP	Fluo-IAPP-GI	Self-Ass.
IAPP(8-18)Aoc(22-28)-GI	430 nM	489 nM	642 nM	84 nM
IAPP(8-18)Adc(22-28)-GI	754 nM	1,45 µM	87 nM	76 nM
IAPP(8-18)PEG(22-28)-GI	1,2 µM	363 nM	110 nM	36 nM

3.4.2 Effects of peptides containing sequences of three amino acids as linkers between IAPP(8-18) and IAPP(22-28)-GI on Aβ40 fibrillogenesis and cytotoxicity

To investigate further the effects of differences between the linkers of the two hot regions, IAPP(8-18) and IAPP(22-28)-GI, a systematic study on analogues containing linkers with differences with regard to steric hindrance and hydrophobicity was performed. Linkers consisted of three amino acids to ensure the presence of the same number of possible H-bond donor/acceptor moieties as in the natively occurring IAPP(19-21) (SSN) peptide sequence. Thereby, the IAPP(19-21) sequence was substituted by different tripeptide units in order to yield linkers with gradually increased steric effect as well as hydrophobicity. Accordingly, sequence SSN was replaced by a sequence consisting of three glycines (no side chain), three alanines (simple hydrophobic side chain), three valines (β-branched chain), or three leucines (γ-branched chain) (Fig. 37). On the basis of their hydropathy index the above residues are on the following row: Gly (-0,4)< Ala (1,8) < Leu (3,8) ≤ Val (4,2) [190].
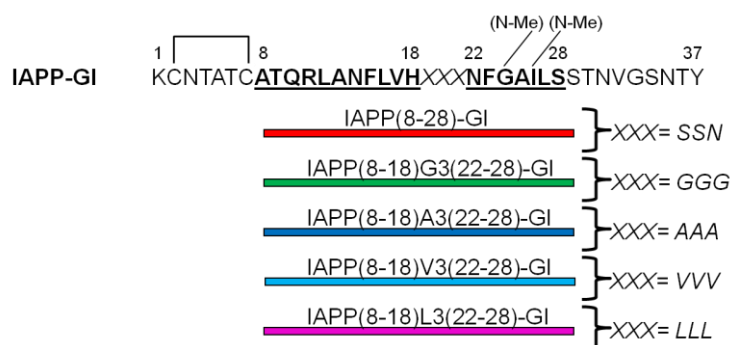
Fig. 37. Primary structure of IAPP-GI. Domains suggested to be hot regions of the Aβ40-IAPP interaction interface are bold and underlined. Designed peptide studied in this chapter: IAPP(8-28)-GI (red), IAPP(8-18)G3(22-28)-GI (green), IAPP(8-18)A3(22-28)-GI (blue), IAPP(8-18)V3(22-28)-GI (cyan) and IAPP(8-18)L3(22-28)-GI (magenta).

Peptides were synthesized by solid phase peptide synthesis (SPPS) utilizing Fmoc-strategy. They were purified by HPLC and MALDI mass spectrometry was used to determine their mass as shown in Table 14.

Table 14. Characterization of peptides synthesized by Fmoc-chemistry (C-terminal amides) via their HPLC retention time (rt) and MS.

	HPLC prg.	rt (min)	$[M+H]^+$ expected	$[M+H]^+$ found
IAPP(8-28)-GI	Fast	19´	2288	2287
IAPP(8-18)G3(22-28)-GI	Fast	18,7´	2171	2171
IAPP(8-18)A3(22-28)-GI	Slow	24,1´	2213	2213
IAPP(8-18)V3(22-28)-GI	Fast	21,5´	2298	2298
IAPP(8-18)L3(22-28)-GI	Slow	23,3´	2340	2340

Next, the question was addressed whether the IAPP(8-28)-GI analogs could intervene with Aβ self-assembly into fibrils and affect formation of cytotoxic Aβ40 aggregates. Aβ40 alone (16.5 µM, pH 7.4) and the mixture of Aβ40 with these peptides (16.5 µM each, pH 7.4) were incubated for 7 days and fibrillogenesis and cytotoxicity were followed by the ThT binding and the MTT reduction assay (Fig. 38). According to the ThT binding assay, Aβ40 fibrillogenesis exhibited a lag-time of ~48 h and reached completion at 96 h (Fig. 38A). In chapter 3.3.1, it was shown that IAPP(8-28)-GI and IAPP(8-18)G3(22-28)-GI cannot block Aβ40 fibril formation while IAPP(8-18)A3(22-28)-GI can inhibit Aβ40 fibrillogenesis. In the presence of IAPP(8-18)V3(22-28)-GI and IAPP(8-18)L3(22-28)-GI, Aβ40 fibrillogenesis was also nearly completely suppressed.

To evaluate the effect of these peptides on formation of cytotoxic Aβ40 aggregates, the peptide incubations which were use for ThT assay were added to the PC-12 cells at various time points of incubation (between 0 h and 7 days) and cell viabilities were assessed by the MTT reduction assay. Aβ40 alone was not toxic when added to the cells immediately after solution preparation (data not shown). Aβ40 cytotoxicity increased, however, within 72 h and reached a maximum after 7 days of incubation (Fig. 38B-C). As already mentioned (chapter 3.3.1) IAPP(8-28)-GI and IAPP(8-18)G3(22-28)-GI did not inhibit 72 h aged Aβ40 cytotoxicity while IAPP(8-18)A3(22-28)-GI partially inhibited. The 72 h aged mixture of Aβ40 with IAPP(8-18)V3(22-28)-GI also was significantly less toxic then 72 h aged Aβ40 (Fig. 38B). Moreover, in the presence of IAPP(8-18)L3(22-28)-GI a complete suppression of Aβ40 cytotoxicity was

observed at 72 h of incubation (Fig. 38B). The MTT assay at 7 days of incubation revealed that the inhibitory effect of IAPP(8-18)A3(22-28)-GI and IAPP(8-18)V3(22-28)-GI observed at 72 h of incubation did not last in the 7 days aged mixtures (Fig. 38C). By contrast, in the presence of IAPP(8-18)L3(22-28)-GI, a complete suppression of Aβ40 cytotoxicity was observed after 7 days of incubation (Fig. 38C). These results gave a clear hint about the structural requirements of the tripeptide sequence between the hot regions with regard to inhibition of Aβ40 fibrillogenesis and cytotoxicity. In particular, the inhibitory capacity of the IAPP(8-28)-GI analogs appeared to considerably improve by increasing the steric hindrance and hydrophobicity of the side chain of the three amino acids, linking the two IAPP hot regions. These results suggest that the effectiveness of the inhibitor depends completely on the nature of the linker connecting IAPP(8-18) and IAPP(22-28)-GI.
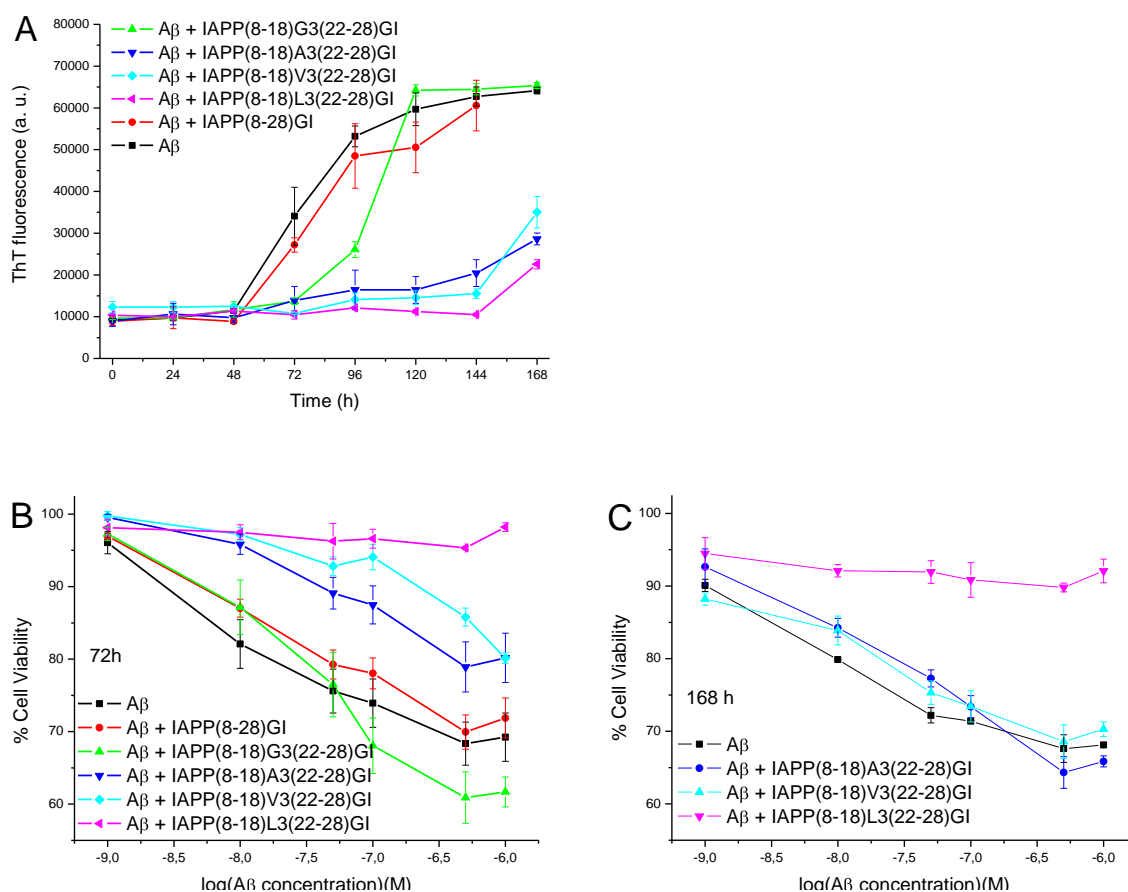

Fig. 38. Effect of the peptides IAPP(8-28)-GI, IAPP(8-18)G3(22-28)-GI, IAPP(8-18)A3(22-28)-GI, IAPP(8-18)V3(22-27)-GI and IAPP(8-18)L3(22-28)-GI on Aβ40 cytotoxicity and fibrillogenesis. (A) Fibrillogenesis of Aβ40 (16.5 μM in 50 mM sodium phosphate buffer, pH 7.4, containing 100 mM NaCl and 1% HFIP) and of 1:1 mixtures of Aβ40 with peptides as indicated was followed by the ThT binding assay. (B) Aβ40 and mixtures of Aβ40 with peptides (16.5 μM in 50 mM sodium phosphate buffer, pH 7.4, containing 100 mM NaCl and 1% HFIP) were incubated for 3 days. Aliquots were then diluted with cell culture medium and added to PC-12 cells at the indicated final concentrations. Following 24 h incubation at 37°C cell viabilities were assessed via the MTT reduction assay. (C) Aβ40-peptide mixtures which were found to inhibit at the incubation time point of 3 days

incubation were added to PC-12 cells at the time point of 7 days. Cell viabilities were determined as under (B). Data are means (±SEM) of 3 assays (performed in triplicates).

Next, far UV-CD was used to study the conformation of the above IAPP(8-28)-GI analogs. Peptides were dissolved in 10 mM sodium phosphate buffer, pH 7.4, containing 1% HFIP and CD spectra were measured immediately thereafter. To determine the aggregation propensity of these peptides in aqueous solution, CD spectra were measured at different peptide concentrations (Fig. 39). It was previously shown (3.3.1), that IAPP(8-28)-GI, IAPP(8-18)G3(22-28)-GI and IAPP(8-18)A3(22-28)-GI exhibited a pronounced minimum around 200 nm indicative of random coil and a second minimum around 225 nm indicative of β-sheet- and/or β-turn (Fig. 39A-C-D). These three peptides formed soluble aggregates at a concentration of 100 µM as indicated by the observed CD signal loss. By contrast, IAPP(8-18)V3(22-28)-GI and IAPP(8-18)L3(22-28)-GI showed even at very low concentrations such as 1 µM predominantly a minimum around 220 nm which was typical of β-sheet conformation and only a very weak random coil signal at 200 nm (Fig. 39E-F). When increasing the peptide concentration to 5 or 10 µM, a red shift of the β-sheet minimum to 228 nm was observed, most likely characteristic of β-sheet oligomer formation [191]. In addition, a maximum around 200 nm was detected indicating β-sheet formation. Both peptides exhibited a very low signal at 50 µM suggesting that IAPP(8-18)V3(22-28)-GI and IAPP(8-18)L3(22-28)-GI had higher aggregation propensity as compared to IAPP(8-28)-GI, IAPP(8-18)G3(22-28)-GI and IAPP(8-18)A3(22-28)-GI. In Fig. 39B the MREs of the peptides at 200 nm (n → π*) and at 225 nm (π → π*) at 10 µM concentration are presented. Interestingly, the CD signal at 200 nm is negative for IAPP(8-28)-GI, IAPP(8-18)G3(22-28)-GI and IAPP(8-18)A3(22-28)-GI indicating the presence of unordered structure mainly. The highest amount of random coil content was reached by IAPP(8-18)A3(22-28)-GI. By contrast, the CD signal at 200 nm is positive for IAPP(8-18)V3(22-28)-GI and IAPP(8-18)L3(22-28)-GI indicating β-sheet structure. Thereby, the highest amount was reached by IAPP(8-18)L3(22-28)-GI. The amount of β-sheet/β-turn contents at 225 nm was higher for IAPP(8-18)A3(22-28)-GI, IAPP(8-18)V3(22-28)-GI and IAPP(8-18)L3(22-28)-GI than IAPP(8-28)-GI, IAPP(8-18)G3(22-28)-GI. In conclusion, the CD data indicate significant changes in peptide conformation when the hydrophobicity of the side chain of the linkers (GGG < AAA << LLL ≤ VVV) is increased. It appears, thus, that the hydrophobic tripeptide linkers IAPP(8-18)V3(22-28)-GI and IAPP(8-18)L3(22-28)-GI promote mainly the formation of β-sheet conformers.
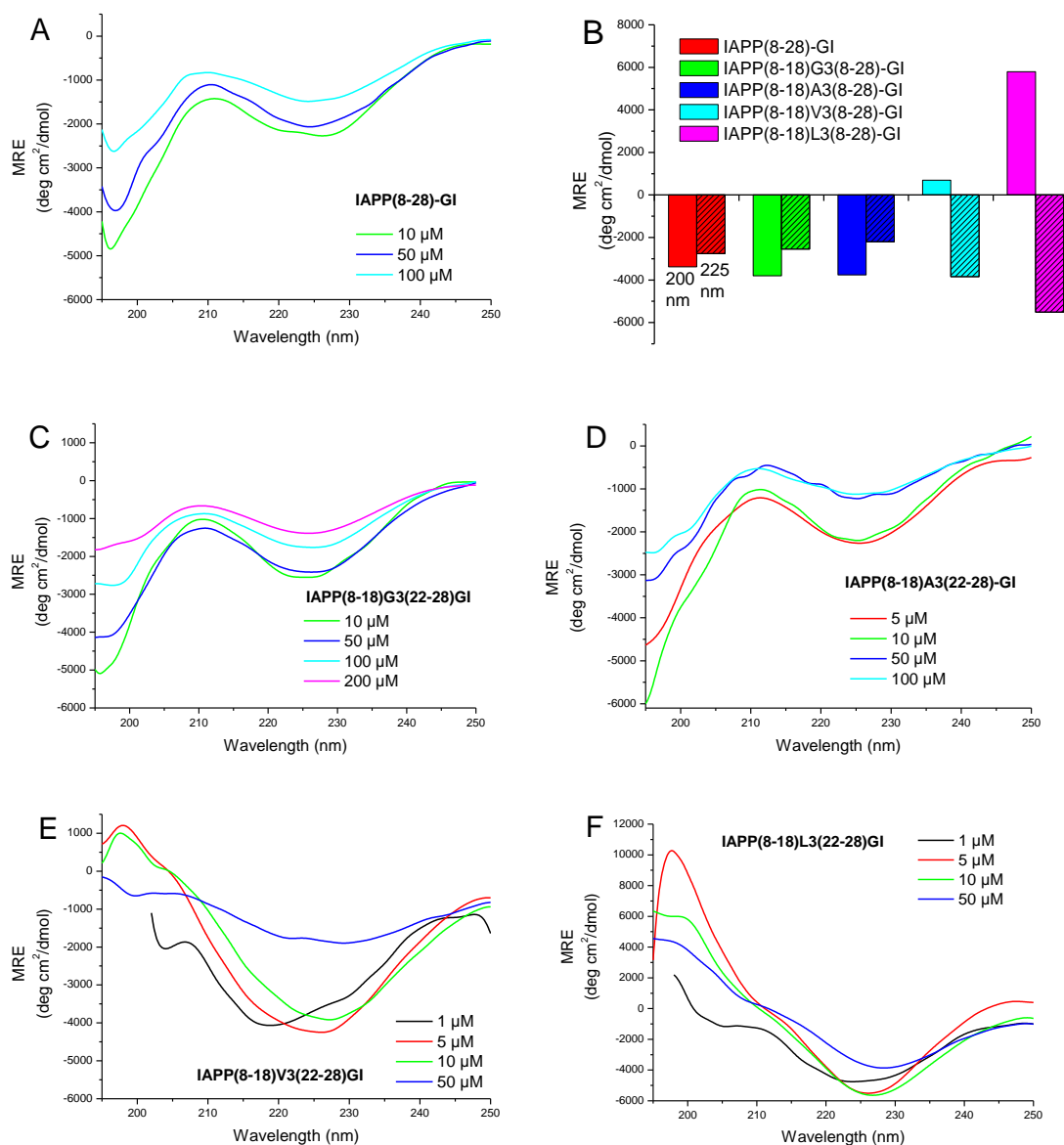
Fig. 39. Concentration dependence of the conformation of IAPP(8-28)-GI (A), IAPP(8-18)G3(22-28)-GI (B), IAPP(8-18)A3(22-28)-GI (C), IAPP(8-18)V3(22-28)-GI (D) and IAPP(8-18)L3(22-28)-GI (E) as assessed by far-UV spectroscopy. Experiments were performed at the indicated peptide concentration in 10 mM sodium phosphate buffer, pH 7.4, containing 1% HFIP. (B) MRE at 200 nm (no pattern) and at 225 nm (striped pattern) for each of the peptides at 10 µM.

Next, the effects of trifluoroethanol (TFE) on the conformation of the above peptides were investigated. As mentioned above, the CD spectra of the peptides when examined in pure aqueous 10 mM sodium phosphate buffer (1% HFIP) indicated significant differences between the conformations depending on the nature of the linker between the two hot regions. By increasing the TFE concentration, strong CD changes were observed which were indicative of α-helix formation (two minima around 208 nm and 222 nm) (Fig. 40). All peptides populated significant amounts of α-helical conformations already at 20% TFE. The

results of the TFE titrations suggested formation of different amounts of helix depending on the linker sequence (Fig. 40B). In particular, IAPP(8-18)G3(22-28)-GI showed the poorest helix propensity in good agreement with the fact that α-helix is entropically expensive for Gly [186]. IAPP(8-18)A3(22-28)-GI and IAPP(8-18)L3(22-28)-GI exhibited the highest helix propensity consistent with the well-known α-helical propensity of Ala and Leu [186]. IAPP(8-28)-GI, IAPP(8-18)V3(22-28)-GI had a intermediate helix forming propensity. Taken together, the results of MTT assays, ThT assays, and CD studies suggested that the inhibitory capacity improved by increasing the steric effect and the hydrophobicity of the linker. Additionally, the peptides which inhibited Aβ40 fibrillogenesis and cytotoxicity were found to be able to form similar and significant amounts of α-helix under TFE-α-helix inducing conditions.
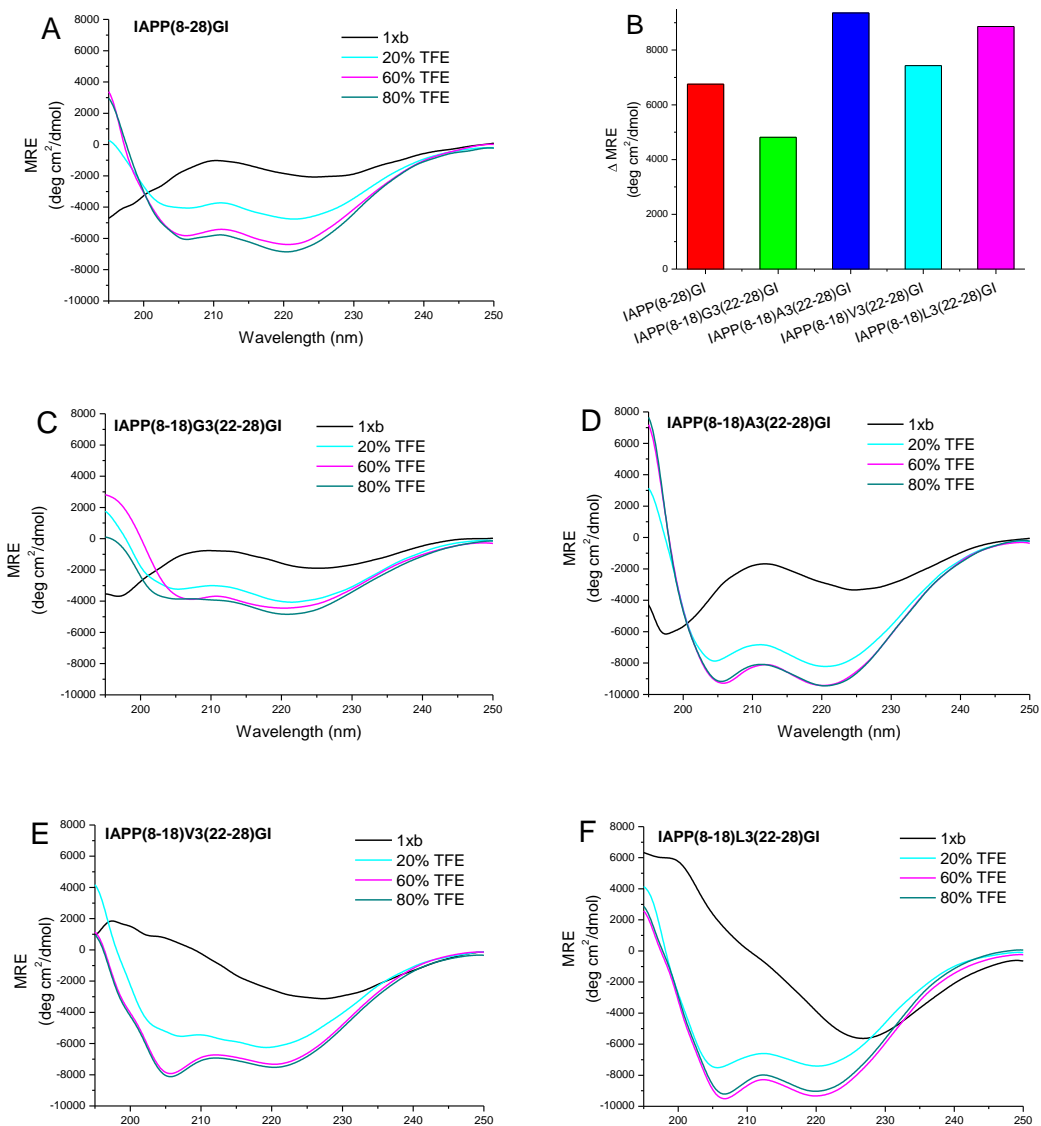

Fig. 40. Effects of TFE on conformation of aqueous solutions of IAPP(8-28)-GI (A), IAPP(8-18)G3(22-28)-GI (C), IAPP(8-18)A3(22-28)-GI (D), IAPP(8-18)V3(22-28)-GI (E) and IAPP(8-18)L3(22-28)-GI (F) assessed by far-UV

spectroscopy. Experiments were performed at a peptide concentration of 10 µM in 10 mM sodium phosphate buffer, pH 7.4, containing 1% HFIP with the indicated amounts of TFE. (B) Plot of the difference between the MRE in pure acqueus buffer and the MRE in 80% TFE (maximal helix form) at 222 nm of the CD spectra in (A)(C)(D)(E)(F).

Next, a fluorescence titration assays were used to determine whether different binding affinities to Aβ40 may correlate with the different inhibitory effects of these peptides on Aβ40 fibril formation and cytotoxicity. In addition, the binding affinities of the peptides to IAPP (IAPP-GI) and to themselves were also examined (Table 15). All tested peptides were found to bind Dac-Aβ40 and their binding affinities were in the low micro- to submicromolar range. The strongest Aβ40 ligands were IAPP(8-28)-GI ($K_{d,app}$= 196±20 nM) and IAPP(8-18)A3(22-28)-GI ($K_{d,app}$= 49 nM). The other peptides bound Dac-Aβ40 in the micromolar range: IAPP(8-18)G3(22-28)-GI ($K_{d,app}$= 1 µM), IAPP(8-18)V3(22-28)-GI ($K_{d,app}$= 794 nM) and IAPP(8-18)L3(22-28)-GI ($K_{d,app}$= 635±32 nM). These results, together with the results of the MTT and ThT assays, suggested that there is not a correlation between binding affinities to Dac-Aβ40 and ability to inhibit Aβ40 aggregation and cytotoxicity.

The above mentioned peptides also bound Fluo-IAPP and Fluo-IAPP-GI with low nanomolar affinities except for IAPP(8-18)G3(22-28)-GI that bound with an affinity in the upper nanomolar range.

Table 15. Apparent affinities (app. Kd) of interaction of IAPP(8-28)-GI, IAPP(8-18)G3(22-28)-GI, IAPP(8-18)A3(22-28)-GI, IAPP(8-18)V3(22-28)-GI and IAPP(8-18)L3(22-28)-GI with Dac-Aβ40, Fluo-IAPP, Fluo-IAPP-GI and their N-terminal Fluo labeled form as determined by fluorescence titration binding assays. The measurements were carried out in 10 mM sodium phosphate buffer, pH 7.4, 1% HFIP and at room temperature. The concentration of the fluorescent labeled peptide was 10 nM for Dac-Aβ40 and 5 nM for Fluo-peptide. $K_{d,app}$ values were determined from one or three binding curves (± SEM where indicated).

	Dac-Aβ40	Fluo-IAPP	Fluo-IAPP-GI	Self-Ass.
IAPP(8-28)-GI	196±20 nM	195 nM	126 nM	71±10 nM
IAPP(8-18)G3(22-28)-GI	1 µM	913 nM	615 nM	91 nM
IAPP(8-18)A3(22-28)-GI	49 nM	24 nM	393 nM	2,7 µM
IAPP(8-18)V3(22-28)-GI	794 nM	95 nM	61 nM	283 nM
IAPP(8-18)L3(22-28)-GI	635±32 nM	61 nM	43 nM	378 nM

3.4.3 Effects of peptides containing constrained linkers between IAPP(8-18) and IAPP(22-28)-GI on Aβ40 fibrillogenesis and cytotoxicity

The results of the previous chapter (3.4.2) indicated that the inhibitory potency of the hot regions IAPP(8-18) and IAPP(22-28)-GI improved as a consequence of increasing the steric hindrance of the linker which might be related to a specific conformation of the strand-turn-

strand structure of these analogues. It could be possible, for example, that the steric effect/hydrophobicity of the linker contributed to stabilize IAPP(8-18) and IAPP(22-28)-GI in a specific strand-turn-strand conformation which is required for inhibition of Aβ40 aggregation and toxicity. To prove this hypothesis, peptides containing covalently constrained linkers were designed (Fig. 41). The most potent inhibitor identified in this work so far, IAPP(8-18)L3(22-28)-GI, was used as a template and an analogue was designed which was "forced" to adopt a turn structure between the 18th and 22nd amino acid position (Fig. 41). In this analogue, IAPP(8-18)L3(22-28)-GI-cyclo, whose side chains were covalently linked via amide bond formation, residues His^{18} and Asn^{22} of the native IAPP sequence were substituted with 2,3-diaminopropionic acid (Dap) and aspartic acid (Asp), respectively. Of note, the amino acids at the 18th and 22nd positions were chosen to be substituted based on the findings of Ala-scan studies (unpublished results of our group). In fact, [A^{18}]-IAPP(8-18) and [A^{22}]-IAPP(22-28)-GI showed similar binding affinities to Aβ40 as the respective non-substituted sequences. However, to obtain direct evidence that the substitution did not affect the properties of the peptide, the same peptide with the two substitutions at the 18th and 22nd positions but without a covalent link between the side chains IAPP(8-18)L3(22-28)-GI-linear was also synthesized and tested (Fig. 41). Furthermore, a peptide whose linker would be unable to bend was also designed. For this purpose, a rigid linker consisting of p-aminobenzoic acid (Ab) and p-aminomethylbenzoic acid (Amb) was used and IAPP(8-18)Amb-Ab(22-28)-GI was designed and synthesized (Fig. 41) [192]. Additionally, a sequence containing this type of linker would be able to form hydrogen bonds and also retain the distance between the two hot regions as in IAPP(8-28)-GI.
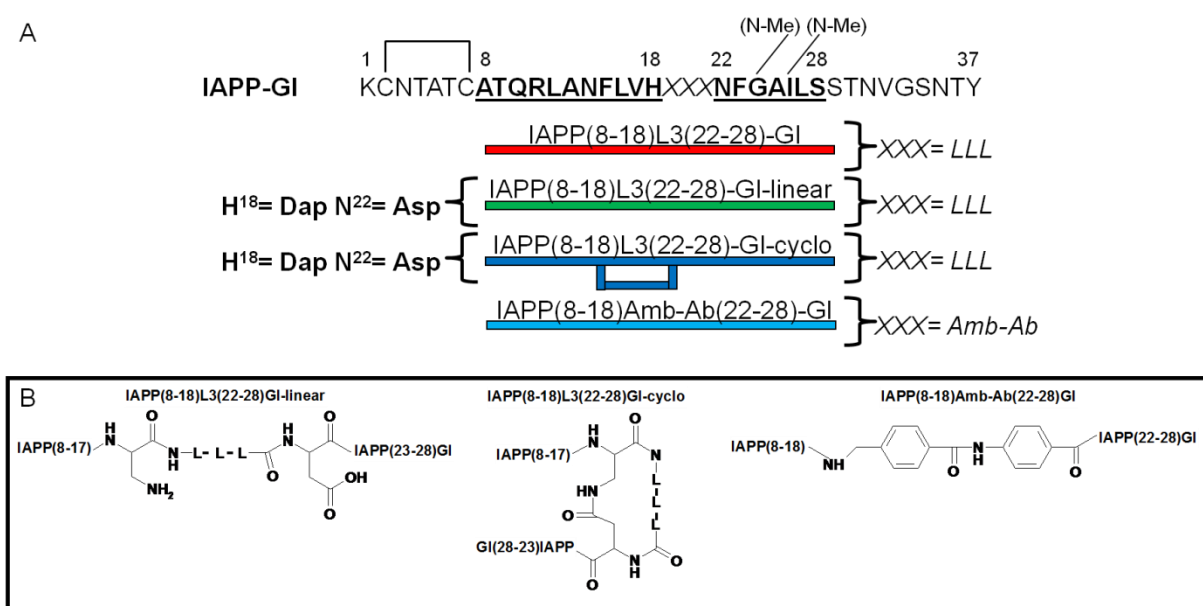

Fig. 41. (A) Primary structure of IAPP-GI. Domains suggested to be hot regions of the Aβ40-IAPP interaction interface are bold and underlined. Schematic presentation of designed inhibitors studied in this chapter: IAPP(8-

18)L3(22-28)-GI (red), IAPP(8-18)L3(22-28)-GI-linear (green), IAPP(8-18)L3(22-28)-GI-cyclo (blue) and IAPP(8-18)Amb-Ab(22-28)-GI (cyan). (B) Chemical structures of the loop region of the three peptides: IAPP(8-18)L3(22-28)-GI-linear, IAPP(8-18)L3(22-28)-GI-cyclo, and IAPP(8-18)Amb-Ab(22-28)-GI.

Peptides were synthesized by solid phase peptide synthesis (SPPS) utilizing Fmoc-strategy. They were purified by HPLC and MALDI mass spectrometry was used to determine their mass as shown in Table 16.

Table 16. Characterization of peptides synthesized by Fmoc-chemistry (C-terminal amides) via their HPLC retention time (rt) and MS.

	HPLCprg.	rt (min)	[M+H]⁺ expected	[M+H]⁺ found
IAPP(8-18)L3(22-28)-GI-linear	Fast	19,5´	2271	2271
IAPP(8-18)L3(22-28)-GI-cyclo	Fast	26´	2289	2288
IAPP(8-18)Amb-Ab(22-28)-GI	Fast	19,5´	2252	2251

Next, the effects of the peptides on Aβ40 self-assembly were studied. Aβ40 was incubated alone or with IAPP(8-18)L3(22-28)-GI, IAPP(8-18)L3(22-28)-GI-linear, IAPP(8-18)L3(22-28)-GI-cyclo and IAPP(8-18)Amb-Ab(22-28)-GI at 1/1. Fibrillization of Aβ40 versus the mixtures was followed via the ThT binding assay and cytotoxicities were assessed by the MTT reduction assay at various time points (Fig. 42). According to the ThT binding assay (Fig. 42A), IAPP(8-18)L3(22-28)-GI-linear blocked fibril formation with a similar potency to IAPP(8-18)L3(22-28)-GI confirming that the two substitutions did not strongly affect the properties of the peptide. On the other hand, IAPP(8-18)L3(22-28)-GI-cyclo could only delay Aβ40 fibrillogenesis by 24 h but did not block it, consistent with a strong difference between the interactions of IAPP(8-18)L3(22-28)-GI and IAPP(8-18)L3(22-28)-GI-cyclo with Aβ40. The peptide with the rigid linker, IAPP(8-18)Amb-Ab(22-28)-GI only weakly suppressed fibril formation. To evaluate the potencies of the inhibitory effects of these analogues on formation of cytotoxic Aβ40 aggregates, aliquots of the mixture of Aβ40 with each of them and of Aβ40 alone (16.5 µM) (solutions used for the ThT binding) were added to PC-12 cells at 72 h and 7 days and cell viabilities were determined. Aβ40 alone was not toxic when added to the cells immediately after solution preparation (data not shown). After 72 h of incubation Aβ40 cytotoxicity increased and the mixture of Aβ40 with IAPP(8-18)L3(22-28)-GI-cyclo was found to be nearly as toxic as the 72 h aged Aβ40 alone (Fig. 42B). By contrast, the mixtures of Aβ40 with IAPP(8-18)L3(22-28)-GI-linear and with IAPP(8-18)L3(22-28)-GI were not cytotoxic (Fig. 42B). When Aβ40 was mixed with IAPP(8-18)Amb-Ab(22-28)-GI (at 1/1) no cytotoxic Aβ40 species were found to be present after 72h of incubation (Fig. 42B). The effects of these analogs on Aβ40 toxicity was further tested at the time point of 168 h

incubation (Fig. 42C). In the presence of IAPP(8-18)Amb-Ab(22-28)-GI and IAPP(8-18)L3(22-28)-GI-linear, formation of cytotoxic Aβ40 species was strongly suppressed while in the presence of IAPP(8-18)L3(22-28)-GI-cyclo the formation of cytotoxic Aβ40 species in the mixture was similar to Aβ40 alone. Taken together, these results showed that: a) IAPP(8-18)L3(22-28)-GI-cyclo corresponding to IAPP(8-18)L3(22-28)-GI containing a covalently constrained turn structure entirely its inhibitory capacity as compared to IAPP(8-18)L3(22-28)-GI, b) the designed IAPP(8-18)Amb-Ab(22-28)-GI with the rigid extended linker was a very effective inhibitor.
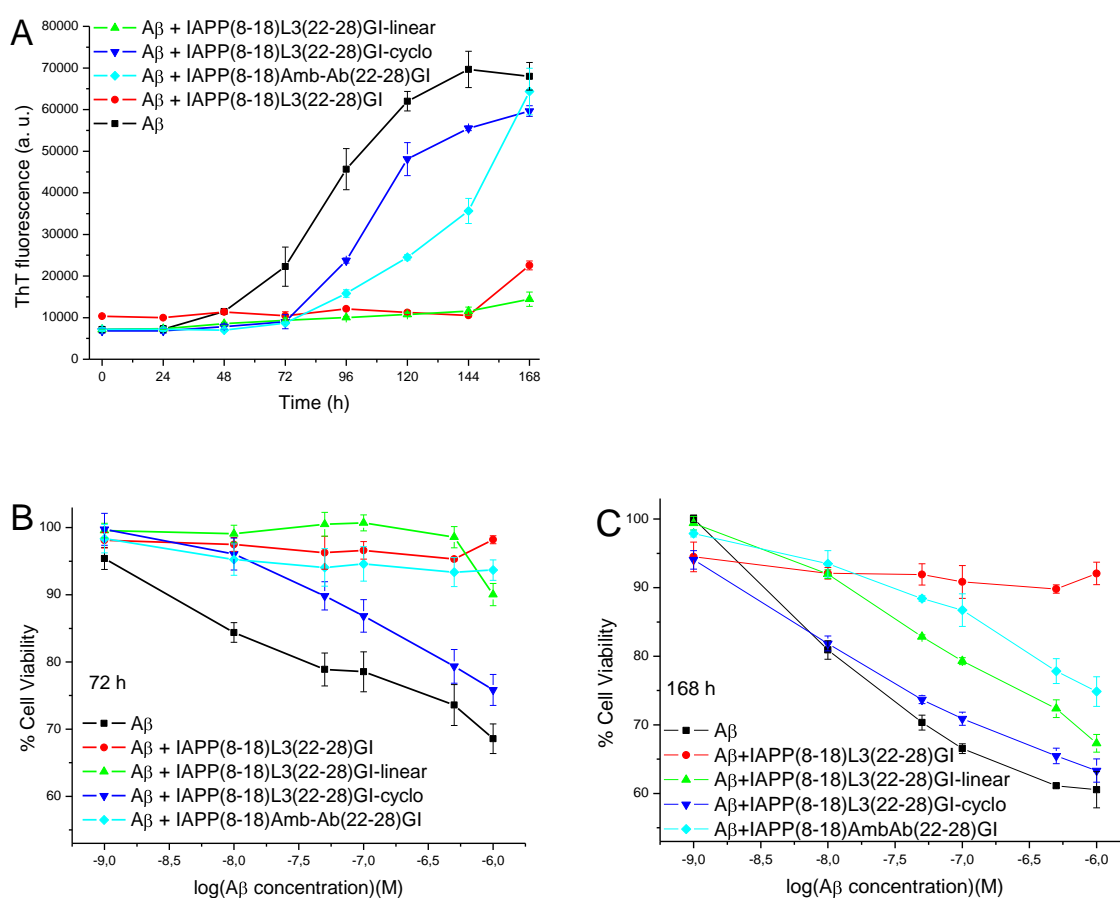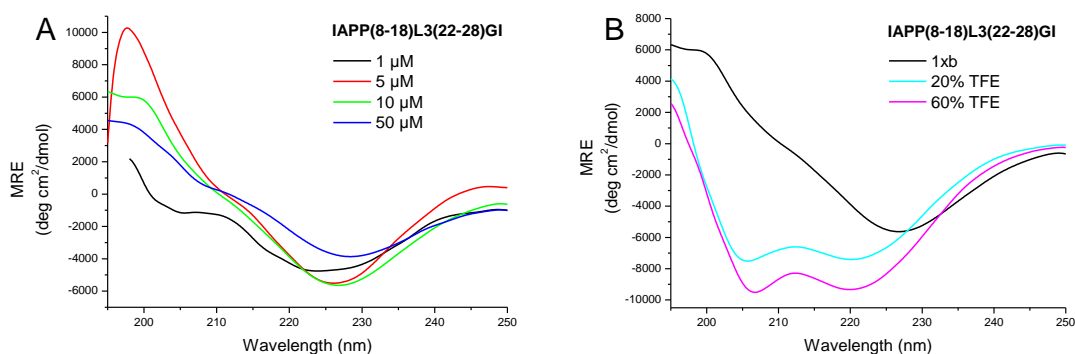

Fig. 42. Effect of IAPP(8-18)L3(22-28)-GI, IAPP(8-18)L3(22-28)-GI-linear, IAPP(8-18)L3(22-28)-GI-cyclo and IAPP(8-18)Amb-Ab(22-28)-GI on Aβ40 fibrillogenesis and cytotoxicity. (A) Fibrillogenesis of Aβ40 (16.5 μM in 50 mM sodium phosphate buffer, pH 7.4, containing 100 mM NaCl and 1% HFIP) and of a mixture of Aβ40 and peptides (1:1) was followed by the ThT binding assay. (B) MTT reduction assay of Aβ40 and a mixture of Aβ40 with peptides (16.5 μM in 50 mM sodium phosphate buffer, pH 7.4, containing 100 mM NaCl and 1% HFIP) after 3 days incubation. (C) MTT assay of Aβ40 and of the above used mixtures of Aβ40 with peptides at the 7 days incubation time point.

Next, the conformation of the above peptides was determined by far-UV CD spectroscopy (Fig. 43). For these measurements, peptides were dissolved in aqueous buffer (pH 7.4) and CD spectra were measured at several peptide concentrations. As already shown (3.4.2),

IAPP(8-18)L3(22-28)-GI exhibited even at 1 µM a main minimum around 223 nm which could be due to β-sheet/β-turn conformation and only a weak random coil signal at 200 nm; 5 and 10 µM exhibited mainly β-sheet conformation while at 50 µM a significant signal loss was observed likely due to aggregation (Fig. 43A). The spectra of IAPP(8-18)L3(22-28)-GI-linear were similar to the ones of IAPP(8-18)L3(22-28)-GI indicating that the substitution of the two amino acids at positions 18 and 22 did not affect the overall conformation and assembly properties of the peptide (Fig. 43C). Concentration-dependence CD studies showed that IAPP(8-18)L3(22-28)-GI-cyclo populated at 1 µM random coil and β-sheet/β-turn conformation but further aggregated already at 10 µM into β-sheet oligomers (Fig. 43E). In fact the cyclic conformational constraint in IAPP(8-18)L3(22-28)-GI-cyclo should favor the formation of a β-sheet structure. The CD spectrum of IAPP(8-18)Amb-Ab(22-28)-GI indicated the presence of random coil and β-sheet conformation only at 1 µM while the spectra corresponding to the 5 and 10 µM peptide concentration were indicative of predominantly β-sheet contents. At 50 µM the signal was very weak consistent with the formation of a soluble oligomeric structure (Fig. 43G). Of note, no further speculations can be made on the conformational studies of IAPP(8-18)Amb-Ab(22-28)-GI since it is known that aromatic contribution can mix the optical transition [193].

Next, the effects of trifluoroethanol (TFE) on the conformation of the above peptides were investigated. The linear control peptide, IAPP(8-18)L3(22-28)-GI-linear, showed a typical increase of the signal with minima indicative of α-helical conformation already at 20% TFE (Fig. 43B). A similar conformational transition was observed for IAPP(8-18)L3(22-28)-GI (Fig. 43D). By contrast, TFE was not able to induce α-helical conformation in the cyclic peptide, IAPP(8-18)L3(22-28)-GI-cyclo, that adopted mainly a random coil structure (minimum at 200 nm) with a β-sheet/β-turn component (minimum at 220-225 nm) (Fig. 43F). TFE appeared to induce random coil rather than α-helix in IAPP(8-18)Amb-Ab(22-28)-GI (Fig. 43H). Both peptides, IAPP(8-18)L3(22-28)-GI-cyclo and IAPP(8-18)Amb-Ab(22-28)-GI, exhibited a distinct behavior in the presence of TFE most likely due to the presence of the conformational constraints (respectively cyclization and rigid linkers).
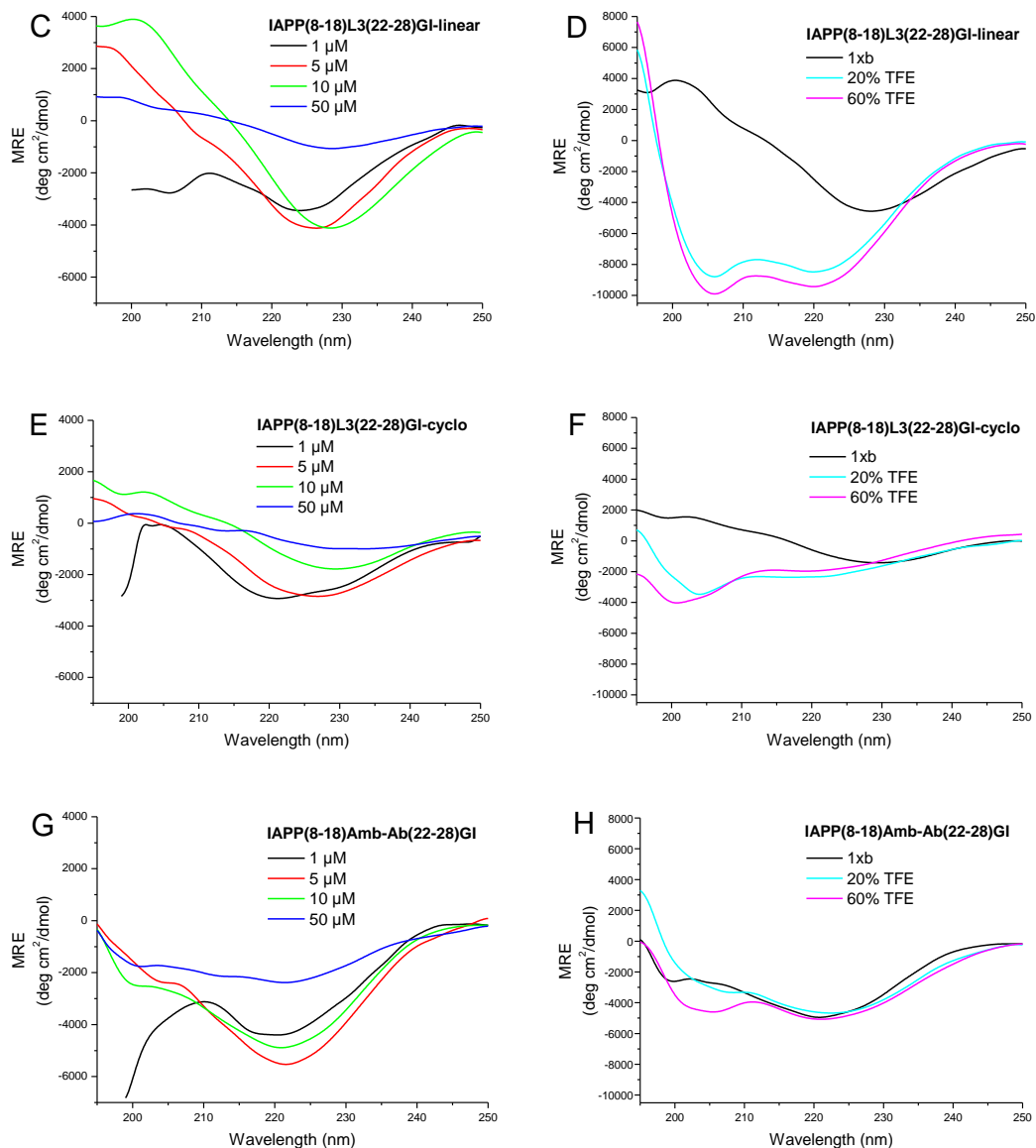
Fig. 43. Concentration dependence of the conformation of IAPP(8-18)L3(22-28)-GI (A), IAPP(8-18)L3(22-28)-GI-linear (C), IAPP(8-18)L3(22-28)-GI-cyclo (E), IAPP(8-18)Amb-Ab(22-28)-GI (G) assessed by far-UV CD spectroscopy. Measurements were performed in solutions of the peptides in 10 mM sodium phosphate buffer, pH 7.4, containing 1% HFIP. Effects of TFE on conformation of aqueous solution of IAPP(8-18)L3(22-28)-GI (B), IAPP(8-18)L3(22-28)-GI-linear (D), IAPP(8-18)L3(22-28)-GI-cyclo (F), IAPP(8-18)Amb-Ab(22-28)-GI (H) assessed by far-UV spectroscopy. Measurements were performed at a peptide concentration of 10 μM in 10 mM sodium phosphate buffer, pH 7.4, containing 1% HFIP and the indicated amount of TFE.

To assess whether these peptides are able to bind Aβ, IAPP, IAPP-GI and to self-associate, fluorescence spectroscopy binding assays were applied. Thereby, titrations using fluorescently labeled Aβ40, IAPP, IAPP-GI, or the analogues by themselves were performed (Table 17). The binding affinities of Dac-Aβ40 to all above analogs were very similar to each

other and were in the upper nanomolar to low micromolar range. Therefore, no direct correlation was deduced between cytotoxicity, fibrillogenesis and binding affinity to Aβ. The affinities to Dac-Aβ were, thus, not very high although IAPP(8-18)L3(22-28)-GI, IAPP(8-18)L3(22-28)-GI-linear, and IAPP(8-18)Amb-Ab(22-28)-GI were found to be very potent Aβ40 aggregation and toxicity inhibitors. In addition, the interaction of IAPP(8-18)L3(22-28)-GI-cyclo with Aβ40 had an apparent dissociation constant which was in the same range as the other analogues but it was found to be only a week inhibitor of Aβ40 aggregation and cytotoxicity. By contrast, low nanomolar $K_{d,app}$s were found for the interaction of all these analogues with Fluo-IAPP and Fluo-IAPP-GI. Thus, the higher affinities of these peptides to Fluo-IAPP and Fluo-IAPP-GI rather than Dac-Aβ40 may be related to the sequence similarity.

Table 17. Apparent affinities (app. Kd) of interaction of IAPP(8-18)L3(22-28)-GI, IAPP(8-18)L3(22-28)-GI-linear, IAPP(8-18)L3(22-28)-GI-cyclo and IAPP(8-18)Amb-Ab(22-28)-GI with Dac-Aβ40, Fluo-IAPP, Fluo-IAPP-GI and their N-terminal Fluo labeled form as determined by fluorescence titration binding assays. The measurements were carried out in 10 mM sodium phosphate buffer, pH 7.4, 1% HFIP and at room temperature. The concentration of the fluorescence labeled peptide was 10 nM for Dac-Aβ40 and 5 nM for Fluo-peptide. $K_{d,app}$ values were determined from one or three binding curves (± SEM where indicated).

	Dac-Aβ40	Fluo-IAPP	Fluo-IAPP-GI	Self-Ass.
IAPP(8-18)L3(22-28)-GI	635±32 nM	61 nM	43 nM	378 nM
IAPP(8-18)L3(22-28)-GI-linear	2,1 µM	82 nM	91 nM	375 nM
IAPP(8-18)L3(22-28)-GI-cyclo	1 µM	97 nM	89 nM	41 nM
IAPP(8-18)Amb-Ab(22-28)-GI	2,3±0,4 µM	300 nM	118 nM	62 nM

3.4.4 Effects of designed analogues of IAPP(8-18)A3(22-28)-GI containing structure stabilizing or destabilizing charged residues at specific sequence positions on Aβ40 fibrillogenesis and cytotoxicity

In chapter 3.1.3, it was shown that the analog in which the two hot regions are connected with a rigid and extended linker (IAPP(8-18)Amb-Ab(22-28)-GI) was an efficient Aβ40 aggregation inhibitor while the peptide with a rigid and likely β-turn inducing cyclic constraint (IAPP(8-18)L3(22-28)-GI-cyclo) was not capable of inhibiting Aβ40 aggregation. To test the hypothesis that a stabilized β-hairpin structure does not yield an Aβ40 aggregation inhibitor, a different strategy was exploited here: accordingly, analogues of IAPP(8-18)A3(22-28)-GI, which had been found to be a flexible medium potency inhibitor were synthesized. These analogues were devised by adding three charged amino acids at the N- and C-termini of IAPP(8-18)A3(22-28)-GI in order to either disturb or promote the potential strand-turn-strand

conformation of IAPP(8-18)A3(22-28)-GI (Fig. 44). A peptide which consisted of the template IAPP(8-18)A3(22-28)-GI with three lysines at the N-terminus and three at the C-terminus was designed (K3-IAPP(8-18)A3(22-28)-GI-K3). These additional charged amino acids were expected a) to improve the solubility and b) to destabilize the strand-turn-strand conformation via electrostatic repulsion. In addition, a peptide was designed with three glutamic acids at the C-terminal and three lysines at the N-terminal (E3-IAPP(8-18)A3(22-28)-GI-K3). These residues were expected to stabilize the potential strand-turn-strand conformation via electrostatic attraction between side chains of the glutamic acids and lysines. Finally, as K3-IAPP(8-18)A3(22-28)-GI-K3 proved to be an effective inhibitor (as the following studies will show), several control peptides were later also synthesized: a peptide with a sequence of three lysines only at the N-terminus (K3-IAPP(8-18)A3(22-28)-GI), a peptide with a sequence of three lysines only at the C-terminus (IAPP(8-18)A3(22-28)-GI-K3) and a peptide with six acetylated lysines at the N- and C-termini (K3*-IAPP(8-18)A3(22-28)-GI-K3*). The same concept was applied to the native partial IAPP sequence IAPP(8-28)-GI which was found to be unable to inhibit Aβ40 aggregation and cytotoxicity (see chapter 3.2). The sequence IAPP(8-28)-GI was used as template and an analogue with three lysines at the N- and three at the C-terminus (K3-IAPP(8-28)-GI-K3) was synthesized and studied. This analogue was designed in order to test whether the electrostatic repulsion at the N-and C-termini were sufficient to improve the inhibitory properties of an inactive sequence.
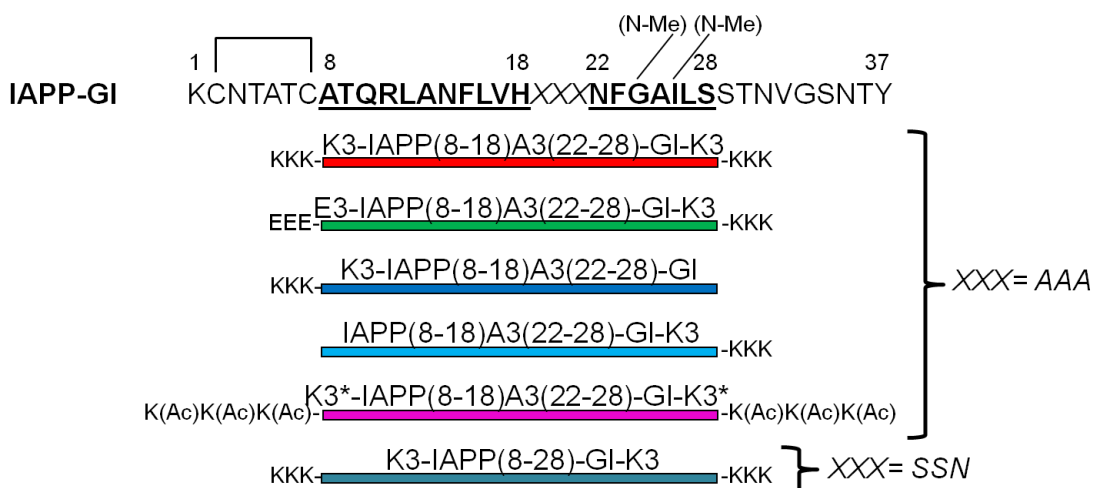
Fig. 44. Primary structure of IAPP-GI. Domains found to be hot regions of the Aβ40-IAPP interaction interface are bold and underlined. Design of analogues studied in this chapter: K3-IAPP(8-18)A3(22-28)-GI-K3 (red), E3-IAPP(8-18)A3(22-28)-GI-K3 (green), K3-IAPP(8-18)A3(22-28)-GI (blue), IAPP(8-18)A3(22-28)-GI-K3 (cyan), K3*-IAPP(8-18)A3(22-28)-GI-K3* (magenta) and K3-IAPP(8-28)-GI-K3 (dark cyan).

These peptides were synthesized by solid phase peptide synthesis (SPPS) utilizing Fmoc-strategy by Dr. A. Caporale. They were purified by HPLC and MALDI mass spectrometry was used to determine their mass as shown in Table 18.

Table 18. Characterization of peptides synthesized by Fmoc-chemistry (C-terminal acids) via their HPLC retention time (rt) and MS.

|	HPLC prg	rt (min)	[M+H]+ expected	[M+H]+ found
K3-IAPP(8-18)A3(22-28)-GI-K3	Fast	18´	2983	2983
E3-IAPP(8-18)A3(22-28)-GI-K3	Fast	20´	2986	2986
K3-IAPP(8-18)A3(22-28)-GI	Fast	18,5´	2599	2599
IAPP(8-18)A3(22-28)-GI-K3	Fast	18,5´	2599	2599
K3*-IAPP(8-18)A3(22-28)-GI-K3*	Fast	21,2´	3225	3225
K3-IAPP(8-28)-GI-K3	Slow	16´	3058	3059

To determine whether the interaction of the above peptides with Aβ40 could inhibit Aβ40 fibrillogenesis and cytotoxicity, incubations of Aβ40 in their absence or presence (at 1/1) were performed. Aβ40 fibrillogenesis and cytotoxicity were assessed by ThT binding and MTT reduction assays. Aβ40 (16.5 µM, pH 7.4) and the mixtures of Aβ40 with the analogues (16.5 µM each) were incubated for 7 days. As shown in Fig. 45A, fibrillogenesis of Aβ40 alone had a lag-phase of 48 h. The steep increase of ThT binding between 48-120 h was followed by a plateau which indicated the end of the fibrillization process. In the presence of E3-IAPP(8-18)A3(22-28)-GI-K3, IAPP(8-18)A3(22-28)-GI-K3 and K3*-IAPP(8-18)A3(22-28)-GI-K3* (at 1/1) the ThT fluorescence increased in the same way as Aβ40 alone suggesting that these peptides did not inhibit Aβ40 fibrillogenesis (Fig. 45A). By contrast, the mixture of Aβ40 and K3-IAPP(8-18)A3(22-28)-GI-K3, K3-IAPP(8-18)A3(22-28)-GI and K3-IAPP(8-28)-GI-K3 completely suppressed Aβ40 fibril formation (Fig. 45A). To examine if the interaction of the peptides with Aβ40 could also inhibit formation of cytotoxic Aβ40 aggregates, aliquots of the incubations of the ThT binding assays were added to PC-12 cells at 3 and 7 days and cytotoxicities were assessed by MTT reduction assay (Fig. 45C-D). Immediately after solution preparation Aβ40 was non-toxic but its cytotoxicity increased following aging for 72 h. The results of Fig. 45B indicated that K3-IAPP(8-18)A3(22-28)-GI-K3, K3-IAPP(8-18)A3(22-28)-GI and K3-IAPP(8-28)-GI-K3 (at 1:1) were able to strongly suppress formation of cytotoxic Aβ40 assemblies. By contrast, E3-IAPP(8-18)A3(22-28)-GI-K3, IAPP(8-18)A3(22-28)-GI-K3 and K3*-IAPP(8-18)A3(22-28)-GI-K3* did not show any effect on formation of cytotoxic Aβ40 species (Fig. 45C). The cytotoxicity of Aβ40 reached the maximum following aging for the 168 h and incubations of Aβ40 with the peptides that inhibited Aβ40 cytotoxicity at 72 h time-point where subjected to MTT reduction assay at 168 h time-point as well (Fig. 45D). K3-IAPP(8-18)A3(22-28)-GI-K3 was found to be the only analogue which was still able to inhibit quite efficiently Aβ40 cytotoxicity whereas K3-IAPP(8-18)A3(22-28)-GI and K3-IAPP(8-28)-GI-K3 did not inhibit.

These results suggested that K3-IAPP(8-18)A3(22-28)-GI-K3 was the most potent inhibitor of this series of analogs. Notably, the electrostatic repulsion likely present between the K3-stretches in the peptide K3-IAPP(8-18)A3(22-28)-GI-K3 considerably improved the inhibitory effect of IAPP(8-18)A3(22-28)-GI which was only a modest inhibitor of Aβ40 aggregation (Fig. 45B and chapter 3.4.2). In the case of the likely present electrostatic attraction between the E3- and K3-streches as in the peptide E3-IAPP(8-18)A3(22-28)-GI-K3, the inhibitory capacity of the template peptide-IAPP(8-18)A3(22-28)-GI was completely abolished. This peptide did not block Aβ40 aggregation and fibrillization likely due to stabilization of a strand-turn-strand conformation which may have cause a shielding of its interacting sites with Aβ40. The two control peptides, K3-IAPP(8-18)A3(22-28)-GI and IAPP(8-18)A3(22-28)-GI-K3, showed clear differences in their inhibitory potentials. When the three lysines were placed at the N-terminus of IAPP(8-18)A3(22-28)-GI, the resulting K3-IAPP(8-18)A3(22-28)-GI analog was found to be able to inhibit Aβ40 aggregation and fibrillization although not as good as K3-IAPP(8-18)A3(22-28)-GI-K3. By contrast, when the three lysines were placed at the C-terminus, the resulting peptide IAPP(8-18)A3(22-28)-GI-K3 was weaker inhibitor than IAPP(8-18)A3(22-28)-GI (Fig. 45B). Importantly, K3*-IAPP(8-18)A3(22-28)-GI-K3* which had N^{ε}-amino groups of both K3-stretches acetylated, was completely inactive providing evidence that the positive charges and thus likely the electrostatic repulsion are necessary for the inhibitory effect on Aβ40 aggregation and toxicity. Finally, K3-IAPP(8-28)-GI-K3 was an effective Aβ40 aggregation and toxicity inhibitor although IAPP(8-28)-GI did not inhibit (Fig. 45B). These results showed that the inhibitory effect of these analogues can be controlled by electrostatic interaction between residues at the edges of the hot-spot regions IAPP(8-18) and IAPP(22-28)-GI.
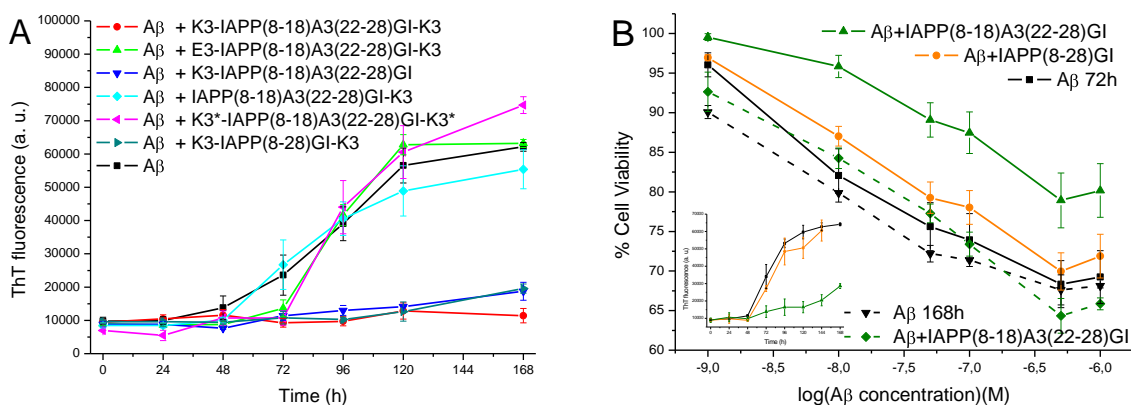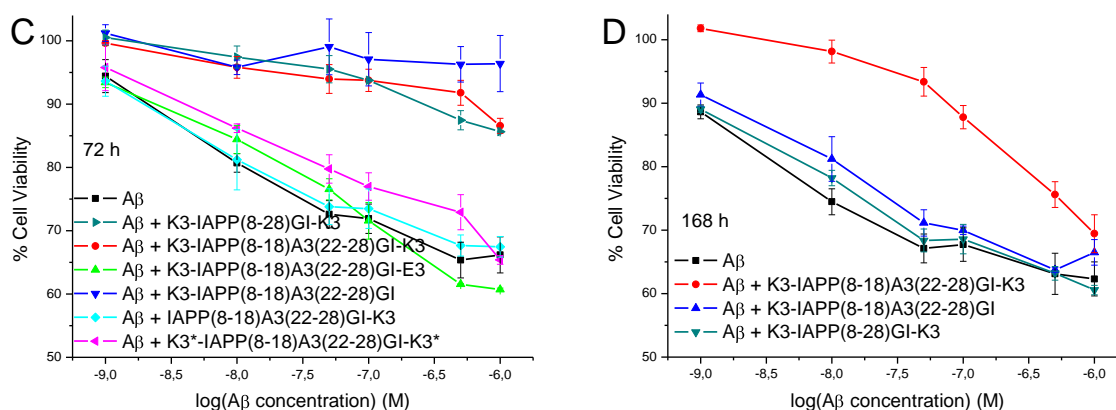
Fig. 45. Effect of the peptides K3-IAPP(8-18)A3(22-28)-GI-K3, E3-IAPP(8-18)A3(22-28)-GI-K3, K3-IAPP(8-18)A3(22-28)-GI, IAPP(8-18)A3(22-28)-GI-K3, K3*-IAPP(8-18)A3(22-28)-GI-K3* and K3-IAPP(8-28)-GI-K3 on Aβ40 fibrillogenesis and cytotoxicity. (A) Fibrillogenesis of Aβ40 (16.5 μM in 50 mM sodium phosphate buffer, pH 7.4, containing 100 mM NaCl and 1% HFIP) and of a mixture of Aβ40 and peptides (1:1) was followed by the ThT binding assay. (B) For comparison, MTT reduction assay (at 3 and 7 days of incubation) and ThT assay (inset) of a mixture of Aβ40 with IAPP(8-28)-GI and IAPP(8-18)A3(22-28)-GI as compared to Aβ40 alone. (C) MTT reduction assay of Aβ40 and a mixture of Aβ40 with peptides (16.5 μM in 50 mM sodium phosphate buffer, pH 7.4, containing 100 mM NaCl and 1% HFIP) after 3 days incubation. Aliquots were then diluted with cell culture medium and added to PC-12 cells at the indicated final concentrations. Followed 24h incubation at 37°C, cell viabilities were assessed via the MTT reduction assay. (D) Aβ40-inhibitor mixtures which were found to inhibit following 3 days incubation were added to PC-12 cell at the time point 7 days. Cell viabilities were determined as under (B). Data are means (±SEM) of 3 assays (performed in triplicates).

To obtain more information about the structural properties of these peptides, various far-UV CD measurements were performed. First, it was examined whether and how the conformation of the peptides in aqueous buffer changed by increasing the concentration of the peptide. In general, the CD spectra of K3-IAPP(8-18)A3(22-28)-GI-K3 and K3-IAPP(8-28)-GI-K3 exhibited a prominent minimum at 190 nm indicating unordered structure and a weaker minimum at 225 nm typical for the β-sheet/β-turn components (Fig. 46A-D). The ratio of the two minima was circa 4(random coil):1(β-sheet/β-turn) which was quite different from the ratio of the corresponding to the "template" peptides IAPP(8-18)A3(22-28)-GI and IAPP(8-28)-GI where the ratio was 2:1. These results suggested that the conformational flexibility of both peptides was increased by the addition of the K3-stretches at the edges, likely due to the charges. The aggregation potential of these two peptides was low as no concentration dependence was observed in the spectra between 10 and 100 μM while the respective "template" peptides formed soluble oligomers between 50 and 100 μM (Fig. 46A-D)(see also Fig. 27A-E). The ratio of the two minima for E3-IAPP(8-18)A3(22-28)-GI-K3 was 2(RC):1(β-sheet/β-turn) as for IAPP(8-18)A3(22-28)-GI (Fig. 46B). In fact, it appears that the opposite charges at the N- and C- termini of the peptide imposed a higher structural order to

IAPP(8-18)A3(22-28)-GI as compared to the positive charges at both ends. This would be consistent with a stabilization of β-sheet/β-turn in E3-IAPP(8-18)A3(22-28)-GI-K3 and a destabilization of β-sheet/β-turn K3-IAPP(8-18)A3(22-28)-GI-K3. In any case, the charges contributed to the solubility of E3-IAPP(8-18)A3(22-28)-GI-K3 which did not aggregate up to a concentration of 100 µM (Fig. 46B). By contrast, K3*-IAPP(8-18)A3(22-28)-GI-K3* formed soluble oligomers already at 50 µM likely due to the fact that N^ε-amino groups of the K3-stretches were acetylated and no charges were thus present at these side chains (Fig. 46C).

Fig. 46. Concentration dependence of the conformation of K3-IAPP(8-18)A3(22-28)-GI-K3 (A), E3-IAPP(8-18)A3(22-28)-GI-K3 (B), K3*-IAPP(8-18)A3(22-28)-GI-K3* (C) and K3-IAPP(8-28)-GI-K3 (D) assessed by far-UV CD spectroscopy. Measurements were performed in solutions of the peptides in 10 mM sodium phosphate buffer, pH 7.4, containing 1% HFIP.

In order to understand the effects of the charges on the structure of these peptides, pH dependence studies were also performed. CD spectra were recorded in phosphate buffer at pH 7.4, 2, and 9 at a peptide concentration of 10 µM. The spectra of K3-IAPP(8-18)A3(22-28)-GI-K3 and K3-IAPP(8-28)-GI-K3 did not exhibit any significant difference between the pH 2, 7.4, and 9 and the slight variations in the spectra could be attributed to other charged side chains present in the peptide (Fig. 47A-D). In fact, the N^ε-amino groups of the lysines should be mainly in a protonated state (pKa(Lys)= 10,5) under all three pH conditions. Indeed the same small variations were also observed in K3*-IAPP(8-18)A3(22-28)-GI-K3* where the K3-

stretches were acetylated (Fig. 47C). The CD spectrum of E3-IAPP(8-18)A3(22-28)-GI-K3 at pH 2 showed less β-sheet/β-turn contribution than the ones at pH 7.4 and 9 in agreement with the fact that at pH 2 the carboxylic function of Glu is not charged (pKa(Glu)= 4.3) (Fig. 47C). These results suggested that when the coulombic attraction decreases, the turn likely present in E3-IAPP(8-18)A3(22-28)-GI-K3 is destabilized.
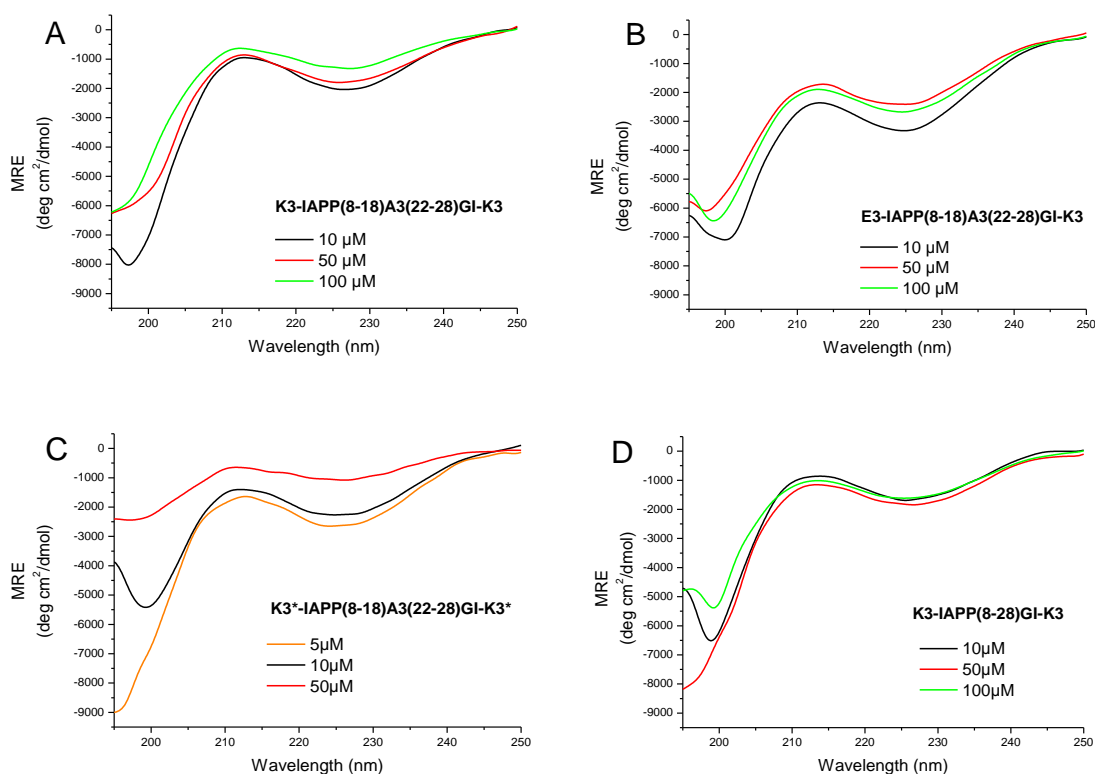

Fig. 47. pH dependence studies of K3-IAPP(8-18)A3(22-28)-GI-K3 (A), E3-IAPP(8-18)A3(22-28)-GI-K3 (B), K3*-IAPP(8-18)A3(22-28)-GI-K3* (C) and K3-IAPP(8-28)-GI-K3 (D) performed at a peptide concentration of 10 µM in 10 mM sodium phosphate buffer containing 1% HFIP, pH 7.4 (line), pH 2.0 (dash) or pH 9.0 (dot).

Lastly, the effects of TFE on the conformation of the above peptides were investigated. In all cases, strong CD changes were observed by increasing the TFE concentration indicating α-helix formation (two minima around 208 nm and 222 nm) (Fig. 48). All peptides formed α-helices already at 20% TFE and the α-helical contents reached the maximum amounts at 60% TFE. In general, the results of the TFE titration studies did not indicate strong differences between the α-helical propensities of the various peptides.

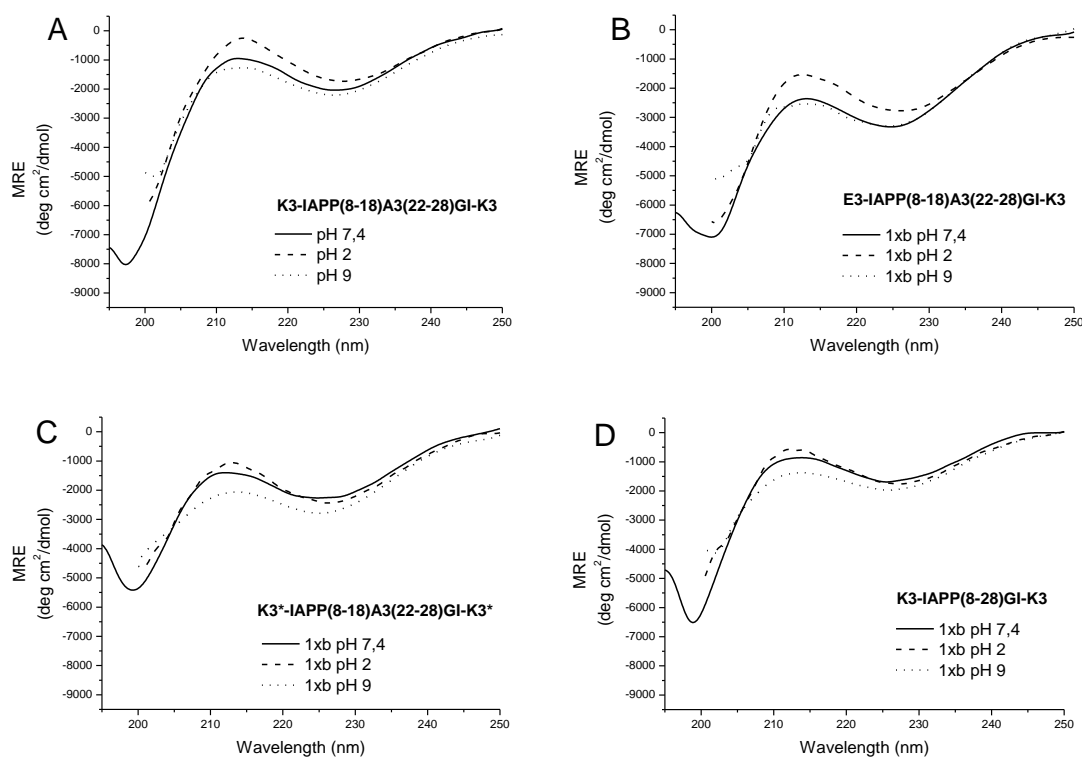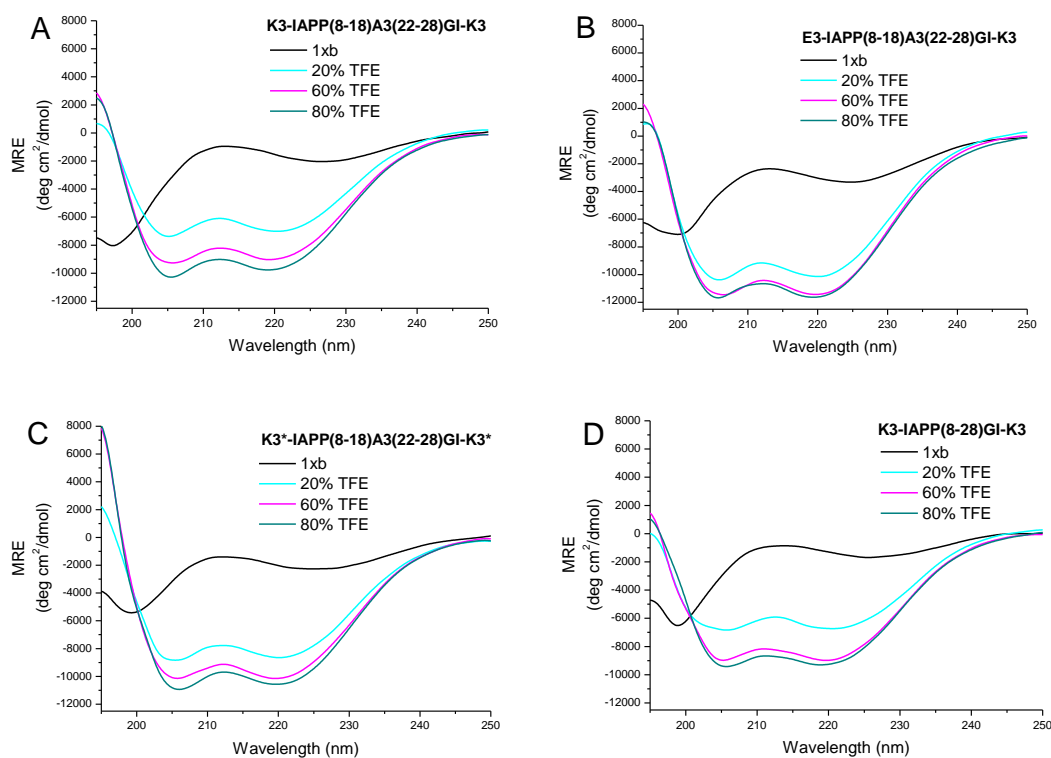Fig. 48. Effects of TFE on conformation of aqueous solution of K3-IAPP(8-18)A3(22-28)-GI-K3 (A), E3-IAPP(8-18)A3(22-28)-GI-K3 (B), K3*-IAPP(8-18)A3(22-28)-GI-K3* (C) and K3-IAPP(8-28)-GI-K3 (D). Measurements were performed at a peptide concentration of 10 μM in 10 mM sodium phosphate buffer, pH 7.4, containing 1% HFIP and the indicated amounts of TFE.

The interaction of the above peptides with Aβ40, IAPP, IAPP-GI and their self-association as well were then studied via fluorescence titration binding assays (Table 19). All tested peptides bound Dac-Aβ40 with dissociation constants in the nanomolar range. The strongest inhibitor studied in this chapter, K3-IAPP(8-18)A3(22-28)-GI-K3, bound Dac-Aβ40 with low nanomolar affinity ($K_{d,app}= 23\pm1$ nM) whereas the weakest inhibitor, E3-IAPP(8-18)A3(22-28)-GI-K3, showed six times weaker affinity to Dac-Aβ40 ($K_{d,app}= 151\pm15$ nM). The remaining peptides bound Aβ40 with similar app. K_ds although the inhibitory potencies differed significantly. Nanomolar $K_{d,app}$s were also found for the interactions of these peptides with Fluo-IAPP or Fluo-IAPP-GI with the exception for E3-IAPP(8-18)A3(22-28)-GI-K3 for which micromolar affinity was found. A relatively similar relationship was observed between the affinities of Fluo-IAPP or Fluo-IAPP-GI towards K3-IAPP(8-18)A3(22-28)-GI-K3 and E3-IAPP(8-18)A3(22-28)-GI-K3 as for the affinities of Dac-Aβ40 to K3-IAPP(8-18)A3(22-28)-GI-K3 and E3-IAPP(8-18)A3(22-28)-GI-K3. In fact, K3-IAPP(8-18)A3(22-28)-GI-K3 proved to bind stronger Dac-Aβ40, Fluo-IAPP, and Fluo-IAPP-GI than E3-IAPP(8-18)A3(22-28)-GI-K3. Of note, all examined peptides in this chapter exhibited self-association affinities in the low

nanomolar range. Therefore, their binding to Dac-Aβ40, Fluo-IAPP and Fluo-IAPP-GI may be affected by competitive self-association processes.

Table 19. Apparent affinities (app. Kd) of interaction of K3-IAPP(8-18)A3(22-28)-GI-K3, E3-IAPP(8-18)A3(22-28)-GI-K3, K3-IAPP(8-18)A3(22-28)-GI, IAPP(8-18)A3(22-28)-GI-K3, K3*-IAPP(8-18)A3(22-28)-GI-K3* and K3-IAPP(8-28)-GI-K3 with Dac-Aβ40, Fluo-IAPP, Fluo-IAPP-GI and their N-terminal Fluo labeled form as determined by fluorescence titration binding assays. The measurements were carried out in 10 mM sodium phosphate buffer, pH 7.4, 1% HFIP and at room temperature. The concentration of the fluorescently labeled peptide was 10 nM for Dac-Aβ40 and 5 nM for the Fluo-peptide. $K_{d,app}$ values were determined from one or three binding curves (± SEM where indicated).

	Dac-Aβ40	Fluo-IAPP	Fluo-IAPP-GI	Self-Ass.
K3-IAPP(8-18)A3(22-28)-GI-K3	23±1 nM	40 nM	96 nM	64 nM
E3-IAPP(8-18)A3(22-28)-GI-K3	151±15 nM	570 nM	1,8 µM	99 nM
K3-IAPP(8-18)A3(22-28)-GI	312 nM	98 nM	83 nM	83 nM
IAPP(8-18)A3(22-28)-GI-K3	338 nM	249 nM	81 nM	87 nM
K3*-IAPP(8-18)A3(22-28)-GI-K3*	138 nM	114 nM	50 nM	10 nM
K3-IAPP(8-28)-GI-K3	860 nM	52 nM	24 nM	14 nM

3.4.5 **Comparison of the effects of the strongest inhibitors on Aβ fibrillogenesis toxicity**

In the previous chapters, three IAPP-GI analogues were identified to be the strongest Aβ40 aggregation inhibitors. Here, the inhibitory potentials of these analogues IAPP(8-18)L3(22-28)-GI, IAPP(8-18)Amb-Ab(22-28)-GI, and K3-IAPP(8-18)A3(22-28)-GI-K3 were compared to each other in order to determine which one has the best inhibitory properties.

First, the ability of the IAPP-GI analogues to inhibit Aβ40 fibrillogenesis and cytotoxicity was tested in the same experimental set up of the Aβ-inhibitors mixtures. Aβ40 fibrillogenesis and cytotoxicity were assessed by the ThT binding and the MTT reduction assays. Aβ40 (16.5 µM, pH 7.4) and the mixtures of Aβ40 with the analogues (16.5 µM each) were incubated for 14 days. As shown in Fig. 49A, fibrillogenesis of Aβ40 alone had a lag-phase of 48 h. The steep increase of ThT binding between 48-144 h was followed by a plateau which indicated the end of the fibrillization process. In the presence of IAPP(8-18)L3(22-28)-GI, IAPP(8-18)Amb-Ab(22-28)-GI, and K3-IAPP(8-18)A3(22-28)-GI-K3 (at 1/1), Aβ40 fibril formation was suppressed up to 7 days (Fig. 49A). No differences between the inhibitory potencies on Aβ40 fibrillogenesis could thus be observed between these three inhibitors. To study formation of cytotoxic Aβ40 aggregates, aliquots of the incubations of the ThT binding assays were added to PC-12 cells at the time point of 3 and 7 days and cytotoxicities were assessed by the MTT reduction assay (Fig. 49B-C-D). The results of Fig. 49B indicated that all three analogs (at

1:1) completely suppressed formation of cytotoxic Aβ40 assemblies at the 72 h incubation time point. By contrast, the 7 days aged mixtures of the peptides with Aβ40 were partly cytotoxic (Fig. 49C): IAPP(8-18)L3(22-28)-GI-K3 was found to be the only analogue which was still able to completely inhibit Aβ40 cytotoxicity whereas IAPP(8-18)Amb-Ab(22-28)-GI and K3-IAPP(8-18)A3(22-28)-GI-K3 only partially inhibited formation of cytotoxic Aβ40 aggregates. These results suggested that IAPP(8-18)L3(22-28)-GI was the most potent Aβ40 aggregation inhibitor if compared to the other two potent Aβ40 aggregation inhibitors IAPP(8-18)Amb-Ab(22-28)-GI and K3-IAPP(8-18)A3(22-28)-GI-K3.
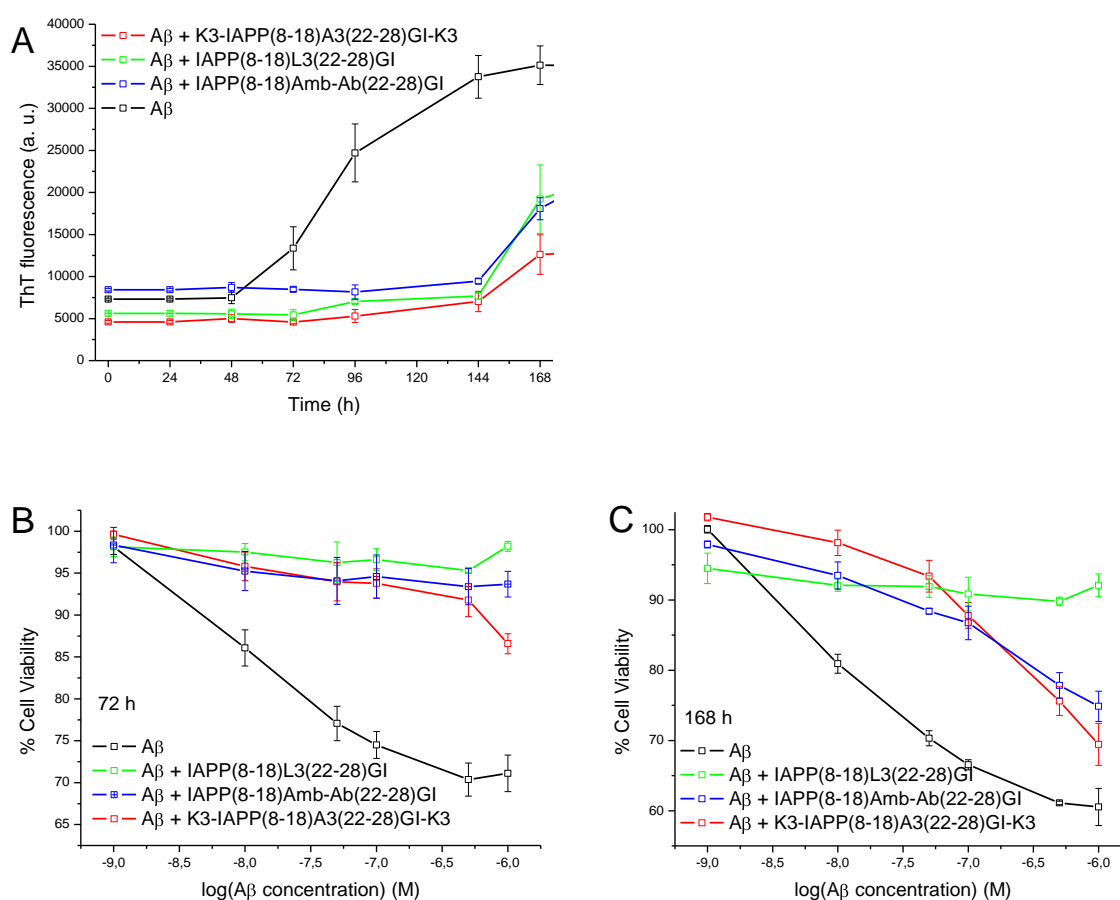
Fig. 49. Effect of the peptides IAPP(8-18)L3(22-28)-GI, IAPP(8-18)Amb-Ab(22-28)-GI, K3-IAPP(8-18)A3(22-28)-GI-K3 on Aβ40 fibrillogenesis and cytotoxicity. (A) Fibrillogenesis of Aβ40 (16.5 µM in 50 mM sodium phosphate buffer, pH 7.4, containing 100 mM NaCl and 1% HFIP) and of a mixture of Aβ40 and peptides (1:1) was followed by the ThT binding assay. (B) Aβ40 and mixtures of Aβ40 with peptides at 1:1 (16.5 µM in 50 mM sodium phosphate buffer, pH 7.4, containing 100 mM NaCl and 1% HFIP) were incubated for 3 days. Aliquots were then diluted with cell culture medium and added to PC-12 cells at the indicated final concentrations. Following 24 h incubation at 37°C cell viabilities were assessed via the MTT reduction assay. (C) Cell viabilities were determined as under (A) at the incubation time point of 7. Data are means (±SEM) of 3 assays (performed in triplicates).

In order to compare the different inhibitory potencies of the three peptides toward formation of cytotoxic Aβ40 aggregates, the half maximal inhibitory concentration (IC_{50}) assay was

determined next. Aβ40 was mixed with different amount of peptides and, following 72 h incubation, cytotoxicities were assessed by the MTT reduction assay (Fig. 50). The titrations of the mixture of Aβ40 (at 100 nM) with IAPP(8-18)L3(22-28)-GI showed that the inhibitory effect of IAPP(8-18)L3(22-28)-GI had an IC_{50} of 95±16 nM (Fig. 50B). Titrations of the mixture of Aβ40 (at 100 nM) with IAPP(8-18)Amb-Ab(22-28)-GI showed that the inhibitory effect of IAPP(8-18)Amb-Ab(22-28)-GI had an IC_{50} of 158±36 nM and titrations of the mixture of Aβ40 (at 100 nM) with K3-IAPP(8-18)A3(22-28)-GI-K3 showed that the inhibitory effect of K3-IAPP(8-18)A3(22-28)-GI-K3 had an IC_{50} of 292±78 nM (Fig. 50D-F). For comparison, the same assay was performed also with IAPP-GI which exhibited an IC_{50} of 63 nM which was consistent with previously reported IC_{50} of IAPP-GI with regard to inhibition of Aβ40 toxicity [167]. Therefore, these findings suggested that IAPP(8-18)L3(22-28)-GI is the most potent inhibitor of Aβ40 cytotoxic self-assembly as compared to the other here presented IAPP-GI analogues and that IAPP(8-18)L3(22-28)-GI showed a similar IC_{50} as IAPP-GI. Based on these findings it appears possible that the interaction between Aβ40 and IAPP(8-18)L3(22-28)-GI might result in formation of non-toxic hetero-oligomeric complexes as it has been previously shown for Aβ40 and IAPP-GI.
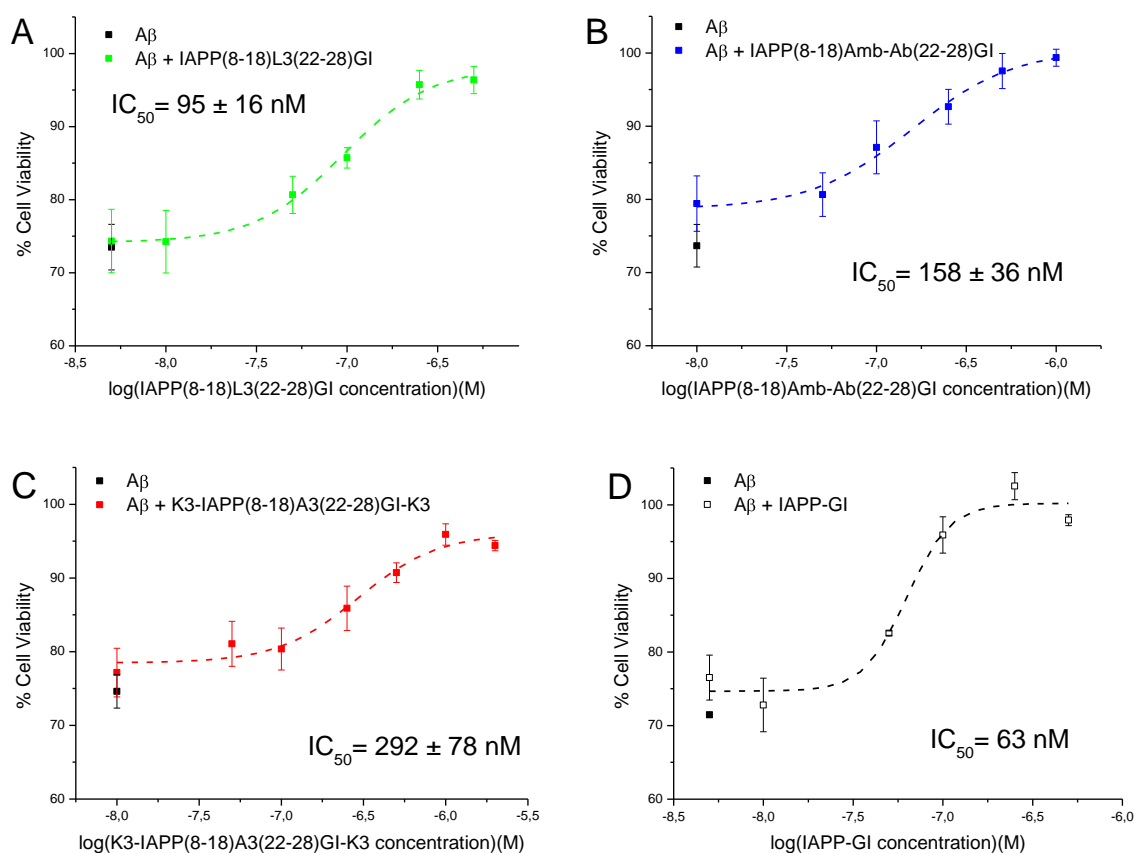

Fig. 50. Determination of the IC_{50} of the inhibitory effect of IAPP(8-18)L3(22-28)-GI (A), IAPP(8-18)Amb-Ab(22-28)-GI (B), K3-IAPP(8-18)A3(22-28)-GI-K3 (C) compared to IAPP-GI (D) on PC-12 cell toxicity of Aβ40 via MTT reduction assay. Aβ40 (16.5 μM in 50 mM sodium phosphate buffer, pH 7.4, containing 100 mM NaCl and 1%

HFIP) and mixtures of Aβ40 with peptides at the indicated amounts were incubated for 3 days. Aliquots were then diluted with cell culture medium and added to PC-12 cells at the final Aβ40 concentration of 100 nM. Data are means (±SEM) of 3 assays (performed in triplicates) except for IAPP-GI which data are means (±SEM) of 1 assay (performed in triplicates).

Next, the capability of these peptides to reverse the cytotoxic effect of already formed cytotoxic Aβ40 aggregates was examined. Aβ40 (16.5 µM, pH 7.4) was aged for 7 days to reach the steady-state of the cytotoxic self-assembly process. At this incubation time point, the peptides (at 100-fold molar excess, 165 µM) were added to the aged and cytotoxic Aβ40 solutions (1.65 µM). Cytotoxicities of the solution were then assessed following 24 h incubation (Fig. 51). The data showed that solutions of Aβ40 with IAPP(8-18)L3(22-28)-GI (100-fold excess) were not cytotoxic anymore whereas the Aβ40 solution was cytotoxic. Thus IAPP(8-18)L3(22-28)-GI was found to be able to block cytotoxicity of already formed Aβ40 aggregates. The mixture of Aβ40 with a 100-fold molar excess of IAPP(8-18)Amb-Ab(22-28)-GI exhibited also partially reduced toxicity as compared to the Aβ40 alone solution. By contrast, a 100-fold molar excess of K3-IAPP(8-18)A3(22-28)-GI-K3 did not affect the already formed cytotoxic Aβ40 aggregates. Thus, data demonstrated that IAPP(8-18)L3(22-28)-GI and IAPP(8-18)Amb-Ab(22-28)-GI were able to block cytotoxicity of already formed Aβ40 assemblies.
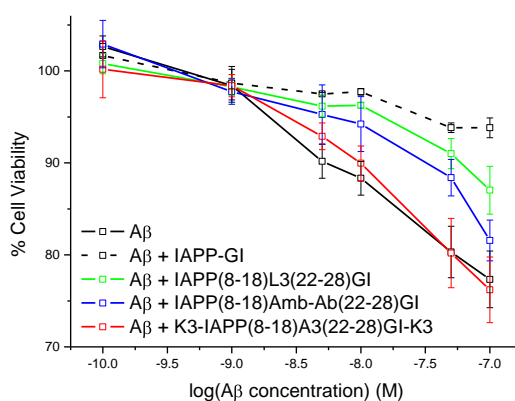
Fig. 51. Effects of IAPP(8-18)L3(22-28)-GI, IAPP(8-18)Amb-Ab(22-28)-GI, and K3-IAPP(8-18)A3(22-28)-GI-K3, as compared to IAPP-GI on already formed cytotoxic Aβ40 aggregates. A 7 days aged 16.5 µM cytotoxic Aβ40 solution was first diluted to 1.65 µM with buffer (50 mM sodium phosphate buffer, pH 7.4, containing 100 mM NaCl and 1% HFIP) and then mixed with 100-fold excess of the peptides. The solutions, including a control solution of aged Aβ40 alone, were incubated for 24 h and added to PC-12 cells at the indicated final concentrations. Cell viabilities were assessed via the MTT reduction assay. Data are means (±SEM) of 3 assays (performed in triplicates).

Taken together, IAPP(8-18)L3(22-28)-GI proved to be strongest Aβ40 inhibitor of Aβ40 self-assembly as it was found capable of a) completely suppressing Aβ40 fibrillogenesis and

cytotoxicity with an IC_{50} in the same low nanomolar range as IAPP-GI and b) blocking cytotoxicity of preformed Aβ40 cytotoxic aggregates. Of note, the other two potent Aβ40 aggregation and toxicity inhibitors, IAPP(8-18)Amb-Ab(22-28)-GI and K3-IAPP(8-18)A3(22-28)-GI-K3 were found by direct comparison to IAPP(8-18)L3(22-28)-GI to be less effective and K3-IAPP(8-18)A3(22-28)-GI-K3 could not block cytotoxicity of already formed Aβ40 cytotoxic aggregates.

4 Discussion

Up-normal protein aggregation is linked to protein folding and misfolding processes. Protein misfolding can cause formation of insoluble aggregates that can be disordered as in the inclusion bodies or ordered as in the amyloid plaques. The formation of amyloid fibrils is associated to many cell degenerative diseases, such as Alzheimer's disease and type 2 diabetes. The two diseases are characterized by the aggregation of two amyloidogenic polypeptides: the 40- 42- residue β-amyloid-peptide (Aβ) in AD and the 37-residue islet amyloid polypeptide (IAPP) in T2D. Surprisingly, it has been recently shown in vitro that these two peptides are able to cross-interact. In fact, Aβ40 binds IAPP with low nanomolar affinity in vitro ($K_{d,app}$= 50 nM) when both peptides are in a non-fibrillar and non-cytotoxic state [167]. Additionally, it has been found that the hetero-association of Aβ40 and IAPP attenuates cytotoxic self-assembly and fibrillogenesis of both peptides [167]. These findings suggested that the Aβ-IAPP interaction - if existent in vivo – may be a molecular link between AD and T2D [167]. An interaction between Aβ and IAPP is possible in vivo since both peptides are present in similar concentrations in serum and cerebrospinal fluid [194].

The first question which was addressed in this work was what are the regions of Aβ and IAPP which are involved in their hetero-association. Thereby, array of membrane-bound peptide decamers were used [177]. The results are presented in chapters 3.1.1 and 3.1.2 and are summarized here in Scheme 3. For these studies and for solubility reasons the N-methylated IAPP mimic IAPP-GI was used instead of IAPP and it was found to bind Aβ40 in regions Aβ(12-24) and Aβ(26-37) which are both regions previously suggested to mediate Aβ40 self-association [61, 62]. On the other side, Aβ40 bound mainly the IAPP(1-20) region and part of the C-terminal IAPP region which have been previously also suggested to be involved in IAPP self-association [137, 142, 152, 166, 178]. Therefore, the Aβ40 and IAPP peptide arrays were also tested with regard to their binding to Aβ40 respectively IAPP. Thereby, the Aβ40 and IAPP peptide membranes were incubated with full length Biotin-Aβ40 and Biotin-IAPP-GI respectively. These studies confirmed that regions which are important for the Aβ-IAPP hetero-association mediated also their self-association (Scheme 3). In parallel to the above studies using membrane-bond peptide arrays, the regions (19-22), Aβ(27-32), Aβ(35-40), IAPP(8-18) and IAPP(22-28) were found by fluorescence based solution binding studies to correspond to the shortest regions or "hot regions" responsible for the Aβ-IAPP interaction [177]. Therefore, the binding sites of the determined Aβ and IAPP hot regions were in the course of my studies also investigated using the IAPP or Aβ membrane bound decamers, respectively. In order to simplify the assays with membrane-bound peptide arrays, segments Aβ(15-24), Aβ(25-35), IAPP(10-18), and IAPP(20-29) were

used (Scheme 3; red and blue letters). The Aβ regions Aβ(15-24) and Aβ(25-35) were found to cross-interact with IAPP regions IAPP(1-20) and IAPP(16-29) (Scheme 3; red and blue underlining). IAPP(10-18) was shown to interact only with the C-terminus of Aβ Aβ(26-37) while IAPP(20-29) bound both Aβ regions Aβ(11-25) and Aβ(23-37) (Scheme 3; red and blue dashed underlining). As summarized in Scheme 3, a broad network of self- and cross-interactions between the hot regions of Aβ and IAPP was found.
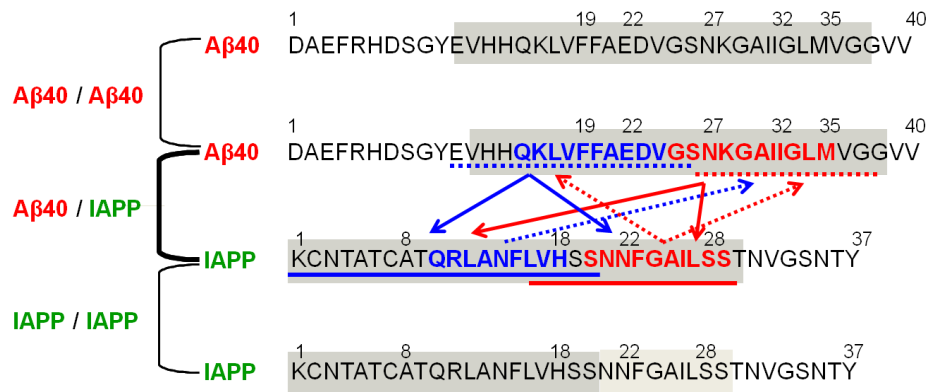
Scheme 3. Cross- and self-interacting regions of Aβ40 and IAPP as indicated by binding studies with peptide arrays (gray bars; light gray: weak interaction). The following sequences were used for the cross-interaction assays: Aβ(15–24) (blue letters), Aβ(25–35) (red letters), IAPP(10-18) (blue letters) and IAPP(20–29) IAPP(red letters). Red and blue underlinings represent the domains that were found in the cross-interaction assay. (The figure was adapted from Ref. [177].)

Given that the self-assembly process of Aβ42 is considered to play a main role in the pathogenesis of AD, the Aβ42 region that interact with IAPP were also determined using IAPP decamers on membrane [195]. Aβ42 showed similar binding behavior towards IAPP region as Aβ40.The results of the binding assays using membrane-bound peptide arrays helped in obtaining first information about the regions involved in the Aβ-IAPP interaction. As mentioned above, to determine more precisely the hot spot regions of the Aβ40-IAPP interaction interface, a number of partial Aβ40 and IAPP sequences and their fluorescently labeled analogues were synthesized - based on the results of the membrane bound peptide arrays -, and their interactions with IAPP and Aβ40 were characterized by fluorescence titration binding assays [177]. These studies identified five short peptide segments of Aβ and IAPP i.e. Aβ(19-22), Aβ(27-32), Aβ(35-40), IAPP(8-18), and IAPP(22-28) as hot regions of the Aβ40-IAPP cross-interaction interface and in addition they showed that these peptide regions are able to self- and to cross-interact (Scheme 4) [177]. As these peptide regions were also found to be high-affinity ligands of both Aβ and IAPP (app. K_ds in the nanomolar to low micromolar range) these results also suggested that the hetero-association between Aβ40 and IAPP proceeds via their self-association regions. Interestingly, it has been recently shown that the here identified IAPP hot regions IAPP(8-18) and IAPP(22-28) are also

involved in the binding to insulin [137, 166, 178, 196, 197]. Furthermore, two of the three Aβ hot regions found here to be involved in Aβ40-IAPP association Aβ(27-32) and Aβ(35-40) have been recently shown to also mediate binding of Aβ to tau [198].

The identified broad interaction network between the hot regions of Aβ and IAPP with regard to both self- and cross-interactions suggests that these segments interact with each other in a competitive way during Aβ and IAPP self- or hetero-association. As Aβ and IAPP are linear and conformationally flexible polypeptides in their early pre-fibrillar states, multiple-interactions would be possible and are consistent with the polymorphism observed in Aβ and IAPP fibrils [45].
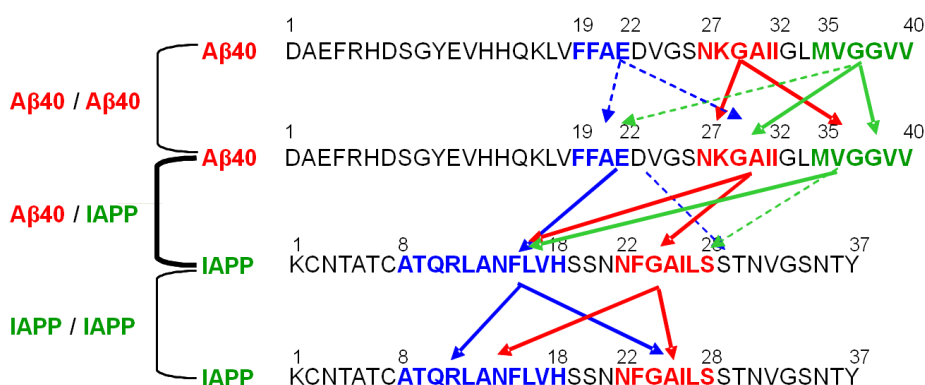
Scheme 4. Summary of the determined cross- and self-interactions between the hot (solid arrows) or slightly longer sequences (dashed arrows) of the Aβ40-IAPP interaction interface (hot regions in blue, red, and green). For interactions involving longer regions, the following sequences were used: Aβ(15-24) instead of Aβ(19-22), Aβ(25-35) instead of Aβ(27-32), and IAPP(20-29) instead of IAPP(22-28). (The figure was taken from Ref. [177].)

Based on the above results and on the earlier finding of our group that IAPP is able to suppress cytotoxic self-association of Aβ40 and vice versa, a study of the effect of the individual regions of IAPP on Aβ40 self-association into cytotoxic aggregates and fibrils was performed next [167]. Most likely due to the fact that native IAPP is a very amyloidogenic and cytotoxic peptide, its effect on suppressing cytotoxicity in 1/1 Aβ-IAPP solutions is weaker when compared to the effect of its non-amyloidogenic and non-toxic analogue IAPP-GI [167]. Therefore, the effects of the regions of both IAPP and IAPP-GI on Aβ40 cytotoxicity and fibrillogenesis were studied [199]. Since IAPP-GI is a very potent inhibitor of Aβ40 aggregation and toxicity and IAPP(8-18) and IAPP(22-28)-GI were identified as "hot regions" of the Aβ-IAPP and Aβ40-IAPP-GI interaction interface, it was expected that IAPP(8-28)-GI consisting of the two hot regions of the Aβ-IAPP interaction interface would also inhibit. Surprisingly, the results reported in chapter 3.2 showed that IAPP(8-28)-GI is unable to inhibit Aβ40 fibrillogenesis and toxicity as well as IAPP(8-28). As expected, no effects of the segments IAPP(1-7) and IAPP(30-37), which have been found to not bind Aβ40, on Aβ40 fibrillogenesis and cytotoxicity were observed [177].

Next, the role of the N- and C-terminal IAPP domains in inhibition of Aβ40 fibrillogenesis and toxicity was investigated by extending the hot regions of Aβ-IAPP interaction interface either to the N- or to the C- terminal direction. The segment IAPP(1-28)-GI was found to be a strong inhibitor of Aβ40 fibrillogenesis and toxicity although not as potent as IAPP-GI while IAPP(8-37)-GI was unable to suppress Aβ40 fibrillogenesis and toxicity. Taken together, these results suggest that the N-terminal sequence of IAPP(1-7) plays an important role in the inhibition of Aβ40 self-assembly although the domain IAPP(1-7) per se does not bind Aβ40 [177]. By contrast, the C-terminal region IAPP(30-37) appeared to be not required for inhibitory function even in combination with IAPP(8-28)-GI as in IAPP(8-37)-GI. However, the presence of IAPP(1-7) together with IAPP(30-37) as in full length IAPP-GI results in the strongest inhibitory effect [167]. The importance of the N-terminal region IAPP(1-7) for the inhibitory effect of IAPP-GI on Aβ40 aggregation and toxicity was further confirmed by studies on the effects of IAPP(8-18) and IAPP(1-18). In fact, both peptides could in part delay Aβ40 fibrillogenesis but only IAPP(1-18) was able to partially suppress formation of cytotoxic Aβ40 species as well while IAPP(8-18) had no effect. Both peptides IAPP(8-18) ($K_{d,app}$= 275±28 nM) and IAPP(1-18) ($K_{d,app}$= 183±56 nM) exhibited a similar binding affinity to Aβ40 suggesting that the N-terminus does not strongly contribute to the binding affinity of IAPP(1-18) to Aβ40 [177].
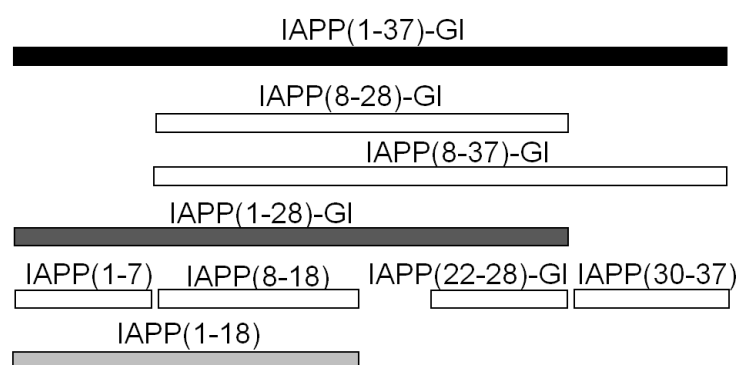
Scheme 5. Schematic summary of the effects of the IAPP-GI (and IAPP) region on Aβ40 amyloid formation and cytotoxicity. Bars in dark colour indicate regions found to inhibit both Aβ40 fibrillization and toxicity; the intensity of the colour correlates to their inhibitory potency. White bars indicate segments that had no effect on both of these two processes. (The figure was taken from Ref. [199].)

The second IAPP (IAPP-GI) "hot region" of IAPP (IAPP-GI) in the Aβ-IAPP interaction interface IAPP(22-28) (or IAPP(22-28)-GI) was also found to be unable to affect Aβ40 fibrillogenesis and toxicity. These findings together with the data on the effects of IAPP(8-18) are consistent with the results of the studies on the IAPP(8-28)-GI region which comprises both "hot regions".

In order to better understand the role of the N-terminus, conformational studies on the self-assembly propensity of IAPP(8-28)-GI and IAPP(1-28)-GI were performed using CD spectroscopy. IAPP(8-28)-GI forms mainly disordered soluble oligomers between 10 and 100 µM while IAPP(1-28)-GI exhibits likely a more stable structured oligomeric state between 10 and 100 µM. Thus, it appears that the N-terminus region IAPP(1-7) stabilizes a specific conformation of IAPP(1-28)-GI. These findings suggest that a specific conformation is required for the inhibition of Aβ40 self-assembly which is not significantly populated in IAPP(8-28)-GI. Previous studies have shown that the N-terminus in full length IAPP acts on the kinetics of fibril formation and mediates the conformational transition of IAPP into high order fibrillar aggregates though not being directly involved its self-association [136, 166, 178, 200]. Thus, it appears that the IAPP N-terminus plays an important role in both self- and hetero-association with Aβ40.

Similar self-association propensities were found for IAPP(8-28)-GI ($K_{d,app}$= 71±10 nM) and IAPP(1-28)-GI ($K_{d,app}$= 44±2 nM). By contrast, full length IAPP-GI had a much lower self association propensity ($K_{d,app}$= 4 nM) [155]. Thus, the differences in the inhibitory abilities of IAPP(8-28)-GI, IAPP(1-28)-GI, and IAPP-GI might be related to the differences between self-assembly potentials of these three peptides. The binding affinities of these peptides to Dac-Aβ40 were also determined. The affinities of Dac-Aβ40 to IAPP(8-28)-GI ($K_{d,app}$= 196±20 nM) and to IAPP(1-28)-GI ($K_{d,app}$= 192±10 nM) were very similar to the affinity toward IAPP-GI ($K_{d,app}$= 267±49 nM) [167]. Of note, the binding affinity of Dac-Aβ40 to IAPP(8-37)-GI, which was found to be unable to interfere with Aβ40 aggregation was in the nanomolar range as well ($K_{d,app}$= 74 nM). These results suggested that the apparent affinities of the interactions of the above IAPP-GI segments with Dac-Aβ40 do not directly correlate with their ability -or inability- to intervene with Aβ40 fibrillogenesis and cytotoxicity processes.

Next, a closer examination on the role of the N-terminal region IAPP(1-7) in the interaction of IAPP-GI with Aβ40 was carried out by using two different strategies. First, the effects of sequences IAPP(8-28)-GI vs. IAPP(1-28)-GI on Aβ40 fibrillogenesis and cytotoxicity were compared to the effects of analogs containing the "hot regions" IAPP(8-18) and IAPP(22-28)-GI which have been connected with each other by using two different tripeptide sequences (chapter 3.3.1). These two peptides containing (Gly-Gly-Gly) and (Ala-Ala-Ala) linkers belong to the series of designed peptides as inhibitors of Aβ40 aggregation which will be discussed later. Second, a systematic analysis on the specific role of the residues within the region of IAPP(1-7) was performed (chapter 3.3.2).

In the first approach, the influence of the N-terminus was examined through the maintenance of the hot regions, IAPP(8-18) and IAPP(22-28)-GI, and the substitution of the three residues between them in the native IAPP(8-28)-GI sequence with three glycines or three alanines.

The following peptides were generated and their properties compared to each other: IAPP(8-28)-GI vs. IAPP(1-28)-GI, IAPP(8-18)G3(22-28)-GI vs. IAPP(1-18)G3(22-28)-GI, IAPP(8-18)A3(22-28)-GI vs. IAPP(1-18)A3(22-28)-GI. Under the IAPP(8-28)-GI analogues, only IAPP(8-18)A3(22-28)-GI inhibited Aβ40 fibril formation and partially suppressed formation of cytotoxic Aβ40 species while IAPP(8-28)-GI and IAPP(8-18)G3(22-28)-GI were unable to do so. By contrast, the three different IAPP(1-28)-GI analogues were found to completely suppress formation of fibrils and toxic Aβ40 assemblies at the 72 h incubation time point. After incubation of 7 days, the mixtures of Aβ40 with IAPP(1-28)-GI or IAPP(1-18)A3(22-28)-GI were found to be as toxic as Aβ40 whereas the mixture of Aβ40 with IAPP(1-18)G3(22-28)-GI was still not toxic. These results suggested once again that the N-terminus plays an important role in the inhibitory effect of IAPP-GI of Aβ40 fibrillogenesis and cytotoxicity. Conformational studies on the IAPP(8-28)-GI analogues by CD spectroscopy revealed higher contents of disordered soluble oligomers between 10 and 100 µM. By contrast, the IAPP(1-28)-GI analogues consisted of more ordered and stable oligomers between 10 and 100 µM. These results suggested that the N-terminus stabilizes a specific conformation in the IAPP(1-28)-GI analogues which appears to play an important role in the inhibitory effect of Aβ40 fibrillogenesis and cytotoxicity.

Many studies have shown that peptide aggregation can occur by a conformational transition of α-helical or random coil states to β-sheets [138, 201, 202]. Additionally, it has been shown that the N-terminal region of IAPP IAPP(1-18) has an α-helical propensity [138, 197]. Therefore, TFE titration studies were performed next in order to compare the α-helical propensities of the different analogues. Both the IAPP(8-28)-GI and the IAPP(1-28)-GI analogues were found to form α-helices and the midpoints of the transitions were at similar TFE concentrations. These results indicated that the α-helical propensities of the IAPP(8-28)-GI and the IAPP(1-28)-GI analogues is not directly related to their different potencies with regard to inhibition Aβ40 fibrillogenesis and cytotoxicity. These studies also showed that the N-terminal region does not significantly contribute to the stabilization of the α-helical structure in IAPP(1-28)-GI. Next, the affinities of interaction of these peptides with Aβ40 were determined by fluorescence based binding assays in solution. Affinities in the micro- to low nanomolar range were found for all studied interactions consistent with no correlation between binding affinities and inhibitory effects on Aβ40 aggregation and toxicity.

In order to investigate the potential role of the specific residues within the N-terminal sequence IAPP(1-7) on Aβ40 aggregation and toxicity, the following peptides were synthesized and studied: G7-IAPP(8-28)-GI, A7-IAPP(8-28)-GI, (A1-3)IAPP(1-28)-GI, (A4-6)IAPP(1-28)-GI, and IAPP(1-28)-GI-red. Thereby, G7-IAPP(8-28)-GI and A7-IAPP(8-28)-GI were proved to be weaker inhibitors of Aβ40 fibrillogenesis and cytotoxicity as compared to IAPP(1-28)-GI. On the other hand, these two peptides were clearly more potent inhibitors of

Aβ40 aggregation and toxicity as compared to IAPP(8-28)-GI indicating that part of this inhibitory effect can be obtained by adding a peptide sequence to the N-terminus of IAPP(8-28)-GI. However, (A1-3)IAPP(1-28)-GI and (A4-6)IAPP(1-28)-GI were found to inhibit Aβ40 fibrillogenesis and cytotoxicity in a similar manner as IAPP(1-28)-GI. These data suggested that, unlike the substitution of all 7 residues, substitution of only two residues in the IAPP(1-7) region is not sufficient to affect the inhibitory effect of IAPP(1-28)-GI on Aβ40 aggregation and toxicity. The reduced form of IAPP(1-28)-GI IAPP(1-28)-GI-red was found to have similar inhibitory property as IAPP(1-28)-GI proving that the disulfide bridge between Cys^2 and Cys^7 does not play a crucial role in the inhibition of Aβ40 aggregation. The disulfide bridge in IAPP is highly conserved between the various species, it is required for the biological activity of IAPP, and prevents the N-terminus from forming a β-strand [187, 203]. On the other hand the disulfide bridge does not contribute to the formation of the fibrillar core structure but it appears to play an important role in IAPP self-assembly [187]. The results of the here presented work would suggest that the similarly strong inhibitory effects of the oxidized and reduced forms of IAPP(1-28)-GI as compared to the lack of effects of IAPP(8-28)-GI, G7-IAPP(8-28)-GI and A7-IAPP(8-28)-GI might be due to differences between the interactions of these peptides with Aβ40. In other words, the different IAPP(1-28)-GI analogues may likely adopt different conformations and would thus interact in different ways with Aβ40. The results of the CD concentration dependence studies of the IAPP(1-28)-GI analogues indicated formation of mainly disordered soluble oligomers for G7-IAPP(8-28)-GI and A7-IAPP(8-28)-GI between 10 and 200 µM while a quite stable structured oligomeric state was found to be populated by (A1-3)IAPP(1-28)-GI and (A4-6)IAPP(1-28)-GI between 5 and 50 µM. TFE titration studies showed that A7-IAPP(8-28)-GI has the highest α-helical content followed by (A1-3)IAPP(1-28)-GI and (A4-6)IAPP(1-28)-GI in agreement with the presence of the α-helix inducing substituent Ala. G7-IAPP(8-28)-GI was found to exhibit a similar α-helical content to IAPP(1-28)-GI. Taken together, these results suggested that (A1-3)IAPP(1-28)-GI and (A4-6)IAPP(1-28)-GI may populate a specific conformer which might be also populated by IAPP(1-28)-GI and which may be important for inhibition of Aβ40 self-assembly. By contrast G7-IAPP(8-28)-GI and A7-IAPP(8-28)-GI appear to exhibit higher disordered secondary structural contents than IAPP(1-28)-GI. Self-association affinities and binding affinities to Dac-Aβ40 of the IAPP(1-28)-GI analogues were found to be in the low nanomolar range. Since the binding affinities to Dac-Aβ40 of these different peptides were very similar to each other, it appears that they do not correlate to their effects on Aβ40 fibrillogenesis and cytotoxicity. It is known that the sequence IAPP(1-7) alone does not bind IAPP and Aβ40; thus, the binding affinities toward Dac-Aβ40 are the result of the interaction of the IAPP hot regions with Dac-Aβ40 [177].

The next question which was addressed in my thesis was whether it is possible to devise a potent inhibitor of Aβ40 aggregation by covalently linking the previously identified IAPP hot regions of the Aβ-IAPP interaction interface to each other. Given that IAPP(8-28)-GI, which contains these two "hot regions" IAPP(8-18) and IAPP(22-28)-GI linked to each other by the tripeptide sequence SSN, was found to be unable to inhibit Aβ40 aggregation and toxicity, the design of these novel peptides focused on using different linkers to connect the hot regions.

As first, the sequence SSN was replaced by non-native hydrophobic or hydrophilic linkers generating the following peptides: IAPP(8-18)Aoc(22-28)-GI, IAPP(8-18)Adc(22-28)-GI and IAPP(8-18)PEG(22-28)-GI (chapter 3.4.1). IAPP(8-18)Adc(22-28)-GI was found to partially inhibit Aβ40 fibrillogenesis and cytotoxicity whereas IAPP(8-18)Aoc(22-28)-GI and IAPP(8-18)PEG(22-28)-GI were completely inactive. The linkers Aoc and PEG had a similar length which corresponds to the length of a tripeptide in an extended conformation as in the IAPP(8-28)-GI sequence; however, Aoc is hydrophobic and PEG hydrophilic. These two peptides were found to be unable to suppress Aβ40 aggregation and toxicity as was also found for IAPP(8-28)-GI. On the other side, IAPP(8-18)Adc(22-28)-GI, the peptide with the longer spacer Adc (corresponding approximately to the length of a tetrapeptide), slightly inhibited Aβ40 fibrillogenesis and cytotoxicity suggesting that the length of the spacer might play an important role. The common denominator of the above analogues was the high degree of flexibility of the linkers which might have favored the self association rather than the interaction with Aβ40.

The conformational studies of the above peptides indicated significant differences between their conformations related to the nature of the linkers. IAPP(8-18)Aoc(22-28)-GI exhibited a mixture of disordered and β-sheet structures at low concentrations and mainly β-sheet structures at higher concentrations. The elongation of Aoc by two methylene groups as in IAPP(8-18)Adc(22-28)-GI resulted in an increase of the hydrophobic character of the linker. The Adc peptide exhibited pronounced β-sheet structure even at low concentrations. By contrast, IAPP(8-18)PEG(22-28)-GI forms mainly disordered soluble oligomers. The hydrophobic character of Aoc and Adc and the absence of hydrogen bond forming capacity of the methylene groups of these two residues likely underlies the results of the TFE titration studies of IAPP(8-18)Aoc(22-28)-GI and IAPP(8-18)Adc(22-28)-GI. In fact, only low amounts of α-helical conformers were observed for both peptides following TFE titration studies. By contrast, strong α-helical stabilization was observed in IAPP(8-18)PEG(22-28)-GI likely due to the hydrophilic character and hydrogen bond forming ability of the (O-CH$_2$-CH$_2$) unit in PEG.

Next, the sequence SSN between the two "hot regions" was substituted for tripeptide sequences with side chains of different hydrophobicity and steric hindrance yielding the peptides IAPP(8-18)G3(22-28)-GI, IAPP(8-18)A3(22-28)-GI, IAPP(8-18)V3(22-28)-GI, and IAPP(8-18)L3(22-28)-GI (chapter 3.4.2). Their effects on inhibition of Aβ40 fibrillogenesis and cytotoxicity were found to correlate well with hydrophobicity or steric hindrance of the side chains of the amino acids in the linker sequences. In fact, IAPP(8-18)L3(22-28)-GI was found to be the most potent inhibitor whereas IAPP(8-28)-GI and IAPP(8-18)G3(22-28)-GI had no effect and IAPP(8-18)A3(22-28)-GI and IAPP(8-18)V3(22-28)-GI had an intermediate effect on Aβ40 aggregation and cell toxicity. These results suggested that a potent inhibitor was obtained by increasing the hydrophobicity and the steric hindrance of the side chains of the linker between the two hot regions. According to the hydropathic scale of Kite and Doolittle, Val is the most hydrophobic amino acid used as a linker in the series of IAPP(8-28)-GI analogues [190]. This would suggest that both the hydrophobicity character and the steric hindrance imposed by the methyl groups on the C^β of Val play an important role in the effect of this peptide on Aβ40 aggregation and cell toxicity. Additional information was obtained by CD studies on the conformation; thus, IAPP(8-28)-GI, IAPP(8-18)G3(22-28)-GI, and IAPP(8-18)A3(22-28)-GI exhibited mainly disordered oligomeric structures in aqueous solution pH 7.4 between 10 and 100 µM whereas IAPP(8-18)V3(22-28)-GI and IAPP(8-18)L3(22-28)-GI were found to form mainly oligomeric β-sheet structures. The CD data suggest that analogues adopting mainly β-sheet/β-turn structures are more likely suitable to intervene with Aβ40 self-assembly. The CD TFE titration studies revealed that the α-helical content can be modulated by changing the residues between the "hot-regions"; namely, IAPP(8-18)A3(22-28)-GI and IAPP(8-18)L3(22-28)-GI had the highest α-helical contents in agreement with the high α-helical propensity of Ala and Leu [186]. However, no correlation of α-helix forming propensity and inhibitory potentials was found. The binding affinities of these peptides to Dac-Aβ40 were in micro- to low nanomolar range which indicated that they are not strongly related to the inhibitory effects on Aβ40 fibrillogenesis and cytotoxicity.

In order to obtain more evidence for the hypothesis that a specific conformation of the inhibitor consisting of linked IAPP hot regions and bulky side chains between the hot regions are key components of a potent Aβ inhibitor another class of constrained peptides was devised consisting of IAPP(8-18)L3(22-28)-GI-cyclo and IAPP(8-18)Amb-Ab(22-28)-GI (chapter 3.4.3). IAPP(8-18)L3(22-28)-GI-cyclo is the cyclic analogue of IAPP(8-18)L3(22-28)-GI which was found to be a potent inhibitor of Aβ40 aggregation and toxicity. The linker in IAPP(8-18)Amb-Ab(22-28)-GI was selected due to its extended nature and rigidity in order to devise an analogue with diminished intramolecular association of the two hot regions [192]. Aβ40 fibrillogenesis and cytotoxicity assays revealed that IAPP(8-18)L3(22-28)-GI-cyclo

could not intervene with Aβ40 self-assembly and toxicity whereas IAPP(8-18)Amb-Ab(22-28)-GI strongly suppressed Aβ40 cytotoxicity and fibril formation. Both peptides bound Dac-Aβ40 with low micromolar affinities while their self association affinities were in the low nanomolar range. Therefore, no correlation was found between their effects on Aβ40 cytotoxicity and fibrillogenesis and binding affinities to Dac-Aβ40. The apparent affinity of self-association of IAPP(8-18)L3(22-28)-GI-cyclo was 10 times lower than in the case of IAPP(8-18)L3(22-28)-GI indicating that the cyclic constraint in IAPP(8-18)L3(22-28)-GI-cyclo may promote self-association. CD concentration dependence studies confirmed that IAPP(8-18)L3(22-28)-GI-cyclo had a higher aggregation propensity than IAPP(8-18)L3(22-28)-GI. IAPP(8-18)Amb-Ab(22-28)-GI formed also oligomeric β-sheet structures likely due to the hydrophobicity of the linker. The behavior of these two peptides in TFE-containing solutions was quite atypical: thus, IAPP(8-18)L3(22-28)-GI-cyclo adopted mainly disordered conformations while IAPP(8-18)Amb-Ab(22-28)-GI exhibited weak α-helical contents. Thus, the constraints imposed on the above two analogues by the linkers had remarkable effects on their structures and their effects on Aβ40 aggregation and toxicity. In fact, the potent inhibitor IAPP(8-18)L3(22-28)-GI became totally inactive when constrained - likely in a β-hairpin conformation - as in IAPP(8-18)L3(22-28)-GI-cyclo while the presence of a rigid extended linker as in IAPP(8-18)Amb-Ab(22-28)-GI was found to yield a potent inhibitor of Aβ40 aggregation and toxicity.

The last part of the designed inhibitors of Aβ40 aggregation and toxicity focused on analogues containing β-hairpin stabilizing or destabilizing charges at the N- or C-termini of the IAPP(8-18)A3(22-28)-GI (chapter 3.4.4). The following three analogues were designed and tested: K3-IAPP(8-18)A3(22-28)-GI-K3, E3-IAPP(8-18)A3(22-28)-GI-K3, K3-IAPP(8-28)-GI-K3. In addition, several control peptides were also tested. K3-IAPP(8-18)A3(22-28)-GI-K3 was found to be the strongest inhibitor whereas E3-IAPP(8-18)A3(22-28)-GI-K3 was completely inactive. These findings suggested that coulombic repulsion between the lysines present in K3-IAPP(8-18)A3(22-28)-GI-K3 might have destabilize a β-hairpin which may have caused more effective interaction with Aβ40 with regard to inhibition of Aβ40 self-association and toxicity. Instead, the coulombic attraction forces between the side chains of the E3- and K3-streches might have promoted the β-hairpin in peptide E3-IAPP(8-18)A3(22-28)-GI-K3. Studies on β-hairpins have shown that the peptides with β-hairpin forming propensities can become stabilized by inserting at the peptide edges electrostatic pair residues [204]. Interestingly, IAPP(8-28)-GI which was completely inactive with regard to the inhibition of Aβ40 aggregation and toxicity changed completely its properties when three lysines were added at the N- and C- termini as in K3-IAPP(8-28)-GI-K3 demonstrating the importance of the charges and the conformation stabilized by their presence for the inhibitory effect on

Aβ40 fibrillogenesis and cytotoxicity. As expected by the above findings, the control peptide with six N^ε-acetylated lysine residues K3*-IAPP(8-18)A3(22-28)-GI-K3* was found to be unable to inhibit Aβ40 aggregation and toxicity. Further, the control peptide K3-IAPP(8-18)A3(22-28)-GI was found to partially inhibit while IAPP(8-18)A3(22-28)-GI-K3 did not. These latter finding raised the question whether the basic residues at the N-terminus of IAPP(8-18)A3(22-28)-GI are more important for the inhibition than the one at the C-terminus. Previous studies suggested that the high affinity of the B10 antibody to Aβ40 is related to the basic residues located on the antibody which are establishing electrostatic interactions with the acidic residues of Aβ40 mainly located in the N-terminus [205].

Next, the affinities of the above analogues with Aβ40 were determined by fluorescence based binding studies. Thereby, binding affinities in the nanomolar range were determined. The apparent self-association affinities were, however, lower than the app. K_ds to Dac-Aβ40 except for the strongest Aβ40 aggregation inhibitor, K3-IAPP(8-18)A3(22-28)-GI-K3, for which the self-association affinity ($K_{d,app}$= 64 nM) was in the same range as the affinity of the interaction with Dac-Aβ40 ($K_{d,app}$= 23±1 nM).

As a final point, a comparison of the inhibitory potencies of the strongest inhibitors identified in this work was performed (chapter 3.4.5). Three peptides were found to be the most efficient Aβ40 aggregation inhibitors: IAPP(8-18)L3(22-28)-GI, IAPP(8-18)Amb-Ab(22-28)-GI, and K3-IAPP(8-18)A3(22-28)-GI-K3. First, cytotoxicity assays at the 7 days incubation time point with Aβ40 were performed and IAPP(8-18)L3(22-28)-GI was found to be the strongest inhibitor: in fact, it suppressed formation of cytotoxic Aβ40 species up to the time point of 7 days. K3-IAPP(8-18)A3(22-28)-GI-K3 also inhibited at that time-point albeit it had a weaker effect than IAPP(8-18)L3(22-28)-GI whereas no inhibitory effect was found for IAPP(8-18)Amb-Ab(22-28)-GI. Studies on the half maximal inhibitory concentration (IC_{50}) for the inhibitory effects of these peptides on formation of cytotoxic Aβ40 species designated IAPP(8-18)L3(22-28)-GI to be the peptide with the strongest inhibitory capacity (IC_{50}= 95±16 nM) which was very similar to the IC_{50} of the effect of IAPP-GI on Aβ40 cytotoxicity (IC_{50}= 63 nM). Slightly lower inhibitory potencies were found for IAPP(8-18)Amb-Ab(22-28)-GI (IC_{50}= 158±36 nM) and K3-IAPP(8-18)A3(22-28)-GI-K3 (IC_{50}= 292±78 nM). Finally, it was examined whether these peptides could block toxicity of already formed cytotoxic Aβ40 aggregates. IAPP(8-18)L3(22-28)-GI was found to block toxicity of already formed Aβ40 cytotoxic assemblies at a 100-fold excess to Aβ40. IAPP(8-18)Amb-Ab(22-28)-GI could only partially reverse the cytotoxicity of already formed Aβ40 aggregates under these conditions and K3-IAPP(8-18)A3(22-28)-GI-K3 had no effect. Of note, IAPP-GI has been previously found to redissociate already formed fibrils and cytotoxic Aβ40 aggregates at a 50-fold excess to Aβ40 [167].

In conclusion, IAPP(8-18)L3(22-28)-GI is a designed IAPP-GI analogue whose properties with regard to inhibition of Aβ40 aggregation and toxicity are very similar to the properties of IAPP-GI. In fact, IAPP(8-18)L3(22-28)-GI was found to be an inhibitor of Aβ40 cytotoxic oligomerization and fibrillogenesis with low nanomolar activity and additionally it is able to reverse the cytotoxic effect of already formed Aβ40 aggregates.

A schematic summary of the results obtained in this thesis IAPP-GI-derived inhibitors of Aβ40 aggregation and toxicity is presented in Fig. 52. It has been previously shown that IAPP-GI is a conformationally stabilized non-amyloidogenic conformer of IAPP [155, 167]. A model of IAPP fibrils obtained by solid state NMR studies has suggested a parallel in-register assembly with a β-strand-loop-β-strand motif [142]. Additionally, studies carried out by ion mobility mass spectrometry combined with molecular dynamics have suggested the presence of two types of monomeric IAPP: a helix coil family and a β-hairpin one [139]. Following studies of the same group on IAPP dimers proposed that the β-hairpin family will further aggregate to fibrils [206]. It was also reported that the binding between two β-hairpins occurs side by side rather than stacking one over the other suggesting a possible mechanism for the observed inhibitory effect of N-methylated IAPP sequences or the IAPP mimic IAPP-GI on IAPP aggregation and toxicity [155, 206]. In fact, the N-methylations in IAPP-GI would allow the binding on one side and block the side-by-side sheet assembly via the other side [206]. Thus, a novel designed peptide inhibitor containing the two IAPP hot regions IAPP(8-18) and IAPP(22-28)-GI might possibly have to mimic a specific IAPP-GI conformer in order to inhibit Aβ40 fibrillogenesis and cytotoxicity. Four different chemical ways were found here to be effective in generating such inhibitory potential (Fig. 52). First, the addition of the N-terminal sequence to IAPP(8-28)-GI IAPP(1-7) as in IAPP(1-28)-GI which may have contributed to stabilization of a preferred conformation in IAPP(1-28)-GI [199]. In fact, CD data have indicated a higher conformational flexibility in IAPP(8-28)-GI as compared to IAPP(1-28)-GI. Second, the insertion of a sterically hindered hydrophobic linker between the hot regions as in IAPP(8-18)L3(22-28)-GI which appears to stabilize a specific β-sheet/β-turn conformation. Third, the introduction of an extended rigid linker between the hot regions as in IAPP(8-18)Amb-Ab(22-28)-GI which also exhibited a prominent β-sheet/β-turn stabilization. Fourth, the introduction of positively charged residues at the N- and C-termini of the covalently linked hot regions as in K3-IAPP(8-18)A3(22-28)-GI-K3. The CD data of all here identified IAPP-derived inhibitors of Aβ40 aggregation and toxicity indicated always at least in part β-sheet/β-turn contents, especially in the case of IAPP(8-18)L3(22-28)-GI which was the most potent Aβ40 fibrillogenesis and cytotoxicity inhibitor. The potent inhibitors found in this work may thus bind to a specific Aβ40 conformation such as a β-hairpin and prevent its further aggregation. In fact, it has been shown that a stabilized β-

hairpin of Aβ, obtained by a double cysteine mutation of Aβ followed by formation of intramolecular disulfide bridge, produces neurotoxic oligomers [207].
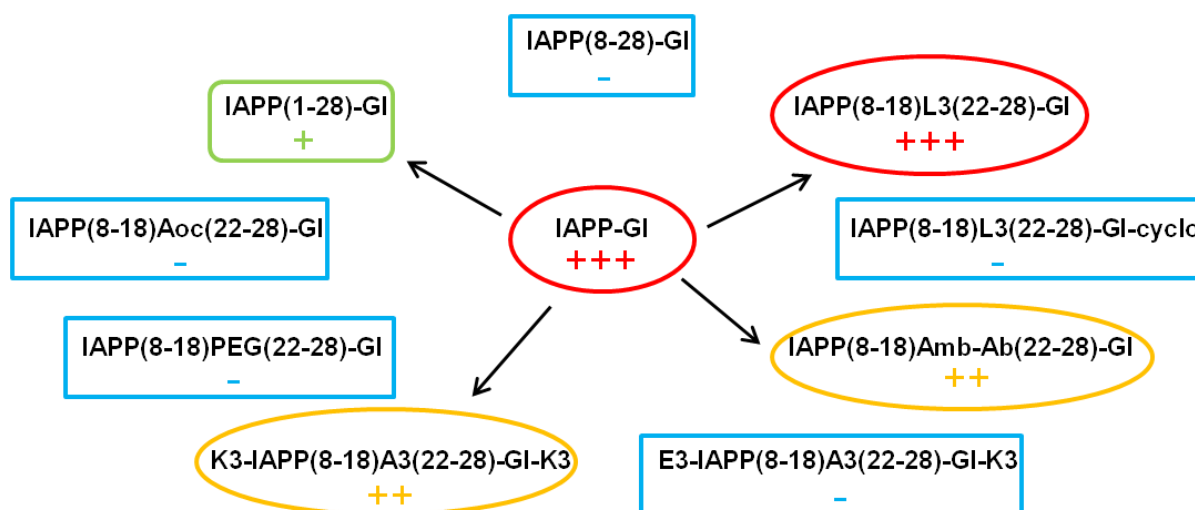
Fig. 52. Summary of the effects of IAPP-GI and suitable representatives of the here presented analogs. The ability of these peptides to inhibit Aβ40 aggregation and toxicity is represented with +++ (potent inhibitor), ++ (good inhibitor), + (middle inhibitor), and – (ineffective).

By contrast, peptides as IAPP(8-28)-GI, IAPP(8-18)Aoc(22-28)-GI, IAPP(8-18)PEG(22-28)-GI which were found to be ineffective in the inhibition of Aβ40 aggregation and toxicity might be unable to stabilize a specific conformation which mimics the IAPP-GI conformation and would be efficient in the inhibition of Aβ40 aggregation. On the other side IAPP(8-18)L3(22-28)-GI-cyclo and E3-IAPP(8-18)A3(22-28)-GI-K3 which were also found to be unable to inhibit Aβ40 aggregation and toxicity might be constrained into a specific conformation that might be not capable to interact with the specific Aβ40 conformation and block its conversion into toxic aggregates.

The studies presented in this work resulted in a first generation of IAPP-GI-derived peptides with different biophysical properties and inhibitory effects on Aβ40 aggregation and toxicity. Under these peptides, IAPP(8-18)L3(22-28)-GI was found to have similar properties as IAPP-GI and is thus one of the most potent ligands and inhibitors of Aβ40 aggregation and toxicity reported so far. In fact, other reported inhibitors are active only at the micromolar concentration range and block only partially Aβ40 fibrillogenesis and cytotoxic self-assembly [208]. For example, inhibitors containing N-methyl amino acids as in the case of K(N-Me)LV(N-Me)FF(N-Me)AE, a peptide based on the Aβ core region with three N-methyl amino acids, has been shown to inhibit Aβ fibril formation but only when it is added at much higher fold excess [108]. Further, a dipeptide without sequence similarity to Aβ40 containing an aromatic moiety and a β-sheet breaking element i.e. D-Trp-Aib has been recently also shown

to be a potent inhibitor of Aβ fibril formation but also when it is added at much higher fold excess [209].

Detailed studies on the conformation of the individual IAPP-GI analogues alone and in complex with Aβ will now be a very important next step towards understanding the mechanism of their action.

.

5 References

1.	Clamp, M., Fry, B., Kamal, M., Xie, X., Cuff, J., Lin, M.F., Kellis, M., Lindblad-Toh, K., and Lander, E.S. (2007). Distinguishing protein-coding and noncoding genes in the human genome. Proc Natl Acad Sci U S A *104*, 19428-19433.

2.	Dobson, C.M. (2003). Protein folding and misfolding. Nature *426*, 884-890.

3.	Anfinsen, C.B., Haber, E., Sela, M., and White, F.H., Jr. (1961). The kinetics of formation of native ribonuclease during oxidation of the reduced polypeptide chain. Proc Natl Acad Sci U S A *47*, 1309-1314.

4.	Anfinsen, C.B. (1973). Principles that govern the folding of protein chains. Science *181*, 223-230.

5.	Levinthal, C. (1968). Are there pathways for protein folding? Extrait du Journal de Chimie Physique *65*, 44.

6.	Dill, K.A., and Chan, H.S. (1997). From Levinthal to pathways to funnels. Nat Struct Biol *4*, 10-19.

7.	Dill, K.A., Fiebig, K.M., and Chan, H.S. (1993). Cooperativity in protein-folding kinetics. Proc Natl Acad Sci U S A *90*, 1942-1946.

8.	Fersht, A.R. (1997). Nucleation mechanisms in protein folding. Curr Opin Struct Biol *7*, 3-9.

9.	Bryngelson, J.D., Onuchic, J.N., Socci, N.D., and Wolynes, P.G. (1995). Funnels, pathways, and the energy landscape of protein folding: a synthesis. Proteins *21*, 167-195.

10.	Wright, P.E., and Dyson, H.J. (1999). Intrinsically unstructured proteins: re-assessing the protein structure-function paradigm. J Mol Biol *293*, 321-331.

11.	Uversky, V.N., and Dunker, A.K. Understanding protein non-folding. Biochim Biophys Acta *1804*, 1231-1264.

12.	Dunker, A.K., Lawson, J.D., Brown, C.J., Williams, R.M., Romero, P., Oh, J.S., Oldfield, C.J., Campen, A.M., Ratliff, C.M., Hipps, K.W., Ausio, J., Nissen, M.S., Reeves, R., Kang, C., Kissinger, C.R., Bailey, R.W., Griswold, M.D., Chiu, W., Garner, E.C., and Obradovic, Z. (2001). Intrinsically disordered protein. J Mol Graph Model *19*, 26-59.

13.	Hardesty, B., and Kramer, G. (2001). Folding of a nascent peptide on the ribosome. Prog Nucleic Acid Res Mol Biol *66*, 41-66.

14.	Lee, S., and Tsai, F.T. (2005). Molecular chaperones in protein quality control. J Biochem Mol Biol *38*, 259-265.

15.	Hartl, F.U., and Hayer-Hartl, M. (2002). Molecular chaperones in the cytosol: from nascent chain to folded protein. Science *295*, 1852-1858.

16.	Hartl, F.U. (1996). Molecular chaperones in cellular protein folding. Nature *381*, 571-579.

17.	Frydman, J. (2001). Folding of newly translated proteins in vivo: the role of molecular chaperones. Annu Rev Biochem *70*, 603-647.

18.	Stevens, F.J., and Argon, Y. (1999). Protein folding in the ER. Semin Cell Dev Biol *10*, 443-454.

19.	Groll, M., Bochtler, M., Brandstetter, H., Clausen, T., and Huber, R. (2005). Molecular machines for protein degradation. Chembiochem *6*, 222-256.

20.	Horwich, A.L., Weber-Ban, E.U., and Finley, D. (1999). Chaperone rings in protein folding and degradation. Proc Natl Acad Sci U S A *96*, 11033-11040.

21.	Yerbury, J.J., Rybchyn, M.S., Easterbrook-Smith, S.B., Henriques, C., and Wilson, M.R. (2005). The acute phase protein haptoglobin is a mammalian extracellular chaperone with an action similar to clusterin. Biochemistry *44*, 10914-10925.

22.	Yerbury, J.J., Stewart, E.M., Wyatt, A.R., and Wilson, M.R. (2005). Quality control of protein folding in extracellular space. EMBO Rep *6*, 1131-1136.

23.	Humphreys, D.T., Carver, J.A., Easterbrook-Smith, S.B., and Wilson, M.R. (1999). Clusterin has chaperone-like activity similar to that of small heat shock proteins. J Biol Chem *274*, 6875-6881.

24.	French, K., Yerbury, J.J., and Wilson, M.R. (2008). Protease activation of alpha2-macroglobulin modulates a chaperone-like action with broad specificity. Biochemistry *47*, 1176-1185.

25. Coker, A.R., Purvis, A., Baker, D., Pepys, M.B., and Wood, S.P. (2000). Molecular chaperone properties of serum amyloid P component. FEBS Lett *473*, 199-202.

26. Wilson, M.R., Yerbury, J.J., and Poon, S. (2008). Potential roles of abundant extracellular chaperones in the control of amyloid formation and toxicity. Mol Biosyst *4*, 42-52.

27. Amaral, M.D. (2004). CFTR and chaperones: processing and degradation. J Mol Neurosci *23*, 41-48.

28. Lomas, D.A., and Carrell, R.W. (2002). Serpinopathies and the conformational dementias. Nat Rev Genet *3*, 759-768.

29. Chiti, F., and Dobson, C.M. (2006). Protein misfolding, functional amyloid, and human disease. Annu Rev Biochem *75*, 333-366.

30. Sunde, M., and Blake, C. (1997). The structure of amyloid fibrils by electron microscopy and X-ray diffraction. Adv Protein Chem *50*, 123-159.

31. Eanes, E.D., and Glenner, G.G. (1968). X-ray diffraction studies on amyloid filaments. J Histochem Cytochem *16*, 673-677.

32. Stromer, T., and Serpell, L.C. (2005). Structure and morphology of the Alzheimer's amyloid fibril. Microsc Res Tech *67*, 210-217.

33. Herczenik, E., and Gebbink, M.F. (2008). Molecular and cellular aspects of protein misfolding and disease. FASEB J *22*, 2115-2133.

34. Jimenez, J.L., Guijarro, J.I., Orlova, E., Zurdo, J., Dobson, C.M., Sunde, M., and Saibil, H.R. (1999). Cryo-electron microscopy structure of an SH3 amyloid fibril and model of the molecular packing. EMBO J *18*, 815-821.

35. Caughey, B., and Lansbury, P.T. (2003). Protofibrils, pores, fibrils, and neurodegeneration: separating the responsible protein aggregates from the innocent bystanders. Annu Rev Neurosci *26*, 267-298.

36. Tycko, R. (2006). Molecular structure of amyloid fibrils: insights from solid-state NMR. Q Rev Biophys *39*, 1-55.

37. Serpell, L.C., and Smith, J.M. (2000). Direct visualisation of the beta-sheet structure of synthetic Alzheimer's amyloid. J Mol Biol *299*, 225-231.

38. Serpell, L.C., Sunde, M., Benson, M.D., Tennent, G.A., Pepys, M.B., and Fraser, P.E. (2000). The protofilament substructure of amyloid fibrils. J Mol Biol *300*, 1033-1039.

39. Nilsson, M.R. (2004). Techniques to study amyloid fibril formation in vitro. Methods *34*, 151-160.

40. Bauer, H.H., Aebi, U., Haner, M., Hermann, R., Muller, M., and Merkle, H.P. (1995). Architecture and polymorphism of fibrillar supramolecular assemblies produced by in vitro aggregation of human calcitonin. J Struct Biol *115*, 1-15.

41. Goldsbury, C.S., Cooper, G.J., Goldie, K.N., Muller, S.A., Saafi, E.L., Gruijters, W.T., Misur, M.P., Engel, A., Aebi, U., and Kistler, J. (1997). Polymorphic fibrillar assembly of human amylin. J Struct Biol *119*, 17-27.

42. Sawaya, M.R., Sambashivan, S., Nelson, R., Ivanova, M.I., Sievers, S.A., Apostol, M.I., Thompson, M.J., Balbirnie, M., Wiltzius, J.J., McFarlane, H.T., Madsen, A.O., Riekel, C., and Eisenberg, D. (2007). Atomic structures of amyloid cross-beta spines reveal varied steric zippers. Nature *447*, 453-457.

43. Lue, L.F., Kuo, Y.M., Roher, A.E., Brachova, L., Shen, Y., Sue, L., Beach, T., Kurth, J.H., Rydel, R.E., and Rogers, J. (1999). Soluble amyloid beta peptide concentration as a predictor of synaptic change in Alzheimer's disease. Am J Pathol *155*, 853-862.

44. Stefani, M., and Dobson, C.M. (2003). Protein aggregation and aggregate toxicity: new insights into protein folding, misfolding diseases and biological evolution. J Mol Med *81*, 678-699.

45. Uversky, V.N., and Fink, A.L. (2004). Conformational constraints for amyloid fibrillation: the importance of being unfolded. Biochim Biophys Acta *1698*, 131-153.

46. Otzen, D.E., Kristensen, O., and Oliveberg, M. (2000). Designed protein tetramer zipped together with a hydrophobic Alzheimer homology: a structural clue to amyloid assembly. Proc Natl Acad Sci U S A *97*, 9907-9912.

47. Chiti, F., Taddei, N., Baroni, F., Capanni, C., Stefani, M., Ramponi, G., and Dobson, C.M. (2002). Kinetic partitioning of protein folding and aggregation. Nat Struct Biol *9*, 137-143.

48. Schwartz, R., Istrail, S., and King, J. (2001). Frequencies of amino acid strings in globular protein sequences indicate suppression of blocks of consecutive hydrophobic residues. Protein Sci *10*, 1023-1031.

49. Schmittschmitt, J.P., and Scholtz, J.M. (2003). The role of protein stability, solubility, and net charge in amyloid fibril formation. Protein Sci *12*, 2374-2378.

50. Kallberg, Y., Gustafsson, M., Persson, B., Thyberg, J., and Johansson, J. (2001). Prediction of amyloid fibril-forming proteins. J Biol Chem *276*, 12945-12950.

51. Fratiglioni, L., Launer, L.J., Andersen, K., Breteler, M.M., Copeland, J.R., Dartigues, J.F., Lobo, A., Martinez-Lage, J., Soininen, H., and Hofman, A. (2000). Incidence of dementia and major subtypes in Europe: A collaborative study of population-based cohorts. Neurologic Diseases in the Elderly Research Group. Neurology *54*, S10-15.

52. Grundke-Iqbal, I., Iqbal, K., Quinlan, M., Tung, Y.C., Zaidi, M.S., and Wisniewski, H.M. (1986). Microtubule-associated protein tau. A component of Alzheimer paired helical filaments. J Biol Chem *261*, 6084-6089.

53. Masters, C.L., Simms, G., Weinman, N.A., Multhaup, G., McDonald, B.L., and Beyreuther, K. (1985). Amyloid plaque core protein in Alzheimer disease and Down syndrome. Proc Natl Acad Sci U S A *82*, 4245-4249.

54. Hardy, J., and Selkoe, D.J. (2002). The amyloid hypothesis of Alzheimer's disease: progress and problems on the road to therapeutics. Science *297*, 353-356.

55. Goldgaber, D., Lerman, M.I., McBride, O.W., Saffiotti, U., and Gajdusek, D.C. (1987). Characterization and chromosomal localization of a cDNA encoding brain amyloid of Alzheimer's disease. Science *235*, 877-880.

56. Mattson, M.P. (1997). Cellular actions of beta-amyloid precursor protein and its soluble and fibrillogenic derivatives. Physiol Rev *77*, 1081-1132.

57. Turner, P.R., O'Connor, K., Tate, W.P., and Abraham, W.C. (2003). Roles of amyloid precursor protein and its fragments in regulating neural activity, plasticity and memory. Prog Neurobiol *70*, 1-32.

58. Esler, W.P., and Wolfe, M.S. (2001). A portrait of Alzheimer secretases--new features and familiar faces. Science *293*, 1449-1454.

59. De Strooper, B. (2003). Aph-1, Pen-2, and Nicastrin with Presenilin generate an active gamma-Secretase complex. Neuron *38*, 9-12.

60. Czech, C., Tremp, G., and Pradier, L. (2000). Presenilins and Alzheimer's disease: biological functions and pathogenic mechanisms. Prog Neurobiol *60*, 363-384.

61. Petkova, A.T., Ishii, Y., Balbach, J.J., Antzutkin, O.N., Leapman, R.D., Delaglio, F., and Tycko, R. (2002). A structural model for Alzheimer's beta -amyloid fibrils based on experimental constraints from solid state NMR. Proc Natl Acad Sci U S A *99*, 16742-16747.

62. Luhrs, T., Ritter, C., Adrian, M., Riek-Loher, D., Bohrmann, B., Dobeli, H., Schubert, D., and Riek, R. (2005). 3D structure of Alzheimer's amyloid-beta(1-42) fibrils. Proc Natl Acad Sci U S A *102*, 17342-17347.

63. Hardy, J.A., and Higgins, G.A. (1992). Alzheimer's disease: the amyloid cascade hypothesis. Science *256*, 184-185.

64. Kirschner, D.A., Abraham, C., and Selkoe, D.J. (1986). X-ray diffraction from intraneuronal paired helical filaments and extraneuronal amyloid fibers in Alzheimer disease indicates cross-beta conformation. Proc Natl Acad Sci U S A *83*, 503-507.

65. Malinchik, S.B., Inouye, H., Szumowski, K.E., and Kirschner, D.A. (1998). Structural analysis of Alzheimer's beta(1-40) amyloid: protofilament assembly of tubular fibrils. Biophys J *74*, 537-545.

66. Sikorski, P., Atkins, E.D., and Serpell, L.C. (2003). Structure and texture of fibrous crystals formed by Alzheimer's abeta(11-25) peptide fragment. Structure *11*, 915-926.

67. Balbach, J.J., Petkova, A.T., Oyler, N.A., Antzutkin, O.N., Gordon, D.J., Meredith, S.C., and Tycko, R. (2002). Supramolecular structure in full-length Alzheimer's beta-amyloid fibrils: evidence for a parallel beta-sheet organization from solid-state nuclear magnetic resonance. Biophys J *83*, 1205-1216.

68. Antzutkin, O.N., Balbach, J.J., and Tycko, R. (2003). Site-specific identification of non-beta-strand conformations in Alzheimer's beta-amyloid fibrils by solid-state NMR. Biophys J *84*, 3326-3335.

69. Petkova, A.T., Yau, W.M., and Tycko, R. (2006). Experimental constraints on quaternary structure in Alzheimer's beta-amyloid fibrils. Biochemistry *45*, 498-512.

70. Riek, R., Guntert, P., Dobeli, H., Wipf, B., and Wuthrich, K. (2001). NMR studies in aqueous solution fail to identify significant conformational differences between the monomeric forms of two Alzheimer peptides with widely different plaque-competence, A beta(1-40)(ox) and A beta(1-42)(ox). Eur J Biochem *268*, 5930-5936.

71.   http://www.clinicaltrials.gov/ct2/results?term=alzheimer.

72.   Hong, L., Koelsch, G., Lin, X., Wu, S., Terzyan, S., Ghosh, A.K., Zhang, X.C., and Tang, J. (2000). Structure of the protease domain of memapsin 2 (beta-secretase) complexed with inhibitor. Science *290*, 150-153.

73.   Willem, M., Garratt, A.N., Novak, B., Citron, M., Kaufmann, S., Rittger, A., DeStrooper, B., Saftig, P., Birchmeier, C., and Haass, C. (2006). Control of peripheral nerve myelination by the beta-secretase BACE1. Science *314*, 664-666.

74.   Hartmann, D., Tournoy, J., Saftig, P., Annaert, W., and De Strooper, B. (2001). Implication of APP secretases in notch signaling. J Mol Neurosci *17*, 171-181.

75.   Kukar, T.L., Ladd, T.B., Bann, M.A., Fraering, P.C., Narlawar, R., Maharvi, G.M., Healy, B., Chapman, R., Welzel, A.T., Price, R.W., Moore, B., Rangachari, V., Cusack, B., Eriksen, J., Jansen-West, K., Verbeeck, C., Yager, D., Eckman, C., Ye, W., Sagi, S., Cottrell, B.A., Torpey, J., Rosenberry, T.L., Fauq, A., Wolfe, M.S., Schmidt, B., Walsh, D.M., Koo, E.H., and Golde, T.E. (2008). Substrate-targeting gamma-secretase modulators. Nature *453*, 925-929.

76.   Kukar, T., and Golde, T.E. (2008). Possible mechanisms of action of NSAIDs and related compounds that modulate gamma-secretase cleavage. Curr Top Med Chem *8*, 47-53.

77.   Schenk, D., Barbour, R., Dunn, W., Gordon, G., Grajeda, H., Guido, T., Hu, K., Huang, J., Johnson-Wood, K., Khan, K., Kholodenko, D., Lee, M., Liao, Z., Lieberburg, I., Motter, R., Mutter, L., Soriano, F., Shopp, G., Vasquez, N., Vandevert, C., Walker, S., Wogulis, M., Yednock, T., Games, D., and Seubert, P. (1999). Immunization with amyloid-beta attenuates Alzheimer-disease-like pathology in the PDAPP mouse. Nature *400*, 173-177.

78.   Bard, F., Cannon, C., Barbour, R., Burke, R.L., Games, D., Grajeda, H., Guido, T., Hu, K., Huang, J., Johnson-Wood, K., Khan, K., Kholodenko, D., Lee, M., Lieberburg, I., Motter, R., Nguyen, M., Soriano, F., Vasquez, N., Weiss, K., Welch, B., Seubert, P., Schenk, D., and Yednock, T. (2000). Peripherally administered antibodies against amyloid beta-peptide enter the central nervous system and reduce pathology in a mouse model of Alzheimer disease. Nat Med *6*, 916-919.

79.   Weiner, H.L., Lemere, C.A., Maron, R., Spooner, E.T., Grenfell, T.J., Mori, C., Issazadeh, S., Hancock, W.W., and Selkoe, D.J. (2000). Nasal administration of amyloid-beta peptide decreases cerebral amyloid burden in a mouse model of Alzheimer's disease. Ann Neurol *48*, 567-579.

80.   Birmingham, K., and Frantz, S. (2002). Set back to Alzheimer vaccine studies. Nat Med *8*, 199-200.

81.   Orgogozo, J.M., Gilman, S., Dartigues, J.F., Laurent, B., Puel, M., Kirby, L.C., Jouanny, P., Dubois, B., Eisner, L., Flitman, S., Michel, B.F., Boada, M., Frank, A., and Hock, C. (2003). Subacute meningoencephalitis in a subset of patients with AD after Abeta42 immunization. Neurology *61*, 46-54.

82.   Lee, M., Bard, F., Johnson-Wood, K., Lee, C., Hu, K., Griffith, S.G., Black, R.S., Schenk, D., and Seubert, P. (2005). Abeta42 immunization in Alzheimer's disease generates Abeta N-terminal antibodies. Ann Neurol *58*, 430-435.

83.   Town, T., Tan, J., Sansone, N., Obregon, D., Klein, T., and Mullan, M. (2001). Characterization of murine immunoglobulin G antibodies against human amyloid-beta1-42. Neurosci Lett *307*, 101-104.

84.   Agadjanyan, M.G., Ghochikyan, A., Petrushina, I., Vasilevko, V., Movsesyan, N., Mkrtichyan, M., Saing, T., and Cribbs, D.H. (2005). Prototype Alzheimer's disease vaccine using the immunodominant B cell epitope from beta-amyloid and promiscuous T cell epitope pan HLA DR-binding peptide. J Immunol *174*, 1580-1586.

85.   Maier, M., Seabrook, T.J., Lazo, N.D., Jiang, L., Das, P., Janus, C., and Lemere, C.A. (2006). Short amyloid-beta (Abeta) immunogens reduce cerebral Abeta load and learning deficits in an Alzheimer's disease mouse model in the absence of an Abeta-specific cellular immune response. J Neurosci *26*, 4717-4728.

86.   Schenk, D. (2002). Amyloid-beta immunotherapy for Alzheimer's disease: the end of the beginning. Nat Rev Neurosci *3*, 824-828.

87.   DeMattos, R.B., Bales, K.R., Cummins, D.J., Dodart, J.C., Paul, S.M., and Holtzman, D.M. (2001). Peripheral anti-A beta antibody alters CNS and plasma A beta clearance and decreases brain A beta burden in a mouse model of Alzheimer's disease. Proc Natl Acad Sci U S A *98*, 8850-8855.

88.   Ellis, R.J., van der Vies, S.M., and Hemmingsen, S.M. (1989). The molecular chaperone concept. Biochem Soc Symp *55*, 145-153.

89.   Evans, C.G., Wisen, S., and Gestwicki, J.E. (2006). Heat shock proteins 70 and 90 inhibit early stages of amyloid beta-(1-42) aggregation in vitro. J Biol Chem *281*, 33182-33191.

90.   Westermark, P. (2005). Aspects on human amyloid forms and their fibril polypeptides. FEBS J *272*, 5942-5949.

91.   Yerbury, J.J., Poon, S., Meehan, S., Thompson, B., Kumita, J.R., Dobson, C.M., and Wilson, M.R. (2007). The extracellular chaperone clusterin influences amyloid formation and toxicity by interacting with prefibrillar structures. FASEB J *21*, 2312-2322.

92.   Sabate, R., and Estelrich, J. (2005). Stimulatory and inhibitory effects of alkyl bromide surfactants on beta-amyloid fibrillogenesis. Langmuir *21*, 6944-6949.

93.   Bush, A.I. (2002). Metal complexing agents as therapies for Alzheimer's disease. Neurobiol Aging *23*, 1031-1038.

94.   Yang, F., Lim, G.P., Begum, A.N., Ubeda, O.J., Simmons, M.R., Ambegaokar, S.S., Chen, P.P., Kayed, R., Glabe, C.G., Frautschy, S.A., and Cole, G.M. (2005). Curcumin inhibits formation of amyloid beta oligomers and fibrils, binds plaques, and reduces amyloid in vivo. J Biol Chem *280*, 5892-5901.

95.   Pappolla, M., Bozner, P., Soto, C., Shao, H., Robakis, N.K., Zagorski, M., Frangione, B., and Ghiso, J. (1998). Inhibition of Alzheimer beta-fibrillogenesis by melatonin. J Biol Chem *273*, 7185-7188.

96.   Salomon, A.R., Marcinowski, K.J., Friedland, R.P., and Zagorski, M.G. (1996). Nicotine inhibits amyloid formation by the beta-peptide. Biochemistry *35*, 13568-13578.

97.   Tomiyama, T., Shoji, A., Kataoka, K., Suwa, Y., Asano, S., Kaneko, H., and Endo, N. (1996). Inhibition of amyloid beta protein aggregation and neurotoxicity by rifampicin. Its possible function as a hydroxyl radical scavenger. J Biol Chem *271*, 6839-6844.

98.   Podlisny, M.B., Walsh, D.M., Amarante, P., Ostaszewski, B.L., Stimson, E.R., Maggio, J.E., Teplow, D.B., and Selkoe, D.J. (1998). Oligomerization of endogenous and synthetic amyloid beta-protein at nanomolar levels in cell culture and stabilization of monomer by Congo red. Biochemistry *37*, 3602-3611.

99.   Kelenyi, G. (1967). On the histochemistry of azo group-free thiazole dyes. J Histochem Cytochem *15*, 172-180.

100. Nakagami, Y., Nishimura, S., Murasugi, T., Kaneko, I., Meguro, M., Marumoto, S., Kogen, H., Koyama, K., and Oda, T. (2002). A novel beta-sheet breaker, RS-0406, reverses amyloid beta-induced cytotoxicity and impairment of long-term potentiation in vitro. Br J Pharmacol *137*, 676-682.

101. Walsh, D.M., Townsend, M., Podlisny, M.B., Shankar, G.M., Fadeeva, J.V., El Agnaf, O., Hartley, D.M., and Selkoe, D.J. (2005). Certain inhibitors of synthetic amyloid beta-peptide (Abeta) fibrillogenesis block oligomerization of natural Abeta and thereby rescue long-term potentiation. J Neurosci *25*, 2455-2462.

102. Necula, M., Kayed, R., Milton, S., and Glabe, C.G. (2007). Small molecule inhibitors of aggregation indicate that amyloid beta oligomerization and fibrillization pathways are independent and distinct. J Biol Chem *282*, 10311-10324.

103. Tjernberg, L.O., Naslund, J., Lindqvist, F., Johansson, J., Karlstrom, A.R., Thyberg, J., Terenius, L., and Nordstedt, C. (1996). Arrest of beta-amyloid fibril formation by a pentapeptide ligand. J Biol Chem *271*, 8545-8548.

104. Cairo, C.W., Strzelec, A., Murphy, R.M., and Kiessling, L.L. (2002). Affinity-based inhibition of beta-amyloid toxicity. Biochemistry *41*, 8620-8629.

105. Lowe, T.L., Strzelec, A., Kiessling, L.L., and Murphy, R.M. (2001). Structure-function relationships for inhibitors of beta-amyloid toxicity containing the recognition sequence KLVFF. Biochemistry *40*, 7882-7889.

106. Soto, C., Kindy, M.S., Baumann, M., and Frangione, B. (1996). Inhibition of Alzheimer's amyloidosis by peptides that prevent beta-sheet conformation. Biochem Biophys Res Commun *226*, 672-680.

107. Soto, C., Sigurdsson, E.M., Morelli, L., Kumar, R.A., Castano, E.M., and Frangione, B. (1998). Beta-sheet breaker peptides inhibit fibrillogenesis in a rat brain model of amyloidosis: implications for Alzheimer's therapy. Nat Med *4*, 822-826.

108. Gordon, D.J., Sciarretta, K.L., and Meredith, S.C. (2001). Inhibition of beta-amyloid(40) fibrillogenesis and disassembly of beta-amyloid(40) fibrils by short beta-amyloid congeners containing N-methyl amino acids at alternate residues. Biochemistry *40*, 8237-8245.

109. Hughes, E., Burke, R.M., and Doig, A.J. (2000). Inhibition of toxicity in the beta-amyloid peptide fragment beta -(25-35) using N-methylated derivatives: a general strategy to prevent amyloid formation. J Biol Chem *275*, 25109-25115.

110. Wild, S., Roglic, G., Green, A., Sicree, R., and King, H. (2004). Global prevalence of diabetes: estimates for the year 2000 and projections for 2030. Diabetes Care *27*, 1047-1053.

111. Onkamo, P., Vaananen, S., Karvonen, M., and Tuomilehto, J. (1999). Worldwide increase in incidence of Type I diabetes--the analysis of the data on published incidence trends. Diabetologia *42*, 1395-1403.

112. Foulis, A.K. (1987). C. L. Oakley lecture (1987). The pathogenesis of beta cell destruction in type I (insulin-dependent) diabetes mellitus. J Pathol *152*, 141-148.

113. Westermark, P., and Grimelius, L. (1973). The pancreatic islet cells in insular amyloidosis in human diabetic and non-diabetic adults. Acta Pathol Microbiol Scand A *81*, 291-300.

114. Opie, E.L. (1900). Pathological Changes Affecting the Islands of Langerhans of the Pancreas. J Boston Soc Med Sci *4*, 251-260.

115. Westermark, P., Wernstedt, C., Wilander, E., and Sletten, K. (1986). A novel peptide in the calcitonin gene related peptide family as an amyloid fibril protein in the endocrine pancreas. Biochem Biophys Res Commun *140*, 827-831.

116. Howard, C.F., Jr. (1978). Insular amyloidosis and diabetes mellitus in Macaca nigra. Diabetes *27*, 357-364.

117. Maloy, A.L., Longnecker, D.S., and Greenberg, E.R. (1981). The relation of islet amyloid to the clinical type of diabetes. Hum Pathol *12*, 917-922.

118. Westermark, P. (1972). Quantitative studies on amyloid in the islets of Langerhans. Ups J Med Sci *77*, 91-94.

119. Clark, A., Wells, C.A., Buley, I.D., Cruickshank, J.K., Vanhegan, R.I., Matthews, D.R., Cooper, G.J., Holman, R.R., and Turner, R.C. (1988). Islet amyloid, increased A-cells, reduced B-cells and exocrine fibrosis: quantitative changes in the pancreas in type 2 diabetes. Diabetes Res *9*, 151-159.

120. Westermark, P. (1973). Fine structure of islets of Langerhans in insular amyloidosis. Virchows Arch A Pathol Pathol Anat *359*, 1-18.

121. Couce, M., Kane, L.A., O'Brien, T.D., Charlesworth, J., Soeller, W., McNeish, J., Kreutter, D., Roche, P., and Butler, P.C. (1996). Treatment with growth hormone and dexamethasone in mice transgenic for human islet amyloid polypeptide causes islet amyloidosis and beta-cell dysfunction. Diabetes *45*, 1094-1101.

122. MacArthur, D.L., de Koning, E.J., Verbeek, J.S., Morris, J.F., and Clark, A. (1999). Amyloid fibril formation is progressive and correlates with beta-cell secretion in transgenic mouse isolated islets. Diabetologia *42*, 1219-1227.

123. O'Brien, T.D., Butler, P.C., Westermark, P., and Johnson, K.H. (1993). Islet amyloid polypeptide: a review of its biology and potential roles in the pathogenesis of diabetes mellitus. Vet Pathol *30*, 317-332.

124. Mirzabekov, T.A., Lin, M.C., and Kagan, B.L. (1996). Pore formation by the cytotoxic islet amyloid peptide amylin. J Biol Chem *271*, 1988-1992.

125. Lorenzo, A., Razzaboni, B., Weir, G.C., and Yankner, B.A. (1994). Pancreatic islet cell toxicity of amylin associated with type-2 diabetes mellitus. Nature *368*, 756-760.

126. Cooper, G.J., Willis, A.C., and Leighton, B. (1989). Amylin hormone. Nature *340*, 272.

127. Glenner, G.G., Eanes, E.D., and Wiley, C.A. (1988). Amyloid fibrils formed from a segment of the pancreatic islet amyloid protein. Biochem Biophys Res Commun *155*, 608-614.

128. Betsholtz, C., Christmansson, L., Engstrom, U., Rorsman, F., Svensson, V., Johnson, K.H., and Westermark, P. (1989). Sequence divergence in a specific region of islet amyloid polypeptide (IAPP) explains differences in islet amyloid formation between species. FEBS Lett *251*, 261-264.

129. Westermark, P., Engstrom, U., Johnson, K.H., Westermark, G.T., and Betsholtz, C. (1990). Islet amyloid polypeptide: pinpointing amino acid residues linked to amyloid fibril formation. Proc Natl Acad Sci U S A *87*, 5036-5040.

130. Betsholtz, C., Christmanson, L., Engstrom, U., Rorsman, F., Jordan, K., O'Brien, T.D., Murtaugh, M., Johnson, K.H., and Westermark, P. (1990). Structure of cat islet amyloid polypeptide and identification of amino acid residues of potential significance for islet amyloid formation. Diabetes *39*, 118-122.

131. Kapurniotu, A. (2001). Amyloidogenicity and cytotoxicity of islet amyloid polypeptide. Biopolymers *60*, 438-459.

132. Chou, P.Y., and Fasman, G.D. (1978). Empirical predictions of protein conformation. Annu Rev Biochem *47*, 251-276.

133. Wood, S.J., Wetzel, R., Martin, J.D., and Hurle, M.R. (1995). Prolines and amyloidogenicity in fragments of the Alzheimer's peptide beta/A4. Biochemistry *34*, 724-730.

134. Ryan, G.J., Jobe, L.J., and Martin, R. (2005). Pramlintide in the treatment of type 1 and type 2 diabetes mellitus. Clin Ther *27*, 1500-1512.

135. Nilsson, M.R., and Raleigh, D.P. (1999). Analysis of amylin cleavage products provides new insights into the amyloidogenic region of human amylin. J Mol Biol *294*, 1375-1385.

136. Jaikaran, E.T., Higham, C.E., Serpell, L.C., Zurdo, J., Gross, M., Clark, A., and Fraser, P.E. (2001). Identification of a novel human islet amyloid polypeptide beta-sheet domain and factors influencing fibrillogenesis. J Mol Biol *308*, 515-525.

137. Shim, S.H., Gupta, R., Ling, Y.L., Strasfeld, D.B., Raleigh, D.P., and Zanni, M.T. (2009). Two-dimensional IR spectroscopy and isotope labeling defines the pathway of amyloid formation with residue-specific resolution. Proc Natl Acad Sci U S A *106*, 6614-6619.

138. Kayed, R., Bernhagen, J., Greenfield, N., Sweimeh, K., Brunner, H., Voelter, W., and Kapurniotu, A. (1999). Conformational transitions of islet amyloid polypeptide (IAPP) in amyloid formation in vitro. J Mol Biol *287*, 781-796.

139. Dupuis, N.F., Wu, C., Shea, J.E., and Bowers, M.T. (2009). Human islet amyloid polypeptide monomers form ordered beta-hairpins: a possible direct amyloidogenic precursor. J Am Chem Soc *131*, 18283-18292.

140. Clark, A., and Nilsson, M.R. (2004). Islet amyloid: a complication of islet dysfunction or an aetiological factor in Type 2 diabetes? Diabetologia *47*, 157-169.

141. Jayasinghe, S.A., and Langen, R. (2004). Identifying structural features of fibrillar islet amyloid polypeptide using site-directed spin labeling. J Biol Chem *279*, 48420-48425.

142. Luca, S., Yau, W.M., Leapman, R., and Tycko, R. (2007). Peptide conformation and supramolecular organization in amylin fibrils: constraints from solid-state NMR. Biochemistry *46*, 13505-13522.

143. Wiltzius, J.J., Sievers, S.A., Sawaya, M.R., Cascio, D., Popov, D., Riekel, C., and Eisenberg, D. (2008). Atomic structure of the cross-beta spine of islet amyloid polypeptide (amylin). Protein Sci *17*, 1467-1474.

144. Aitken, J.F., Loomes, K.M., Konarkowska, B., and Cooper, G.J. (2003). Suppression by polycyclic compounds of the conversion of human amylin into insoluble amyloid. Biochem J *374*, 779-784.

145. Tomiyama, T., Kaneko, H., Kataoka, K., Asano, S., and Endo, N. (1997). Rifampicin inhibits the toxicity of pre-aggregated amyloid peptides by binding to peptide fibrils and preventing amyloid-cell interaction. Biochem J *322 (Pt 3)*, 859-865.

146. Harroun, T.A., Bradshaw, J.P., and Ashley, R.H. (2001). Inhibitors can arrest the membrane activity of human islet amyloid polypeptide independently of amyloid formation. FEBS Lett *507*, 200-204.

147. Lin, Y.M., Raffen, R., Zhou, Y., Cassidy, C.S., Flavin, M.T., and Stevens, F.J. (2001). Amyloid fibril formation in microwell plates for screening of inhibitors. Amyloid *8*, 182-193.

148. Scrocchi, L.A., Chen, Y., Waschuk, S., Wang, F., Cheung, S., Darabie, A.A., McLaurin, J., and Fraser, P.E. (2002). Design of peptide-based inhibitors of human islet amyloid polypeptide fibrillogenesis. J Mol Biol *318*, 697-706.

149. Gilead, S., and Gazit, E. (2004). Inhibition of amyloid fibril formation by peptide analogues modified with alpha-aminoisobutyric acid. Angew Chem Int Ed Engl *43*, 4041-4044.

150. Elgersma, R.C., Mulder, G.E., Kruijtzer, J.A., Posthuma, G., Rijkers, D.T., and Liskamp, R.M. (2007). Transformation of the amyloidogenic peptide amylin(20-29) into its corresponding peptoid and retropeptoid: access to both an amyloid inhibitor and template for self-assembled supramolecular tapes. Bioorg Med Chem Lett *17*, 1837-1842.

151. Kapurniotu, A., Schmauder, A., and Tenidis, K. (2002). Structure-based design and study of non-amyloidogenic, double N-methylated IAPP amyloid core sequences as inhibitors of IAPP amyloid formation and cytotoxicity. J Mol Biol *315*, 339-350.

152. Tenidis, K., Waldner, M., Bernhagen, J., Fischle, W., Bergmann, M., Weber, M., Merkle, M.L., Voelter, W., Brunner, H., and Kapurniotu, A. (2000). Identification of a penta- and hexapeptide of islet amyloid polypeptide (IAPP) with amyloidogenic and cytotoxic properties. J Mol Biol *295*, 1055-1071.

153. Tatarek-Nossol, M., Yan, L.M., Schmauder, A., Tenidis, K., Westermark, G., and Kapurniotu, A. (2005). Inhibition of hIAPP amyloid-fibril formation and apoptotic cell death by a designed hIAPP amyloid- core-containing hexapeptide. Chem Biol *12*, 797-809.

154. Griffiths J.M., A.T.T., Auger M., Costa P.R., Griffin R.C., Lansbury P.T. (1995). Rotational Resonance Solid-State NMR Elucidates a Structural Model of Pancreatic Amyloid. J. Am. Chem. Soc. *117*, 3539-3546.

155. Yan, L.M., Tatarek-Nossol, M., Velkova, A., Kazantzis, A., and Kapurniotu, A. (2006). Design of a mimic of nonamyloidogenic and bioactive human islet amyloid polypeptide (IAPP) as nanomolar affinity inhibitor of IAPP cytotoxic fibrillogenesis. Proc Natl Acad Sci U S A *103*, 2046-2051.

156. Selkoe, D.J. (1997). Alzheimer's disease: genotypes, phenotypes, and treatments. Science *275*, 630-631.

157. Hoppener, J.W., Ahren, B., and Lips, C.J. (2000). Islet amyloid and type 2 diabetes mellitus. N Engl J Med *343*, 411-419.

158. Haan, M.N. (2006). Therapy Insight: type 2 diabetes mellitus and the risk of late-onset Alzheimer's disease. Nat Clin Pract Neurol *2*, 159-166.

159. de la Monte, S.M., and Wands, J.R. (2005). Review of insulin and insulin-like growth factor expression, signaling, and malfunction in the central nervous system: relevance to Alzheimer's disease. J Alzheimers Dis *7*, 45-61.

160. Li, L., and Holscher, C. (2007). Common pathological processes in Alzheimer disease and type 2 diabetes: a review. Brain Res Rev *56*, 384-402.

161. Hoyer, S. (2004). Glucose metabolism and insulin receptor signal transduction in Alzheimer disease. Eur J Pharmacol *490*, 115-125.

162. Qiu, W.Q., and Folstein, M.F. (2006). Insulin, insulin-degrading enzyme and amyloid-beta peptide in Alzheimer's disease: review and hypothesis. Neurobiol Aging *27*, 190-198.

163. Nicolls, M.R., D'Antonio, J.M., Hutton, J.C., Gill, R.G., Czwornog, J.L., and Duncan, M.W. (2003). Proteomics as a tool for discovery: proteins implicated in Alzheimer's disease are highly expressed in normal pancreatic islets. J Proteome Res *2*, 199-205.

164. David, D.C., Ittner, L.M., Gehrig, P., Nergenau, D., Shepherd, C., Halliday, G., and Gotz, J. (2006). Beta-amyloid treatment of two complementary P301L tau-expressing Alzheimer's disease models reveals similar deregulated cellular processes. Proteomics *6*, 6566-6577.

165. Degrado, W.F. (1988). Design of peptides and proteins. Adv Protein Chem *39*, 51-124.

166. Mazor, Y., Gilead, S., Benhar, I., and Gazit, E. (2002). Identification and characterization of a novel molecular-recognition and self-assembly domain within the islet amyloid polypeptide. J Mol Biol *322*, 1013-1024.

167. Yan, L.M., Velkova, A., Tatarek-Nossol, M., Andreetto, E., and Kapurniotu, A. (2007). IAPP mimic blocks Abeta cytotoxic self-assembly: cross-suppression of amyloid toxicity of Abeta and IAPP suggests a molecular link between Alzheimer's disease and type II diabetes. Angew Chem Int Ed Engl *46*, 1246-1252.

168. Felix, A.M., Heimer, E.P., Wang, C.T., Lambros, T.J., Fournier, A., Mowles, T.F., Maines, S., Campbell, R.M., Wegrzynski, B.B., Toome, V., and et al. (1988). Synthesis, biological activity and conformational analysis of cyclic GRF analogs. Int J Pept Protein Res *32*, 441-454.

169. Kaiser, E., Colescott, R.L., Bossinger, C.D., and Cook, P.I. (1970). Color test for detection of free terminal amino groups in the solid-phase synthesis of peptides. Anal Biochem *34*, 595-598.

170. Vojkovsky, T. (1995). Detection of secondary amines on solid phase. Pept Res *8*, 236-237.

171. Han, Y., Albericio, F., and Barany, G. (1997). Occurrence and Minimization of Cysteine Racemization during Stepwise Solid-Phase Peptide Synthesis(1)(,)(2). J Org Chem *62*, 4307-4312.

172. King, D.S., Fields, C.G., and Fields, G.B. (1990). A cleavage method which minimizes side reactions following Fmoc solid phase peptide synthesis. Int J Pept Protein Res *36*, 255-266.

173. Gill, S.C., and von Hippel, P.H. (1989). Calculation of protein extinction coefficients from amino acid sequence data. Anal Biochem *182*, 319-326.

174. Pace, C.N., Vajdos, F., Fee, L., Grimsley, G., and Gray, T. (1995). How to measure and predict the molar absorption coefficient of a protein. Protein Sci *4*, 2411-2423.

175. Frank, R. (2002). The SPOT-synthesis technique. Synthetic peptide arrays on membrane supports--principles and applications. J Immunol Methods *267*, 13-26.

176. Greene, L.A., and Tischler, A.S. (1976). Establishment of a noradrenergic clonal line of rat adrenal pheochromocytoma cells which respond to nerve growth factor. Proc Natl Acad Sci U S A *73*, 2424-2428.

177. Andreetto, E., Yan, L.M., Tatarek-Nossol, M., Velkova, A., Frank, R., and Kapurniotu, A. (2010). Identification of hot regions of the Abeta-IAPP interaction interface as high-affinity binding sites in both cross- and self-association. Angew Chem Int Ed Engl *49*, 3081-3085.

178. Wiltzius, J.J., Sievers, S.A., Sawaya, M.R., and Eisenberg, D. (2009). Atomic structures of IAPP (amylin) fusions suggest a mechanism for fibrillation and the role of insulin in the process. Protein Sci *18*, 1521-1530.

179. LeVine, H., 3rd (1993). Thioflavine T interaction with synthetic Alzheimer's disease beta-amyloid peptides: detection of amyloid aggregation in solution. Protein Sci *2*, 404-410.

180. LeVine, H., 3rd (1999). Quantification of beta-sheet amyloid fibril structures with thioflavin T. Methods Enzymol *309*, 274-284.

181. Mosmann, T. (1983). Rapid colorimetric assay for cellular growth and survival: application to proliferation and cytotoxicity assays. J Immunol Methods *65*, 55-63.

182. Yamaguchi, K., Naiki, H., and Goto, Y. (2006). Mechanism by which the amyloid-like fibrils of a beta 2-microglobulin fragment are induced by fluorine-substituted alcohols. J Mol Biol *363*, 279-288.

183. Holtzer, M.E., and Holtzer, A. (1992). Alpha-helix to random coil transitions: determination of peptide concentration from the CD at the isodichroic point. Biopolymers *32*, 1675-1677.

184. Liebes, L.F., Zand, R., and Phillips, W.D. (1975). Solution behavior, circular dichroism and 22 HMz PMR studies of the bovine myelin basic protein. Biochim Biophys Acta *405*, 27-39.

185. Sancho, J., Neira, J.L., and Fersht, A.R. (1992). An N-terminal fragment of barnase has residual helical structure similar to that in a refolding intermediate. J Mol Biol *224*, 749-758.

186. Pace, C.N., and Scholtz, J.M. (1998). A helix propensity scale based on experimental studies of peptides and proteins. Biophys J *75*, 422-427.

187. Koo, B.W., and Miranker, A.D. (2005). Contribution of the intrinsic disulfide to the assembly mechanism of islet amyloid. Protein Sci *14*, 231-239.

188. Khemtemourian, L., Engel, M.F., Kruijtzer, J.A., Hoppener, J.W., Liskamp, R.M., and Killian, J.A. The role of the disulfide bond in the interaction of islet amyloid polypeptide with membranes. Eur Biophys J *39*, 1359-1364.

189. Veronese, F.M., and Harris, J.M. (2002). Introduction and overview of peptide and protein pegylation. Adv Drug Deliv Rev *54*, 453-456.

190. Kyte, J., and Doolittle, R.F. (1982). A simple method for displaying the hydropathic character of a protein. J Mol Biol *157*, 105-132.

191. Kapurniotu, A., Bernhagen, J., Greenfield, N., Al-Abed, Y., Teichberg, S., Frank, R.W., Voelter, W., and Bucala, R. (1998). Contribution of advanced glycosylation to the amyloidogenicity of islet amyloid polypeptide. Eur J Biochem *251*, 208-216.

192. Vagner, J., Handl, H.L., Monguchi, Y., Jana, U., Begay, L.J., Mash, E.A., Hruby, V.J., and Gillies, R.J. (2006). Rigid linkers for bioactive peptides. Bioconjug Chem *17*, 1545-1550.

193. Sreerama, N., Manning, M.C., Powers, M.E., Zhang, J.X., Goldenberg, D.P., and Woody, R.W. (1999). Tyrosine, phenylalanine, and disulfide contributions to the circular dichroism of proteins: circular dichroism spectra of wild-type and mutant bovine pancreatic trypsin inhibitor. Biochemistry *38*, 10814-10822.

194. Nicolls, M.R. (2004). The clinical and biological relationship between Type II diabetes mellitus and Alzheimer's disease. Curr Alzheimer Res *1*, 47-54.

195. Findeis, M.A. (2007). The role of amyloid beta peptide 42 in Alzheimer's disease. Pharmacol Ther *116*, 266-286.

196. Gilead, S., Wolfenson, H., and Gazit, E. (2006). Molecular mapping of the recognition interface between the islet amyloid polypeptide and insulin. Angew Chem Int Ed Engl *45*, 6476-6480.

197. Mishra, R., Geyer, M., and Winter, R. (2009). NMR spectroscopic investigation of early events in IAPP amyloid fibril formation. Chembiochem *10*, 1769-1772.

198. Guo, J.P., Arai, T., Miklossy, J., and McGeer, P.L. (2006). Abeta and tau form soluble complexes that may promote self aggregation of both into the insoluble forms observed in Alzheimer's disease. Proc Natl Acad Sci U S A *103*, 1953-1958.

199. Andreetto, E., Yan, L.M., Caporale, A., and Kapurniotu, A. (2011). Dissecting the Role of Single Regions of an IAPP Mimic and IAPP in Inhibition of Abeta40 Amyloid Formation and Cytotoxicity. Chembiochem *12*, 1313-1322.

200. Goldsbury, C., Goldie, K., Pellaud, J., Seelig, J., Frey, P., Muller, S.A., Kistler, J., Cooper, G.J., and Aebi, U. (2000). Amyloid fibril formation from full-length and fragments of amylin. J Struct Biol *130*, 352-362.

201.   Soto, C., and Frangione, B. (1995). Two conformational states of amyloid beta-peptide: implications for the pathogenesis of Alzheimer's disease. Neurosci Lett *186*, 115-118.

202.   Shen, C.L., and Murphy, R.M. (1995). Solvent effects on self-assembly of beta-amyloid peptide. Biophys J *69*, 640-651.

203.   Cooper, G.J. (1994). Amylin compared with calcitonin gene-related peptide: structure, biology, and relevance to metabolic disease. Endocr Rev *15*, 163-201.

204.   Ramirez-Alvarado, M., Blanco, F.J., and Serrano, L. (2001). Elongation of the BH8 beta-hairpin peptide: Electrostatic interactions in beta-hairpin formation and stability. Protein Sci *10*, 1381-1392.

205.   Haupt, C., Morgado, I., Kumar, S.T., Parthier, C., Bereza, M., Hortschansky, P., Stubbs, M.T., Horn, U., and Fandrich, M. Amyloid fibril recognition with the conformational B10 antibody fragment depends on electrostatic interactions. J Mol Biol *405*, 341-348.

206.   Dupuis, N.F., Wu, C., Shea, J.E., and Bowers, M.T. The amyloid formation mechanism in human IAPP: dimers have beta-strand monomer-monomer interfaces. J Am Chem Soc *133*, 7240-7243.

207.   Sandberg, A., Luheshi, L.M., Sollvander, S., Pereira de Barros, T., Macao, B., Knowles, T.P., Biverstal, H., Lendel, C., Ekholm-Petterson, F., Dubnovitsky, A., Lannfelt, L., Dobson, C.M., and Hard, T. Stabilization of neurotoxic Alzheimer amyloid-beta oligomers by protein engineering. Proc Natl Acad Sci U S A *107*, 15595-15600.

208.   Cohen, F.E., and Kelly, J.W. (2003). Therapeutic approaches to protein-misfolding diseases. Nature *426*, 905-909.

209.   Frydman-Marom, A., Rechter, M., Shefler, I., Bram, Y., Shalev, D.E., and Gazit, E. (2009). Cognitive-performance recovery of Alzheimer's disease model mice by modulation of early soluble amyloidal assemblies. Angew Chem Int Ed Engl *48*, 1981-1986.

6 Abbreviations

α	Alpha
A	Absorbance
Å	Angstrom
Aβ	β-amyloid peptide
Aβ40	β-amyloid peptide (sequence [1-40])
Aβ42	β-amyloid peptide (sequence [1-42])
ACN	Acetonitrile
Ac_2O	Acetic anhydride
AD	Alzheimer's Disease
AFM	Atomic force microscopy
APP	Amyloid precursor protein
β	Beta
BCA	Bicinchoninic acid
BSA	Bovine serum albumin
CD	Circular dichroism
CR	Congo red
CSF	Cerebrospinal fluid
DAC	7-Diethylaminocoumarine-3-carboxylic acid
DCM	Dichlormethane
DIC	Diisopropylcarbodiimide
DIEA	Diisopropylethylamine
DMF	Dimethylformamid
DMS	Dimethysulfide
DMSO	Dimethylsulfoxide
EDT	1,2-ethandithiol
EDTA	Ethylenediaminetetraacetic acid
ER	Endoplasmic reticulum
FCS	Fetal calf serum
Fluo	5(6)-Carboxyfluorescein
Fmoc	9-fluorenylmethoxycarbonyl
FTIR	Fourier transform infrared spectroscopy
Gdn-HCl	Guanidinium-HCl
h	Hour
HCl	Hydrogen chloride
HFIP	1,1,1,3,3,3-hexafluoro-2-propanol
HATU	2-(7-Aza-1H-benzotriazole-1-yl)-1,1,3,3-tetramethyluroniumhexafluorophosphate
HOBt	1-hydroxybenzotriazole
H_2O_2	Hydrogen peroxide
IC_{50}	Half maximal inhibitory concentration
IAPP	Islet amyloid polypeptide (human)
IAPP-GI	Double N-methylated IAPP analog [(N-Me)G24, (N-Me)I26]-IAPP
IDE	Insulin-degrading enzyme
M	Molar

MALDI	Matrix-assisted laser desorption ionization mass spectrometry
mg	Milligram
min	Minutes
mM	Millimolar
ml	Milliliter
µg	Microgram
µM	Micromolar
µl	Microliter
MTT	3-(4,5-dimethylthiazol-2-yl)-2,5-diphenyltetrazolium bromide
MW	Molecular weight
nm	Nanometer
nM	Nanomolar
NMR	Nuclear magnetic resonance
NSAID's	Nonsteroidal anti-inflammatory drugs
PC-12	Rat pheochromocytoma cell line
POD	Peroxidase
prg.	Program
QC	Quality control
rIAPP	Rat IAPP
RP-HPLC	Reverse phase high performance liquid chromatography
rt	Retention time
SEM	Standard error of mean
SPPS	Solid phase peptide synthesis
SDS	Sodium dodecyl sulfate
SS-NMR	Solid state nuclear magnetic resonance
TBS	Tris buffered saline
TBTU	N,N,N′,N′-Tetramethyl-O-(benzotriazol-1-yl)uronium tetrafluoroborate
tBu	tert-butyl
TEM	Transmission electron microscopy
TFA	Trifluoroacetic acid
THA	Thioanisole
ThT	Thioflavin T
TIS	Triisopropylsilan
Tris-HCl	2-Amino-2-(hydroxymethyl)-1,3-propanediol hydrochloride
Trt	Trityl
UV	Ultraviolet

7 Curriculum Vitae

<u>Personal data</u>

Name: Andreetto Erika

Date of birth: July 30, 1981

Place of birth: Verona

Citizenship: Italian

<u>Education</u>

09. 1986 - 06. 1992	Lower-School in Castel d´Azzano
09. 1992 - 06. 1995	Middle-School in Castel d´Azzano
09. 1995 - 06. 2000	High-School in Istituto Statale "G. Galilei", Verona
09. 2000 - 10. 2005	Chemistry Studies in University of Padova
01. 2005 - 10. 2005	Experimental work for master degree. Thesis in the laboratories of the Department of Chemistry of the University of Padova. Title of the Thesis: "Role of side-chain chiral centers in the screw sense of peptide helices". Advisor : Prof. Fernando Formaggio
02. 2006 - 03. 2007	Fellowship in the laboratories for Bioorganic and Medicinal Chemistry, Institute of Biochemistry, University Hospital RWTH Aachen. Advisor : Prof. Aphrodite Kapurniotu
06. 2007 - 09. 2007	Scientific collaborator in the laboratories for Bioorganic and Medicinal Chemistry, Institute of Biochemistry, University Hospital RWTH Aachen.
10. 2007 - 01. 2011	PhD student in the laboratories for Peptide Biochemistry, Technical University Munich Freising-Weihenstephan
02. 2011 - 07. 2011	Fellowship with the program "equal opportunity for women in science and teaching" in the laboratories for Peptide Biochemistry, Technical University Munich Freising-Weihenstephan

8 Acknowledgments

Many people have contributed to this thesis.

First of all I would like to thank Prof. Dr. Aphrodite Kapurniotu for giving me the opportunity to perform my PhD work under her supervision. I thank her for the several scientific advices and her constant supervision from the preliminary to the concluding level of my scientific work. I'm grateful to her also for making me a stronger person than I was.

A thank also to Prof. Dr. Jürgen Bernhagen for the cooperation over the last years.

I would like to thank Prof. Dr. Horst Kessler to have accepted to be my reviewer.

I would also like to thank all of the members of Kapurniotu's research group from Aachen, especially Dr. Alexandra Velkova, Dr. Li-Mei Yan and Marianna Tatatrek-Nossol not only for being nice co-workers but also for providing much needed humor and entertainment. And now all of the members of Kapurniotu's research group from Freising, especially Andrea Karine, and Michael. I additionally thank Dr. Andrea Caporale for the help in peptide synthesis and purification; Daniel Hornburg and Vanessa Ecker for peptide purification.

This is a great opportunity to express my gratitude to all the people I got to know over these years in Germany. A special thank to those who constantly support me with their friendship and who share with me a lot of the great parties: Aleksandra, Radek, Pia, Corinna, Steffi, Li-Mei, Ben, Moritz, Andrea, Michelino and Karine.

Now let me switch to Italian in order to thank the transalpine part.

Prima di tutto un ringraziamento speciale va ai miei genitori, Rosmin e Rob, per aver sempre creduto in me e per il continuo supporto. Senza di voi non credo che sarei riuscita a ultimare questo lungo viaggio.

Vorrei anche ringraziare la mia grossa e rumorosa famiglia per avermi sempre tenuto aggiornata, per avermi sempre ricordato quali sono le mie radici e l'importanza del valore della famiglia.

Durante questi anni ho compreso che le amicizie vere non finiscono a causa della distanza quindi un grazie anche a voi: Silvia, Fren, Sari, Clari e Fra.

9 Declaration

I, Erika Andreetto, declare that I have written this thesis independently, exclusively based on the literature and tools mentioned in the thesis. This document has not previously been submitted for a degree at any other institution than the Technical University of Munich.

Freising, ……………

_____

Erika Andreetto